University of Alberta

A Three-Dimensional Slope Stability Method Based on Finite Element Stress Analysis and Dynamic Programming

by

Jason Robert Stianson

A thesis submitted to the Faculty of Graduate Studies and Research
in partial fulfillment of the requirements for the degree of **Doctor of Philosophy.**

in

Geotechnical Engineering

Department of Civil & Environmental Engineering

Edmonton, Alberta
Fall 2008

Library and Archives Canada

Published Heritage Branch

395 Wellington Street
Ottawa ON K1A 0N4
Canada

Bibliothèque et Archives Canada

Direction du Patrimoine de l'édition

395, rue Wellington
Ottawa ON K1A 0N4
Canada

Your file Votre référence
ISBN: 978-0-494-46433-5
Our file Notre référence
ISBN: 978-0-494-46433-5

NOTICE:
The author has granted a non-exclusive license allowing Library and Archives Canada to reproduce, publish, archive, preserve, conserve, communicate to the public by telecommunication or on the Internet, loan, distribute and sell theses worldwide, for commercial or non-commercial purposes, in microform, paper, electronic and/or any other formats.

The author retains copyright ownership and moral rights in this thesis. Neither the thesis nor substantial extracts from it may be printed or otherwise reproduced without the author's permission.

AVIS:
L'auteur a accordé une licence non exclusive permettant à la Bibliothèque et Archives Canada de reproduire, publier, archiver, sauvegarder, conserver, transmettre au public par télécommunication ou par l'Internet, prêter, distribuer et vendre des thèses partout dans le monde, à des fins commerciales ou autres, sur support microforme, papier, électronique et/ou autres formats.

L'auteur conserve la propriété du droit d'auteur et des droits moraux qui protège cette thèse. Ni la thèse ni des extraits substantiels de celle-ci ne doivent être imprimés ou autrement reproduits sans son autorisation.

In compliance with the Canadian Privacy Act some supporting forms may have been removed from this thesis.

While these forms may be included in the document page count, their removal does not represent any loss of content from the thesis.

Conformément à la loi canadienne sur la protection de la vie privée, quelques formulaires secondaires ont été enlevés de cette thèse.

Bien que ces formulaires aient inclus dans la pagination, il n'y aura aucun contenu manquant.

Canada

Dedication

To my mother Darlene, my father Stan and my wife Kristina.

Abstract

The application of limit equilibrium finite element slope stability methods is examined. Two-dimensional studies are presented to provide a better understanding of the interaction between a stress - deformation analysis and the slope stability calculations. Special attention is directed towards the influence of the stress - strain characteristics of the soil, the influence of Poisson's ratio and stress history. Studies are presented to investigate concerns that an isotropic linear elastic soil model might not provide a reliable estimate of the factor of safety in slopes where there is potential for extensive yielding, because the shear stress is permitted to increase beyond the shear strength of the soil. The influence of Poisson's ratio and stress history is shown to be related to the rotation of the principal stress that is part of the collapse process. The accuracy of the factor of safety is shown to depend on the degree of compatibility between the orientation of the principal stress and the admissibility criteria used to control the shape of the slip surface. The fluctuations in the factor of safety can be eliminated using an elasto-plastic stress analysis and kinematic admissibility criteria can be used to control the shape of the slip surface.

The development of a stress-based three-dimensional slope stability method is also presented. The factor of safety is computed based on the results of an independent stress-deformation analysis. The resulting factor of safety equation is determinate, linear and satisfies all conditions of equilibrium. The search for the slip surface is completed using traditional trial and error techniques where the shape of the critical slip surface is pre-defined along with a more advanced non-linear

searching procedure. The characteristics of the derived factor of safety equation support the design of a searching algorithm based on a combination of dynamic programming and a series of geometric and kinematic admissibility criteria. The admissibility criteria are used to refine the searching procedure and distinguish between reasonable and unreasonable slip surfaces. The shape of the slip surface becomes part of the slope stability evaluation and is integrated with the method used to compute the factor of safety.

Acknowledgements

I would like to express my sincere gratitude to some of the individuals who have supported the completion of this research.

Dr. D.G. Fredlund provided generous funding, thorough evaluation of my research and guidance through many difficult decisions. Dr. D.H. Chan offered thoughtful encouragement, insightful comments and the opportunity for beneficial teaching experience. Dr. N.R. Morgenstern and Dr. C.D. Martin made themselves available on numerous occasions to discuss my work and provided valuable advice. The Natural Sciences and Engineering Research Council of Canada and Dr. M.D. Fredlund of SoilVision Systems Ltd. provided funding to support this research. I would also like to thank the members of my committee for taking the time to examine my research and make the necessary arrangements to attend my defense.

Many professors and fellow graduate students at the University of Alberta have contributed to the value of this experience. Most notably, Xioabo Wang and Seung Sik Lim took time for many rich discussions regarding our families and research.

I would like to extend special thanks to my parents Stan and Darlene Stianson, sister Michelle Gregor, sister and brother-in-law Lorelei and Brent Johnston, parents in-law Ron and Linda Hallden, brother- and sister-in-law Craig and Marcy Hallden and all my extended family for their encouragement and prayers. I am especially grateful to my wife Kristina, daughter Liv and son Will for the sacrifices they have made so that we could take advantage of this opportunity. This journey holds considerably more meaning because I was able to share it with them (I love you with all my heart).

Finally, I would like to thank my Lord and Savior Jesus Christ. The completion of this degree is a testament to His love, grace, faithfulness and attention to prayer.

Table of Contents

1 Introduction **1**

1.1 Factor of Safety 2
1.2 Searching Techniques 6
1.3 Overview of Research Project 8
1.4 Organization of Dissertation 9
1.5 Bibliography 11

2 Dynamic Programming Slope Stability Analyses Based on Linear Elastic and Elasto-Plastic Stress Analyses **15**

2.1 Introduction 15
2.2 Background 17
2.2.1 Slope Stability Comparisons Involving Elasto-Plastic Stress Analysis 17
2.2.2 Slope Stability Method used to Perform a Comparison Between Slope Stability Results Based on Linear Elastic or Elasto-Plastic Stresses 21
2.2.2.1 Calculation of the Factor of Safety Based on Stresses from an Independent Stress-Deformation Analysis 23
2.2.2.2 Application of the Dynamic Programming Searching Technique 25
2.3 Comparing Slope Stability Analysis Based on Linear Elastic or Elasto-Plastic Stresses 29
2.3.1 Methodology and Scope 29
2.3.2 Presentation of Results 32
2.3.2.1 Homogeneous Dry Slope 32
2.3.2.2 Homogeneous Wet and Submerged Slope 41
2.3.2.3 Two Layer Slope 42
2.3.2.4 Three Layer Slope 43
2.4 The Effects of the Linear Elastic or Elasto-Plastic Constitutive Model on the Slope Stability Calculation 45
2.5 Conclusions 50
2.6 Bibliography 51

3 The Role of Admissibility Criteria in Stress-Based Slope Stability Methods **54**

3.1 Introduction 54
3.2 Background 55
3.3 Admissibility Criteria Developed to Govern the Shape of Potential Slip Surfaces 58
3.4 Influence of Poisson's Ratio on Normally Consolidated Slopes 60

3.4.1 Section No. 1: Influence of Poisson's Ratio when the Slip Surface is Assumed to be Circular 63
3.4.2 Section No. 2: Influence of Poisson's Ratio when Kinematic Admissibility Criteria are used to Control the Shape of the Critical Slip Surface. 64
3.5 The use of 'Admissibility Plots' to Illustrate the Interaction between the Internal Stress Distribution and the Application of Kinematic Admissibility Criteria 71
3.5.1 Interaction between Stress Rotation and Admissibility Criteria 76
3.5.2 Interaction between Kinematic Admissibility Criteria and the Internal Stress Distribution for 0verconsolidated Slopes 81
3.6 Discussion 84
3.6.1 Potential Violation of Kinematic Admissibility using Grid and Radius Searches 85
3.6.2 Strict Application of Kinematic Admissibility Criteria in Finite Element Slope Stability Methods 89
3.7 Conclusions 90
3.8 Bibliography 92

4 Three-Dimensional Slope Stability Based on Stresses from a Stress-Deformation Analysis 94
4.1 Introduction 94
4.2 Background 95
4.2.1 Developments Related to Two-Dimensional Stress-Based Methods of Slope Stability 96
4.2.2 Extension of Two-Dimensional Stress-Based Methods of Slope Stability to Three Dimensions 98
4.3 Three-Dimensional Limit Equilibrium Slope Stability Analysis Based on Finite Element Stresses 100
4.3.1 Linking the Stress-Deformation Analysis with the Slope Stability Calculations 100
4.3.2 Calculating the Factor of Safety for a Three-Dimensional Slip Surface 101
4.3.3 Restrictions Applied to the Shape of the Slip Surface 107
4.4 Verification Example Problems 108
4.4.1 Verification Example No. 1: Closed Form Solution 108
4.4.1.1 Finite Element Stress Analysis for Verification Example No. 1 109
4.4.1.2 Slope Stability Results for Verification Example No. 1 109
4.4.1.3 Influence of Poisson's Ratio on the Three-Dimensional Factor of Safety 113
4.4.2 Verification Example No. 2: Weak Layer 116

4.4.2.1 Finite Element Stress Analysis for Verification Example No. 2 117
4.4.2.2 Slope Stability Results for Verification Example No. 2 118
4.4.2.3 Influence of Poisson's Ratio on the Three-Dimensional Factor of Safety 121
4.4.3 Verification Example No. 3: Leshchinsky et al. (1985) 123
4.4.4 Verification Example No. 4: Dennhardt and Forster 1985 126
4.5 Discussion 131
4.6 Conclusion 132
4.7 Bibliography 133

5 Three-Dimensional Slope Stability Based on Dynamic Programming and Finite Element Stresses Analysis 136
5.1 Introduction 136
5.2 Background 138
5.3 Application of the Dynamic Programming Optimization Technique to Three-Dimensional Slope Stability 142
5.3.1 Development of a *Stage-State* System 143
5.3.2 Admissibility Criteria Governing the Shape of the Slip Surface Perpendicular to Movement 144
5.3.2.1 Concave Admissibility Criteria 148
5.3.2.2 Earth Pressure Admissibility Criteria 150
5.3.2.3 Grid Aspect Ratio Constraint 150
5.3.2.4 Application of Admissibility Criteria during *State Curve* Generation 152
5.3.3 Admissibility Criteria Governing the Shape of the Slip Surface in the Direction of Movement 155
5.3.4 Definition of the Factor of Safety 155
5.3.5 Dynamic Programming Optimization Procedure 158
5.4 Comparisons with Published Three-Dimensional Solutions 159
5.4.1 Loaded Homogeneous Slope 160
5.4.1.1 Application of the Dynamic Programming Searching Procedure in Combination with Admissibility Criteria 162
5.4.1.2 Slope Stability Results 164
5.4.1.3 Comparison with Critical Ellipsoidal Failure Surface 166
5.4.2 Loaded Homogeneous Slope with Modified Soil Properties 168
5.4.2.1 Slope Stability Results 169
5.4.3 Convex Slope Including Pore-Water Pressures and a Weak Layer 170
5.4.3.1 Slope Stability Results 172
5.5 Discussion 176
5.6 Conclusions 177

5.7 Bibliography 178

6 Summary and Conclusions **181**
6.1 Two-Dimensional Studies 182
6.2 Three-Dimensional Studies 184
6.3 Recommendations for Future Research 186
6.4 Bibliography 187

A Comparing Slope Stability Analysis Based on Linear Elastic or Elasto-Plastic Stresses Using Dynamic Programming Techniques **188**
A.1 Introduction 188
A.2 Background 189
A.3 Verification 190
A.3.1 Vertical Cut analysis 190
A.4 Comparison of Slope Stability Results Based on Linear Elastic or Elasto-Plastic Stress Analysis 191
A.4.1 Scope 191
A.4.1.1 Homogenous Slopes 192
A.4.1.2 Wet and Submerged Slopes 194
A.4.1.3 Slope Angle 194
A.4.1.4 Multi-Layered Slopes 194
A.5 Results 194
A.5.1 Vertical Cut 194
A.5.2 Homogeneous Slope 196
A.5.3 Wet and Submerged Slope 201
A.5.4 Slope Angle 202
A.5.5 Multi-Layer Slopes 203
A.5.5.1 Two Layer Slope 203
A.5.5.2 Three Layer Slope 204
A.6 Conclusions 205
A.7 Bibliography 206

B Methodology to Perform a Three-Dimensional Dynamic Programming Slope Stability Analysis **207**
B.1 Finite Element Analysis 207
B.2 Development of the *Stage-State* System 209
B.2.1 Three-Dimensional Dynamic Programming Search Grid 209
B.2.2 State Curve Generation 215
B.3 Dynamic Programming Search 219
B.3.1 Calculating the Factor of Safety 220
B.3.2 Optimization Procedure 223
B.4 Evaluating the Results 225

List of Tables

Table 1.1: A classification scheme used to compare two-dimensional limit equilibrium factor of safety equations. 3
Table 1.2: Summary of key milestones in the progression from restrictive searching techniques based on geometric admissibility criteria (GAC) to more flexible procedures based on kinematic admissibility criteria (KAC). 6
Table 2.1: A summary of a number of research studies that compare the results between slope stability analyses based on elasto-plastic stresses with other methods of analysis 18
Table 2.2: Factors of safety for families of curves from Toufigh (1997). 21
Table 2.3: Range of soil properties used in the parametric study involving the homogeneous slope 32
Table 3.1: Previous studies regarding the influence of Poisson's ratio on limit equilibrium slope stability calculations. 57
Table 4.1: A comparison between the factors of safety computed for verification example No. 1 113
Table 4.2: A comparison between the factors of safety computed for verification example No. 2 121
Table 5.1: Geometric admissibility criteria applied in two-dimensional slope stability formulations. 138
Table 5.2: Kinematic admissibility criteria applied in two-dimensional slope stability formulations. 140
Table 5.3: Results of a sensitivity study regarding the rigorous treatment of *state curve* generation. 153
Table 5.4: The parameters used to define the dynamic programming search and a summary of the solution details for the comparison involving the loaded homogeneous slope. 163
Table 5.5: Comparison between factors of safety computed by Yamagami and Jiang (1997) and the current slope stability method for Example No. 3 174
Table A.1: Homogeneous slope soil properties 193
Table B.1: Parameters input into the stress-deformation analysis. 208
Table B.2: Parameters required to build the dynamic programming Search Grid.... 212

List of Figures

Figure 2.1: The field of critical planes used to identify the most likely failure surface for a simple homogeneous slope (Huang and Yamasaki 1993). 20
Figure 2.2: Geologically controlled slip surface that illustrates the possibility of the slip surface being convex or concave. 23
Figure 2.3: Components of the dynamic programming method including an example search grid. 27
Figure 2.4: Methodology used to compare the effect of the linear elastic or elasto-plastic models on the slope stability calculation. 30
Figure 2.5: Comparison of the shape, location and average factor of safety for the slip surfaces determined using linear elastic stresses, elasto-plastic stresses and the Morgenstern and Price (1965) method for the 2:1 homogeneous slope at a factor of safety of approximately 1.3. 33
Figure 2.6: Local factor of safety distributions along the slip surfaces determined using linear elastic stresses or elasto-plastic stresses for the 2:1 homogeneous slope at a factor of safety of approximately 1.3..... 34
Figure 2.7: Comparison of the shape, location and average factor of safety for the slip surfaces determined using linear elastic stresses, elasto-plastic stresses and the Morgenstern and Price (1965) method for the 2:1 homogeneous slope at a factor of safety of approximately 1.0. 35
Figure 2.8: Local factor of safety distribution along the slip surface determined using linear elastic stresses or elasto-plastic stresses for the 2:1 homogeneous slope at a factor of safety of approximately 1.0..... 36
Figure 2.9: Comparison of the shape, location and average factor of safety for the slip surfaces determined using linear elastic stresses, elasto-plastic stresses and the Morgenstern and Price (1965) method for the 2:1 homogeneous slope at a factor of safety of less than 1.0..... 38
Figure 2.10: Comparison of the shape, location and average factor of safety for the slip surfaces determined using linear elastic stresses, elasto-plastic stresses and the Morgenstern and Price (1965) method based on the deformed geometry predicted using an elasto-plastic stress analysis..... 39
Figure 2.11: Comparison of the shape, location and average factor of safety for the slip surfaces determined using linear elastic stresses or elasto-plastic stresses for a homogeneous slope with slope angles of 3:1, 2:1 and 1:1..... 41
Figure 2.12: Comparison of the shape, location and average factor of safety for the slip surfaces determined using linear elastic stresses or elasto-plastic stresses for the 2:1 homogeneous slope with a piezometric line (i.e., wet slope) as well as conditions of partial submergence..... 42

Figure 2.13: Comparison of the shape, location and average factor of safety for the slip surfaces determined using linear elastic stresses or elasto-plastic stresses for the 2:1 slope with two soil layers. 43
Figure 2.14: Comparison of the shape, location and average factor of safety for the slip surfaces determined using linear elastic stresses or elasto-plastic stresses for the 2:1 slope with three soil layers including a weak layer. 44
Figure 2.15: Shear strength distributions along the slip surfaces determined using linear elastic stresses or elasto-plastic stresses for the 2:1 homogeneous slope and a factor of safety approximately equal to 1.0. 46
Figure 2.16: Comparing linear elastic versus elasto-perfectly plastic stress analysis. 47
Figure 2.17: Mobilized shear stress distributions along the slip surfaces determined using linear elastic stresses or elasto-plastic stresses for the 2:1 homogeneous slope and a factor of safety approximately equal to 1.0. 48
Figure 2.18: Shear strength for a strain softening material. 49
Figure 3.1: A schematic illustrating the application of kinematic admissibility criteria during the dynamic programming search (Pham and Fredlund 2003). 60
Figure 3.2: Sensitivity study designed to duplicate the controversy observed in previous studies. 62
Figure 3.3: Relationship between Poisson's ratio and the factor of safety assuming the shape of the slip surface is circular. 64
Figure 3.4. Relationship between Poisson's ratio and the factor of safety for the case where the shape of the slip surface is controlled using kinematic admissibility criteria. 65
Figure 3.5: Family of slip surfaces for the case where the stability number is equal to 1.71. 66
Figure 3.6: Family of slip surfaces for the case where the stability number is equal to 0.57. 67
Figure 3.7: Family of slip surfaces for the case where the stability number is equal to 0.14. 68
Figure 3.8: Family of slip surfaces for the case where the stability number is equal to zero. 69
Figure 3.9: Conceptual Mohr-Coulomb failure envelope for a cohesionless material. 70
Figure 3.10: Admissibility plot for the case where Poisson's ratio is equal to 0.48 and the stability number is equal to 1.71 (F_s = 1.24). 72
Figure 3.11: Admissibility plot for the case where Poisson's ratio is equal to 0.48 and the stability number is equal to 0 (F_s = 0.75). 73
Figure 3.12: Admissibility plot for the case where Poisson's ratio is equal to 0.1 and the stability number is equal to 1.71 (F_s = 1.22). 74
Figure 3.13: Admissibility plot for the case where Poisson's ratio is equal to 0.1 and the stability number is equal to 0 (F_s = 1.44). 75

Figure 3.14: Conceptual illustration of how stress rotations can influence the admissibility of line segments considered in the dynamic programming search..... 76
Figure 3.15: Family of slip surfaces computed based on elasto-plastic stresses for the stability number equal to zero case. 79
Figure 3.16: Admissibility plot for the case where Poisson's ratio is equal to 0.1 and the stability number is equal to 0 (F_s = 0.67). 80
Figure 3.17: Comparison of the angle to the direction of the minor principal stress computed using an elasto-plastic or linear elastic stress-deformation analysis. 81
Figure 3.18: Admissibility plot for the case where the internal stresses are computed using a linear elastic analysis for the stability number equal to 1.71 case (F_s = 1.69)..... 83
Figure 3.19: Admissibility plot for the case where the internal stresses are computed using an elasto-plastic analysis for the stability number equal to 1.71 case (F_s = 1.28)..... 84
Figure 3.20: Distribution of shear strength and shear mobilized along the critical slip surface for the stability number equal to zero case and Poisson's ratio is equal to 0.1 (F_s = 0.91). 86
Figure 3.21: Local factor of safety distribution along the circular slip surface computed based on stresses from an linear elastic excavated slope analysis in conditions where Ko is equal 3.0 (F_s = 1.93)..... 88
Figure 3.22: Local factor of safety distribution along the circular slip surface computed based on stresses from an elasto-plastic excavated slope analysis in conditions where Ko is equal 3.0 (F_s = 1.52)..... 89
Figure 4.1: A summary of the finite element procedures for computing the factor of safety in slope stability analysis (Fredlund et al. 1997). 96
Figure 4.2: Illustration of the three-dimensional grid linking the finite element stress analysis with the slope stability calculations. 101
Figure 4.3: A three-dimensional ellipsoidal slip surface approximated by a series of triangular planes. 103
Figure 4.4: Calculating the resisting force, R_{ijl}, and shear force, S_{ijl}, based on the normal stress, $\sigma_{n_{ijl}}$, and mobilized shear stress, τ_{ijl}, acting at the centroid of incremental area A_{ijl}. 105
Figure 4.5: Finite element mesh used to calculate the internal stress state for verification example No. 1..... 109
Figure 4.6: Verification example No. 1: a specified spherical slip surface in a homogeneous purely cohesive slope (Hungr et al. 1989) with c', cohesion; ϕ', friction angle; R, moment arm of the resisting force; γ, unit weight of soil. 110
Figure 4.7: Influence of the finite element mesh, the intermediate grid, and the slip surface discretization on the three-dimensional factor of safety..... 112
Figure 4.8: Influence of Poisson's ratio on the three-dimensional factor of safety for verification example #1..... 115

Figure 4.9: A two-dimensional cross-section illustrating the geometry and soil properties for verification example No. 2. H is the height of the slope and *R* is the radius of the ellipsoid. 116
Figure 4.10: Finite element mesh used to calculate the internal stress state for verification example No. 2 118
Figure 4.11: Slip surface generated for Case 1 considering a slide volume of 13,000m^3. 119
Figure 4.12: Results of a sensitivity study used to determine the appropriate density for the finite element mesh for Case 1. 120
Figure 4.13: Influence of Poisson's ratio on the three-dimensional factor of safety for Case 1 122
Figure 4.14: Comparison of the factor of safety for the three-dimensional slip surfaces found using the variational approach developed by Leshchinsky et al. (1985), the method of columns approach developed by Hungr et al. (1989), and the procedure developed for the current study 124
Figure 4.15: Three-dimensional slip surface found using the procedure developed for the current study 125
Figure 4.16: Slope stability results for a three-dimensional slope with a surcharge load of 55 kPa. Numbers without parentheses are from Hungr et al. (1989). Numbers with parentheses are from Dennhardt and Forster (1985). 127
Figure 4.17: Relationship between the exit distance of the three-dimensional failure surface and the three-dimensional factor of safety. 130
Figure 5.1: Stage-state system proposed by Yamagami and Jiang (1997). 143
Figure 5.2: A series of regular two-dimensional *cross-section grids* generated for a number of *stage cross-sections* for a three-dimensional slope. 145
Figure 5.3: Illustration to describe the generation of state curves. 146
Figure 5.4: Relationship between computing time and the number of *state curve* connections. 147
Figure 5.5: An illustration of the differences between state curves allowed by the three proposed variations of the concave constraint. 149
Figure 5.6: Illustration showing how the number of *state curve* combinations can be increased or decreased depending on the aspect ratio selected for the cross-section grid. 151
Figure 5.7: Illustration showing how information from field investigations can be used to reduce the total number of admissible *state curves* and reduce the solution time. 154
Figure 5.8: A three-dimensional slip surface discretized into a series of triangular planes. 157
Figure 5.9: Plan view and cross-section view of the simple homogeneous slope considered in Example No. 1. 161
Figure 5.10: Critical slip surface found using the proposed slope stability method 164

Figure 5.11: Critical slip surface for the case where the load applied on the crest of the slope is equal to 30 kPa (F_s = 1.30). 166
Figure 5.12: Comparison between the critical slip surface found using the dynamic programming search technique with the critical ellipsoidal slip surface found using a simple grid and radius search technique. 167
Figure 5.13: Cross-section view of the modified slope conditions considered in Example No. 2. 169
Figure 5.14: Slope stability results for the second example where an irregular weak layer is included in the slope. 170
Figure 5.15: Slope geometry and soil conditions considered in the multi-layer conical heap example problem. 171
Figure 5.16: Slope stability results for Example No. 3. 174
Figure A.1: Vertical cut comparison 196
Figure A.2: Dry Homogeneous Slope, F_s~1.3. 198
Figure A.3: Dry Homogeneous Slope, F_s~1.0 198
Figure A.4: Dry Homogeneous Slope, F_s<1.0 199
Figure A.5: Effect of initial stress state on the factor of safety. 201
Figure A.6: Wet and Submerged Slope 202
Figure A.7: Slope Angle. 203
Figure A.8: Two Layer Slope 204
Figure A.9: Three layer slope. 205
Figure B.1: Illustration of the three-dimensional grid linking the stress-deformation analysis with the slope stability calculations. 209
Figure B.2: Profile view (a) and front view (b) illustrating the separation between the intermediate grid and the search grid. 211
Figure B.3: Illustration describing the design of the dynamic programming search grid. 214
Figure B.4: Search grid configurations to facilitate different searching strategies. 215
Figure B.5: Profile view of one stage from Figure B.3 a) illustrating the numbering scheme used in the numerical procedure to generate *state curves*. 216
Figure B.6: Schematic illustrating the application of the earth pressure admissibility criteria. 217
Figure B.7: Schematic illustrating the application of the concave admissibility criteria. 218
Figure B.8: Illustration of a completed sample of *state curves*. 219
Figure B.9: Illustration of a completed *stage-state* system. 219
Figure B.10: Illustration of one triangular plane intersecting an element from the intermediate grid. 220
Figure B.11: Calculating the resisting force, R, and shear force, S, based on the normal stress, σ_n, and mobilized shear stress, τ, acting at the centroid of a triangular plane. 222
Figure B.12: One state curve connection between stage $[i]$ and $[i-1]$. 224

List of Symbols

A – Area

c' – Effective cohesion of soil

δ – Dynamic programming convergence criteria

E – Young's modulus

ϕ^b – Angle of friction with respect to changes in matric suction

ϕ' – Effective angle of internal friction

F_s – Factor of safety

G – Return function

GAC – Geometric admissibility criteria

γ – Unit weight of soil

H – Optimal function

KAC – Kinematic admissibility criteria

ν – Poisson's ratio

R – Resisting force

S – Actuating force

σ_n – Normal stress

σ_x – Horizontal stress

σ_y – Vertical stress

θ – Angle of inclination

τ_{xy} – Shear stress

τ – Mobilized shear stress along a potential slip surface

τ_f – Average shear strength of soil

u_a – Pore air pressure

$(u_a - u_w)$ – Matric suction

Chapter 1

Introduction

The development of limit equilibrium slope stability methods based on stresses from a finite element analysis seems to correspond in maturity with method of slices techniques. The gradual improvement with time of the method of slices technique is marked by the development of methods that satisfy all conditions of equilibrium. Methods satisfying all conditions of equilibrium are required to provide a reliable factor of safety calculation for slip surfaces that might deviate from circular or planar shapes. However, the development of advanced searching procedures is discouraged since the methods do not invoke kinematical considerations regarding soil behavior and require that the shape of the slip surface be assumed (Morgenstern and Price 1965). Deriving the factor of safety equation based on the results from a stress - deformation analysis makes it possible to invoke kinematic admissibility criteria and develop searching procedures that include the shape of the slip surface in the overall slope stability evaluation.

The primary objective of this dissertation is to provide a new finite element slope stability method that can be used to overcome limitations inherited by three-dimensional method of columns. The dissertation describes the details regarding the development of a three-dimensional slope stability method where the factor of safety is computed based on the results of a stress - deformation analysis and the search for the critical slip surface is completed using the dynamic programming method. The following sections present a classification scheme that is used to describe the characteristics of the finite element factor of safety, a review of key milestones regarding the development of two- and three-dimensional searching procedures, followed by an overview of the dissertation

1.1 Factor of Safety

The method of slices represents one of the most widely used numerical techniques to compute the factor of safety. Developmental research related to the method of slices extends over four decades and documents the progression from methods that satisfy force or moment equilibrium to the most advanced methods satisfying all conditions of equilibrium (Fellenius 1936; Bishop 1955; Janbu et al. 1956; Morgenstern and Price 1965; Spencer 1967; Fredlund and Krahn 1977). Classification schemes have been developed to compare the characteristics of each method. Existing classification schemes are used to distinguish between different methods depending on which conditions of equilibrium are met according to the *existing classification scheme* shown in Table 1.1. It is well known that the reliability of the factor of safety (F_s) calculation for slip surfaces of a particular shape is related to the equilibrium conditions that are satisfied. Methods satisfying moment equilibrium are considered to be reliable when the majority of the slip surface is circular and methods satisfying force equilibrium are considered to be reliable when the majority of the slip surface is planar. The need for methods satisfying all conditions of equilibrium is considered necessary given that the critical slip surface may deviate significantly from a circle or a plane.

Table 1.1: A classification scheme used to compare two-dimensional limit equilibrium factor of safety equations.

	Existing classification scheme			Expanded classification scheme		
Method	Moment equilibrium	Vertical force equilibrium	Horizontal force equilibrium	Calculation procedure	Local F_s	Governing admissibility criteria
Method of Slices						
Ordinary or Fellenius (1936)	x			linear	Constant	GAC
Janbu's Simplified (1956)			x	non-linear	Constant	GAC
Simplified Bishop (1955)	x		x	non-linear	Constant	GAC
Spencer (1967)	x	x	x[a]	non-linear	Constant	GAC
Morgenstern-Price (1965)	x	x	x[b]	non-linear	Constant	GAC
GLE (1977)	x	x	x[c]	non-linear	Constant	GAC
Enhanced						
Linear Elastic	x	x	x[d]	linear	Variable	KAC

X represents the inter-slice normal force ; E represents the inter-slice shear force
a X/E is constant
b X/E is variable
c X/E is variable and the factor of safety from moment equilibrium and force equlibrium are solved separately.
d Slices do not exist therefore no assumptions are required regarding the relationship between X and E.
GAC: Geoemetric Admissibility Criteria
KAC: Kinematic Admissibility Criteria
GLE: General Limit Equilibrium Method (Fredlund 1977)

"Enhanced limit strength methods" refers to a procedure where the results from an independent stress-deformation analysis are combined with a limit equilibrium framework to compute the factor of safety (Kulhawy 1969). "Enhanced limit strength methods" require only one finite element analysis to compute the factor of safety for any number of c' and $tan\phi'$ combinations and should not be confused with the finite element slope stability procedure commonly referred to as the "Strength Reduction Technique" (Zienkiewicz et al. 1975; Matsui and San 1992). The "enhanced limit strength method" has been referred to as the "enhanced limit method", "enhanced method" or "finite element slope stability method" following the classification scheme presented by Fredlund and Scoular (1999). The term "stress-based" method is considered to provide a more accurate description of the procedure and is used in this dissertation.

The *existing classification scheme* is expanded to demonstrate the advantages associated with adopting stress-based methods. The *expanded classification scheme* includes three new categories on *calculation procedure, local factor of safety (F_S),*

and *governing admissibility criteria.* The *calculation procedure* refers to the character of the mathematical method that must be used to compute the factor of safety. A linear method indicates a situation where the factor of safety equation is statically determinate and can be solved directly. A non-linear method indicates a situation where the factor of safety equation is statically indeterminate. An estimated factor of safety is used to compute the normal force along the slip surface and the final factor of safety is found through an iterative procedure. The *local factor of safety* distribution is classified as either constant or variable. A variable distribution indicates a situation where the factor of safety for discrete portions of the slip surface can be computed independent of the global factor of safety for the overall slip surface. A constant distribution indicates that the calculation of the local factor of safety and the global factor of safety cannot be separated (i.e., the local factor of safety is equal to the global factor of safety along the entire slip surface.).

Admissibility criteria are used to control the geometry of slip surfaces considered in a slope stability analysis. The *governing admissibility criteria* classification is included to demonstrate that the ability to invoke certain admissibility criteria is related to the method used to compute the factor of safety. It is possible to distinguish between two classes of admissibility criteria; namely, geometric and kinematic admissibility criteria. Geometric admissibility criteria (GAC) are based strictly on the geometric properties of the slip surface. Kinematic admissibility criteria (KAC) can be formulated based on principles of soil behavior and the kinematics required to ensure physically realistic slip surfaces. Kinematic admissibility criteria are generally more flexible than geometric admissibility criteria.

The stress-based method has several advantages when compared to traditional limit equilibrium method of slices techniques.

- The internal stress distribution resulting from a finite element analysis is computed satisfying all the conditions of equilibrium.
- The stress-based slope stability formulation is determinate and does not require assumptions regarding the internal stress conditions. The resulting

factor of safety equation is linear and can be solved without the use of iterative procedures.

- The local factor of safety distribution is variable providing valuable information regarding possible development of failure.
- Kinematic considerations regarding soil behavior can be invoked removing the requirement that the shape of the slip surface be assumed.

The characteristics of the stress-based method have resulted in the development of more advanced searching procedures where kinematic admissibility criteria can be used to control the shape of the slip surface (Pham 2002; Pham and Fredlund 2003). The use of kinematic admissibility criteria makes it possible to determine the shape of the critical slip surface as part of the overall slope stability evaluation.

The development of the method of columns has matured to a similar level as the method slices. The methods of slices listed in Table 1.1 have been extended to equivalent methods of columns techniques and are available in commercial software (Hovland 1977; Chen and Chameau 1982; Hungr 1987; Ugai 1988; Lam and Fredlund 1993; Hungr 2001). Methods of columns techniques resulting from the extension of two-dimensional methods satisfying all conditions of equilibrium provide the ability to compute the factor of safety for three-dimensional slip surfaces of any shape. The method of columns inherits other characteristics from the method of slices resulting in a classification system similar to the *extended classification scheme* in Table 1.1. The method of columns procedures are non-linear. The three-dimensional local factor of safety distribution is constant and no kinematic considerations regarding soil behavior are invoked confirming that the shape of the three-dimensional slip surface must be assumed (i.e., geometric admissibility governs.).

The "hybrid" approach proposed by Loehr (1998) can be considered an extension of the two-dimensional stress-based method to three dimensions and was developed to overcome the limitations associated with the method of columns techniques. Loehr reported difficulties associated with the level of mesh refinement required to provide

an accurate factor of safety calculation. The advantages associated with the stress-based method of slope stability have not been fully realized in three-dimensional analyses.

1.2 Searching Techniques

A factor of safety equation must be combined with a searching procedure to predict the stability of slopes in cases where the location of the slip surface is unknown. The selection of a searching procedure depends largely on the type of admissibility criteria supported by the factor of safety equation. Table 1.2 provides a summary of key milestones in the progression from the use of restrictive searches based on geometric admissibility criteria to more flexible procedures based on kinematic admissibility criteria.

Table 1.2: Summary of key milestones in the progression from restrictive searching techniques based on geometric admissibility criteria (GAC) to more flexible procedures based on kinematic admissibility criteria (KAC).

2D/3D	Factor of Safety	Admissibility	Author
2D	Method of slices	GAC	Bishop (1955); Janbu et. al (1956) Morgenstern and Price (1965) Spencer (1967)
	Method of slices	GAC	Baker (1980)
	Enhanced	GAC	Scoular (1997)
	Enhanced	KAC	Pham (2002)
3D	Method of Columns	GAC	Hungr (2001)
	Method of Columns	GAC	Jiang & Yamagami (2004) Yamagami & Jiang (1997)
	Enhanced	GAC	Loehr (1998), Current research
	Enhanced	KAC	Current research

The first method of slices formulations assumed the shape of the critical slip surface to be circular which led to the use of a trial and error searching procedure

commonly referred to as the "grid and radius" method. The "grid and radius" searching procedure has been modified to include circular slip surfaces intersected by planes or impenetrable soil layers providing the ability to consider composite slip surfaces. Steps have also been taken to automate the trial and error procedure to reduce the effort required to locate the critical slip circle.

The next stage involved the development of a number of searching procedures to remove restrictions placed on the shape of the slip surface such as dynamic programming (Baker 1980), Simplex method (Nguyen 1985), Conjugate Gradient (Greco 1988), Monte Carlo (Greco 1996), Alternating Variable (Celestino and Duncan 1981), Univariate (Greco 1988), Variation Calculus (Baker and Garber 1977) and Steepest Descent (Chen and Shao 1988). The searching procedures were combined with various methods of slices techniques and were limited to the use of geometric admissibility criteria. Baker (1980) demonstrated that the dynamic programming method can be designed to consider admissibility criteria while the search for the critical slip surface is in progress. A new geometric admissibility criterion was proposed that considers slip surfaces to be admissible if the first derivative calculated from the crest to the toe of the slope was greater than or equal to zero (i.e., the slip surface must be concave.). The ability to include concave slip surfaces represents a significant improvement considering that slip surfaces with circular and composite characteristics can be evaluated in a single search.

Scoular (1997) combined the stress-based method with the grid and radius searching procedure assuming that the critical slip surface was circular. Other procedures have been developed based on geometric admissibility criteria providing the ability to search for slip surfaces that might deviate from a circular shape (Yamagami and Ueta 1988b; Kim and Lee 1997). Pham (2002) utilized the full potential of the stress-based method by adopting a kinematic admissibility criterion to govern the search for the critical slip surface. The criterion makes it possible to search for irregular slip surfaces that might follow along unique geological or man made features.

The development of three-dimensional searching procedures has not matured to the same level as two-dimensional methods. A three-dimensional version of the "grid and radius" searching procedure has been developed to search for spherical or ellipsoidal slip surfaces following a similar trial and error procedure (Hungr 2001). Dynamic programming has also been used to search for three-dimensional slip surfaces following the geometric admissibility criteria proposed by Baker (1980) (Yamagami and Jiang 1997; Jiang and Yamagami 2004). Loehr (1998) extended the two-dimensional stress-based method to three dimensions but no formal searching procedure was developed. The author is not aware of any three-dimensional searching algorithms where kinematic admissibility criteria are used to control the shape of the slip surface.

1.3 Overview of Research Project

The development of the stress-based method provides the ability to apply kinematic admissibility criteria and ultimately make the shape of the slip surface part of the slope stability evaluation. The advantages associated with stress-based methods have been realized within the context of two-dimensional slope stability but have not been extended to three-dimensional analyses. There is also a need for more research regarding the interaction between the stress - deformation analysis and the slope stability calculations. The application of the stress-based method introduces new soil parameters that are not typically associated with slope stability calculations. In many cases, the influence of the stress - strain characteristics of the soil, Poisson's ratio and the application of admissibility criteria are not well understood.

This dissertation presents the progression of research that was completed to develop a three-dimensional stress-based slope stability method where the search for the critical slip surface is based on kinematic admissibility criteria. Two-dimensional studies are presented to clarify the interaction between the stress - deformation analysis, the factor of safety calculation and the characteristics of the dynamic programming searching procedure. The second half of the dissertation presents the

development of the three-dimensional slope stability method. The first stage focuses on developing a procedure to compute the three-dimensional factor of safety based on the results of stress - deformation analysis. The second stage involves the integration of the dynamic programming searching procedure including a number of admissibility criteria.

The research required the development of software capable of two- and three-dimensional slope stability calculations. Both the two- and three-dimensional software are designed to search for the critical slip surface or perform back analysis by computing the factor of safety for a known slip surface. The search for the critical two-dimensional slip surface is completed based on the dynamic programming algorithm and the application of kinematic admissibility criteria. The search for the critical three-dimensional slip surface can be completed based on an extension of the dynamic programming algorithm to three-dimensions. A trial and error procedure based on the assumption that the critical slip surface is ellipsoidal (i.e., similar to the 'grid and radius' method in two-dimensions) can also be used. The slope stability software is designed to interface with commercially available stress - deformation software products. Two products were used during the course of this research including SVSolid™ and FLAC™. SVSolid™ is a finite element based software product developed by SoilVision Systems Ltd. (SoilVision Systems Ltd. 2006a). FLAC™ is a finite difference based software product developed by the Itasca Consulting Group Inc. (Itasca Consulting Group Inc. 2000). Other commercial software products used during the course of this research include GeoStudio™ (GEO-SLOPE International Ltd. 2004), SVFlux™ and Tecplot™ (Tecplot Inc. 2003).

1.4 Organization of Dissertation

The dissertation is presented in paper-based format and consists of four main chapters, supplemented by two appendices. Each chapter is an article that has been prepared for submission to a peer reviewed journal and includes an independent literature review and citations. The literature review consists of published work

related to two- and three-dimensional slope stability including numerical procedures to compute the factor of safety, searching procedures, case histories and laboratory studies. The dissertation itself is occasionally referenced due to the nature of the paper based thesis format.

Chapter 2 presents a comparison of two-dimensional slope stability analyses based on isotropic linear elastic or elasto-plastic stresses. The study examines the accuracy of the factor of safety calculation based on a linear elastic stress analysis in slope conditions where there is the potential for extensive yielding. The internal stresses are generated by the 'switch on' gravity method because the study is directed towards normally consolidated slope conditions. Chapter 3 is an extension of the two-dimensional analyses completed in Chapter 2. A sensitivity analysis is designed to examine the potential influence that Poisson's ratio and Young's modulus might have on the calculation of the factor of safety. This part of the study is limited to normally consolidated slopes (i.e., stress conditions generated by the 'switch on' gravity method.) to remain consistent with the types of analyses considered in previous research. The study goes on to examine whether an isotropic linear elastic stress analysis can provide a reasonable representation of the stresses in over-consolidated soil conditions. Discussion is also provided regarding the merits related to the strict application of kinematic admissibility criteria in the dynamic programming searching procedure and the potential to violate kinematic admissibility in searching procedures based exclusively on geometric admissibility criteria.

Chapter 4 is focused on the development of a procedure where stresses from a finite element analysis are incorporated into a limit equilibrium framework to compute the factor of safety for three-dimensional slip surfaces. A series of verification examples and sensitivity studies are presented to determine if the proposed method provides the required accuracy and flexibility to assess the stability of slopes typically encountered in practice. Chapter 5 presents the details surrounding the integration of the three-dimensional dynamic programming searching procedure. Geometric and kinematic admissibility criteria are developed to train the searching procedure to distinguish between reasonable and unreasonable slip

surfaces. A series of stability evaluations are presented to discover if the admissibility criteria can be used to provide a balance between the number of slip surfaces considered in the analysis and the solution time.

Appendix A consists of a conference paper presented at the Canadian Geotechnical Conference in 2004 (Stianson et al. 2004). The paper presents the results from a preliminary two-dimensional study that was completed to verify the operability of the two-dimensional slope stability software and begin to study the differences between slope stability calculations based on linear elastic or elasto-plastic stresses. Appendix B provides detailed information regarding the procedure that was designed to complete a three-dimensional dynamic programming slope stability analysis.

1.5 Bibliography

Baker, R. 1980. Determination of the critical slip surface in slope stability computations. International Journal For Numerical and Analytical Methods in Geomechanics, 4(4): 333-359.

Baker, R., and Garber, M. 1977. Variational approach to slope stability. *In* Proceedings of the 9th International Conference on Soil Mechanics and Foundation Engineering. Tokyo, Vol.2, pp. 9-12.

Bishop, A.W. 1955. The use of the slip circle in the stability analysis of slopes. Geotechnique, 5(1): 7-17.

Celestino, T.B., and Duncan, J.M. 1981. Simplified search for noncircular slip surfaces. *In* Proceedings of the 10th International Conference on Soil Mechanics and Foundation Engineering. Stockholm, Sweden, Vol.3, pp. 391-394.

Chen, R.H., and Chameau, J.L. 1982. Three-dimensional limit equilibrium analysis of slopes. Geotechnique, 33(1): 31-40.

Chen, Z.-Y., and Shao, C.-M. 1988. Evaluation of minimum factor of safety in slope stability analysis. Canadian Geotechnical Journal, 25(4): 735-748.

Fellenius, W. 1936. Calculations of the stability of earth dams. *In* Transaction of the 2nd Congress on Large Dams. Washington DC, Vol.4, p. 445

Fredlund, D.G., and Krahn, J. 1977. Comparison of slope stability methods of analysis. Canadian Geotechnical Journal, 14(3): 429-439.

Fredlund, D.G., and Scoular, R.E.G. 1999. Using limit equilibrium concepts in finite element slope stability analysis. *In* Proceedings of the International Symposium on Slope Stability Engineering-IS-Shikoku'99. Japan. November 8-11, pp.31-47.

GEO-SLOPE International Ltd. 2004. GeoStudio. Version 6.22, Calgary, Alberta.

Greco, V.R. 1988. Numerical methods for locating the critical slip surface in slope stability analysis. *In* Proceedings of the 6th International Conference on Numerical Methods in Geotechnical Engineering. Innsbruck, pp. 1219-1223.

Greco, V.R. 1996. Efficient Monte-Carlo technique for locating critical slip surface. Journal of Geotechnical Engineering, ASCE, 122(7): 517-525.

Hovland, H.J. 1977. Three-dimensional slope stability analysis method. Journal of Soil Mechanics and Foundations Division, ASCE, 103(GT9): 971-986.

Hungr, O. 1987. An extension of Bishop's simplified method of slope stability analysis to three dimensions. Geotechnique, 37(1): 113-117.

Hungr, O. 2001. CLARA-W: Slope Stability Analysis in two or three Dimensions for microcomputers. O. Hungr Geotechnical Research, Vancouver, B.C., p. 76.

Itasca Consulting Group Inc. 2000. FLAC - Fast Lagrangian Analysis of Continua. Version 4.0, Minneapolis, MN.

Janbu, N., Bjerrum, L., and Kjaernsli, B. 1956. Soil mechanics applied to some engineering problems. Norwegian Geotechnical Institute, Publication No. 16 (in Norwegian).

Jiang, J.-C., and Yamagami, T. 2004. Three-dimensional slope stability analysis using an extended spencer method. Soils and Foundations, 44(4): 127-135.

Kim, J.Y., and Lee, S.R. 1997. Improved search strategy for the critical slip surface using finite element stress fields. Computers and Geotechnics, 21(4): 295-313.

Kulhawy, F.H. 1969. Finite element analysis of the behavior of embankments. Dissertation, University of California, California, USA.

Lam, L., and Fredlund, D.G. 1993. General Limit Equilibrium Model for Three-Dimensional Slope Stability Analysis. Canadian Geotechnical Journal, 30(6): 905-919.

Loehr, J.E. 1998. Development of a hybrid limit equilibrium-finite element procedure for three-dimensional slope stability analysis. Dissertation, The University of Texas at Austin, Texas, USA.

Matsui, T., and San, K.-C. 1992. Finite element slope stability analysis by shear strength reduction technique. Soils and Foundations, 32(1): 59-70.

Morgenstern, N.R., and Price, V.E. 1965. The analysis of slope stability of general slip surfaces. Geotechnique, 15(1): 79-63.

Naylor, D.J. 1982. Finite Elements and Slope Stability. *In* Numerical Methods in Geomechanics, Proceedings of the NATO Advanced Study Institute. Vimeiro, Port. D. Reidel Public Co, Dordrecht, Netherlands, Vol.92, pp. 229-244.

Nguyen, V.U. 1985. Determination of critical slope failure surfaces. Journal of Geotechnical Engineering, ASCE, 111(2): 238-250.

Pham, H.T.V. 2002. Slope Stability Analysis Using Dynamic Programming Method Combined With a Finite Element Stress Analysis. Thesis, University of Saskatchewan, Saskatoon, Canada.

Pham, H.T.V., and Fredlund, D.G. 2003. The application of dynamic programming to slope stability analysis. Canadian Geotechnical Journal, 40(4): 830-847.

Scoular, R.E.G. 1997. Limit equilibrium slope stability analysis using a stress analysis. Thesis, University of Saskatchewan, Saskatoon, Canada.

SoilVision Systems Ltd. 2006. User's Manual, SVSolid Version 4.0, Saskatoon, SK.

Spencer, E. 1967. A method for analysis of the stability of embankments assuming parallel interslice forces. Geotechnique, 17(1): 11-26.

Stianson, J., Chan, D., and Fredlund, D.G. 2004. Comparing slope stability analysis based on linear elastic or elasto-plastic stresses using dynamic programming

techniques. *In* 57th Canadian Geotechnical Conference. Quebec City, Quebec, Canada, Session 7c, pp. 23-30.

Tecplot Inc. 2003. Tecplot. Version 10.0, Bellevue, WA.

Ugai, K. 1988. Three-dimensional slope stability analysis by slice method. *In* Proceedings of the 6th International Conference on Numerical Methods in Geomechanics. Innsbruck, Swoboda, Vol.2, pp. 1369-1374.

Yamagami, T., and Ueta, Y. 1988b. Search for critical slip lines in finite element stress field by dynamic programming. *In* Proceedings of the 6th International Conference on Numerical Methods in Geomechanics. Innsbruck, pp. 1347-1352.

Yamagami, T., and Jiang, J.C. 1997. A search for the critical slip surface in three dimensional slope stability analysis. Soils and Foundations, 37(3): 1-16.

Zienkiewicz, O.C., Humpheson, C., and Lewis, R.W. 1975. Associated and non associated visco-plasticity and plasticity in Soil Mechanics. Geotechnique, 25(4): 671-689.

Chapter 2

Dynamic Programming Slope Stability Analyses Based on Linear Elastic and Elasto-Plastic Stress Analyses

2.1 Introduction

A number of limit equilibrium slope stability methods have been developed where the overall factor of safety is calculated based on stresses from a separate finite element analysis (Yamagami and Ueta 1988b; Zou et al. 1995; Fredlund et al. 1997; Pham 2002). The proposed finite element methods are reported to have several advantages when compared to traditional limit equilibrium method of slices techniques (Fredlund et al. 1997).

- The slope stability formulations based on finite element stresses are determinate and do not require assumptions regarding internal stress conditions that are typically required for conventional method of slices techniques.
- The factor of safety equation based on finite element stresses can be solved without the use of iterative procedures. The factor of safety equation is linear because the normal stresses acting at specific locations along potential slip surfaces are known.
- The distribution in the local factor of safety can be computed and used to provide further information regarding the character of the instability.

One of the main motivations behind the development of slope stability methods based on finite element stresses is the ability to include the stress-strain characteristics of the soil in the stability calculations. Scoular (1997) performed extensive comparisons between slope stability results from a finite element slope stability method with results from the traditional methods of slices. The intent was to investigate differences that might occur between factor of safety calculations where the stress-strain characteristics of the soil are included and cases which use force equilibrium on a simple slice. The comparisons were carried out for a range of soil conditions where slopes were stable and slopes were failing. In all cases, the finite element factors of safety were computed based on stresses generated from an isotropic linear elastic "switch-on" gravity analysis. The results demonstrated that factors of safety computed using the method of slices and the finite element method were similar, even for unstable slopes where the factor of safety was less than 1.0. The results also showed that the location of the critical slip surface might be different in some cases.

The agreement in the factors of safety near failure might come as a surprise considering that the finite element slope stability calculations were based on linear elastic stresses. It appeared possible that a slope stability analysis based on elasto-plastic stresses would provide a more reasonable calculation of the factor of safety and the location of the critical slip surface for slopes that are near failure. On the other hand, it also appeared possible that a slope stability analysis based on a linear elastic analysis might be adequate when the slope is not near failure (Naylor 1982). In either case, the sensitivity of the slope stability calculations to the selected constitutive model was not well defined.

The purpose of this study is to investigate differences that might occur in slope stability calculations as a result of using differing soil behavior models. A series of example problems are presented that compare slope stability results based on stresses generated from either an isotropic linear elastic or elasto-plastic stress analysis. The results are compared by evaluating the differences in the shape, location, and factor of safety of the critical slip surface determined using either constitutive model. The

same searching procedure was used to determine the critical slip surface when using linear elastic or elasto-plastic stresses. The examples are selected to ensure that the comparison includes both stable and failing slopes.

2.2 Background

A review of previous research involving comparisons between slope stability analyses based on elasto-plastic stresses is presented. The majority of the previous studies involved the comparison of slope stability calculations based on elasto-plastic stresses with one or more of the method of slices techniques. One study (Zienkiewicz et al. 1975), reported difficulties associated with restrictions typically placed on the shape of the slip surface in conventional method of slices techniques. Additional research is presented to discuss the rationale that was used to select an appropriate searching procedure to overcome the difficulties reported in previous studies. The slope stability method selected to perform the proposed comparison is presented including the procedure used to search for the critical slip surface and the definition of the factor of safety.

2.2.1 Slope Stability Comparisons Involving Elasto-Plastic Stress Analysis

Table 2.1 provides a summary of a number of research studies that include comparisons between the results of slope stability analyses based on elasto-plastic stresses with results from other methods.

Table 2.1: A summary of a number of research studies that compare the results between slope stability analyses based on elasto-plastic stresses with other methods of analysis.

Author	Elasto-plastic slope stability method	Slope stability method used in the comparison	Comparison Results
Zienkiewicz et al. (1975)	Strength reduction technique	Bishop (1955), (Morgenstern and Price 1965)	Agreement for simple homogeneous slopes; diverged for more complex slopes
Snitbhan and Chen (1978)	Strength reduction technique	Limit analysis	Agreement for simple homogeneous slopes
Kohgo and Yamashita (1988)	Strength reduction technique	(Fellenius 1936), Bishop (1955), (Morgenstern and Price 1965)	Agreement for simple homogeneous slopes
Huang and Yamasaki (1993a)	Local factor of safety technique	Bishop (1955), (Sarma 1973)	Agreement in factor of safety; Slip surface did not agree in some cases
Toufigh (1997)	Local displacement	Linear elastic versus elasto-plastic stresses	Significant variation attributed to the soil behavior models

Several comparisons were completed using elasto-plastic stresses in combination with the strength reduction technique (Zienkiewicz et al. 1975; Snitbhan and Chen 1978; Kohgo and Yamashita 1988). The soil properties corresponding to the collapse of a slope were determined by monitoring the displacement at an appropriate location within the slope (usually a point near the toe). Failure (F_s = 1.0) was assumed to occur when the displacement at the monitored point increased excessively due to an incremental decrease in strength or an incremental increase in the unit weight of the soil. The failure surface was approximated by observing patterns in the velocity vectors and contours of shear strain. The critical slip surface was considered to coincide with a path following along locations in the slope displaying the largest velocity vectors and values of shear strain. Subsequent slope stability analyses were carried out using the methods listed in Table 2.1. The results of the slope stability calculations compared the shape, location, and factor of safety of the critical slip surface. The factor of safety and critical slip surfaces were reported to be in good agreement for cases where simple homogeneous slopes were considered.

Zienkiewicz et al. (1975) went on to show that the same agreement might not be expected for composite embankments with irregular soil layers. One embankment consisting of manmade material in combination with existing geological features was analyzed. The factors of safety computed using the Bishop (1955) or Morgenstern and Price (1965) methods of analysis were found to be 12% and 24% higher than the factor of safety computed using the strength reduction technique, respectively. The mode of failure observed from the strength reduction analysis was clearly non-circular. The differences reported in the Bishop and Morgenstern and Price factors of safety were attributed to the manner in which the equilibrium of each slice was satisfied and the restriction that only circular slip surfaces could be considered in the search for the critical slip surface.

Huang and Yamasaki (1993) presented a comparison between a new local factor of safety technique with Bishop's (1955) and Sarma's (1973) methods of slices. The proposed local factor of safety technique was based on stresses generated from a separate finite element analysis. The procedure involved the calculation of a local factor of safety for every node on the finite element mesh. A procedure using Mohr circles in combination with a Mohr-Coulomb failure envelope was developed to determine the orientation of the plane with the lowest local factor of safety at each node. The local factor of safety was defined as the available shear strength divided by the shear stress acting on the critical plane. Individual line segments were drawn with orientations corresponding to the critical planes at nodes where the local factor of safety was less than or equal to some pre-determined threshold value. The line segments were used as a guide to trace a continuous slip surface extending from the crest to the toe of the slope. The critical slip surface was identified through visual inspection and was defined as the deepest continuous slip surface that could be traced by connecting a series of line segments.

Figure 2.1 illustrates the field of critical planes used to identify the most likely failure surface for a simple homogeneous slope. The planes were drawn at nodes in the finite element mesh where the local factor of safety was less than or equal to 1.0.

The slip surface shown in Figure 2.1 was traced by connecting the planes that would result in the deepest continuous slip surface.

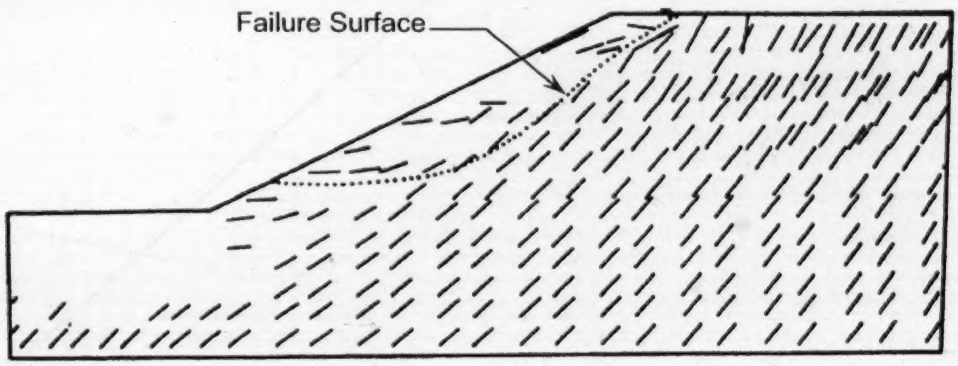

Figure 2.1: The field of critical planes used to identify the most likely failure surface for a simple homogeneous slope (Huang and Yamasaki 1993).

The comparisons presented by Huang and Yamasaki (1993) included several homogeneous slopes as well as the analysis of Springfield dam. The factors of safety from all analyses were reported to be in good agreement with the exception of the location of the slip surface in some instances.

Toufigh (1997) reported the results of a study where the slope stability results based on elasto-plastic stresses were compared with results based on linear elastic stresses. The displacement fields computed from the finite element stress analysis were used to generate a family of slip surfaces to be considered in the slope stability analysis. Each slip surface was generated beginning at an arbitrary point at the top of the slope. A series of line segments were drawn tangent to intersecting displacement vectors until the slip surface exited at a point near the base of the slope. A family of slip surfaces were generated by repeating the process beginning at a number of different points along the crest of the slope. The factor of safety of each slip surface was calculated using the Mohr-Coulomb failure criteria and stresses from the finite element analysis.

Table 2.2: Factors of safety for families of curves from Toufigh (1997).

No. of curve	1	2	3	4	5	6
Elastoplastic behaviour	*	14.25	9.11	2.07	0.96	0.97
Linear elastic behaviour	*	*	12.96	9.24	6.58	4.27

* unacceptable factors of safety due to boundary conditions used in model

Table 2.2 shows a comparison between the factors of safety computed for a family of six curves generated for a homogeneous 1:2 slope. The factors of safety computed based on linear elastic stresses were significantly higher when compared to the factors of safety computed based on elasto-plastic stresses. The variations in the factors of safety were attributed to the differences in the two soil behavior models.

2.2.2 Slope Stability Method used to Perform a Comparison Between Slope Stability Results Based on Linear Elastic or Elasto-Plastic Stresses

Traditional limit equilibrium factors of safety are typically computed within the framework of one of the method of slices formulations. Methods of slices that satisfy both force and moment equilibrium are generally preferred. The factor of safety equations associated with the more rigorous methods are non-linear and must be solved using an iterative procedure. The computational difficulties are generally accepted based on the grounds that the factor of safety calculations are more reliable. However, the reliability of the procedure used to search for the slip surface with the lowest factor of safety is often overlooked. Simple trial and error searching procedures are typically used in combination with the most advanced method of slices formulations. The search is normally restricted to circular failure surfaces while other potentially admissible slip surfaces are arbitrarily excluded from the search. The deficiencies that could enter into the slope stability analysis due to the use of

inadequate searching procedures might be as detrimental as using a factor of safety equation that was formulated without considering all the conditions of equilibrium. The computational complexities that arise from the combination of non-linear factor of safety equations with more advanced non-linear searching procedures have likely contributed to the continued use of simple trial and error techniques.

Replacing trial and error searching techniques with a more advanced dynamic programming optimization procedure permits the development of more general criteria to govern the shape of admissible slip surfaces (Baker 1980; Yamagami and Ueta 1988b; Zou et al. 1995; Pham 2002). Baker (1980) combined dynamic programming with the factor of safety equation developed by Spencer (1967). Baker developed a new criterion to govern the shape of admissible slip surfaces considered in the dynamic programming procedure. Slip surfaces were considered to be admissible if the first derivative calculated from the crest to the toe of the slope was greater than or equal to zero (i.e., the slip surface must be concave.). The ability to include concave slip surfaces represents a significant improvement considering that slip surfaces following along weak layers can be included in the search. The dynamic programming procedure has also been applied in combination with finite element slope stability methods (Yamagami and Ueta 1988b; Zou et al. 1995; Pham 2002; Pham and Fredlund 2003). Studies have shown that computational complexities associated with the application of the dynamic programming method are significantly reduced when the factor of safety equation is linear. Pham and Fredlund (2003) also demonstrated that the stresses from the finite element analysis could be used to develop a new kinematic admissibility criterion. The criterion is based on the principle that the resisting force must always act in a direction opposite to the mass movement and does not pose direct restrictions on the geometry of the slip surface. The criterion makes it possible to search for irregular slip surfaces that might follow along unique geological or man made features, as shown in Figure 2.2.

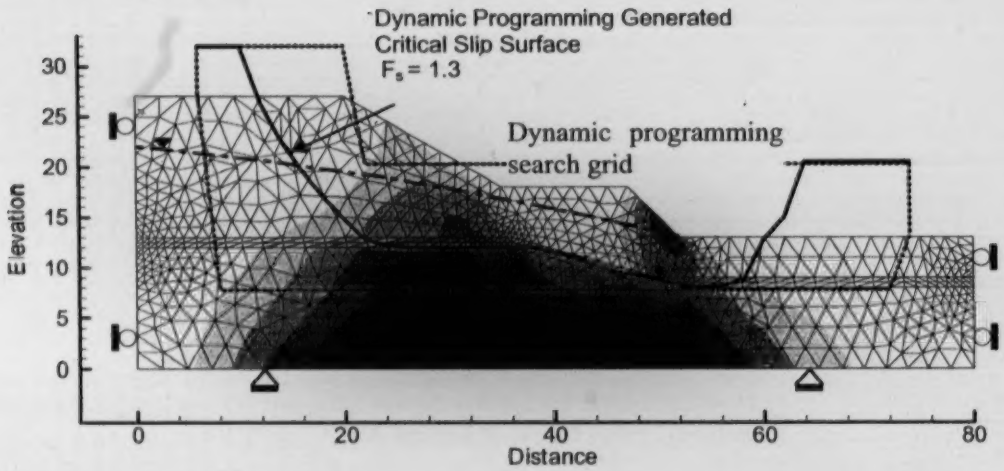

Figure 2.2: Geologically controlled slip surface that illustrates the possibility of the slip surface being convex or concave.

The dynamic programming procedure is used in combination with the finite element factor of safety equation to ensure consistency in the comparison between slope stability analyses based on linear elastic or elasto-plastic stress. The slope stability method is also considered to represent a move towards a more exact solution when compared with the method of slices techniques (Pham and Fredlund 2003). A brief description of the factor of safety equation and the dynamic programming formulation is provided. A more detailed discussion is provided in Pham and Fredlund (2003).

2.2.2.1 Calculation of the Factor of Safety Based on Stresses from an Independent Stress-Deformation Analysis

The dynamic programming method is a numerical algorithm used to optimize sequential multi-stage decision problems (Bellman 1957). Multi-stage decision problems are solved using a system of "stages" and "states". The "stage-state"

system consists of a grid of points organized into rows and columns. The "stage-state" system is used to search for the critical slip surface and is known as the search grid. The points from the search grid can be connected to form linear line segments. It is assumed that a continuous slip surface can be approximated by connecting a series of n linear line segments. The overall factor of safety (F_s) can be defined as follows:

$$[2.1] \qquad F_s = \frac{\sum_{i=1}^{n} \tau_{f_i} \Delta L_i}{\sum_{i=1}^{n} \tau_i \Delta L_i}$$

where n is the total number of individual line segments, τ_{f_i} is the shear strength, τ_i is the shear stress, and ΔL_i is the length of one line segment (Naylor 1982).

The shear strength along the i^{th} line segment can be computed using the extended Mohr-Coulomb equation for saturated-unsaturated soil (Fredlund and Rahardjo 1993) given by the following equation;

$$[2.2] \qquad \tau_{f_i} = c' + (\sigma_n - u_a)\tan\phi' + (u_a - u_w)\tan\phi^b$$

where $(\sigma_n - u_a)$ is the net normal stress acting on the ith segment, $(u_a - u_w)$ is the matric suction, and c', ϕ', and ϕ^b are the effective shear strength parameters for a saturated-unsaturated soil.

The normal stress, σ_n, and the actuating shear stress, τ_n, acting at the orientation of the i^{th} line segment are determined using Eq. [2.3] and Eq. [2.4] derived from the Mohr circle of stresses (Terzaghi and Peck 1948);

$$[2.3] \qquad \sigma_n = \sigma_x * \sin^2\theta + \sigma_y \cos^2\theta - \tau_{xy} \sin 2\theta$$

$$[2.4] \quad \tau_n = \tau_{xy}\left(\sin^2\theta - \cos^2\theta\right) - \left(\frac{\sigma_x - \sigma_y}{2}\right)\sin 2\theta$$

where θ is the angle of the i^{th} line segment with respect to the horizontal and σ_x, σ_y and τ_{xy} are the normal and shear stresses acting in the x- and y- coordinated directions. The values of σ_x, σ_y and τ_{xy} are computed using a separate numerical stress-deformation analysis. The factor of safety calculations based on finite element stresses falls into the category of a limit equilibrium method since the factor of safety is defined through consideration of the overall limit equilibrium of forces.

2.2.2.2 Application of the Dynamic Programming Searching Technique

The dynamic programming method can only be applied to an additive function. The definition of the factor of safety in Eq. [2.1] is a ratio and can be re-written in an additive form as follows;

$$[2.5] \quad G = \sum_{i=1}^{n}(R_i - FsS_i)$$

where R_i, S_i and F_s are the acting resisting force, acting shear force and factor of safety along the i^{th} line segment, respectively. The resulting equation is called the auxiliary functional (G) (also known as the return function) and can be evaluated for individual line segment considered in the dynamic programming search. The objective is to determine the combination of line segments (i.e., slip surface) where the summation of return function values is the lowest. Minimizing the auxiliary functional has been shown to be equivalent to minimizing the definition of the factor of safety given in Eq. [2.1] (Baker 1980).

A second equation, called the optimal function (Eq. [2.6]), is introduced to keep track of the return function values as the dynamic programming search progresses from one "stage" to the next.

$$[2.6] \quad H_{i+1}(j) = \min[H_i(K) + DG_i(j,K)]$$

K is an array representing the total number of "state" points from "stage" i (NPi), as shown in Figure 2.3. Therefore, $H_i(K)$ represents the value of the optimal function at each of the "state" points in "stage" i. $DG_i(j,K)$ represents an array used to store the values of the return function calculated for the line segments connecting "state" point j in "stage" i+1 to each of the "state" points represented by the K array. The line segment representing the critical path from one of the "state" points in "stage" i to "state" point j in "stage" i+1 (i.e., $H_i+1(j)$) is determined by selecting the minimum value of $H_i(K) + DG_i(j,K)$.

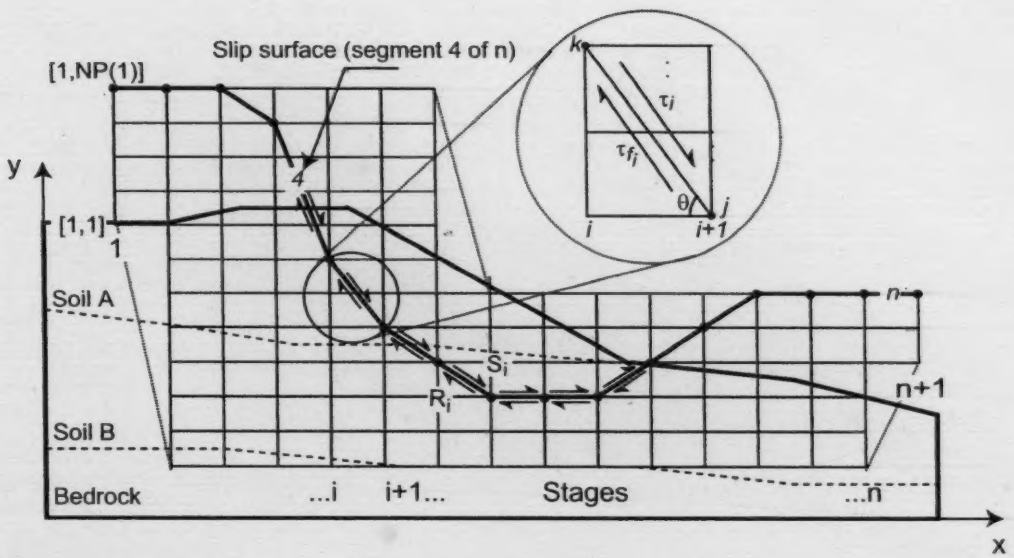

Figure 2.3: Components of the dynamic programming method including an example search grid.

The dynamic programming search is iterative and can be used to solve slope stability problems using the following steps.

1) Solve for the stress state at all points in the slope.
2) Define the dynamic programming search grid. The search grid is divided into "stages" in the horizontal direction and into "states" in the vertical direction. The terms "stages" and "states" are names used to separate the numbering of the grid points in the horizontal and vertical directions. The search grid takes on the character of a series of columns and rows, as shown in
3) Figure 2.3. The grid must contain a number of points outside the slope near the crest and the toe of the slope. This ensures that the entry and exit points of the slip surface are part of the analysis. At least one column of "state" points must be contained entirely within the boundaries of the slope. The column is usually selected near the mid-point of the slope.
4) The complete stress state from the numerical analysis is imported to the points on the dynamic programming search grid. Linear interpolation is used when the

points from the dynamic programming search grid do not exactly correspond to the mesh used in the numerical analysis.

5) The user must select an initial factor of safety that is used in computing the Auxiliary Functional, G, for the first iteration. The value for a convergence criterion (δ) is also selected. The convergence criterion is used to determine when the dynamic programming search has identified the critical slip surface.

6) The value of the Optimal Function, $H_{(1,K)}$, is initialized to zero for all "state" points, K, in the first "stage".

7) It is now possible to determine the most critical path to each point in the search grid by evaluating Eq. [2.6] for all remaining "state" points. The first "state" point to be evaluated is, $j=1$, in "stage", $i+1 = 2$ (i.e., $H_2(1)$). The "state" point, K, from "stage", i, resulting in the minimum Optimal Functional value, $\min[H_i(K)+DG_i(j,K)]$, is recorded and the search proceeds to the next "state" point, $j+1$, in the current stage (i.e., $i+1 = 2$). When all of the "state" points in the current stage have been evaluated, the search proceeds to the next stage and step (6) is repeated.

8) When the search reaches the last "stage", the "state" point with the lowest Optimal Functional value is determined. The information stored at this point corresponds to the combination of line segments with the lowest factor of safety.

9) The actual factor of safety for the combination of line segments determined from step (7) is calculated using Eq. [2.1].

10) The computed factor of safety is compared with the previous factor of safety. If the difference is less than a predetermined convergence criterion, δ, the search is discontinued. If not, the previous factor of safety is replaced with the new factor of safety and another iteration is undertaken repeating steps (6) through (9).

The dynamic programming searching procedure was selected to move away from traditional grid and radius type searching procedures that require significant restrictions on the shape of potential slip surfaces. Dynamic programming provides the ability to develop meaningful admissibility criteria to guide the shape of the slip

surface and is not considered to be as vulnerable to being trapped in local minima as the grid and radius procedure. In addition, it is possible to design the search grid and perform a series of simple checks to reduce the chance of a situation where the searching procedure gets trapped in a local minimum (i.e., include a number of grid points outside the slope, choose a reasonable grid density and search portions of the slope separately etc.).

2.3 Comparing Slope Stability Analysis Based on Linear Elastic or Elasto-Plastic Stresses

A study was undertaken to ascertain the differences that might occur in slope stability analyses based on stresses calculated assuming linear elastic or elasto-plastic soil behavior. The methodology developed to perform the comparisons is presented followed by the results from specific examples.

2.3.1 Methodology and Scope

The methodology used to compare the slope stability calculations is illustrated in the flow chart shown in Figure 2.4.

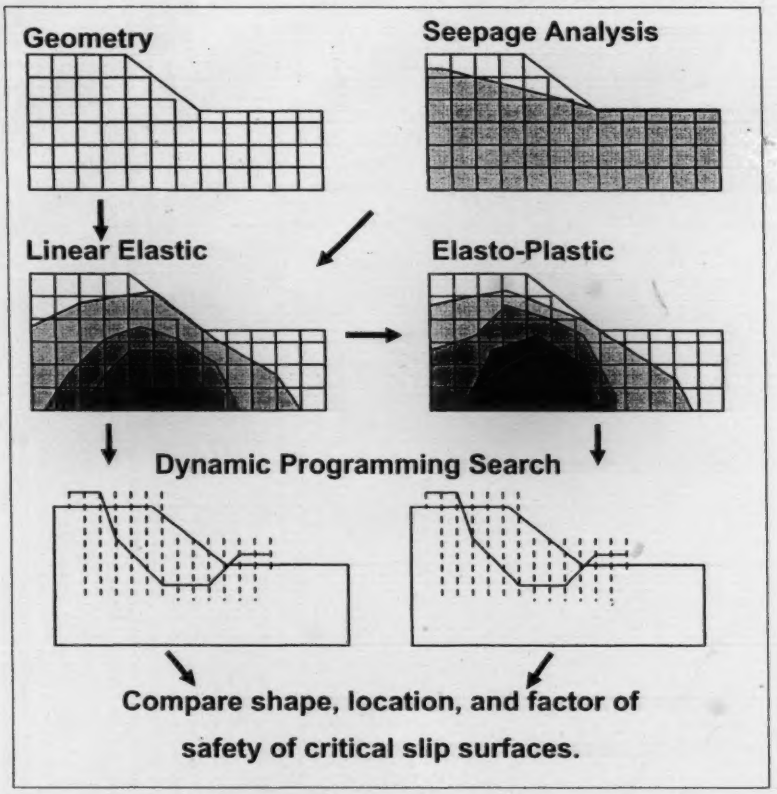

Figure 2.4: Methodology used to compare the effect of the linear elastic or elasto-plastic models on the slope stability calculation.

The geometry of the slope was defined, followed by the generation of the isotropic linear elastic stresses resulting when gravity forces are "switched on". Pore-water pressures were imported from a separate seepage analysis when required. The elasto-plastic stresses were evaluated using the linear elastic conditions as the initial stress state. Next, two separate slope stability analyses were completed; one based on the linear elastic stresses, the other based on the elasto-plastic stresses. The same dynamic programming grid was used to search for the critical slip surface in both cases. Finally, the shape, location and average factor of safety for the critical slip surfaces from the two slope stability analyses were compared. The stress-deformation analyses were completed using FLAC (Itasca Consulting Group Inc.),

the seepage analyses were completed using SVFLUX (SoilVision Systems Ltd.), and the slope stability calculations were completed using a computer code developed specifically for this study.

A variety of slopes with increasing complexity were included in the study to ensure that the comparison would encompass a range of typical conditions. The comparison begins with a parametric study involving a simple homogeneous slope. Next, embankments with various slope angles and pore-water pressure conditions are considered, followed by two multi-layered slope conditions. The current study is a continuation of the research presented by Stianson et al. (2004).

Table 2.3 summarizes the range of soil properties considered in the parametric study completed for the simple homogeneous slope. Four values of Poisson's ratio were considered along with three combinations of c' and ϕ'. The combinations of c' and ϕ' were selected to evaluate cases where the factors of safety ranged from values greater than 1.0 to values less than 1.0, based on computations carried out using linear elastic stresses. Only the results obtained for the case where Poisson's ratio was equal to 0.48 have been included. The comparison for this case is representative of the results observed for other cases; the only differences being that the shape of the slip surface is affected slightly by changing Poisson's ratio. The slope stability results were not sensitive to Young's modulus. Therefore, Young's modulus was not included in the parametric study and was set to 20,000 kPa for all cases. The unit weight of the soil (γ) and the convergence criteria (δ) for the dynamic programming search remained constant throughout the comparison and were set to 18 kN/m^3 and 0.001, respectively. The factors of safety are reported to higher accuracy than is typically used in practice to facilitate a detailed comparison of the results.

Table 2.3: Range of soil properties used in the parametric study involving the homogeneous slope

Unit Weight γ (kN/m^3)	Poisson's Ratio ν	Effective Cohesion c' (kPa)	Effective Friction Angle ϕ' (degrees)
18	0.48	20	10
		17	7
		15	5
18	0.40	20	10
		17	7
		15	5
18	0.33	20	10
		17	7
		15	5
18	0.20	20	10
		17	7
		15	5

2.3.2 Presentation of Results

The results of each comparison are presented beginning with the parametric study involving a homogeneous slope followed by other comparisons involving various pore-water pressure conditions, slope angles, and finally multi-layered slopes.

2.3.2.1 Homogeneous Dry Slope

Figures 2.5, 2.7 and 2.9 provide comparisons of the slope stability results for cases where the factors of safety are approximately 1.3, 1.0 and less than 1.0, respectively. The slip surface defined using square symbols represents the results based on linear elastic stresses while the slip surface described using triangular symbols represents the results based on elasto-plastic stresses. The solid line with no symbols represents the results from a conventional limit equilibrium analysis using the Morgenstern and

Price (1965) method. The linear elastic and elasto-plastic local factor of safety distributions have been included in Figures 2.6 and 2.8 for the first two cases.

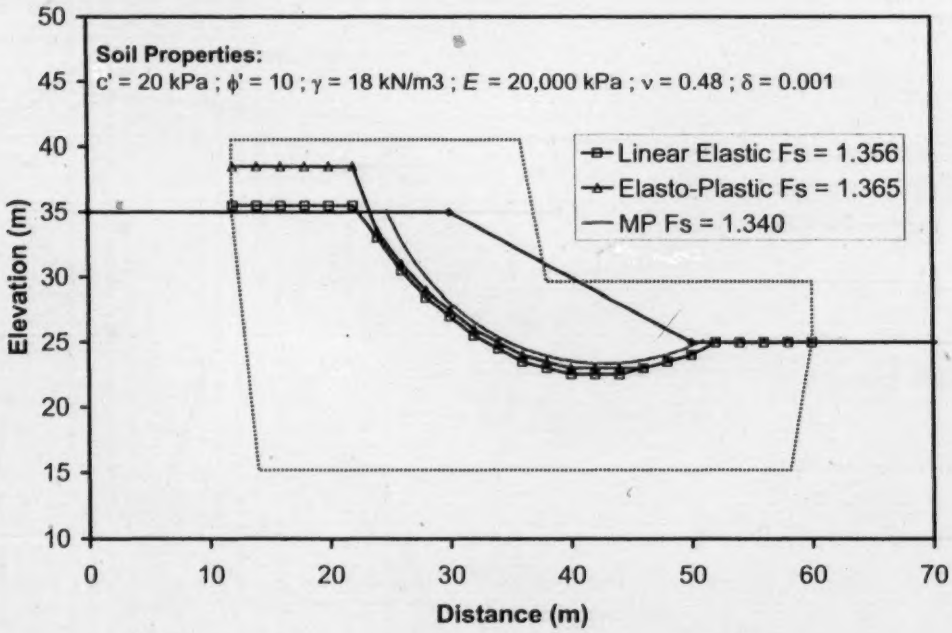

Figure 2.5: Comparison of the shape, location and average factor of safety for the slip surfaces determined using linear elastic stresses, elasto-plastic stresses and the Morgenstern and Price (1965) method for the 2:1 homogeneous slope at a factor of safety of approximately 1.3.

Figure 2.5 confirms that there is reasonably close agreement between all three analytical procedures when relatively stable slope conditions are considered. The shape and location for the critical slip surfaces are similar. The average factors of safety calculated using linear elastic and elasto-plastic stresses are 1.356 and 1.365, respectively. The difference between the two factors of safety values is less than 1%.

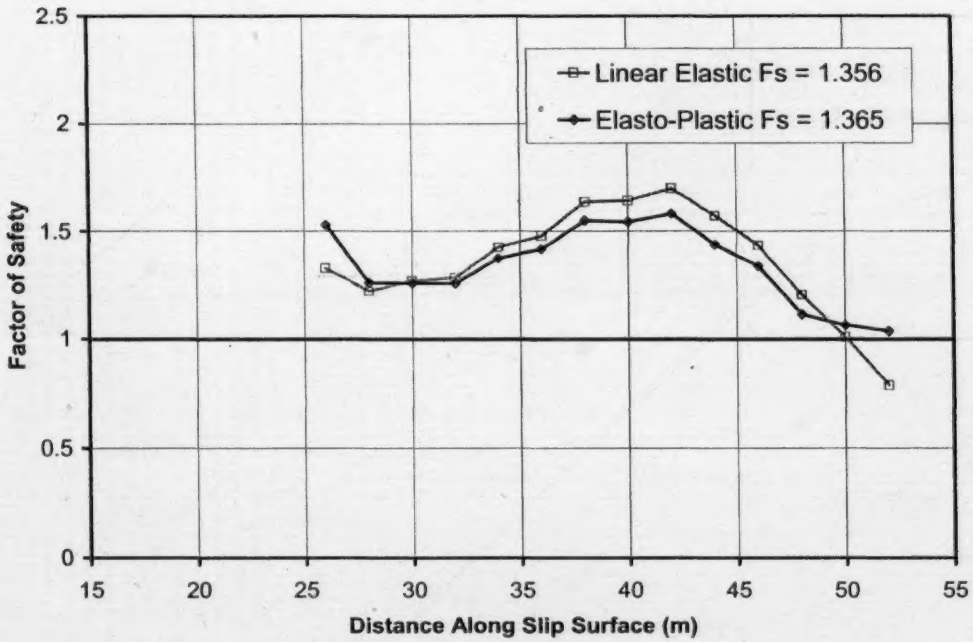

Figure 2.6: Local factor of safety distributions along the slip surfaces determined using linear elastic stresses or elasto-plastic stresses for the 2:1 homogeneous slope at a factor of safety of approximately 1.3.

The local factor of safety distributions along each slip surface for the conditions evaluated in Figure 2.5, are provided in Figure 2.6. The central region of the slope is shown to have the highest local factor of safety followed by the crest of the slope and finally the toe of the slope. The evidence would suggest that failure might start at the toe of the slope as the local factor of safety is less than 1.0 based on elastic stresses and is equal to 1.0 based on elasto-plastic stresses. It can also be noted that the local factors of safety calculated using elasto-plastic stresses to the left of the failing portion at the toe are less than those calculated using elastic stresses. This behavior indicates that the excess stresses are being redistributed to more stable portions of the slope. Even though localized failure has started at the toe of the slope, it has only occurred over a small portion of the slip surface. Therefore, the agreement in the

overall factor of safety and the location of the slip surface illustrated in Figure 2.5 might be expected. The differences might be accentuated as the stability of the slope is reduced and the overall factor of safety approaches 1.0.

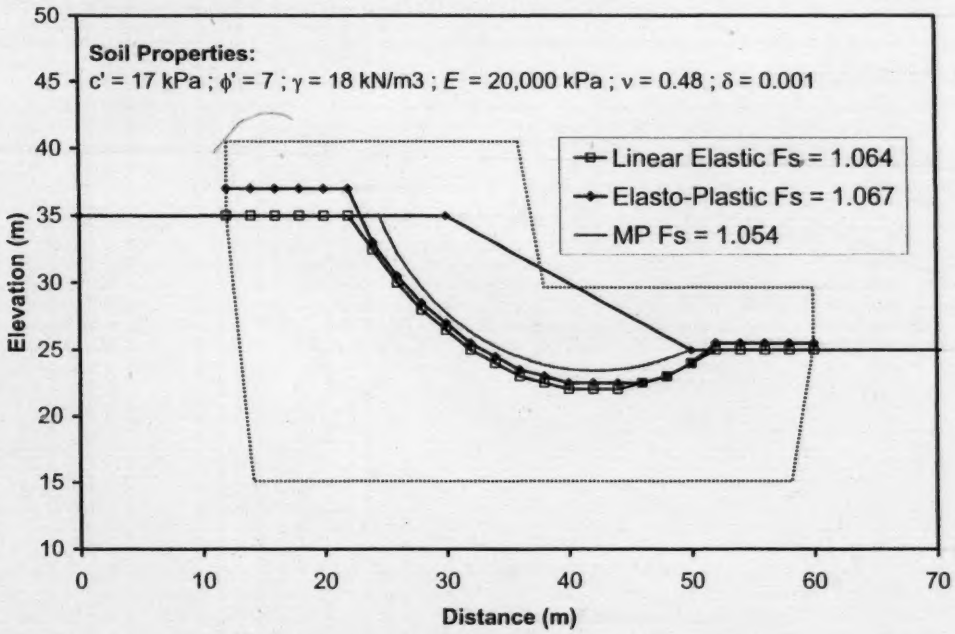

Figure 2.7: Comparison of the shape, location and average factor of safety for the slip surfaces determined using linear elastic stresses, elasto-plastic stresses and the Morgenstern and Price (1965) method for the 2:1 homogeneous slope at a factor of safety of approximately 1.0.

Figure 2.7 demonstrates that the agreement in the slope stability calculations continues as the factor of safety is decreased to approximately 1.0. There is reasonably close agreement between the shape and location of the critical slip surface and there is once again less than 1% difference in the overall factors of safety.

The shape of the local factor of safety distribution based on linear elastic stresses is similar to that of the previous example but the local factors of safety have shifted downward as shown in Figure 2.8. Consequently, a zone at the toe of the slope has failed and failure has been initiated near the crest of the slope. The shape of the local

factor of safety distribution based on elasto-plastic stresses is essentially flat at a factor of safety near 1.0. The shape of the distribution indicates that the maximum amount of stress redistribution has taken place along the slip surface. Even with the large variations in local factor of safety, there is still reasonably close agreement between the shape, location and average factor of safety for the most critical slip surface.

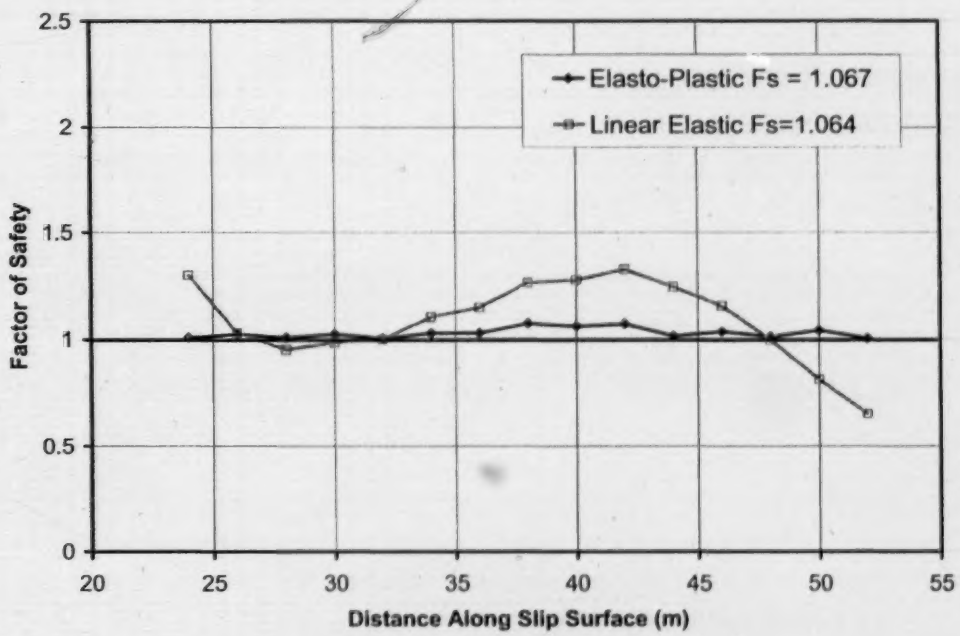

Figure 2.8: Local factor of safety distribution along the slip surface determined using linear elastic stresses or elasto-plastic stresses for the 2:1 homogeneous slope at a factor of safety of approximately 1.0.

A similar comparison was conducted for a case where the strength of the soil was further reduced resulting in an overall factor of safety below 1.0 (based on elastic stresses). The results of the comparison are shown in Figure 2.9. The overall factors of safety calculated using elastic and elasto-plastic stresses were equal to 0.868 and 1.041, respectively. The difference between the two factors of safety is

approximately 16%. The slip surfaces determined from elastic stresses and the Morgenstern and Price method are similar to those found in the previous examples while the slip surface determined using elasto-plastic stresses has moved much deeper into the slope. The deeper slip surface might be a result of the deformed shape predicted in the elasto-plastic stress analysis. In the previous examples where the factors of safety were greater than or equal to 1.0, small displacements were adequate to allow the excess stresses to redistribute resulting in deformed shapes that were reasonably close to the original slope geometry. Further decreasing the soil strength resulted in larger displacements taking place before the excess stresses could be redistributed. It is possible that the increased displacements might have resulted in a deformed shape that deviated from the original slope geometry enough to cause significant differences in the slope stability comparison. An additional comparison was carried out using the deformed slope geometry predicted from the elasto-plastic analysis in an attempt to explain the differences shown in Figure 2.9.

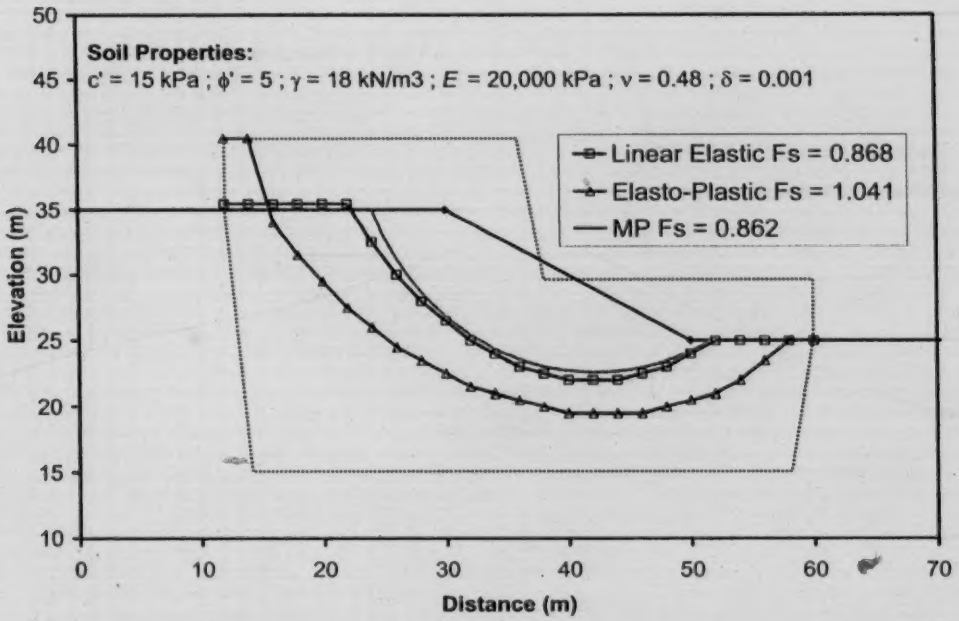

Figure 2.9: Comparison of the shape, location and average factor of safety for the slip surfaces determined using linear elastic stresses, elasto-plastic stresses and the Morgenstern and Price (1965) method for the 2:1 homogeneous slope at a factor of safety of less than 1.0.

The deformed slope geometry is shown in Figure 2.10 (dashed line) along with a comparison of the slope stability results from all three analytical methods. The critical slip surfaces identified using the elastic stress analysis and the Morgenstern-Price method have moved deeper into the slope and the factors of safety have increased to 1.0, as result of the more stable deformed slope geometry. The comparison shows a similar level of agreement to that realized in previous examples where the factors of safety were greater than or equal to 1.0. The improved agreement shown in Figure 2.10 provides evidence that the deformed slope geometry was the cause for the differences in the slope stability results shown in Figure 2.9.

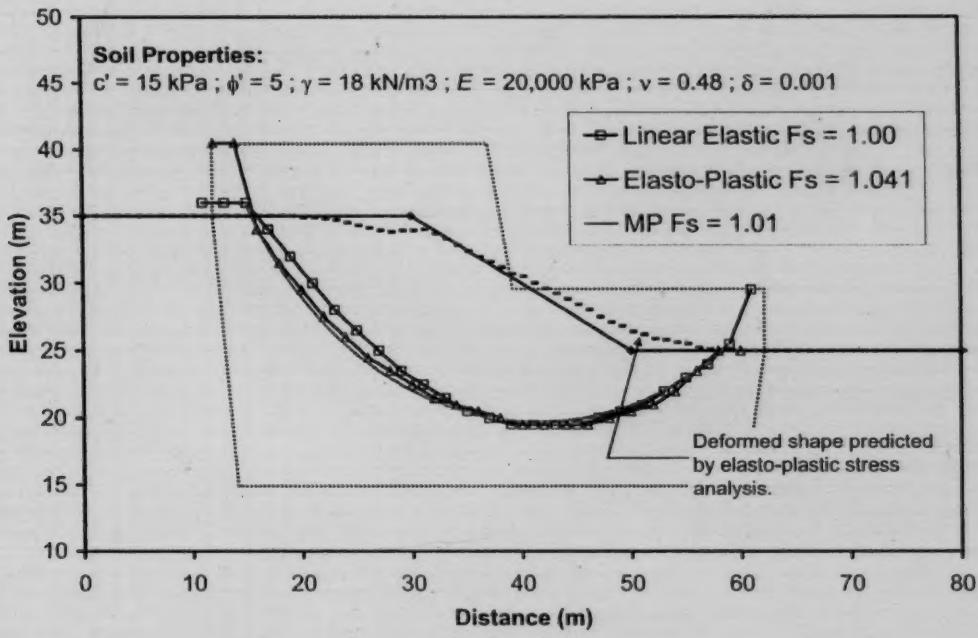

Figure 2.10: Comparison of the shape, location and average factor of safety for the slip surfaces determined using linear elastic stresses, elasto-plastic stresses and the Morgenstern and Price (1965) method based on the deformed geometry predicted using an elasto-plastic stress analysis.

The results presented in Figure 2.5 through Figure 2.8 are meant to compare slope stability calculations considering conditions typically evaluated in practice (i.e., factors of safety from 1.3 to 1.0). The results demonstrate that the soil behavior model can significantly influence the local factor of safety distribution but has little influence on the overall factor of safety. It is understood that it is impossible for the slope conditions evaluated in Figure 2.9 and 2.10 to exist naturally (i.e., factor of safety is less than 1.0). Nevertheless, the results are included to demonstrate that the comparison needs to be extended to the point of unrealistic slope conditions before the slope stability comparison indicates any significant differences. The results emphasize the conclusion that there will be no difference between slope stability calculations based on linear elastic or elasto-plastic stresses as long as the same slope

geometry is being evaluated. The results can be used to explain other cases where the selection of soil properties in the finite element analysis (i.e., strength properties or Young's modulus) might result in a deformed shape that is different than the original shape. The results also show that small changes in geometry can result in a significant difference in the location of the slip surface and the overall factor of safety. The results emphasize the importance of making sure the geometry of the slope is as accurate as possible.

The previous examples compare the slope stability calculations as the slope is brought to failure by decreasing the strength of the soil. Figure 2.11 provides a comparison involving a case where the stability of the slope is reduced by increasing the slope angle while keeping the strength of the soil constant. The cohesion is equal to 20kPa and the angle of internal friction is equal to 10°. Three slope angles are considered including 3:1, 2:1 and 1:1 resulting in factors of safety of approximately 1.5, 1.3 and 1.0. The results confirm that a similar level of agreement is achieved for a case where the stability of the slope is reduced by increasing the slope angle.

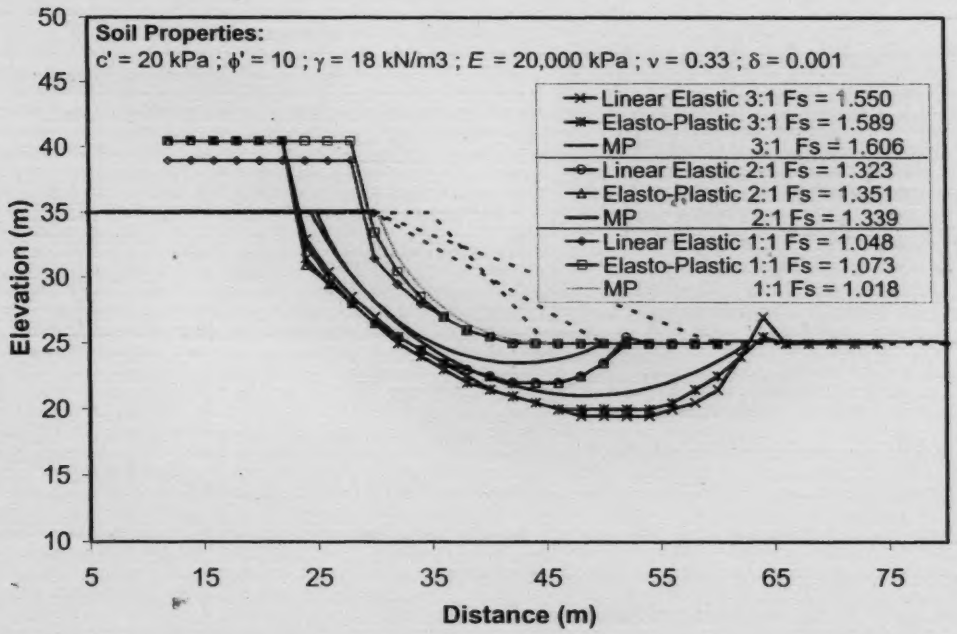

Figure 2.11: Comparison of the shape, location and average factor of safety for the slip surfaces determined using linear elastic stresses or elasto-plastic stresses for a homogeneous slope with slope angles of 3:1, 2:1 and 1:1.

The slope stability comparisons thus far have only given consideration to dry homogeneous slopes. Additional slope stability analyses are presented where the effects of pore-water pressure and multiple soil layers are considered.

2.3.2.2 Homogeneous Wet and Submerged Slope

The stability of a homogeneous embankment with a 2:1 slope angle is evaluated under two conditions including a case where the piezometric line passes through the toe of the slope (i.e., wet slope) as well as a case of partial submergence of the slope (Figure 2.12). The effective cohesion and effective friction angle were arbitrarily selected to be 20 kPa and 10°, respectively. The computed average factors of safety

were approximately 1.22 for the wet slope and approximately 1.25 for the submerged slope. The slope stability analyses based on elastic and elasto-plastic stresses showed reasonably close agreement under both the wet and submerged conditions.

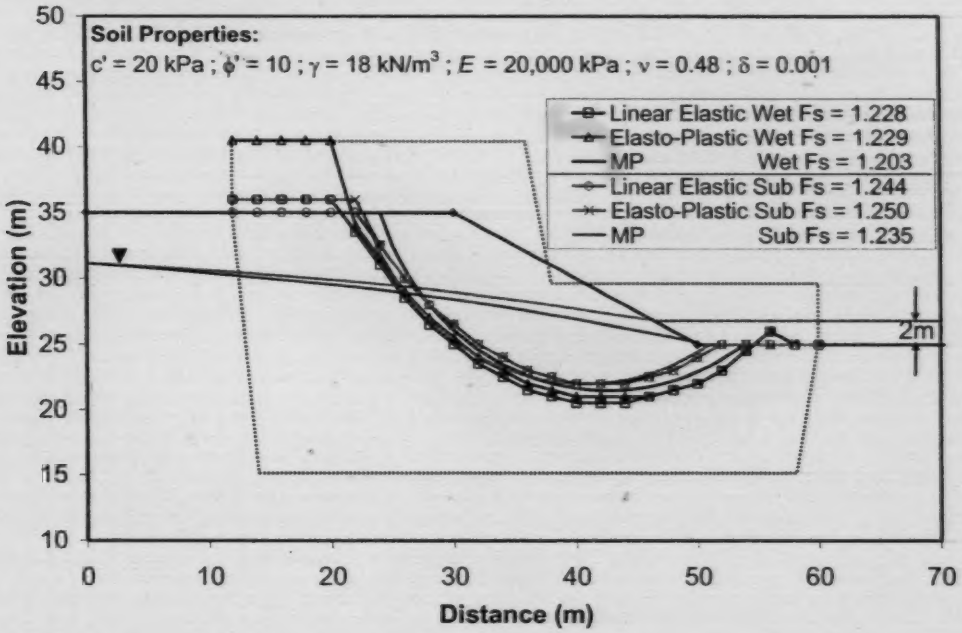

Figure 2.12: Comparison of the shape, location and average factor of safety for the slip surfaces determined using linear elastic stresses or elasto-plastic stresses for the 2:1 homogeneous slope with a piezometric line (i.e., wet slope) as well as conditions of partial submergence.

2.3.2.3 Two Layer Slope

The first multi-layered slope configuration is shown in Figure 2.13. The slope stands at a 2:1 angle and consists of two soil units. The shear strength of both soil layers was selected to result in an overall factor of safety close to 1.0. The final soil properties selected for the analysis are provided in Figure 2.13.

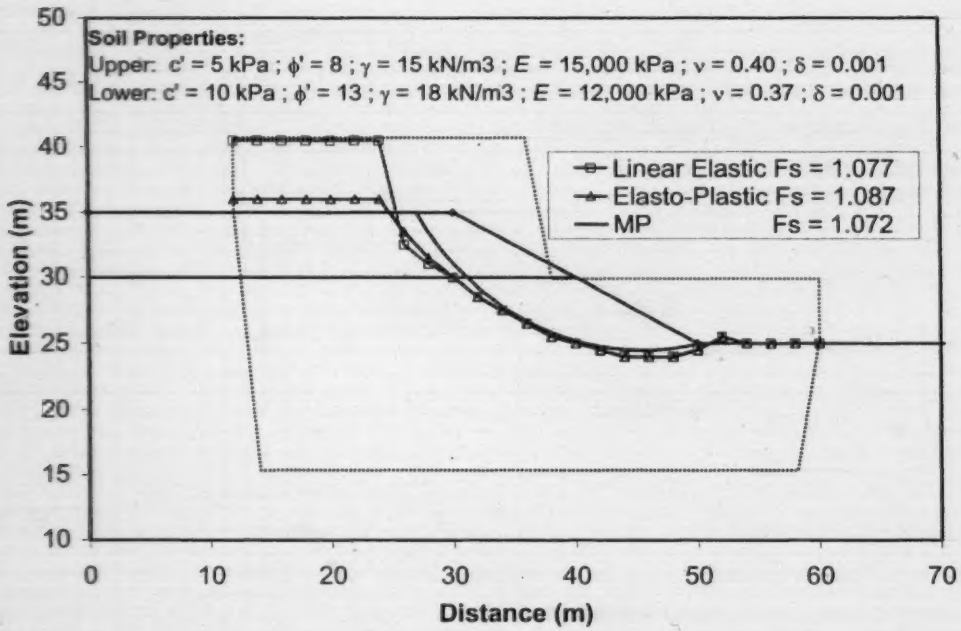

Figure 2.13: Comparison of the shape, location and average factor of safety for the slip surfaces determined using linear elastic stresses or elasto-plastic stresses for the 2:1 slope with two soil layers.

The results shown in Figure 2.13 demonstrate the same level of agreement observed in other examples. The difference between the two factors of safety is less than 1% and there is agreement in the shape and location of the critical slip surface.

2.3.2.4 Three Layer Slope

The second multi-layered slope includes three soil layers. The shear strength properties were selected to result in an average factor of safety near 1.0. A thin, weak layer was also included to illustrate the effect on the shape and location of a slip surface that is controlled by a geological feature.

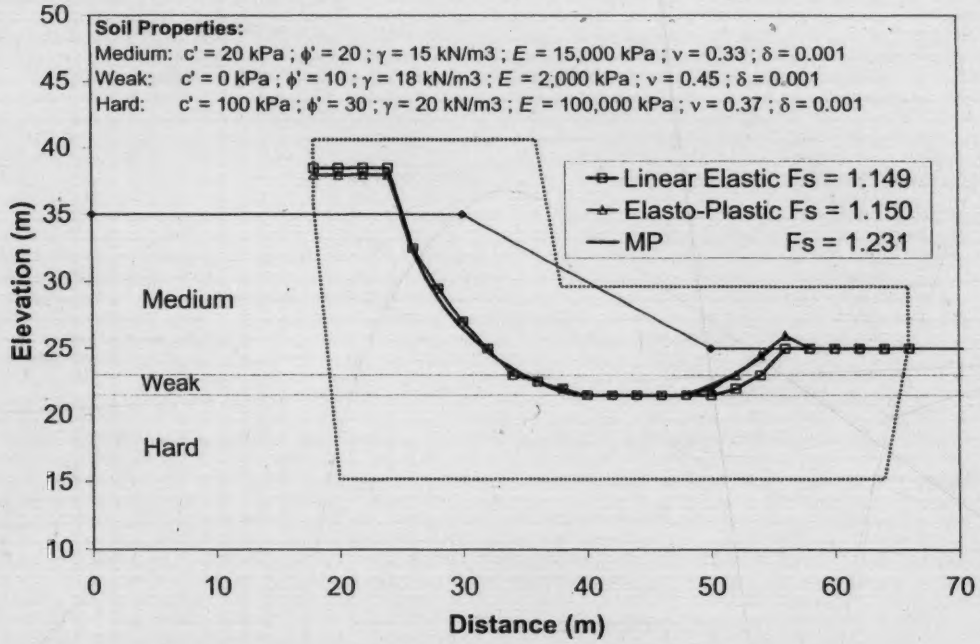
Soil Properties:
Medium: c' = 20 kPa ; ϕ' = 20 ; γ = 15 kN/m3 ; E = 15,000 kPa ; ν = 0.33 ; δ = 0.001
Weak: c' = 0 kPa ; ϕ' = 10 ; γ = 18 kN/m3 ; E = 2,000 kPa ; ν = 0.45 ; δ = 0.001
Hard: c' = 100 kPa ; ϕ' = 30 ; γ = 20 kN/m3 ; E = 100,000 kPa ; ν = 0.37 ; δ = 0.001
Linear Elastic Fs = 1.149
Elasto-Plastic Fs = 1.150
MP Fs = 1.231
Medium
Weak
Hard
Elevation (m)
Distance (m)
50
45
40
35
30
25
20
15
10
0
10
20
30
40
50
60
70

Figure 2.14: Comparison of the shape, location and average factor of safety for the slip surfaces determined using linear elastic stresses or elasto-plastic stresses for the 2:1 slope with three soil layers including a weak layer.

The results in Figure 2.14 show that the same level of agreement is achieved even under more complex stratigraphic conditions. It appears that the same mode of failure is determined assuming either linear elastic or elasto-plastic soil behavior. The application of the dynamic programming optimization technique makes it possible to determine the mode of failure without making any prior assumptions regarding the shape of the slip surface. There is once again less than 1% difference in the average factor of safety and there is good agreement in the shape and location of the critical slip surface.

2.4 The Effects of the Linear Elastic or Elasto-Plastic Constitutive Model on the Slope Stability Calculation

Examination of a number of slope stability comparisons involving various stratigraphic and pore-water pressure conditions shows no significant differences on the slip surface location or the overall factor of safety when linear elastic or elasto-plastic soil behavior is assumed. The differences in the slope stability calculations become apparent when the local factors of safety are compared at individual points along the slip surfaces. These differences are accentuated as the slope becomes close to failure. The following discussion examines why there are large differences in the local factor of safety and proposes a condition where the assumed soil behavior model might significantly influence the calculation of the overall factor of safety.

From Eq. [2.2], the shear strength is dependent on five variables; namely, effective cohesion , c', effective angle of internal friction, ϕ', pore-water pressure distribution, u_w, and the angle defining the ratio of increase in shear strength with respect to soil suction, ϕ^b. Four of the above variables are independent of the stress analysis; namely, c', ϕ', u_w and ϕ^b, in typical slope stability calculations. These variables are assigned values for the various soil layers and held constant throughout the analysis. The normal stress, σ_n, is the only variable that can be influenced by the selected constitutive model. If the stress distribution is approximated by "switching on" gravity forces, the normal stress will be controlled largely by the geometry of the slope. Therefore, it could be expected that similar normal stresses would be calculated regardless of the selected constitutive model as long as the same soil properties and geometry are used.

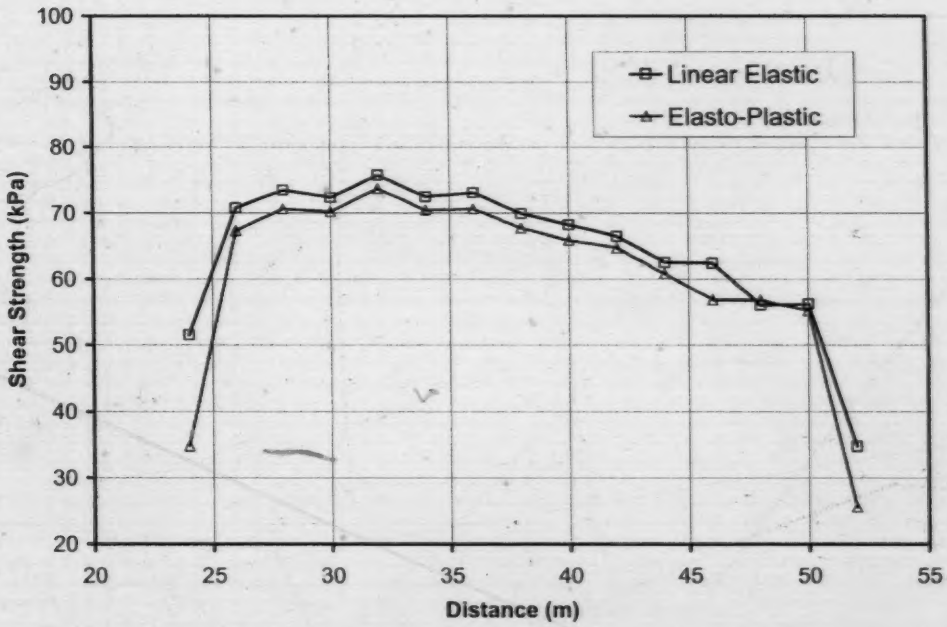

Figure 2.15: Shear strength distributions along the slip surfaces determined using linear elastic stresses or elasto-plastic stresses for the 2:1 homogeneous slope and a factor of safety approximately equal to 1.0.

The above rationale can be described further by considering the local shear strength distributions shown in Figure 2.15. Figure 2.15 shows a plot of the shear strength distribution along the critical elastic and elasto-plastic slip surfaces determined for the homogeneous slope with a factor of safety of approximately 1.0 (i.e., Figure 2.7). The shear strength values based on linear elastic stresses are slightly larger than those based on elasto-plastic stresses. The small differences are due to the fact that the slip surface determined based on elastic stresses is slightly lower than the slip surface determined from elasto-plastic stresses. A lower slip surface will have larger normal stresses and slightly larger shear strengths. Overall, the assumed soil behavior model seems to have little influence on the shape of the shear strength distribution and the magnitude of individual values along the distribution. This would indicate that the variations observed in the local factor of

safety distributions shown in Figure 2.8 do not originate in the shear strength term of the factor of safety equation.

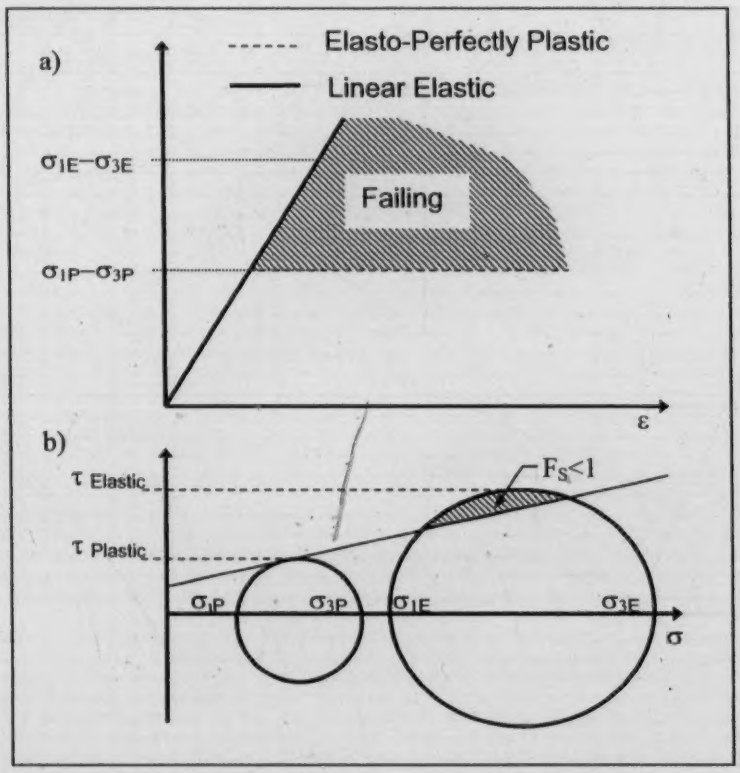

Figure 2.16: Comparing linear elastic versus elasto-perfectly plastic stress analysis.

The mobilized shear stress is calculated using the deviatoric stress from the stress analysis (Figure 2.16a) in combination with Mohr's circle (Figure 2.16b). It is possible to calculate different mobilized shear stresses depending on the stability of the slope and the constitutive model selected for the stress analysis. Referring to Figure 2.16a, the deviatoric stress calculated for failing portions of the slope, using the elasto-plastic model, are only permitted to rise to the shear strength of the soil before being redistributed to other areas of the slope. The deviatoric stresses calculated using the linear elastic constitutive model are permitted to increase beyond the shear strength of the soil. Higher deviatoric stresses produce Mohr's circles with

larger radii, resulting in higher mobilized shear stresses as shown in Figure 2.16b. The shear stress distributions shown in Figure 2.17 confirm that the mobilized shear stress calculated from a linear elastic analysis is higher in failing portions of the slope and seems to explain the origin of the observed variations in the local factor of safety distributions.

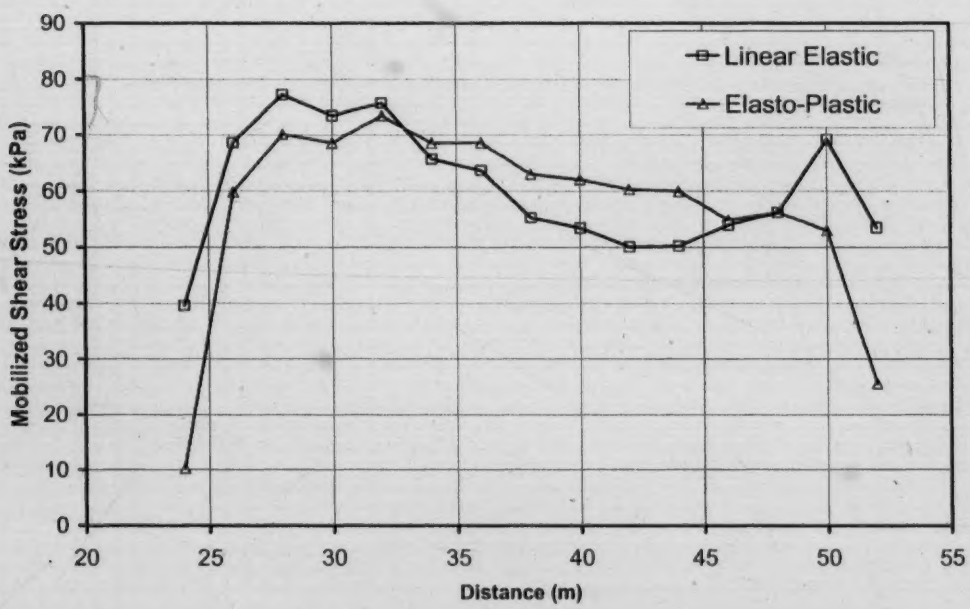

Figure 2.17: Mobilized shear stress distributions along the slip surfaces determined using linear elastic stresses or elasto-plastic stresses for the 2:1 homogeneous slope and a factor of safety approximately equal to 1.0.

All of the slope stability calculations completed in the current study are evaluated based on the assumption that the strength parameters (i.e., c' and ϕ') are constant throughout individual soil units. It is possible that the assumed soil behavior model might influence the slope stability calculations more significantly if attempts were made to capture the strain softening characteristics of the soil. The strength of the soil could be included in the slope stability analysis as a function of the amount of

strain computed from the stress-deformation analysis, according to a relationship similar to that shown in Figure 2.18.

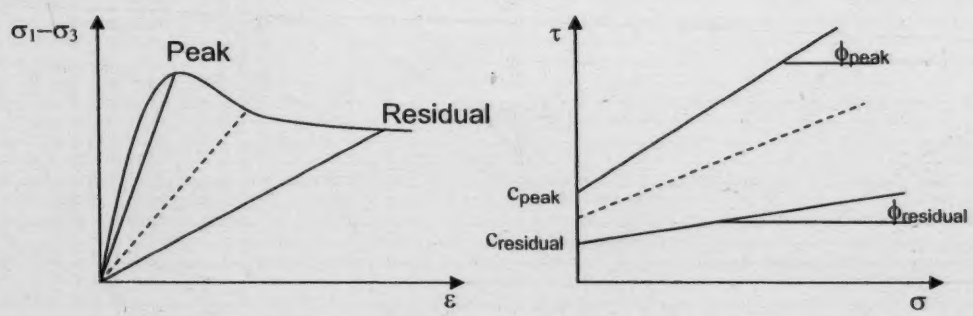

Figure 2.18: Shear strength for a strain softening material.

In certain locations of the slope, the strength of the soil will correspond to the peak strength conditions shown in Figure 2.18. Other locations of the slope might have been subject to additional strains resulting in a loss of strength (i.e., c' and ϕ'). The strength of the soil might exist at some intermediate level (dashed line) or in extreme cases be reduced to a level corresponding to the residual strength of the soil. It is possible to assign the strength at individual locations within the slope according to the strains calculated from a numerical stress-deformation analysis. Significant differences might occur between a slope stability analysis based on linear elastic stresses using constant strength parameters when compared to a slope stability analysis using strain dependent strength properties. The slope stability method used in the current analysis would have to be modified to perform slope stability analyses using strain dependent shear strength properties.

2.5 Conclusions

Slope stability results based on linear elastic or elasto-plastic stress analyses have been compared with respect to the shape, location and overall factor of safety for the most critical slip surface. The following conclusions can be made from this study.

1) There appears to be insignificant differences in the local factors of safety calculated from linear elastic stresses or elasto-plastic stresses for slopes with factors of safety large enough such that localized failure does not occur. The differences in the local factor of safety become larger for slopes that are close to failure and experience localized failure. The local factors of safety determined when using elasto-plastic stresses for slopes at or near failure would appear to be more representative of *in situ* conditions.
2) There are small essentially insignificant differences between the shape, location and the overall factors of safety (i.e., less than 1%) calculated using either the linear elastic or elasto-plastic stress analysis. The use of linear elastic stresses appears to be acceptable when the factor of safety is equal to, greater than, or less than unity and constant shear strength properties are used in the slope stability analysis.
3) Slope stability calculations in engineering practice are generally concerned with the stability of the original slope geometry, not the deformed slope geometry. It is noted that the geometry at the end of the elasto-plastic stress-deformation analysis can be significantly different from the original slope geometry. The geometrical differences can significantly alter the slope stability evaluation.
4) The shape, location, and overall factor of safety predicted using conventional methods of slices agrees with the results based on elastic stresses for factors of safety greater than, equal to, or less than 1.0 for the range of examples presented in this study.
5) The comparisons show no significant deviation in the results based on either soil behavioral model for cases where the factors of safety are greater than or equal to

1.0. When the overall factor of safety is less than 1.0, the linear elastic model and the limit equilibrium method of slices give similar answers. The elasto-plastic model will seek a slip surface location where the factor of safety is 1.0.

The agreement shown in this comparative study confirms that linear elastic stresses can provide a reasonable representation of the stresses at failure for a wide range of conditions. Therefore, linear elastic stresses will likely continue to be found in general usage for limit equilibrium slope stability analysis.

2.6 Bibliography

Baker, R. 1980. Determination of the critical slip surface in slope stability computations. International Journal For Numerical and Analytical Methods in Geomechanics, 4(4): 333-359.

Bellman, R. 1957. Dynamic Programming. Princeton University Press, Princeton, N.J.

Bishop, A.W. 1955. The use of the slip circle in the stability analysis of slopes. Geotechnique, 5(1): 7-17.

Fredlund, D.G., and Rahardjo, H. 1993. Soil Mechanics for Unsaturated Soils. John Wiley & Sons, Inc., New York, N. Y.

Fredlund, D.G., Krahn, J., and Pufahl, D.E. 1981. The relationship between limit equilibrium slope stability methods. *In* Proceedings of the International Conference on Soil Mechanics and Foundations Engineering. Stockholm, Sweden, Vol.3, pp. 409-416.

Fredlund, D.G., Scoular, R.E.G., and Zakerzadeh, N. 1997. Using finite element stress analysis to compute the factor of safety. *In* 52nd Canadian Geotechnical Conference. Regina, Saskatchewan, Canada, pp. 73-80.

Huang, S.L., and Yamasaki, K. 1993. Slope failure analysis using local minimum factor of safety approach. Journal of Geotechnical Engineering, ASCE, 119(12): 1974-1987.

Itasca Consulting Group, I. 1994. FLAC - Fast Lagrangian Analysis of Continua. Version 4.0, Minneapolis, MN.

Kohgo, Y., and Yamashita, T. 1988. Finite element analysis of fill type dams - Stability during construction by using the effective stress concept. *In* Conference on Numerical Methods in Geomechanics, Innsbruck, pp. 1315-1322.

Morgenstern, N.R., and Price, V.E. 1965. The analysis of slope stability of general slip surfaces. Geotechnique, 15(1): 79-63.

Naylor, D.J. 1982. Finite Elements and Slope Stability. *In* Numerical Methods in Geomechanics, Proceedings of the NATO Advanced Study Institute. Vimeiro, Port. D. Reidel Public Co, Dordrecht, Netherlands, Vol.92, pp. 229-244.

Pham, H.T.V. 2002. Slope Stability Analysis Using Dynamic Programming Method Combined With a Finite Element Stress Analysis. Thesis, University of Saskatchewan, Saskatoon, Canada.

Pham, H.T.V., and Fredlund, D.G. 2003. The application of dynamic programming to slope stability analysis. Canadian Geotechnical Journal, 40(4): 830-847.

Sarma, S.K. 1973. Stability analysis of embankments and slopes. Geotechnique, 23(3): 423-433.

Scoular, R.E.G. 1997. Limit equilibrium slope stability analysis using a stress analysis. Thesis, University of Saskatchewan, Saskatoon, Canada.

Snitbhan, N., and Chen, W.-F. 1978. Elastic-plastic large deformation analysis of soil slopes, 9(6): 567-577.

Spencer, E. 1967. A method for analysis of the stability of embankments assuming parallel interslice forces. Geotechnique, 17(1): 11-26.

Stianson, J., Chan, D., and Fredlund, D.G. 2004. Comparing slope stability analysis based on linear elastic or elasto-plastic stresses using dynamic programming techniques. *In* 57th Canadian Geotechnical Conference. Quebec City, Quebec, Canada, Session 7c, pp. 23-30.

Terzaghi, K., and Peck, R.B. 1948. Soil Mechanics in Engineering Practice. John Wiley & Sons, Inc., New York, N. Y.

Toufigh, M.M. 1997. Finite element modelling of embankment stability. International Journal for Engineering Modelling, 10(1-4): 57-62.

Yamagami, T., and Ueta, Y. 1988b. Search for critical slip lines in finite element stress field by dynamic programming. *In* Proceedings of the 6th International Conference on Numerical Methods in Geomechanics. Innsbruck, pp. 1347-1352.

Zienkiewicz, O.C., Humpheson, C., and Lewis, R.W. 1975. Associated and non associated visco-plasticity and plasticity in soil mechanics. Geotechnique, 25(4): 671-689.

Zou, J.Z., Williams, D.J., and Xiong, W.L. 1995. Search for critical slip surfaces based on finite element method. Canadian Geotechnical Journal, 32(2): 233-246.

Chapter 3

The Role of Admissibility Criteria in Stress-Based Slope Stability Methods

3.1 Introduction

The development of slope stability methods where the factor of safety is computed based on stresses from a finite element analysis provide a number of advantages when compared to conventional method of slices techniques. Fredlund and Scoular (1997) report that the factor of safety equation is determinate and linear indicating that no additional assumptions are required regarding the internal forces acting on the sliding mass. Therefore, iterative procedures are not required to compute the factor of safety. Pham and Fredlund (2003) recognized that reducing the complexity of the factor of safety calculation and a priori knowledge of the internal stress distribution provides the ability to adopt more advanced searching procedures and integrate kinematic admissibility criteria to govern the search for the critical slip surface. The end result is a slope stability method that does not require assumptions regarding the shape of potential slip surfaces; rather, the shape of the slip surface becomes part of the slope stability evaluation.

The internal stress distribution is commonly generated using the "switch-on" gravity technique assuming isotropic linear elastic soil behavior. Young's modulus and Poisson's ratio are often assigned at random with little knowledge of how the values will impact the slope stability calculations. Sensitivity studies are sometimes performed as part of the stability analysis to determine if the factor of safety is

sensitive to the selection of Young's modulus or Poisson's ratio. The selection of appropriate values could be simplified if the variability in the factor of safety is low. If the variability in the factor of safety is high, it might mean that more effort is required to determine the most appropriate values to be used in combination with a stability analysis. Most researchers agree that Young's modulus has little to no influence (< 3%) on computed factors of safety (Table 3.1). However, there appears to be different views regarding the overall influence of Poisson's ratio (Table 3.1). In some cases, the factor safety is reported to vary by less than 5% while in other cases the factor of safety is shown to vary by more than 20%.

One of the main objectives of this paper is to determine the influence that Poisson's ratio and Young's modulus might have on finite element slope stability calculations. This part of the study is limited to normally consolidated slopes (i.e., stress conditions generated by the 'switch on' gravity method.) to remain consistent with the types of analyses considered in previous research. The results from a sensitivity study are used to discuss previous experience regarding the influence of Poisson's ratio. The study goes on to examine if a linear elastic stress analysis can be used to capture the collapse process in overconsolidated soil conditions. Discussion is also provided regarding the merits related to the strict application of kinematic admissibility criteria in the dynamic programming searching procedure and the potential to violate kinematic admissibility if searching procedures like the grid and radius method are used.

3.2 Background

A number of studies have been completed to investigate the influence of Poisson's ratio and Young's modulus on the factor of safety calculations (Table 3.1). The slope conditions range from cases such as dams and other embankments, to representative cases including homogeneous and layered slopes. The internal stresses are generated for a range of conditions including excavated slopes, built-up slopes and embankments where gravity forces are 'switched on'. The internal stress distribution

for a particular slope is recalculated a number of times using different values for Poisson's ratio and Young's modulus. Slope stability calculations are completed for each case and the overall variation in the factor of safety is recorded. The factor of safety from various method of slices procedures have been used to provide a context to the results to discover clear trends between finite element based slope stability calculations and method of slices analyses.

Table 3.1 provides a summary of information regarding the range of Poisson's ratios considered in each sensitivity study, the maximum variation in the factor of safety resulting from the selection of different values for Poisson's ratio and the maximum variation in the factor of safety as a result of selecting various values for Young's modulus. Most researchers agree that Young's modulus has little to no influence on the factor of safety for homogeneous conditions and minimal influence (< 3%) on the factor safety for layered conditions (i.e., layers with contrasting Young's modulus values.) (Wang and Sun 1970). Therefore, most of the attention was directed towards studying the influence of Poisson's ratio. Figures illustrating the relationship between the computed factors of safety and Poisson's ratio were presented in addition to recording the maximum variation in the factor of safety.

Table 3.1: Previous studies regarding the influence of Poisson's ratio on limit equilibrium slope stability calculations.

Author	Range of Poisson's ratio	Maximum variation in the factor of safety (%)	
		Poisson's ratio	Young's modulus
Dunlop and Duncan 1970	0.2 - 0.475	-	0
Wang and Sun 1970	0.2 - 0.4	5%	3%
Wright et al. 1973	0.3 - 0.49	6%	-
Fredlund et al. 1997	0.33 and 0.48	1%	-
Fredlund and Scoular 1999	0.33 and 0.48	3%	-
Pham and Fredlund 2003		20%	-
Gitirana Jr. and Fredlund 2003	0.33, 0.43, 0.49	19%	-
Brito et al. 2004	0.3	*	-

* Influence of parameter considered to be significant but value not reported.
- Influence of parameter considered to be negligable but value not reported.

There appears to be some debate regarding the influence of Poisson's ratio on factor of safety calculations. Early studies seem to indicate that Poisson's ratio does not have a significant influence on the computed factor of safety (Dunlop and Duncan 1970; Wang and Sun 1970; Wright et al. 1973; Fredlund et al. 1997). The latest studies suggest that the factor of safety might vary as much as 20% depending on the value selected for Poisson's ratio. The main difference between slope stability methods developed after 1999 is the use of kinematic admissibility criteria to govern the search for the critical slip surface. Slope stability methods developed prior to Pham and Fredlund (2003) assumed that the slip surface was circular. Circular slip surfaces were assumed to be kinematically admissible and no specific checks were performed to confirm the assumption. The following section provides more detail related to the application of kinematic admissibility criteria when the shape of the slip surface is computed as well as the importance of checking for admissibility when the shape of the slip surface is assumed.

3.3 Admissibility Criteria Developed to Govern the Shape of Potential Slip Surfaces

Admissibility criteria can be viewed as a set of rules used to govern the shape of slip surfaces considered in the slope stability analysis. The goal is to select the admissibility criteria that can be used to simulate actual slope stability failures. Admissibility criteria are typically selected to provide a balance between the flexibility that is required to simulate real cases and difficulties encountered in the numerical techniques used to compute the factor of safety and search for the critical slip surface. The application of admissibility criteria has taken on different forms throughout the development of slope stability methods. One example is the use of trial and error searching procedures where the critical slip surface is assumed to be circular. Another example is the development of criteria to evaluate the admissibility of the circular slip surface resulting from the method of slices analysis. These types of admissibility criteria are based on principles of soil mechanics and force equilibrium and are applied by considering the forces acting on individual slices. The admissibility criteria can be used to identify situations where the slope stability results might not be reliable; such as cases where the mobilized shearing resistance becomes large and negative resulting in negative factors of safety or conditions where the total and effective normal force at the base of a slice is negative to maintain force equilibrium (i.e., state of tension is implied) (Ching and Fredlund 1983). These admissibility criteria can be viewed as secondary criteria and are typically applied once the search for the critical slip surface is complete.

More advanced searching procedures have been developed to permit the application of admissibility criteria during the search for the critical slip surface. Certain admissibility criteria are based strictly on the geometry of the slip surface while others are based on physical principles related to the slope movement or principles of soil mechanics. Admissibility criteria based only on the geometry of the slip surface can be classified as geometric admissibility criteria and admissibility

criteria based on some aspect of the physics of the movement can be classified as kinematic admissibility criteria. Kinematic admissibility criteria are generally more flexible and result in fewer restrictions on the shape of the slip surface. However, the ability to apply kinematic admissibility criteria is influenced by the searching procedure and the procedure used to compute the factor of safety (Stianson 2008). Kinematic admissibility criteria can be applied in cases where dynamic programming is used to search for the critical slip surface and the factor of safety is computed based on stresses generated from a separate stress-deformation analysis. Geometric admissibility criteria are typically easier to apply because no prior knowledge of the internal stress distribution is required.

The use of slope stability methods where the factor of safety is computed based on finite element stresses has resulted in the development of new ways to apply kinematic admissibility criteria. Pham and Fredlund (2003) developed a method where kinematic admissibility criteria can be used to control the shape of the slip surface while the search for the critical slip surface is in progress. The method hinges on the use of dynamic programming to search for the critical slip surface. The kinematic admissibility criterion used to control the shape of the slip surface is based on the principle that resisting forces acting along a slip surface must act in a direction opposite to the assumed direction of mass movement (i.e., the mobilized shear forces are assumed to act in the direction of movement.). A Mohr's circle analysis is used to identify the direction of the mobilized shear force acting on individual line segments considered in the dynamic programming search. If the mobilized shear stress is in the direction of slope movement the line segment is included in the search; if not, the line segment is excluded from the search (Figure 3.1). The kinematic admissibility criteria used by Pham and Fredlund (2003) is similar to assumptions made in a method of slices analysis in that: 1) the direction of slope movement is assumed at the beginning the analysis and 2) the mobilized shear force along the base of a slice is required to act in the direction of slope movement.

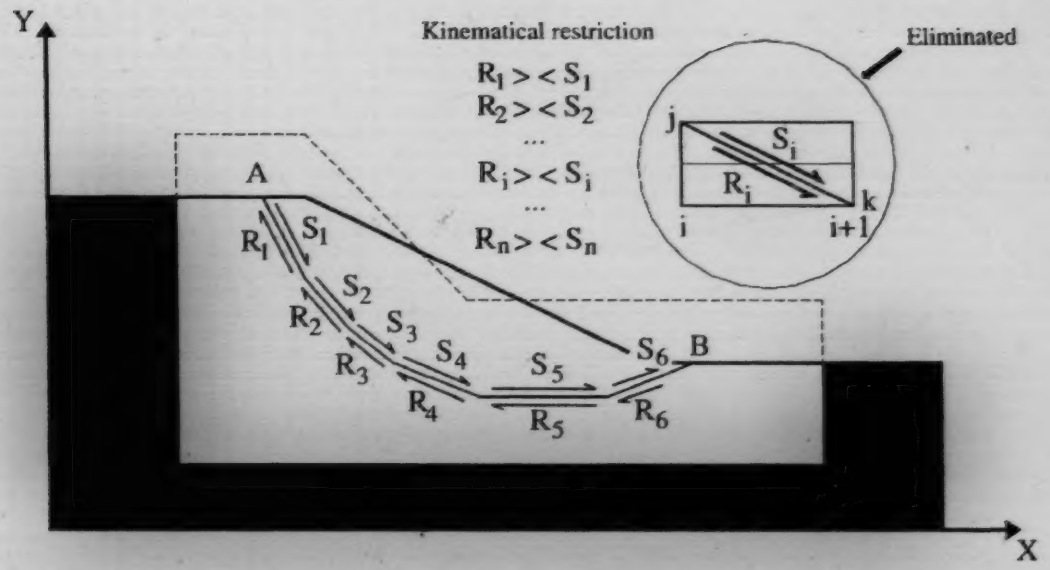

Figure 3.1: A schematic illustrating the application of kinematic admissibility criteria during the dynamic programming search (Pham and Fredlund 2003).

Slip surfaces generated using geometric admissibility criteria are not necessarily kinematically admissible. Circular slip surfaces considered in a "grid and radius" search are often assumed to be kinematically admissible even though no specific checks are performed to confirm the assumption. A number of examples are considered in the current study to investigate whether or not there might be cases where circular slip surfaces might violate the kinematic admissibility criteria described in Figure 3.1.

3.4 Influence of Poisson's Ratio on Normally Consolidated Slopes

A sensitivity study was completed to investigate why some reports suggest the influence of Poisson's ratio is less than 10% while other studies report that the factor of safety might vary as much as 20%. The sensitivity study was designed with the objective of identifying at least one slope configuration where the different levels of

sensitivity observed in previous studies could be duplicated. In other words, identify one case where: 1) the influence of Poisson's ratio is less significant when the shape of the slip surface is assumed to be circular and, 2) the influence of Poisson's ratio is more significant when the search for the slip surface is governed using kinematic admissibility criteria. The sensitivity study is divided into two sections according to the procedure used to control the shape of potential slip surfaces. Slip surfaces are assumed to be circular in the first section and dynamic programming is used to search for the shape of the critical slip surface in the second section. The factor of safety is computed based on finite element stresses in both sections.

Figure 3.2 provides a summary of the methodology that was developed to identify slope conditions that might be used to duplicate the controversy observed in previous studies. Experience seems to indicate that the influence of Poisson's ratio might be related to the location of the critical slip surface (i.e., more significant when the slip surface is shallow). The location of the slip surface in a homogeneous slope can be controlled by selecting different combinations of effective cohesion (c') and angle of internal friction (ϕ'). Deeper slip surfaces result when cohesion dominates the strength of the material. The slip surface moves towards the slope face as the cohesion is decreased to zero.

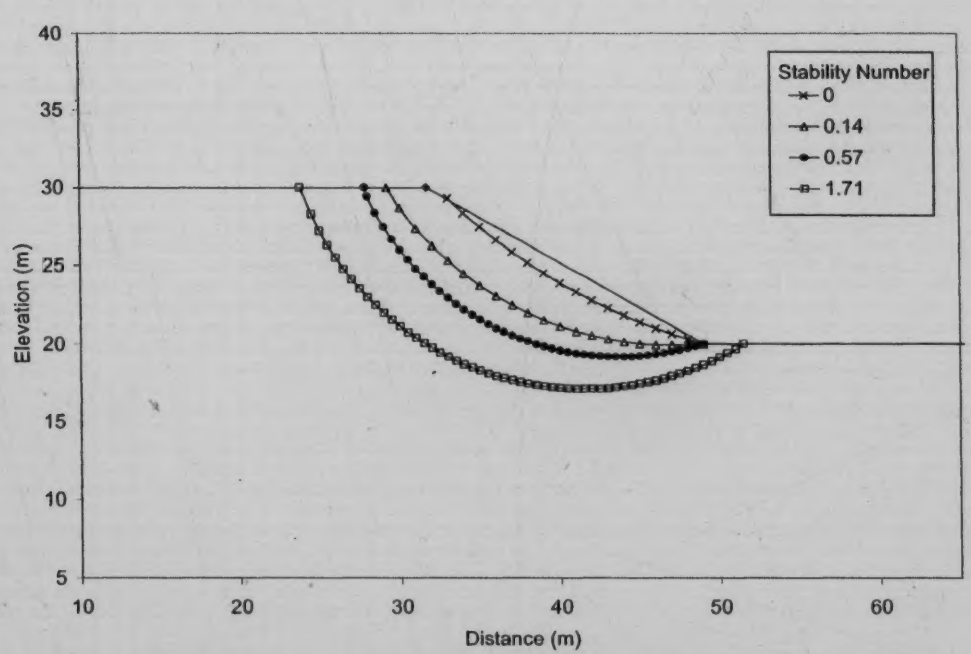

Figure 3.2: Sensitivity study designed to duplicate the controversy observed in previous studies.

A number of c' and ϕ' combinations were considered resulting in deep slip surfaces progressing to conditions where the slip surface approaches the face of the slope. The stability number (N) was calculated for each c' and ϕ' combination, using Eq. [3.1],

$$[3.1] \qquad N = \frac{c'}{\gamma H \tan\phi'}$$

where c' is cohesion, γ is the unit weight, H is the slope height, and ϕ' is the angle of internal friction. Larger stability numbers indicate conditions where cohesion dominates the strength of the soil (i.e., deep slip surfaces) and lower stability numbers indicate conditions where friction dominates the strength of the soil (i.e., shallow slip

surfaces). The angle of internal friction was set to 30 degrees in the stability number equal to zero case to consider the limiting condition where the internal angle of friction is equal to the slope angle.

The internal stress distribution for the slope was generated using an isotropic linear elastic "switch-on" gravity analysis. The internal stresses were re-computed a number of times based on different values of Poisson's ratio ranging from 0.1 to 0.48. Poisson's ratio partially controls the relationship between the horizontal and vertical stress in an isotropic linear elastic analysis. Under no later yield condition for horizontally layered soils, this process generates a Ko value equal to $K_o = \sigma_x/\sigma_y = \nu /(1 - \nu)$). Poisson's ratio were used as a tool to generate a range of stress conditions where Ko varies between 0 and 1.0. For Ko values higher than 1.0, high horizontal stresses were applied on the boundaries. The stability analysis was completed for each Ko condition to evaluate the influence of the internal stress distribution on the factor of safety calculation.

3.4.1 Section No. 1: Influence of Poisson's Ratio when the Slip Surface is Assumed to be Circular

The factor of safety for each c' and ϕ' combination was re-calculated five times using the following values for Poisson's ratio; 0.1, 0.2, 0.3, 0.4, and 0.48. Figure 3.1 illustrates the variability in the factor of safety for the critical slip surface (CSS) corresponding to each stability number. Poisson's ratio is listed along the horizontal axis. The percent difference between the factor of safety computed when Poisson's ratio is equal to 0.48 and the factors of safety computed for the other values of Poisson's ratio (i.e., 0.1, 0.2, 0.3, and 0.4), is listed on the vertical axis.

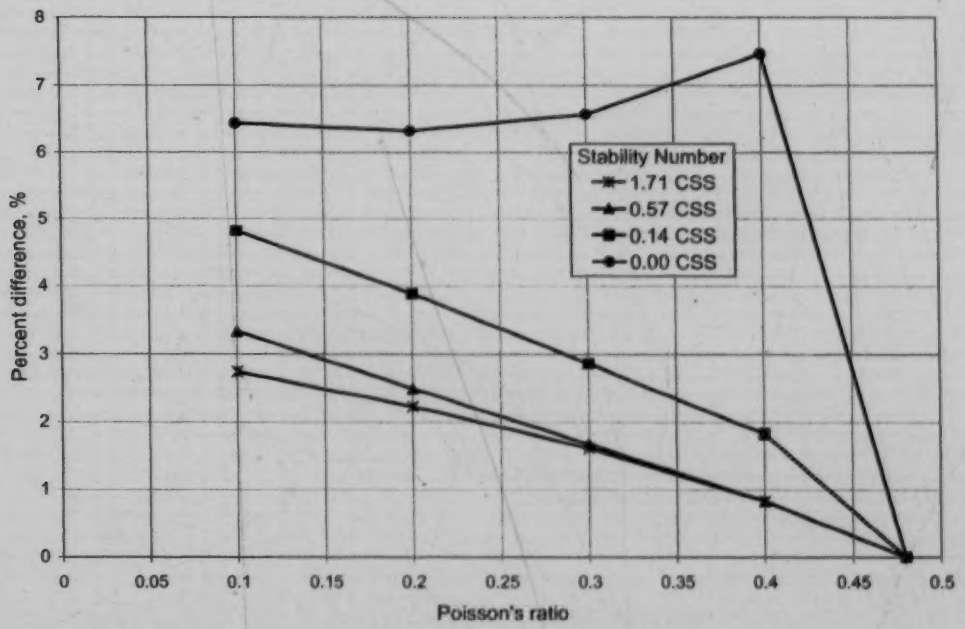

Figure 3.3: Relationship between Poisson's ratio and the factor of safety assuming the shape of the slip surface is circular.

The results seem to follow a trend where the influence of Poisson's ratio becomes more significant as the slip surface becomes shallow (i.e., lower stability number). The maximum variability in the factor of safety is less than 8% and seems to correspond to the results from earlier research listed in Table 3.1.

3.4.2 Section No. 2: Influence of Poisson's Ratio when Kinematic Admissibility Criteria are used to Control the Shape of the Critical Slip Surface.

The sensitivity study described in Figure 3.4 was repeated using a slope stability method where dynamic programming was used in combination with kinematic

admissibility criteria to search for the critical slip surface. The results are presented in Figure 3.4 following the same form as the previous section. Poisson's ratio is plotted along the horizontal axis. The vertical axis lists the difference between the factor of safety computed for the case where Poisson's ratio is equal to 0.48 and the factors of safety computed using other values of Poisson's ratio (i.e., 0.1, 0.2, 0.3, and 0.4). The relationship between Poisson's ratio and the factor of safety is plotted for each stability number.

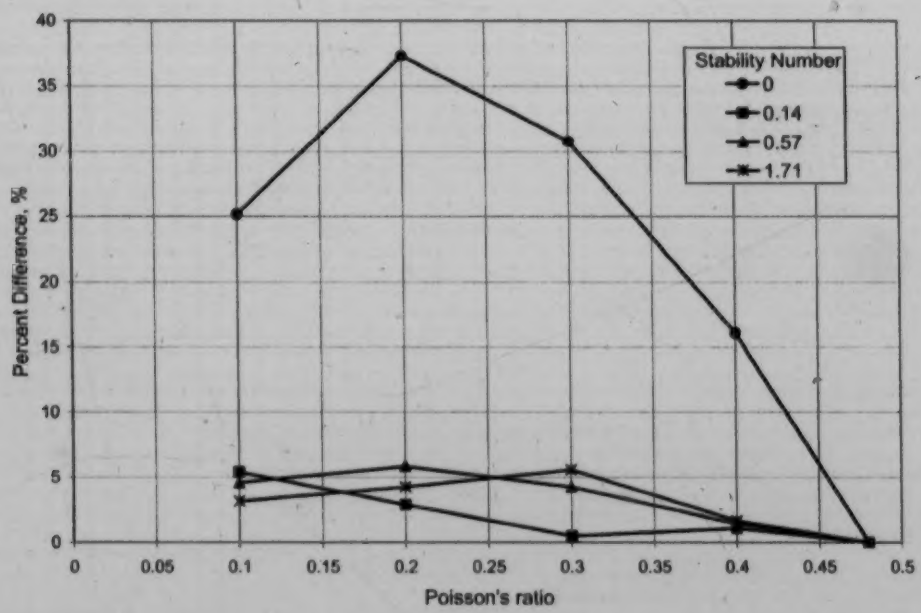

Figure 3.4. Relationship between Poisson's ratio and the factor of safety for the case where the shape of the slip surface is controlled using kinematic admissibility criteria.

The variability in the factor of safety is similar to the results reported in the previous section (< 8%) for the cases where the stability number is greater than or equal to 0.14. However, the maximum variability in the factor of safety occurs for the case where the stability number is equal to zero. The difference is higher than 35%. The stability number equal to zero case is one example that can be used to duplicate the differences observed in previous studies. It appears that the influence of Poisson's

ratio is related to the type of admissibility criteria applied during the search for the critical slip surface.

Figure 3.5 through 3.8 display the variability in the shape and location of the critical slip surface when dynamic programming is combined with kinematic admissibility criteria to search for the critical slip surface. Each figure displays a family of slip surfaces corresponding to the values of Poisson's ratio selected in the finite element stress analysis. There are a total of six slip surfaces on each figure, one for each value of Poisson's ratio (5) and the critical slip surface identified using the Morgenstern-Price (1965) method of slices technique.

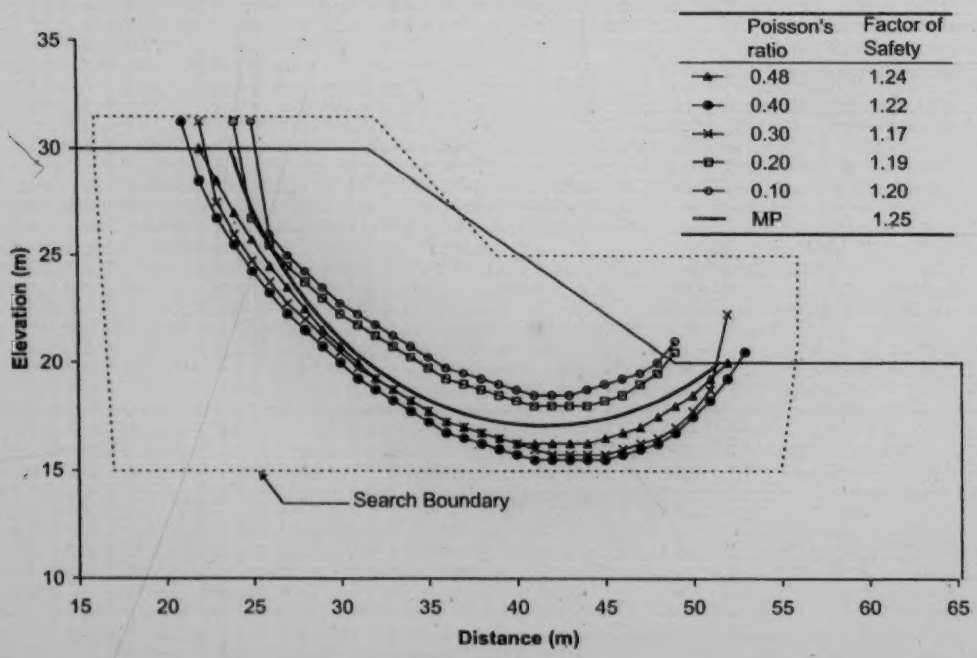

Figure 3.5: Family of slip surfaces for the case where the stability number is equal to 1.71.

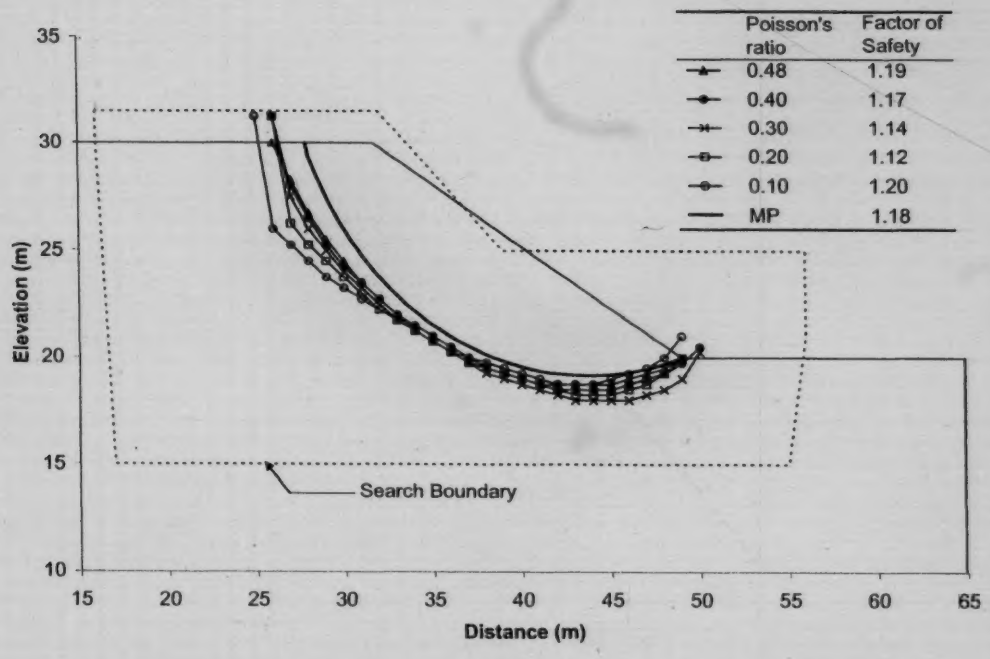

Figure 3.6: Family of slip surfaces for the case where the stability number is equal to 0.57.

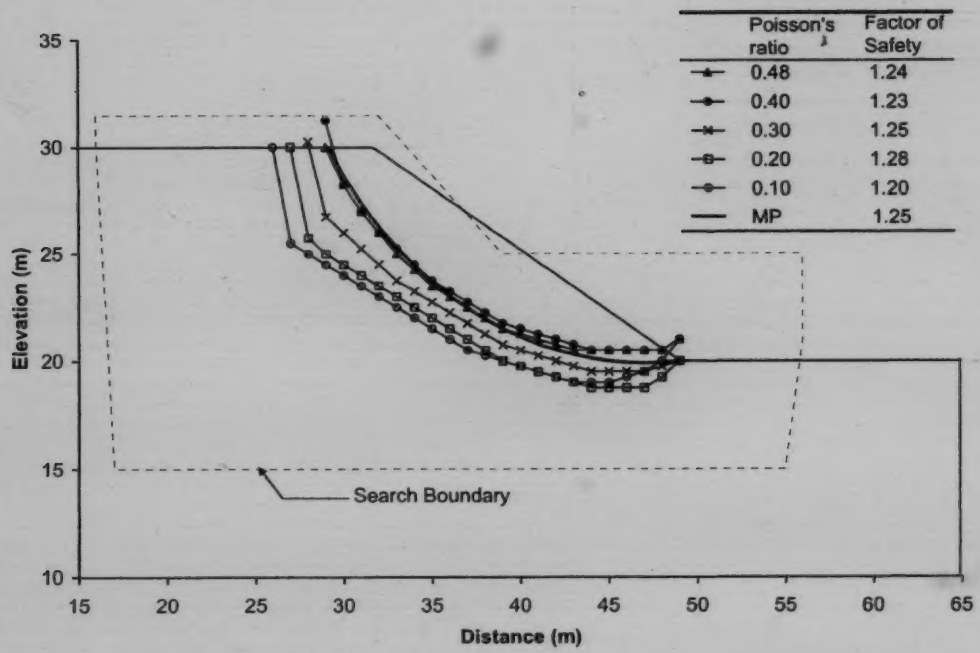

Figure 3.7: Family of slip surfaces for the case where the stability number is equal to 0.14.

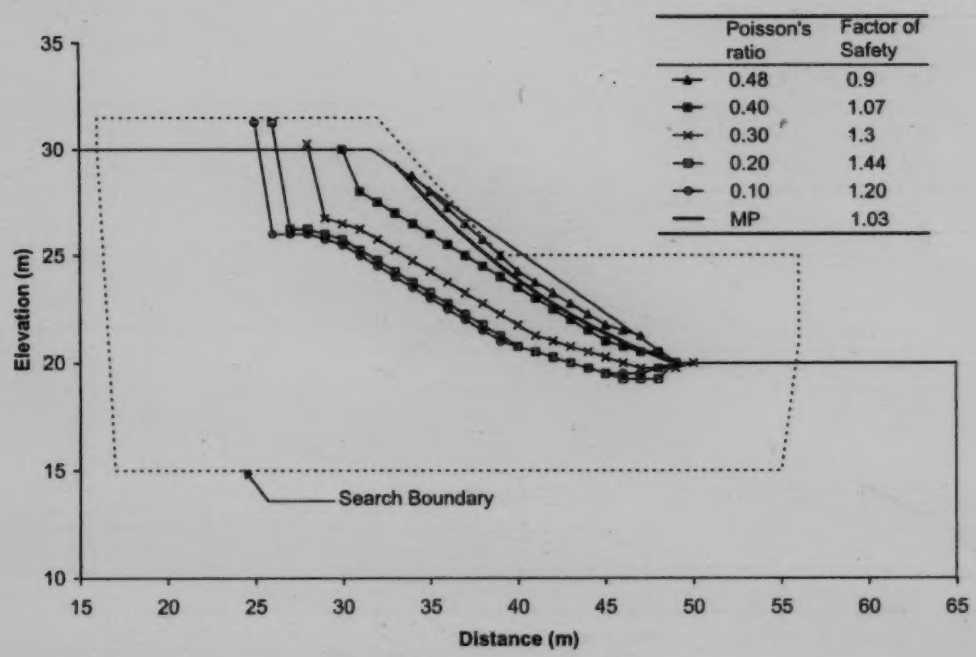

Figure 3.8: Family of slip surfaces for the case where the stability number is equal to zero.

The family of slip surfaces for each stability number follow the general behavior illustrated in Figure 3.2 in that deeper slip surfaces correspond to larger stability numbers. The variability in the shape and location of the critical slip surface seems to fluctuate for different stability numbers. The shape of the slip surfaces is relatively consistent when the stability number is greater than zero. However, there are large differences in the shape and location of the critical slip surface for the case where the stability number is equal to zero. It is interesting to point out that these conditions are also difficult to evaluate using the method of slices. The conditions generally result in shallow localized slip surfaces making it difficult to determine the factor of safety for a global failure condition. A global slip surface is often investigated by artificially increasing the cohesion of the material by small amounts (i.e., 1 to 5 kPa for example.). Increasing the cohesion typically results in a deeper slip surface with a higher factor of safety. The increase in the factor of safety resulting from a small

increase in the cohesion is considered acceptable in return for the ability to investigate the desired global failure condition. A similar procedure was required for the case where Poisson's ratio is equal to 0.48. The search grid was designed to keep the slip surface from rising too close to the slope face resulting in a similar location to the critical slip circle identified by the Morgenstern and Price analysis.

The tendency for the slip surface to rise to the slope face can be explained considering the Mohr-Coulomb failure envelope shown in Figure 3.9. The failure envelope is elevated at the angle of internal friction and passes through the origin when cohesion is equal to zero. The Mohr's circles shown in Figure 3.9 represent potential stress states for a soil element on or near the slope face. The minimum principal stress for a soil element near the slope face is close to zero. The Mohr's circle passes close to the origin and intersects the failure envelope.

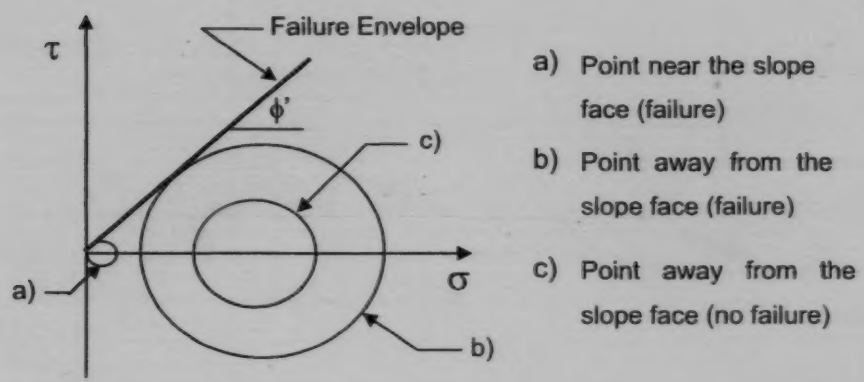

Figure 3.9: Conceptual Mohr-Coulomb failure envelope for a cohesionless material.

The results presented in Figure 3.8 are not consistent with the behavior described above. The critical slip surface is near the slope face when Poisson's ratio is close to 0.5 but moves deeper into the slope as Poisson's ratio is decreased to 0.1, even though the stability number is equal to zero. These results provide evidence that there might be difficulties associated with the strict application of kinematic admissibility criteria during the search for the critical slip surface. It is interesting to note that the critical

slip surface follows the anticipated behavior regardless of the value selected for Poisson's ratio if the search for the critical slip surface is carried out using the grid and radius method where no kinematic admissibility checks are applied. The following section describes a procedure that was developed to evaluate the interaction between the admissibility criteria adopted in the searching procedure and the internal stress distribution computed from the stress-deformation analysis.

3.5 The use of 'Admissibility Plots' to Illustrate the Interaction between the Internal Stress Distribution and the Application of Kinematic Admissibility Criteria

Information gathered during a dynamic programming search can be used to create plots illustrating the influence of the admissibility criteria on the overall slope stability calculations. A significant number of line segments can be evaluated during the search for the critical slip surface. The line segments are created by joining two points from the dynamic programming search grid. It is possible to record the admissibility and local factor of safety for each line segment. The information can be used to identify the combination of line segments resulting in the critical admissible path to any point on the dynamic programming search grid. Plotting the critical path to every point on the search grid is one way to illustrate the interaction between the internal stress distribution and admissibility criteria applied during the search for the critical slip surface. These plots can be used to gain a general understanding regarding the critical trends associated with the overall admissibility of the system and can be referred to as 'admissibility plots'. Urciuoli and Picarelli (2004) use a similar type of plot to illustrate the rotation of failure planes predicted by Mohr's theory during the development of slope failure. It is important to point out that 'admissibility plots' only show a sample of the total number of admissible line segments considered in the dynamic programming search. It would not be possible to distinguish between line segments if all of the admissible line segments were included

in the admissibility plot. Similarly, line segments connecting grid points outside the boundaries of the slope are not included to remove unnecessary clutter. All of the admissibility plots presented below were generated using the same dynamic programming search grid to provide a consistent basis for comparison.

Figure 3.10 and 3.11 are the admissibility plots for the case where Poisson's ratio is equal to 0.48 and the stability numbers are equal to 1.71 and zero, respectively. The critical slip surfaces are included to illustrate the relationship to the overall admissibility of the system.

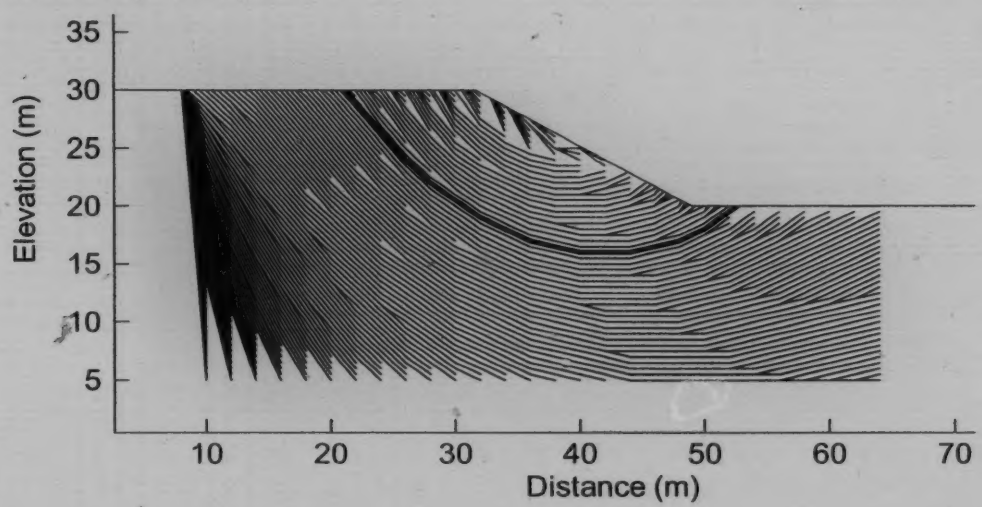

Figure 3.10: Admissibility plot for the case where Poisson's ratio is equal to 0.48 and the stability number is equal to 1.71 ($F_s = 1.24$).

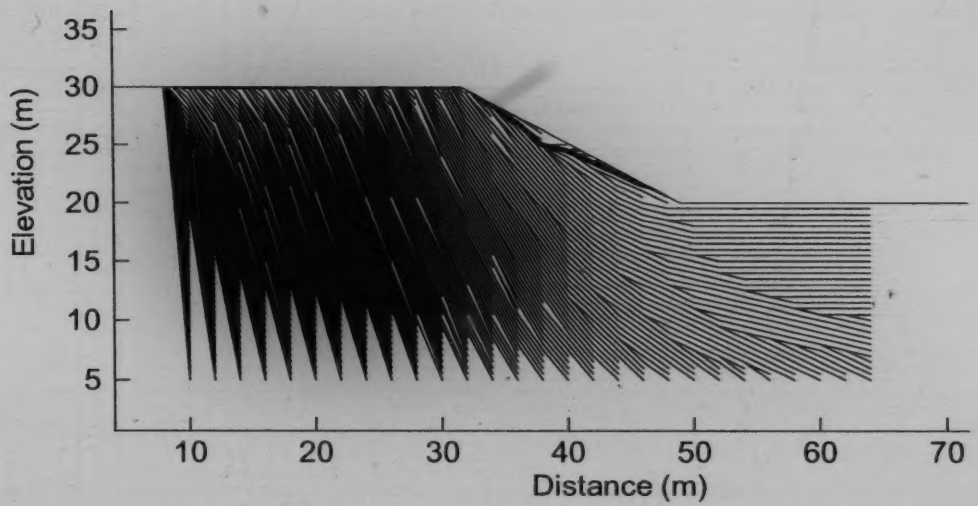

Figure 3.11: Admissibility plot for the case where Poisson's ratio is equal to 0.48 and the stability number is equal to 0 ($F_s = 0.75$).

The admissibility plots confirm that slip surfaces can be expected to be circular for the case where the stability number is equal to 1.71 and slip surfaces can be expected to take on planar characteristics when the stability number is equal to zero. There are a large number of line segments surrounding the critical slip surface in both cases indicating that the search is not restricted due to the presence of inadmissible line segments in critical areas of the slope.

Figure 3.11 and 3.12 are the admissibility plots for the case where Poisson's ratio is equal to 0.1 and the stability numbers are equal to 1.71 and zero, respectively. There is a significant reduction in the number of line segments surrounding the critical slip surface in both cases. It appears that the selection of Poisson's ratio has a significant influence on the admissibility of line segments in certain areas of the slope. The reduction in the number of admissible line segments near the crest of the slope is likely the cause of the variability in the location of the slip surface shown in Figure 3.7 (N = 1.71). It appears that the entry of the slip surface is forced closer to the crest of the slope for the cases where Poisson's ratio is less than 0.3. Pushing the entry point closer to the crest seems to have resulted in shallower slip surfaces. The

restrictions seem to be less significant when the stability number is equal to 0.15 and have the opposite effect when the stability number is 0.14. The admissibility plots seem to be useful in explaining why there is more variability in the location of the slip surface in some cases but not in others (i.e., Figure 3.5, Figure 3.6, Figure 3.7, and Figure 3.8).

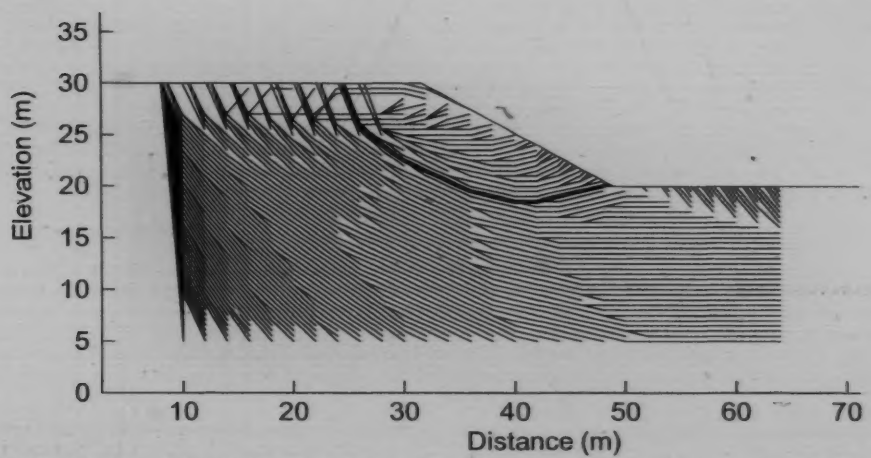

Figure 3.12: Admissibility plot for the case where Poisson's ratio is equal to 0.1 and the stability number is equal to 1.71 ($F_s = 1.22$).

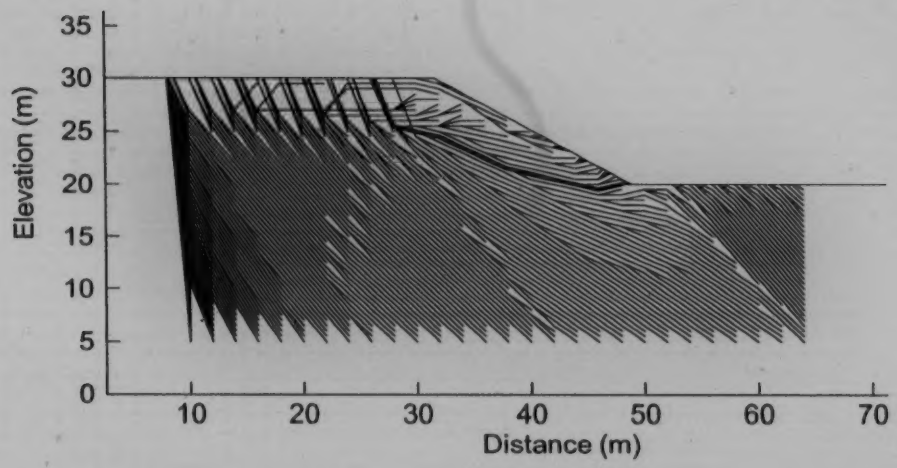

Figure 3.13: Admissibility plot for the case where Poisson's ratio is equal to 0.1 and the stability number is equal to 0 ($F_s = 1.44$).

The reduction in the number of admissible line segments when Poisson's ratio is equal to 0.1 seems to have a significant impact on the location of the critical slip surface when the stability number is equal to zero. Previous discussions indicate that the slip surface should rise to the ground surface when the material is cohesionless and the internal angle of friction is equal to the slope angle. Figure 3.13 illustrates that there are a small number of admissible line segments near the slope face. A close evaluation of those line segments reveals that there is no combination of admissible line segments to provide a continuous slip surface. Some slip surfaces end abruptly before exiting the slope and others have not entry point near the crest of the slope. As a result, the search for the critical slip surface is forced deeper into the slope. The critical slip surface shown in Figure 3.13 is nearly the shallowest set of line segments that can be combined to form a continuous slip surface.

3.5.1 Interaction between Stress Rotation and Admissibility Criteria

The admissibility plots presented above demonstrate that the admissibility of line segments in certain areas of the slope can be affected by the selection of Poisson's ratio. Poisson's ratio, v, partially controls the relationship between the horizontal and vertical stresses and can influence the orientation of the principal stresses. Figure 3.14 demonstrates conceptually how the slope stability calculations can be affected if the orientation of the principal stress is rotated.

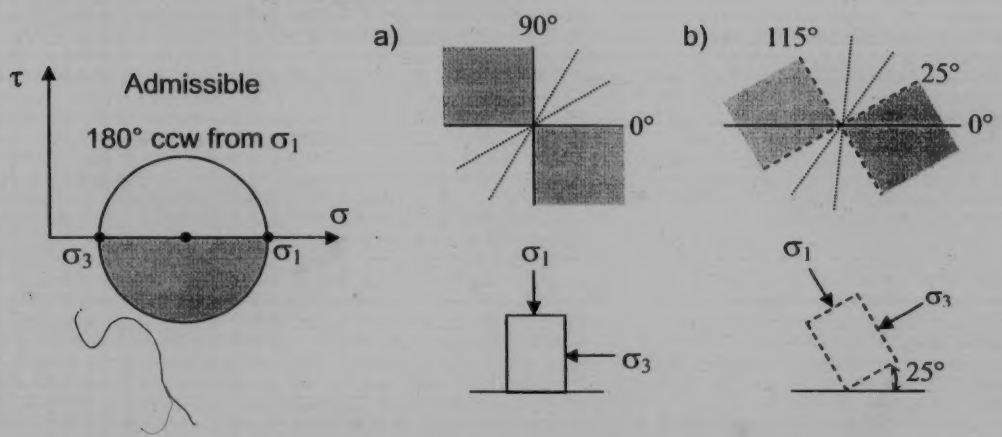

Figure 3.14: Conceptual illustration of how stress rotations can influence the admissibility of line segments considered in the dynamic programming search.

First, let us assume that positive shear stresses correspond to the assumed direction of failure. Therefore, line segments with positive shear stresses are admissible and line segments with negative shear stresses are not admissible. According to Mohr's circle, line segments will have positive shear stress if oriented at angles between 0 and 180 degrees measured counter clockwise (ccw) from the plane where σ_1 acts (or clockwise from the plane where σ_3 acts). Line segments considered in the slope stability analysis will be admissible if oriented at angles between 0 and 90 degrees since angles measured on Mohr's circle are twice the angle measured in reality (i.e., Principal stresses are 90 degrees apart on the soil element which

corresponds to 180 degrees in Mohr's circle.). Let us suppose that scenarios a) and b) represent an element of soil at the same point near the toe of a slope. The internal stress distribution in scenario a) was generated using one value for Poisson's ratio while the internal stresses in scenario b) were generated using a different value of Poisson's ratio. The actual values for Poisson's ratio are not important for this discussion. The main point is that the procedure used to generate the stresses in scenario b) resulted in the rotation of the principal stresses.

In scenario a), σ_1 acts on a horizontal plane. Therefore, line segments oriented between 0 and 90 degrees measured counter clockwise from a horizontal plane are admissible. Two arbitrary admissible line segments are shown along with the shaded zone with no admissible line segments. In scenario b), σ_1 acts on a plane elevated at 25 degrees (ccw) from the horizontal. Therefore, line segments oriented between 25 and 115 degrees are admissible. The discussion demonstrates how the orientation of the principal stresses can influence the orientation of admissible line segments. In this case, admissible line segments in scenario b) are steeper than admissible line segments in scenario a). It should be noted that the line segments considered in the dynamic programming search are created by joining two points from the dynamic programming search grid. In some cases, the rotation of the principal stresses and the grid spacing selected in the dynamic programming search can result in the exclusion of certain line segments as shown in Figure 3.12 and 3.13.

The exclusion of individual line segments based on the strict application of kinematic admissibility criteria could be viewed as a negative characteristic of the dynamic programming searching procedure. It might seem more reasonable to modify the procedure to accept a certain number of inadmissible line segments, providing that the overall slip surface is admissible, in an attempt to reconcile the results illustrated in Figure 3.8. Another alternative is that the kinematic admissibility criterion is being applied properly and the results in Figure 3.8 and the admissibility plot in Figure 3.13 provide evidence that the linear elastic analysis might not provide a reasonable representation of the characteristics of the internal stresses at failure.

Urciuoli (2002) describes the development of collapse as a process where both principal stresses and failure surfaces predicted by Mohr's theory rotate to become kinematically compatible with the geometry of the slope. Naylor (1982) warned that care should be taken in deriving the shape of the slip surface based on the results of a linear elastic analysis because the orientation of the stress field might not result in the proper alignment of failure planes predicted by Mohr's theory. Urciuoli (2002) goes on to suggest that an elasto-plastic analysis might provide a better representation of the stress field because the stress redistribution resulting from local failure results in the rotation of the stress field to an orientation that promotes the development of a continuous slip surface. The stability number equal to zero case was re-analyzed based on stresses from an elasto-plastic analysis and compared to the linear elastic results.

Figure 3.15 illustrates the family of slip surfaces computed using elasto-plastic stresses for the stability number equal to zero case. It appears that using elasto-plastic stresses has corrected the problems associated with Figure 3.8. All of the slip surfaces approach the slope face regardless of the value selected for Poisson's ratio and there is no longer significant variation in the computed factor of safety.

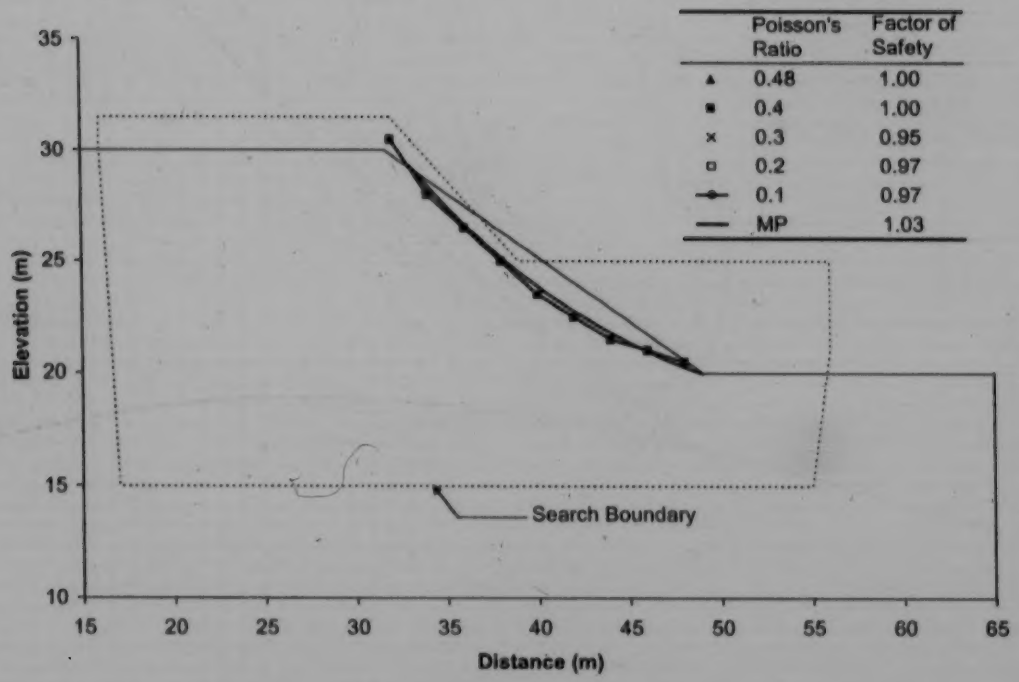

Figure 3.15: Family of slip surfaces computed based on elasto-plastic stresses for the stability number equal to zero case.

Figure 16 represents the admissibility plot generated based on elasto-plastic stresses for the case where Poisson's ratio is equal to 0.1 and the stability number is equal to zero. The results can be directly compared to Figure 3.13 which represents the same case but is generated using linear elastic stresses. The results confirm that the elasto-plastic analysis promotes a dramatic increase in the number of admissible line segments and the number of continuous slip surfaces in critical areas of the slope (i.e., near the slope face.).

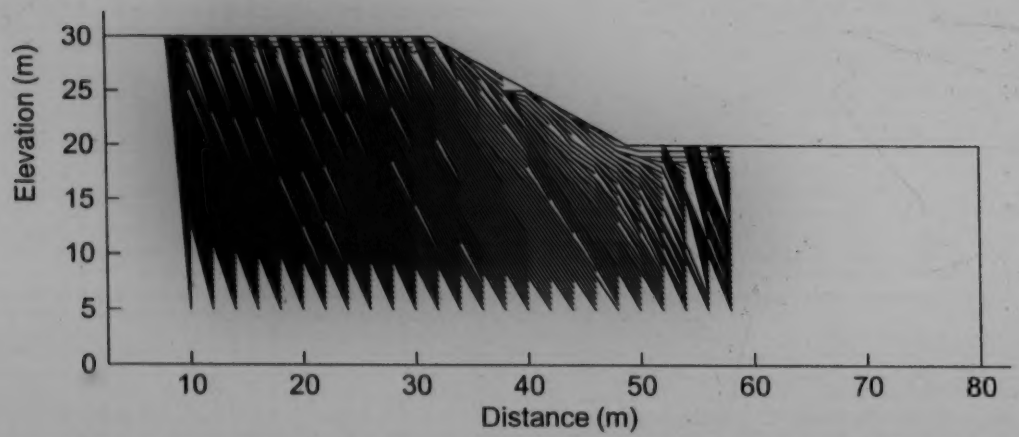

Figure 3.16: Admissibility plot for the case where Poisson's ratio is equal to 0.1 and the stability number is equal to 0 ($F_s = 0.67$).

Figure 3.17 compares the angle to the minor principal stress computed using an elasto-plastic or linear elastic stress analysis for a random selection of points near the slope face (Angle of 60° is perpendicular to the slope face.). The results confirm that there can be significant differences in the orientation of the principal stresses between linear elastic or elasto-plastic stress analyses. The results provide further evidence that the orientation of the principal stresses predicted in the stress-deformation analysis can significantly influence the subsequent slope stability calculations. It appears that a linear elastic stress-deformation analysis does not provide a reasonable representation of the internal stress distribution for this example.

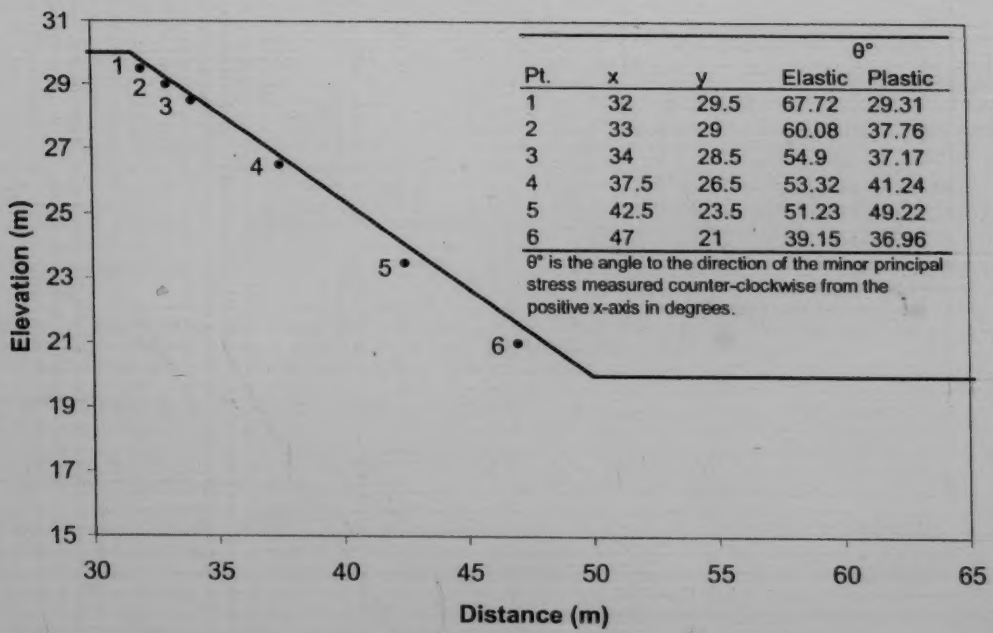

Pt.	x	y	θ° Elastic	θ° Plastic
1	32	29.5	67.72	29.31
2	33	29	60.08	37.76
3	34	28.5	54.9	37.17
4	37.5	26.5	53.32	41.24
5	42.5	23.5	51.23	49.22
6	47	21	39.15	36.96

θ° is the angle to the direction of the minor principal stress measured counter-clockwise from the positive x-axis in degrees.

Figure 3.17: Comparison of the angle to the direction of the minor principal stress computed using an elasto-plastic or linear elastic stress-deformation analysis.

3.5.2 Interaction between Kinematic Admissibility Criteria and the Internal Stress Distribution for 0verconsolidated Slopes

Poisson's ratio has been shown to influence the relationship between the horizontal and vertical stress in normally consolidated soil modeled using a "switch-on" gravity analysis (i.e., $K_o = \sigma_x/\sigma_y = \nu/(1 - \nu)$). The coefficient of lateral earth pressure at rest (K_o) could vary between 1 and 0 for the values of Poisson's ratio considered in the previous analysis. This variation could be viewed as insignificant considering that K_o can be much higher in many overconsolidated soil deposits. It seems reasonable to

extend the analysis to consider overconsolidated slope conditions with the objective of determining if the differences between linear elastic and elasto-plastic slope stability analyses are significantly exaggerated for cases where the variation in K_o is two to three times the values considered previously.

There are many procedures that could be used to generate the initial stress field for various K_o conditions including fluctuation of the water table, removal of surcharge pressure and constant overconsolidated ratio. In this case, an initial linear elastic stress field with a constant overconsolidation ratio (OCR) is generated through the application of external stress boundary conditions applied to the edges of a rectangular block of soil. A slope is excavated in approximately 2m lifts to a depth of 10m creating a slope angle of 30 degrees. The internal stress distribution resulting from the excavation process is solved using linear elastic and an elasto-plastic analysis. Two slope stability analyses are completed, one based on the linear elastic stress field, the other based on the elasto-plastic stress field. Admissibility plots are generated in both cases to illustrate the interaction between the admissibility criteria applied during the dynamic programming search and the internal stress distribution.

Figure 3.18 shows the admissibility plot for the case where the internal stress was computed using a linear elastic analysis. The results confirm that the interaction between the admissibility criteria and a linear elastic approximation of the internal stress distribution in overconsolidated soil conditions is significantly exaggerated when compared to the influence of Poisson's ratio in the previous normally consolidated example (i.e., Figure 3.8). The admissibility plot indicates that the number of admissible slip surfaces is nearly reduced to zero. The reduction in the number of admissible slip surfaces is attributed to the exclusion of individual line segments because the linear elastic stress field results in local failure planes that are not compatible with the formation of a continuous slip surface. The incompatible stress field has resulted in an irregular slip surface with a factor of safety that has been artificially elevated to a value of 1.69.

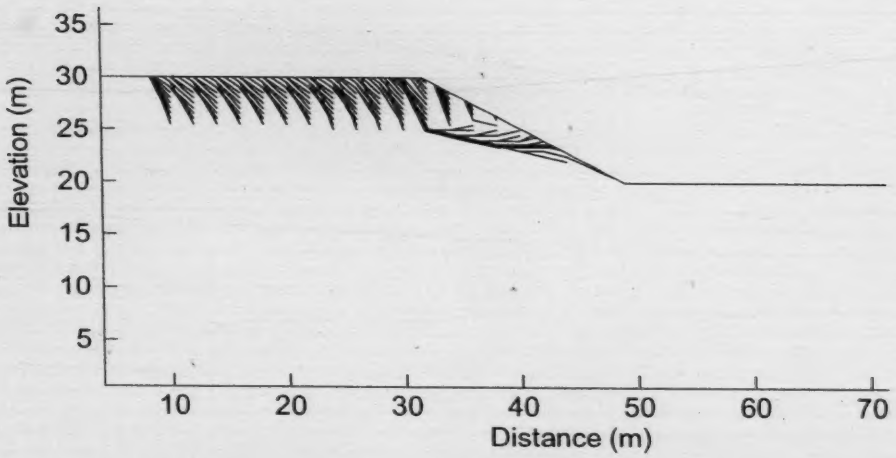

Figure 3.18: Admissibility plot for the case where the internal stresses are computed using a linear elastic analysis for the stability number equal to 1.71 case ($F_s = 1.69$).

The results in Figure 3.19 demonstrate that elasto-plastic analysis provides a better representation of the internal stress distribution. The local failure planes appear to be compatible with the geometry of the slope and promote the development of continuous slip surfaces. The factor of safety has reduced to a reasonable value since the location of the slip surface is no longer influenced by the absence of admissible planes in critical areas of the slope.

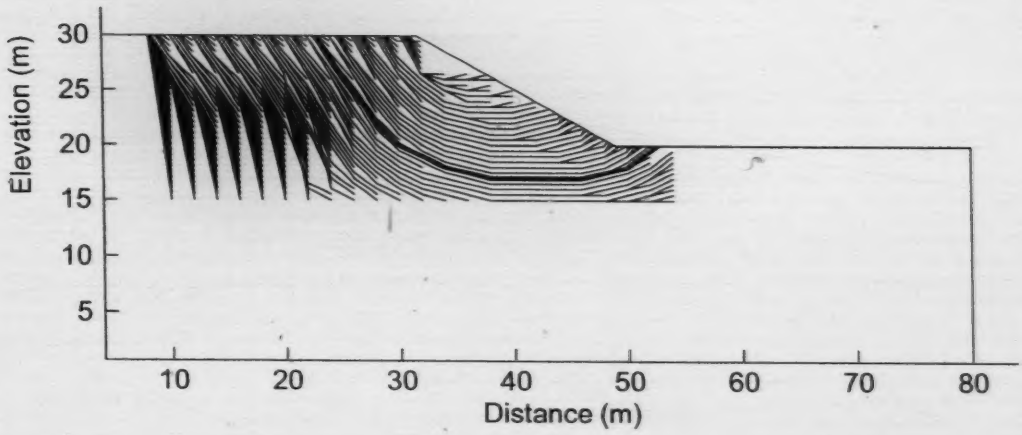

Figure 3.19: Admissibility plot for the case where the internal stresses are computed using an elasto-plastic analysis for the stability number equal to 1.71 case ($F_s = 1.28$).

3.6 Discussion

The results in Figure 3.3 and Figure 3.4 were initially used to explain the different reports regarding the influence of Poisson's ratio on slope stability calculations. It appears that the differences observed in Figure 3.3 and Figure 3.4 can be used to identify conditions where a linear elastic analysis does not provide a reasonable representation of the internal stress distribution to be used in slope stability calculations. Figure 3.3 was presented to confirm the thinking that Poisson's ratio might not have a significant influence on the factor of safety in cases where the shape of the critical slip surface is assumed to be circular (i.e., or any procedure that only considers geometric admissibility, including the 'grid and radius' method.). Those results could be used to argue that the internal stress distribution resulting from a linear elastic analysis is adequate and the variation in the factor of safety observed in Figure 3.4 is due to the application of kinematic admissibility criteria that are too strict. Commercial software is used to re-analyze two cases to explain why it is possible to overlook the problems associated with linear elastic stresses if the search for the critical slip surface is completed using the 'grid and radius' method. Further

discussion of the literature is also provided to support the strict application of kinematic admissibility criteria.

3.6.1 Potential Violation of Kinematic Admissibility using Grid and Radius Searches

A linear elastic "switch-on" gravity analysis was performed to compute the internal stress distribution for the stability number equal to zero case when Poisson's ratio is equal to 0.1. Slope/W™ was used to perform a finite element slope stability analysis where the factor of safety is computed based on the stress distribution from Sigma/W™ and the 'grid and radius' method is used to search for the critical slip surface. The critical slip surface was located near the slope face and the factor of safety was computed to be 0.91, as shown in Figure 3.20. Figure 3.20 also illustrates the shear strength and the shear mobilized for individual line segments along the critical slip surface. The local factor of safety for each line segment is computed by dividing the shear strength by the mobilized shear stress. The information in Figure 3.20, along with the direction of failure assumed at the beginning of the slope stability analysis, makes it possible to evaluate the admissibility of the critical slip surface. The mobilized shear force for each line segment along the slip surface should act in the assumed direction of movement (in this case left to right) to pass the proposed kinematic admissibility criteria. In other words, the mobilized shear stress should be positive. The mobilized shear stress acting on the first three line segments is negative which means that this slip surface is kinematically inadmissible. The presence of inadmissible line segments in an otherwise reasonable slope stability analysis could be used as evidence to suggest that it is acceptable to allow a small number of inadmissible line segments to be included in the slope stability analysis. However, the full implications of including inadmissible line segments is not fully understood without considering the local factor of safety distribution that is ultimately used to compute the overall factor of safety.

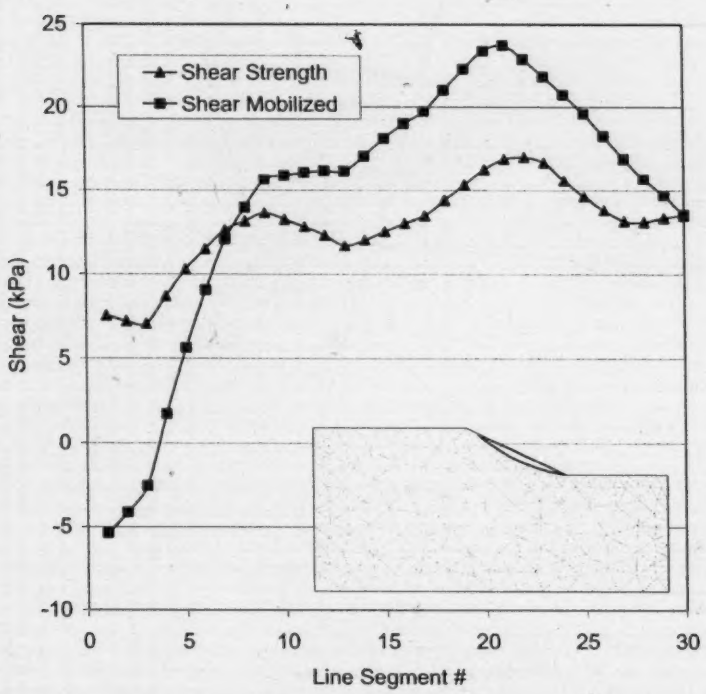

Figure 3.20: Distribution of shear strength and shear mobilized along the critical slip surface for the stability number equal to zero case and Poisson's ratio is equal to 0.1 ($F_s = 0.91$).

The mobilized shear stress and the shear strength for line segment number three are reported to be -2.5667 kPa and 7.0594 kPa, respectively. The shear strength divided by the mobilized shear stress results in a local factor of safety equal to -2.75; however, the slope stability results indicate that the local factor of safety is equal to 5.0. It appears that the local factor of safety has been set to a reasonably large value to indicate that the mobilized shear stress is opposing the movement of the slope resulting in an increased margin of safety.

Figure 3.21 illustrates the slope stability results for the overconsolidated case where K_o is initially equal 3.0. An initial linear elastic stress field with a constant

overconsolidation ratio equal to three is generated through the application of external stress boundary conditions applied to the edges of a rectangular block of soil. A slope is excavated in approximately 1m lifts to a depth of 10m creating a slope angle of 30 degrees. The strength properties correspond to the N = 1.71 case. The impact of including inadmissible planes in the slope stability analysis is significantly exaggerated. The critical slip surface is depressed deep into the slope and the mobilized shear stress is negative on over half of the slip surface corresponding to the line segments where the local factor of safety is shown to be 5.0. All of these factors have resulted in a factor of safety that is artificially elevated to a value of 1.93 when compared to the results shown in Figure 3.5 and Figure 3.19.

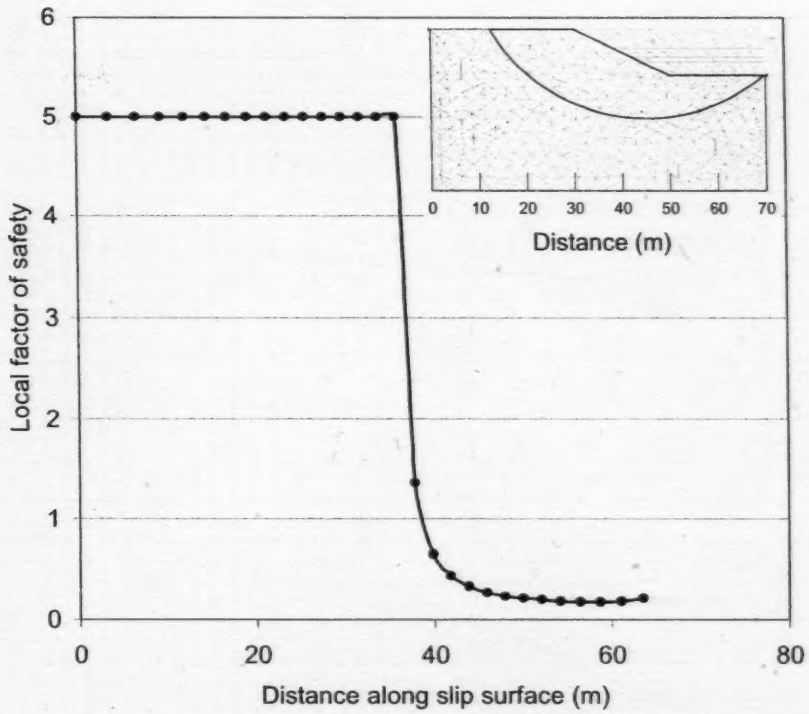

Figure 3.21: Local factor of safety distribution along the circular slip surface computed based on stresses from an linear elastic excavated slope analysis in conditions where Ko is equal 3.0 (F_s = 1.93).

Figure 3.22 illustrates how the results change if the stresses are computed using an elasto-plastic analysis. There are no longer any negative values of mobilized shear stress and the location of the slip surface is more reasonable (The local factor of safety is equal to 5.0 for one line segment but it does not correspond to a case where the mobilized shear stress is negative.) The factor of safety is reduced to 1.52 but is still significantly greater than the factor of safety for the critical slip surface found using dynamic programming (1.27). The results demonstrate the benefits of using searching procedures based on kinematic admissibility criteria that are intimately related to the internal stress distribution of the slope.

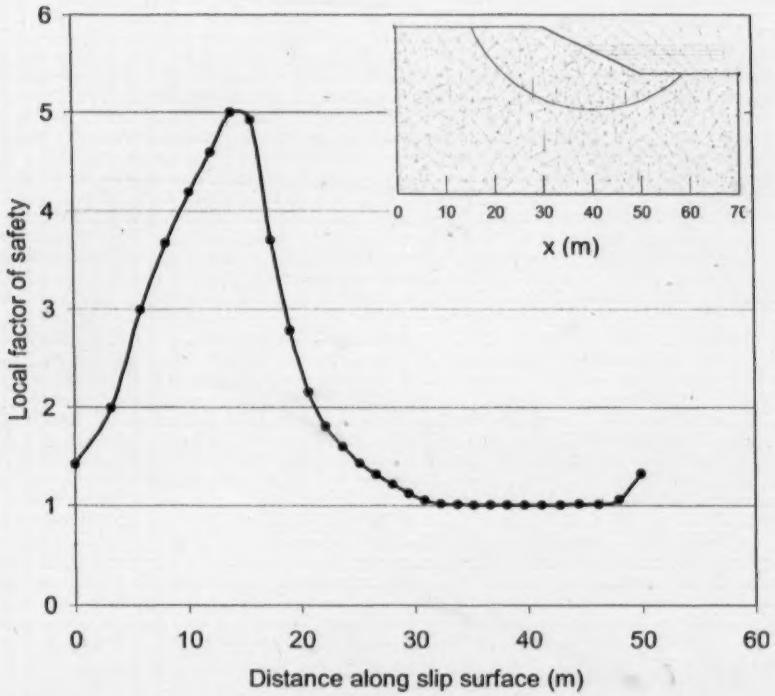

Figure 3.22: Local factor of safety distribution along the circular slip surface computed based on stresses from an elasto-plastic excavated slope analysis in conditions where Ko is equal 3.0 ($F_s = 1.52$).

3.6.2 Strict Application of Kinematic Admissibility Criteria in Finite Element Slope Stability Methods

Urciuoli (2002) and Urciuoli and Picarelli (2004) studied the relationship between stress, strain and displacement during the collapse of an infinite slope. The collapse process is characterized by the rotation of the principal stresses until failure surfaces predicted by Mohr's theory are kinematically compatible with the geometry of the slope. The results from the study provide evidence that slope conditions could exist where linear elastic stresses might not provide a reasonable representation of the

internal stress distribution. The results were used in the current study to direct the selection of an appropriate analysis that could be performed to explain the difficulties associated with the application of kinematic admissibility criteria in finite element slope stability methods.

Urciuoli et al. (2007) state that *"the mechanics of failure in intact soils is complex because the orientation of the developing slip surface must be consistent everywhere with that of the principal stresses. Normally, this is not assured by initial stresses whose direction could lead to local failure planes that are incompatible with the formation of a continuous slip surface"*. These comments suggest that the application of strict admissibility criteria is appropriate since the internal stresses need to rotate into alignment before a continuous slip surface can develop. Urciuoli et al. (2007) includes findings from case studies and laboratory tests to support these conclusions (Morgenstern and Tchalenko 1967; Skempton and Petley 1967) including cases of "unfinished landslides" characterized by the formation of long cracks on the ground surface but no generation of general slope failure (Bernarder 2000).

3.7 Conclusions

A summary of the literature is provided to identify different findings regarding the influence of Poisson's ratio and Young's modulus on the factor of safety. In some cases, the factor safety is reported to vary by less than 5% while in other cases the factor of safety is shown to vary by more than 20%. The results from a sensitivity study were presented to explain the different views surrounding the influence of Poisson's ratio. One example from the sensitivity study was identified where the influence of Poisson's ratio seemed to be related to the method used to search for the critical slip surface. The variation in the factor of safety was found to be less than 10% if the grid and radius method was used to identify the critical slip surface and greater than 35% if the dynamic programming method was used. The different levels of sensitivity were found to be related to the soil behavior model adopted in the stress-deformation analysis and how the searching procedure is designed to interact

with the resulting internal stress distribution of the slope. Further studies were presented to investigate the details surrounding the interaction between admissibility criteria and the internal stress distribution of the slope considering linear elastic and elasto-plastic soil behavior as well as overconsolidated soil conditions. The following conclusions can be made from this study.

1) Poisson's ratio can influence the orientation of the principal stresses in a "switch-on" gravity analysis. The interaction between admissibility criteria and the orientation of the stress field can result in fluctuations in the computed factor of safety. The influence of Poisson's ratio can be minimized by using an elasto-plastic stress analysis which provides a more realistic prediction of the orientation of the principal stresses.
2) A linear elastic analysis is found to provide an inadequate representation of the internal stress distribution in overconsolidated soil conditions where the rotation of the principal stress is required to promote the development of a continuous slip surface.
3) The strict application of kinematic admissibility criteria in the dynamic programming search is appropriate and corresponds to the behavior observed in case histories and in laboratory tests.
4) Information gathered during the dynamic programming search can be used to illustrate the interaction between the kinematic admissibility criteria and the internal stress distribution for the slope in the form of an admissibility plot.
5) Searching procedures that rely on geometric admissibility criteria can result in critical slip surfaces that are not compatible with internal stress distribution. The violation of kinematic admissibility can be recognized by identifying locations along the slip surface where the mobilized shear stress is opposite to the assumed direction of failure (i.e., negative.). The influence on the overall stability analysis depends on how much of the slip surface is inadmissible and how the presence of negative mobilized shear stresses are treated. In most cases the incompatibility results in a factor of safety that is artificially elevated.

3.8 Bibliography

Bernarder, S. 2000. Progressive landslides in long natural slopes. Dissertation, Lulea University of Technology, Lulea, Sweden.

Brito, C.C., Pereira, J.H.F., Gitirana Jr., G.F.N., and Fredlund, D.G. 2004. Transient stability analysis of a collapsible dam using dynamic programming combined with finite element stress state fields. *In* IX International Symposium on Landslides. Rio de Janeiro, Brazil, Vol.2, pp. 1079-1084.

Ching, R.K.H., and Fredlund, D.G. 1983. Some difficulties associated with the limit equilibrium method of slices. Canadian Geotechnical Journal, 20(4): 661-672.

Dunlop, P., and Duncan, J.M. 1970. Development of failure around excavated slopes. Journal of Soil Mechanics and Foundations Division, ASCE, 96(SM2): 471-493.

Fredlund, D.G., and Scoular, R.E.G. 1999. Using limit equilibrium concepts in finite element slope stability analysis. *In* Proceedings of the International Symposium on Slope Stability Engineering-IS-Shikoku'99. Invited Keynote Paper, Matsuyama, Shikoku, Japan. November 8-11, pp. 31-47.

Fredlund, D.G., Scoular, R.E.G., and Zakerzadeh, N. 1997. Using finite element stress analysis to compute the factor of safety. *In* 52nd Canadian Geotechnical Conference. Regina, Saskatchewan, Canada, pp. 73-80.

Gitirana Jr., G.F.N., and Fredlund, D.G. 2003. Analysis of Transient embankment stability analysis using dynamic programming. *In* Proceedings of the 56th Canadian Geotechnical Conference. Winnipeg, Manitoba, Canada, Vol.1, pp. 808-814.

Morgenstern, N.R., and Price, V.E. 1965. The analysis of slope stability of general slip surfaces. Geotechnique, 15(1): 79-63.

Morgenstern, N.R., and Tchalenko, J.S. 1967. Microstructural observations on shear zones from slips in natural clays. *In* Proceedings Geotechnical Conference. Oslo, Norway, Vol.1, pp. 147-152.

Pham, H.T.V., and Fredlund, D.G. 2003. The application of dynamic programming to slope stability analysis. Canadian Geotechnical Journal, 40(4): 830-847.

Skempton, A.W., and Petley, D. 1967. The strength along structural discontinuities in stiff clays. *In* Proceedings Geotechnical Conference, Oslo, Norway, Vol. 1, pp. 55-69.

Stianson, J.R. 2008. A three-dimensional slope stability method based on finite element stress analysis and dynamic programming. Dissertation, University of Alberta, Canada.

Urciuoli, G. 2002. Strains preceding failure in infinite slopes. International Journal of Geomechanics, 2(1): 93-112.

Urciuoli, G., and Picarelli, L. 2004. The shear strength mobilised in first-time slides in highly overconsolidated clays. *In* Advances in Geotechnical Engineering: The Skempton Conference, Mar 29-31 2004. London, United Kingdom. Thomas Telford Services Ltd, pp. 1005-1016.

Urciuoli, G., Picarelli, L., and Leroueil, S. 2007. Local soil failure before general slope failure. Geotechnical and Geological Engineering, 25(1): 103-122.

Wang, F., and Sun, M. 1970. Slope stability analysis by the finite element stress analysis and limiting equilibrium, U.S. Bureau of Mines, Report of Investigations 7341, Washington.

Wright, S.G., Kulhawy, F.H., and Duncan, J.M. 1973. Accuracy of equilibrium slope stability analysis. Journal of Soil Mechanics and Foundations Division, ASCE, 99(SM10): 783-791.

Chapter 4

Three-Dimensional Slope Stability Based on Stresses from a Stress-Deformation Analysis

4.1 Introduction

A variety of procedures are available to evaluate the stability of slopes ranging from simple expressions like the stability number to rigorous numerical methods. The need for more rigorous numerical methods resulted in the development of limit equilibrium formulations categorized as the method of slices (Fellenius 1936; Bishop 1955; Janbu et al. 1956). Significant improvements in the speed and memory capacity of personal computers facilitated the use of the method of slices in engineering practice and promoted research into a series of more rigorous two-dimensional method of slices formulations. These formulations allowed for the extension of the two-dimensional method of slices to the three-dimensional method of columns (Chen and Chameau 1983; Hungr 1987; Lam and Fredlund 1993; Hungr 2001).

The method of slices and the method of columns require the use of assumptions regarding the forces in the sliding mass to render the factor of safety equation determinate. The stress-based method of slope stability incorporates the stresses computed from a stress - deformation analysis into a conventional limit equilibrium factor of safety calculation. The stress-based method was developed to alleviate the use of assumptions regarding the forces in the sliding mass. Fredlund et al. (1997)

identified three important advantages resulting from the use of stress-based methods versus the assumptions typically adopted in method of slices formulations; 1) The stress versus strain relationship of the soils is included in the analysis, 2) the factor of safety equation is determinate and requires no further assumptions to complete the calculation and 3) the factor of safety equation is linear because the normal stresses along the slip surface are known. The application of the stress-based method in two-dimensional slope stability has led to the development of admissibility criteria that can be used to negate the usage of assumptions regarding the shape of the slip surface. It is anticipated that similar three-dimensional admissibility criteria will be developed as a result of the extension of the stress-based method to three dimensions.

The development and wide-spread use of the stress-based method of slope stability has been made possible due to the increased speed of personal computers and the development of commercial software. The increases in computing speed and memory capacity have been so substantial that it has become economical to extend the two-dimensional stress-based method to three dimensions. The objective of this research study is to demonstrate a procedure for combining a finite element stress analysis on a slope with limit equilibrium concepts to calculate the factor of safety for three-dimensional slip surfaces. A series of published example problems are re-analyzed as part of the verification process.

4.2 Background

The following discussion provides a summary of the developments related to two- and three-dimensional stress-based methods of slope stability.

4.2.1 Developments Related to Two-Dimensional Stress-Based Methods of Slope Stability

A detailed summary of finite element methods of slope stability was presented by Scoular (1997). Fredlund et. al. (1997) summarized the development of the two-dimensional finite element methods of slope stability using the flow chart shown in Figure 4.1.

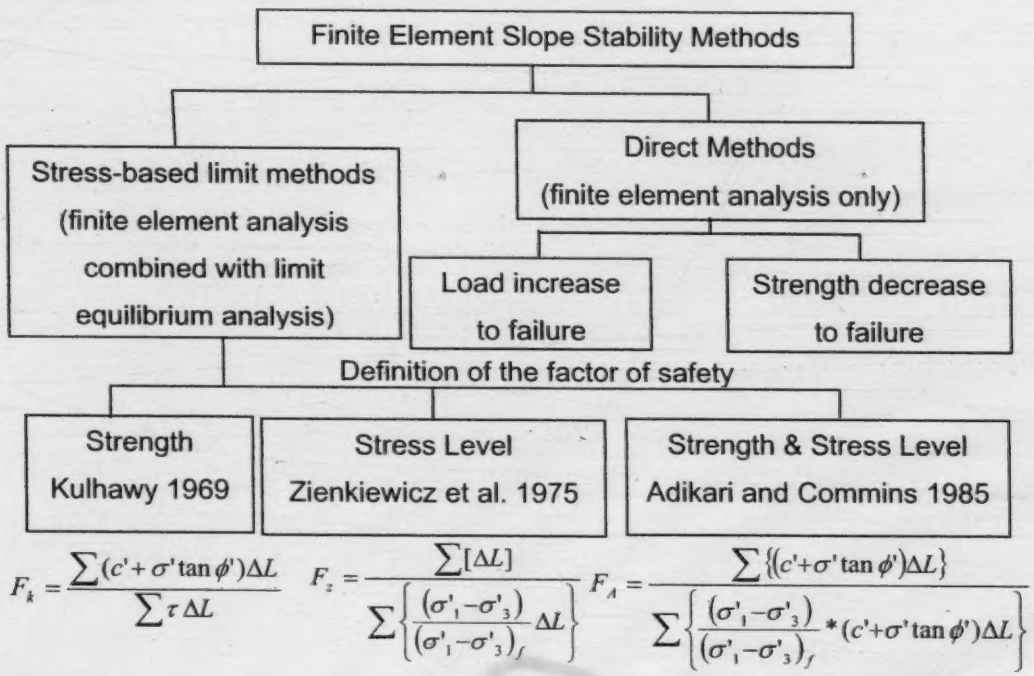
Finite Element Slope Stability Methods
Stress-based limit methods (finite element analysis combined with limit equilibrium analysis)
Direct Methods (finite element analysis only)
Load increase to failure
Strength decrease to failure
Definition of the factor of safety
Strength
Kulhawy 1969
Stress Level
Zienkiewicz et al. 1975
Strength & Stress Level
Adikari and Commins 1985
$F_k = \frac{\sum (c' + \sigma' \tan \phi') \Delta L}{\sum \tau \Delta L}$
$F_z = \frac{\sum [\Delta L]}{\sum \left\{ \frac{(\sigma'_1 - \sigma'_3)}{(\sigma'_1 - \sigma'_3)_f} \Delta L \right\}}$
$F_A = \frac{\sum \{(c' + \sigma' \tan \phi') \Delta L\}}{\sum \left\{ \frac{(\sigma'_1 - \sigma'_3)}{(\sigma'_1 - \sigma'_3)_f} * (c' + \sigma' \tan \phi') \Delta L \right\}}$

Figure 4.1: A summary of the finite element procedures for computing the factor of safety in slope stability analysis (Fredlund et al. 1997).

The finite element slope stability methods have been categorized as either direct or stress-based methods. The "Enhanced limit strength" method originally proposed by Kulhawy (1969) was identified by Scoular (1997) as the most appropriate factor of

safety definition. Scoular (1997) went on to solve a series of slope stability problems verifying the reliability of the method based on the "enhanced limit strength" factor of safety definition. The "stress level" methods have been criticized for using the principal stresses in the factor of safety definition. Fredlund et al. (1999) concluded that by definition, failure does not take place on the plane of principal stress and that any "stress level" method will result in higher factors of safety than "strength" methods. Therefore, the three-dimensional slope stability method presented in the current study is based on the enhanced limit strength factor of safety definition.

Pham (2002) advanced the work of Scoular (1997) by incorporating a more advanced searching procedure that allowed the shape of the slip surface to become part of the analysis. The factor of safety calculation is based on the "enhanced Limit Strength" concept while the dynamic programming optimization technique is used to search for the slip surface with the lowest factor of safety. Pham (2002) demonstrated that the computational complexities associated with the application of more advanced searching procedures are significantly reduced due to the linear nature of the stress-based factor of safety equation. The geometrical restrictions typically placed on the shape of the slip surface can be replaced with a new admissibility criteria based on the kinematics of the failing mass. It seems reasonable to expect that the development of three-dimensional stress-based methods of slope stability will provide similar advantages associated with the application of more advanced non-linear searching techniques.

Stianson (2008) performed a comparative study to investigate the differences that might occur between slope stability calculations depending on the soil behavior model selected in the finite element analysis. The comparative study was completed using a slope stability method that was developed based on the procedure proposed by Pham (2002). The results demonstrated that there are small essentially insignificant differences between slope stability calculations based on stresses generated using a linear elastic or elasto-plastic soil behavior model. Therefore, each of the factor of safety calculations presented in this report are based on stresses generated from a linear elastic switch on gravity analysis.

The research summarized above has laid the groundwork for the extension of the stress-based method of slope stability to three-dimensions. The advantages associated with the stress-based limit equilibrium method have been well documented and recommendations have been made regarding the most appropriate factor of safety definition.

4.2.2 Extension of Two-Dimensional Stress-Based Methods of Slope Stability to Three Dimensions

There has been limited research directed towards the extension of the two-dimensional stress-based methods of slope stability to three dimensions. Chen and Chameau (1982) reported using a method where the stresses from a three-dimensional finite element analysis were combined with a limit equilibrium analysis to assess the stability of a particular embankment. The factor of safety calculated using the finite element stresses was reported to be in reasonable agreement with factors of safety computed using other limit equilibrium methods. Many of the details regarding the application of the method were not provided.

Loehr (1998) developed a hybrid approach where a finite element stress analysis was utilized within a limit equilibrium framework, similar to the work of Chen and Chameau (1982). Potential slip surfaces were discretized using a series of triangular planes. A procedure involving linear interpolation was developed to compute the resisting force and shear force acting at the centroid of individual triangular planes. The forces were computed based on the stresses from a separate finite element analysis. The overall factor of safety was computed by dividing the summation of the resisting forces by the summation of the shear forces acting on the slip surface. Two example problems were considered to test the accuracy of the formulation. The first example consisted of an infinitely long slope with a planar slip surface and the second example involved a symmetrical wedge failure. First, the overall factors of safety for both examples were calculated by hand considering the normal and shear forces

required to satisfy force equilibrium. Next, the normal force, shear force, and factor of safety were computed using the proposed finite element slope stability method. The accuracy of the finite element slope stability method was evaluated by comparing the normal force, shear force, and overall factor of safety to the values determined from the hand calculation.

The results from the finite element method were found to provide an inadequate level of accuracy for both examples. The degree to which the finite element analysis deviated from the manual force equilibrium analysis was considered to be dependent on the density of the finite element mesh and the value of Poisson's ratio selected in the finite element analysis. The influence of Poisson's ratio was reported to diminish as the density of the finite element mesh was increased. The finite element procedure was deemed unreliable due to the computational effort required to increase the density of the finite element mesh to a level that would remove the effect of Poisson's ratio. The procedure used to calculate the forces acting at the centroid of individual triangular surfaces was also considered to contribute to the inadequacies of the method. Loehr went on to propose that the method could be improved by calculating the stresses acting on the slip surface directly from the nodal forces from the finite element analysis.

The reliability of performing limit equilibrium slope stability calculations using stresses imported from a separate finite element analysis appear to be in question. Extensive sensitivity studies were completed using the proposed procedure to evaluate the factors that could influence the accuracy of the factor of safety calculation.

4.3 Three-Dimensional Limit Equilibrium Slope Stability Analysis Based on Finite Element Stresses

The following discussion outlines the details surrounding the calculation of the factor of safety for a three-dimensional slip surface. The factor of safety calculations are based on the combination of a limit equilibrium analysis with stresses from a separate stress-deformation analysis.

4.3.1 Linking the Stress-Deformation Analysis with the Slope Stability Calculations

The internal stress state computed from the finite element analysis is used to determine the forces acting along the three-dimensional slip surface. The interpolation procedure required to determine the stresses acting at discrete points along the slip surface is dependent on the mesh configuration used in the three-dimensional stress-deformation analysis (i.e., tetrahedron, hexahedron etc.). A separate interpolation procedure is required for individual mesh configurations. For simplicity, the stresses from the finite element analysis are exported to a common grid configuration, referred to as the intermediate grid, consisting of rectangular elements (Figure 4.2).

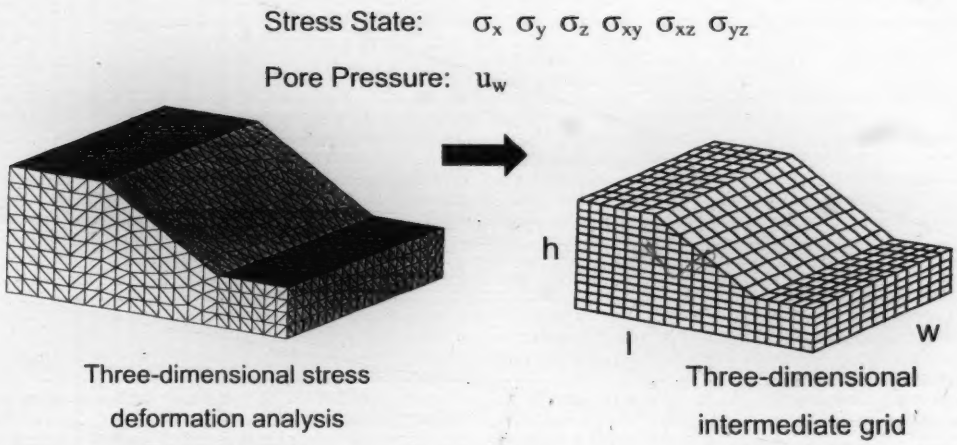

Figure 4.2: Illustration of the three-dimensional grid linking the finite element stress analysis with the slope stability calculations.

Exporting the stresses from the stress-deformation analysis to a rectangular grid configuration means that only one interpolation procedure is required to determine the stresses acting along a slip surface. The density of the intermediate grid is defined by specifying the number of increments in the *x, y,* and *z*-directions (i.e., *w, l,* and *h*). Sensitivity analyses are performed to show that the dimensions of the intermediate grid can be selected so that there are no adverse effects on the accuracy of the factor of safety calculations.

4.3.2 Calculating the Factor of Safety for a Three-Dimensional Slip Surface

The factor of safety equation for an arbitrary three-dimensional slip surface can be defined as:

$$[4.1] \qquad F_S = \frac{\int \tau_f \, dA}{\int \tau \, dA}$$

where τ_f is the shear strength of the soil, τ is the mobilized shear stress, and dA is an incremental area on the slip surface. Assuming that a potential slip surface can be approximated by a series of triangular surfaces (Figure 4.3), it is possible to write the factor of safety equation in discretized form:

$$[4.2] \qquad F_S = \sum_{ijk=1}^{mn2} \tau_{f_{ijk}} A_{ijk} \Big/ \sum_{ijk=1}^{mn2} \tau_{ijk} A_{ijk} = \sum_{ij=1}^{mn} R_{ij} \Big/ \sum_{ij=1}^{mn} S_{ij}$$

where m is the number of dividing lines in the x-direction, n is the number of dividing lines in the y-direction, $\tau_{f_{ijk}}$ is the shear strength, τ_{ijk} is the mobilized shear stress, and A_{ijk} is the area of one triangular plane (The i, j and k subscripts indicate the coordinates of the resultant force in the three-dimensional grid not the components of the vector). The resisting force, R_{ij}, and the shear force, S_{ij}, can be calculated by multiplying the shear strength and the mobilized shear stress by the area of each plane. R_{ij} and S_{ij} are the addition of the resisting forces and shear forces acting on the combination of two triangular planes (i.e., k =1 and 2).

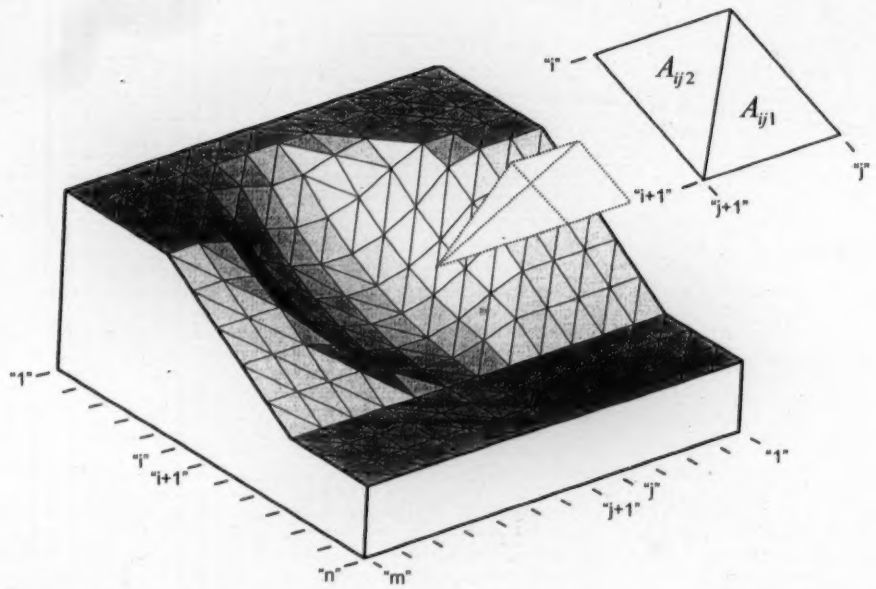

Figure 4.3: A three-dimensional ellipsoidal slip surface approximated by a series of triangular planes.

The slip surface shown in Figure 4.3 is discretized with a total of $m*n*2$ triangular planes. The two triangles between the dividing lines i and $i+1$ in the x-direction and j and $j+1$ in the y-direction can be identified according to the incremental areas A_{ij1} and A_{ij2}. The procedure used to compute the resisting force, R_{ij1}, and the shear force, S_{ij1}, for triangle A_{ij1}, is described below.

The normal and mobilized shear stresses acting on the incremental area, A_{ijk}, can be calculated using the stress state at the centroid of the area A_{ij1} and the unit vector, n, normal to the plane. A search is performed through the intermediate grid to determine the eight nodes surrounding the centroid of a triangle.

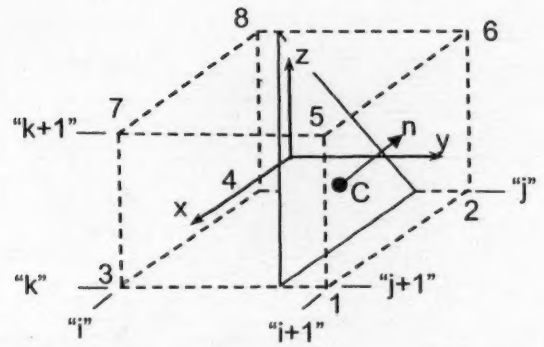

The stress states from the surrounding eight nodes are used to determine the stress state at the centroid of the triangle A_{ijl}, using standard tri-linear interpolation. First, a local coordinate system is defined with an origin located at the centre of the element. Next, the local coordinates (x_c, y_c, z_c) for the centroid, C, of the triangular plane can be computed using the expressions shown in Eq. [4.3].

$$[4.3] \qquad x_c = 2 * \frac{(x - x_i)}{(x_{i+1} - x_i)} - 1 \; ; \; y_c = 2 * \frac{(y - y_j)}{(y_{j+1} - y_j)} - 1 \; ; \; z_c = 2 * \frac{(z - z_k)}{(z_{k+1} - z_k)} - 1$$

The values x, y, z are the coordinates for the centroid of the triangular plane based on the global coordinate system. Likewise, the coordinates x_i, y_i, and z_i are based on the global coordinate system. The local coordinates computed using the expressions given in Eq. [4.3] will always result in values between negative one and one. The local coordinates of the centroid can be used to compute an interpolation factor, N, for each of the eight nodes using the set of expressions given in Eq. [4.4].

$$\begin{aligned}
N_1 &= (1/8) * (1 + x_c) * (1 + y_c) * (1 - z_c) \\
N_2 &= (1/8) * (1 - x_c) * (1 + y_c) * (1 - z_c) \\
N_3 &= (1/8) * (1 + x_c) * (1 - y_c) * (1 - z_c) \\
N_4 &= (1/8) * (1 - x_c) * (1 - y_c) * (1 - z_c) \\
N_5 &= (1/8) * (1 + x_c) * (1 + y_c) * (1 + z_c)
\end{aligned} \qquad [4.4]$$

$$N_6 = (1 / 8) * (1 - x_c) * (1 + y_c) * (1 + z_c)$$
$$N_7 = (1 / 8) * (1 + x_c) * (1 - y_c) * (1 + z_c)$$
$$N_8 = (1 / 8) * (1 - x_c) * (1 - y_c) * (1 + z_c)$$

The parameters describing the stress state at the centroid of the triangular plane (i.e., σ_x, σ_y, σ_z, σ_{xy}, σ_{xz}, σ_{yz}) can be computed as the sum of the parameter multiplied by the corresponding interpolation factor for each of the eight nodes (i.e., $\sigma_x = \sum_{i=1}^{8} \sigma_{x_i} N_i$ etc.). The unit normal vector, n, can be determined using the three coordinates from the triangular plane.

Knowing the stress state at the centroid of the triangle and the unit vector normal to the plane, it is possible to calculate the components of the traction $T^{(n)}$ shown in Figure 4.4, using Eq. [4.5].

[4.5] $$T_i^{(n)} = \sigma_{ij} n_j$$

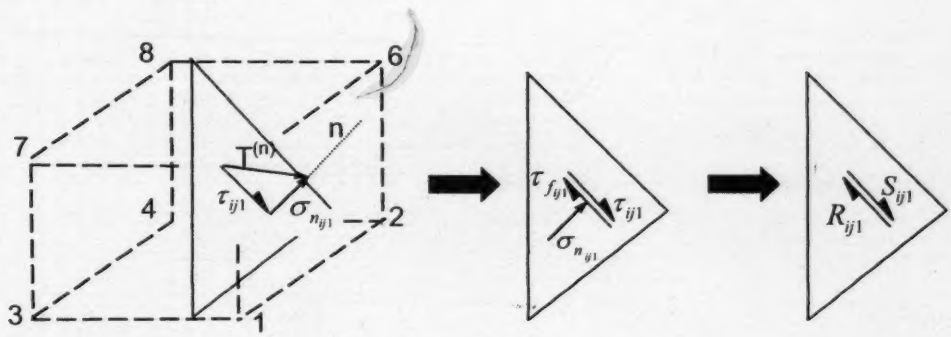

Figure 4.4: Calculating the resisting force, R_{ij1}, and shear force, S_{ij1}, based on the normal stress, $\sigma_{n_{ij1}}$, and mobilized shear stress, τ_{ij1}, acting at the centroid of incremental area A_{ij1}.

The normal stress, $\sigma_{n_{ij1}}$, can be calculated by evaluating the dot product of the traction $T^{(n)}$ and the unit normal vector, n, using Eq. [4.6].

[4.6] $$\sigma_{n_{ijk}} = T^n \bullet n$$

Finally, Pythagoras' theorem can be used to determine the magnitude of the mobilized shear stress, τ_{ijk}, acting at the centroid of the area located at coordinates i, j and k using Eq. [4.7].

[4.7] $$\tau_{ijk} = \sqrt{\left|T^{(n)}\right|^2 - \left|\sigma_{n_{ijk}}\right|^2}$$

The shear force, S_{ijl}, is calculated by multiplying the mobilized shear stress, from Eq. [4.7], by the area of the triangle, A_{ijl}.

The shear strength provided by each incremental area, A_{ijk}, can be calculated using the extended Mohr-Coulomb equation for saturated-unsaturated soil (Fredlund and Rahardjo 1993):

[4.8] $$\tau_{f_{ijk}} = c' + (\sigma_n - u_a)\tan\phi' + (u_a - u_w)\tan\phi^b$$

where c', ϕ', and ϕ^b are the shear strength parameters of a saturated-unsaturated soil, $(\sigma_n - u_a)$ is the net normal stress, and $(u_a - u_w)$ is the matric suction. The resisting force, R_{ijl}, is computed by multiplying the shear strength of the soil, $\tau_{f_{ijl}}$, by the area of the triangle A_{ijl}.

The same procedure can be used to compute the resisting force and shear force for each triangular plane on the slip surface. The summation of the resisting forces divided by the summation of the shear forces can be used to compute the overall factor of safety for the slip surface, according to Eq. [4.2].

4.3.3 Restrictions Applied to the Shape of the Slip Surface

The factor of safety equation defined by Eq. [4.2] can be used to compute the factor of safety for slip surfaces of any shape. However, all of the verification examples selected for the current study consider ellipsoidal slip surfaces, with the exception of one example, where the ellipsoidal slip surface is modified to approximate a translational slide along a weak layer within the slope. The slip surface for this case is defined by an ellipsoid intersected by a plane.

$$[4.9] \qquad \frac{(x-x_c)^2}{a^2}+\frac{(y-y_c)^2}{b^2}+\frac{(z-z_c)^2}{c^2}=1$$

The general equation for an ellipsoidal surface is given by Eq. [4.9]. Each ellipsoidal slip surface is specified by the coordinates of its centre (x_c,y_c,z_c), its radius, and an aspect ratio. The semi-axes b and c are taken to be equal to the radius of the ellipsoid. The semi-axis a, is equal to the radius of the ellipsoid multiplied by the aspect ratio. A ratio of 1 defines a spherical slip surface while a large number (i.e., 1000) defines a cylindrical slip surface. In some cases, a trial and error searching procedure is used to determine the centre, radius, and aspect ratio for the critical ellipsoidal slip surface. The search for the critical slip surface is similar to the procedure developed by Hungr (2001) for use in Clara/W™.

Stianson (2008) demonstrated that the factor of safety computed in two-dimensional finite element slope stability analyses can be affected when circular slip surfaces are assumed to be kinematically admissible. In some cases, the shear forces acting along the slip surface might violate the assumed direction of failure. It is possible that similar effects might occur when ellipsoidal slip surfaces are considered in the current three-dimensional slope stability calculations. The results from the current research will be closely evaluated to check if the forces acting on individual planes along the slip surface might influence the factor of safety calculations.

4.4 Verification Example Problems

The results from four example problems are presented to evaluate the reliability of the proposed procedure for calculating three-dimensional factors of safety based on stresses from a separate finite element analysis. The factors of safety are reported to higher accuracy than is typically used in practice to facilitate a detailed comparison of the results.

4.4.1 Verification Example No. 1: Closed Form Solution

The first verification example problem consists of a symmetrical spherical slip surface intersecting a homogeneous slope made up of purely cohesive soil (Figure 4.6). A closed-form solution for this example problem was presented by Baligh and Azzouz (1975) and Gens et al. (1988). The factor of safety from the closed-form solution was calculated to be 1.402. The factor of safety equal to 1.402 was confirmed by Silvestri (2006b; 2006a). The closed-form solution is a popular benchmark and has been used to evaluate various three-dimensional slope stability formulations (Hungr et al. 1989; Lam and Fredlund 1993; Chen et al. 2001).

The factor of safety computed using the proposed stress-based slope stability method is compared to the results presented in previous research. A series of sensitivity analyses are also presented to determine if the computed factor of safety is sensitive to the density of the finite element mesh, the density of the intermediate grid, the number of planes used to discretize the slip surface and the value of Poisson's ratio selected in the finite element stress analysis.

4.4.1.1 Finite Element Stress Analysis for Verification Example No. 1

The finite element mesh used to compute the internal stress state for the slope is shown in Figure 4.5. Roller boundary conditions are applied to all sides of the problem, the bottom of the problem is pinned, and the top surface of the problem is free to move. The internal stress distribution is computed based on an isotropic linear elastic model using the 'switch on' gravity technique. The dimensions are selected so that the boundary conditions have a limited effect on the stresses near the specified slip.

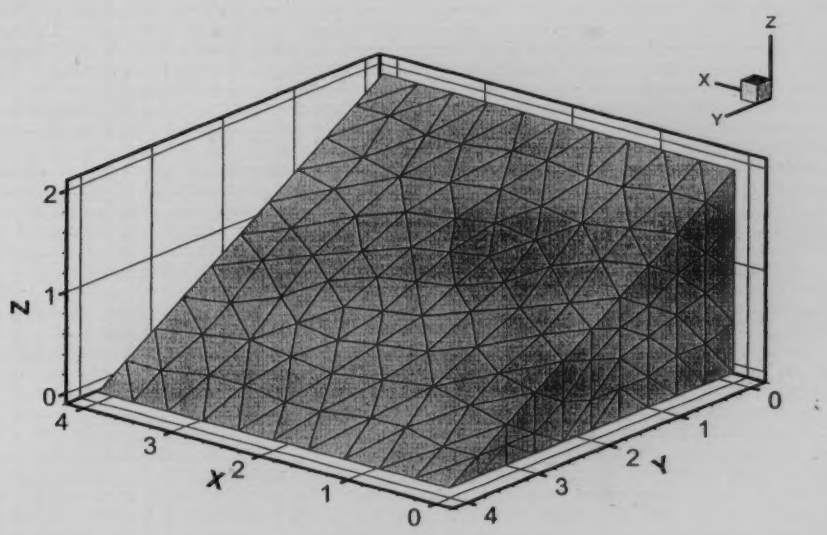

Figure 4.5: Finite element mesh used to calculate the internal stress state for verification example No. 1.

4.4.1.2 Slope Stability Results for Verification Example No. 1

The factor of safety computed using the proposed finite element limit equilibrium method might be affected by three different meshes including: 1) the finite element mesh used to solve for the internal stress state, 2) the intermediate grid used to link the stress-deformation analysis to the limit equilibrium factor of safety calculation, and 3) the number of planes used to discretize the slip surface. The results from a sensitivity analysis considering each of these factors are provided in Figure 4.6.

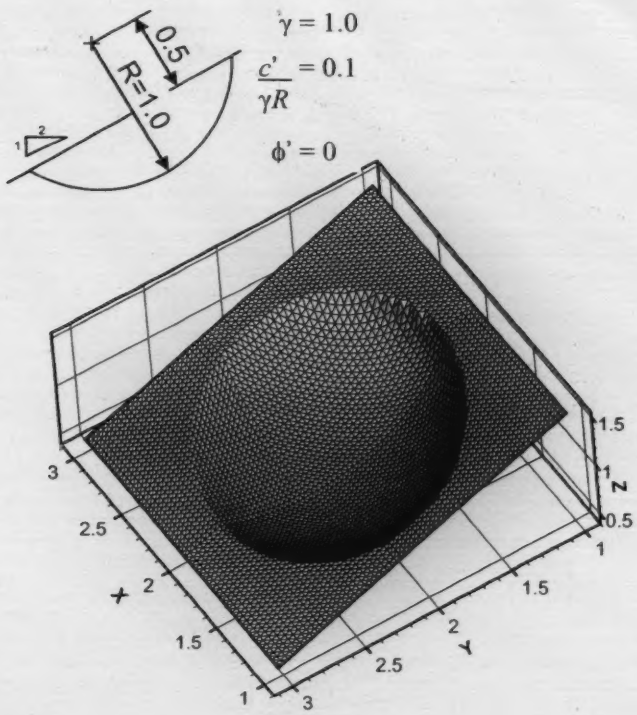

Figure 4.6: Verification example No. 1: a specified spherical slip surface in a homogeneous purely cohesive slope (Hungr et al. 1989) with c', cohesion; ϕ', friction angle; R, moment arm of the resisting force; γ, unit weight of soil.

The curves in Figure 4.7 are labeled according to the dimension of the finite element mesh used to solve for the internal stress state and the dimension of the intermediate grid. A finite element mesh generated with NGRID equal to 10,

indicates that the longest dimension of the problem, in this case 4m, is divided into 10 increments resulting in a grid spacing equal to 0.4m. The finite element mesh throughout the remainder of the problem is modified to comply with the grid spacing of 0.4m required over the longest dimension of the problem. The internal stresses computed from the finite element analysis are exported to an intermediate grid with the same number of divisions in the *x*, *y*, and *z*-directions. Therefore, an intermediate grid with a dimension equal to 16 means that each dimension of the problem (i.e., *x*, *y*, and *z*) is divided into 16 increments.

The *x*-axis in Figure 4.7 reports half the number of triangular planes used to discretize the slip surface. The number of triangular planes is divided by two so that a direct comparison can be made with the number of columns used in previous studies. The three-dimensional factor of safety is reported on the *y*-axis. The grey band through the middle of Figure 4.7 represents the range of factors of safety that are within 1% of the closed-form solution. The computer time required to compute the factor of safety for each case is estimated along the secondary *x*-axis along the top of Figure 4.7. The simulations were run on a 3.00GHz Pentium 4 processor with 1.0GB of random access memory (RAM). All of the models presented in Figure 4.7 were solved using Poisson's ratio equal 0.49 and Young's modulus equal to 10,000 kPa.

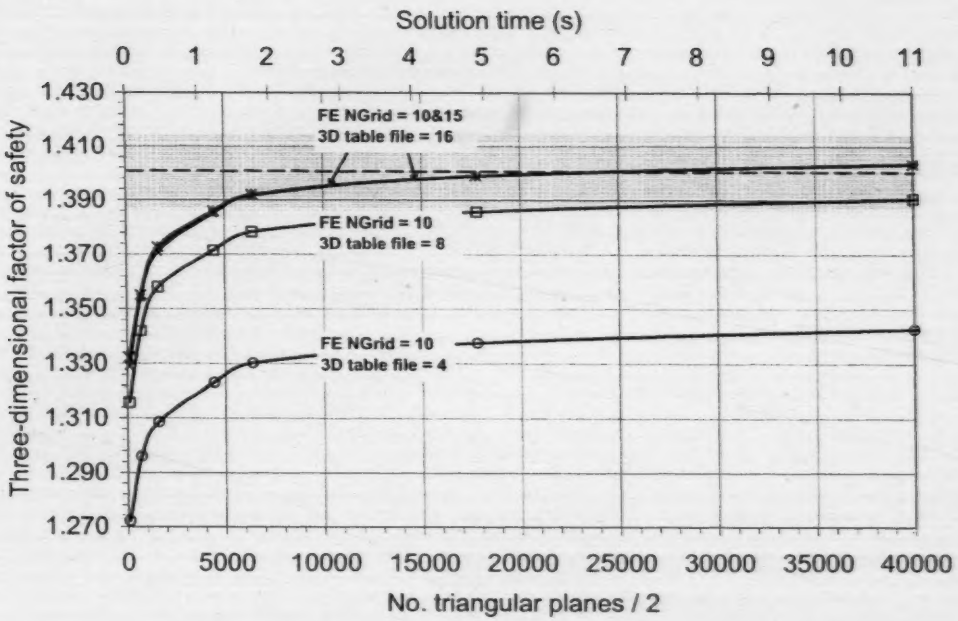

Figure 4.7: Influence of the finite element mesh, the intermediate grid, and the slip surface discretization on the three-dimensional factor of safety.

Initially, the internal stress state was computed using a finite element mesh with NGRID equal to 10. The computed stresses were exported to an intermediate grid with four increments in the *x*, *y*, and *z*-directions. A series of slope stability models were generated to determine the relationship between the computed factor of safety and the number of planes used to discretize the slip surface. The factor of safety increases from 1.272 to 1.324 as the number of planes increases from 100 to 6,400.

The procedure described above is repeated while incrementally increasing the density of the intermediate grid and the finite element mesh. The intent is to determine the condition where additional increases in the density of the grids do not influence the computed factor of safety. In other words, a converged solution is achieved. A converged solution is considered to be achieved for the case where the finite element mesh is generated using NGRID equal to 10 and the stresses are exported to an intermediate grid with 16 increments in the *x*, *y*, and z-directions. The

factor of safety for this case is equal to 1.386 when the slip surface is discretized with 6,400 planes.

The factor of safety computed using the proposed stress-based slope stability method is compared to the factors of safety from other studies in Table 4.1. The factor of safety computed using the stress-based slope stability method appears to be in reasonably close agreement with the closed-form solution and the values reported from other studies.

Table 4.1: A comparison between the factors of safety computed for verification example No. 1.

Author	Method	Three-dimensional factor of safety	% difference
Baligh and Azzouz (1975) ; Gens et al. (1988)	Closed form solution	1.402	-
Hungr et. al. (1989)	Method of columns (Simplified Bishop)	1.422	1.4
Lam and Fredlund (1993) (540 columns)	Method of columns (GLE)	1.402	0.0
Lam and Fredlund (1993) (1200 columns)	Method of columns (GLE)	1.386	-1.2
Chen et. al. (2001a)	Upper bound limit analysis	1.422	1.4
Chen (2004)	Upper bound limit analysis	1.43	2.0
Current Study	Stress-based slope stability method	1.403	0.1

4.4.1.3 Influence of Poisson's Ratio on the Three-Dimensional Factor of Safety

A sensitivity analysis was also completed to determine if the Poisson's ratio (v) used to calculate the internal stress state has a significant effect on the computed factor of

safety. A series of models were completed considering eight values of Poisson's ratio including 0.0, 0.1, 0.2, 0.3, 0.4, 0.42, 0.45, and 0.49.

Figure 4.8 illustrates the relationship between Poisson's ratio and the computed three-dimensional factor of safety. The range of Poisson ratio values are listed on the *x*-axis, the computed three-dimensional factors of safety are shown on the left *y*-axis, and the percent difference from the closed form solution is provided on the right *y*-axis. The figure also provides information regarding the admissibility of individual planes along the slip surface, depending on the Poisson's ratio selected in the finite element stress analysis. The number of planes where the shear force violates the assumed direction of failure is listed for each value of Poisson's ratio. The shear force is considered to be kinematically inadmissible if it acts contrary to the assumed direction of failure.

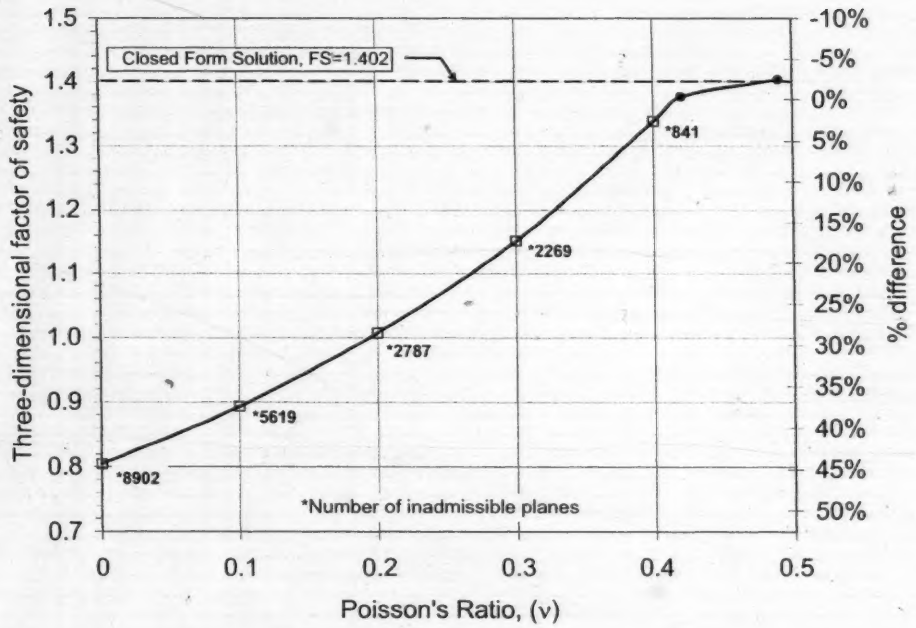

Figure 4.8: Influence of Poisson's ratio on the three-dimensional factor of safety for verification example #1.

The factor of safety increases from approximately 0.8 when Poisson's ratio is equal to 0 to 1.386 when Poisson's ratio is equal to 0.49. The factor of safety varies by more than 40% over the range of Poisson's ratio values considered in the sensitivity study. It appears that the variation in the factor of safety is related to the number of planes along the slip surface where the kinematic admissibility criterion is violated. The factor of safety is closest to the closed-form solution when no planes violate the admissibility criterion and seems to be degraded as the number of inadmissible planes increases. The results confirm the behavior described by Stianson (2008).

4.4.2 Verification Example No. 2: Weak Layer

The second verification example involves a composite slip surface sliding along a weak layer within a homogeneous slope (Figure 4.9). The example problem was originally presented by Fredlund and Krahn (1977) in a two-dimensional slope stability study. Since then, the slope has been extended to three dimensions and used to evaluate three-dimensional slope stability formulations. The factor of safety computed using the stress-based slope stability formulation is compared to the results reported in previous studies (Xing 1988; Hungr et al. 1989; Lam and Fredlund 1993; Chen et al. 2001; Chen 2004).

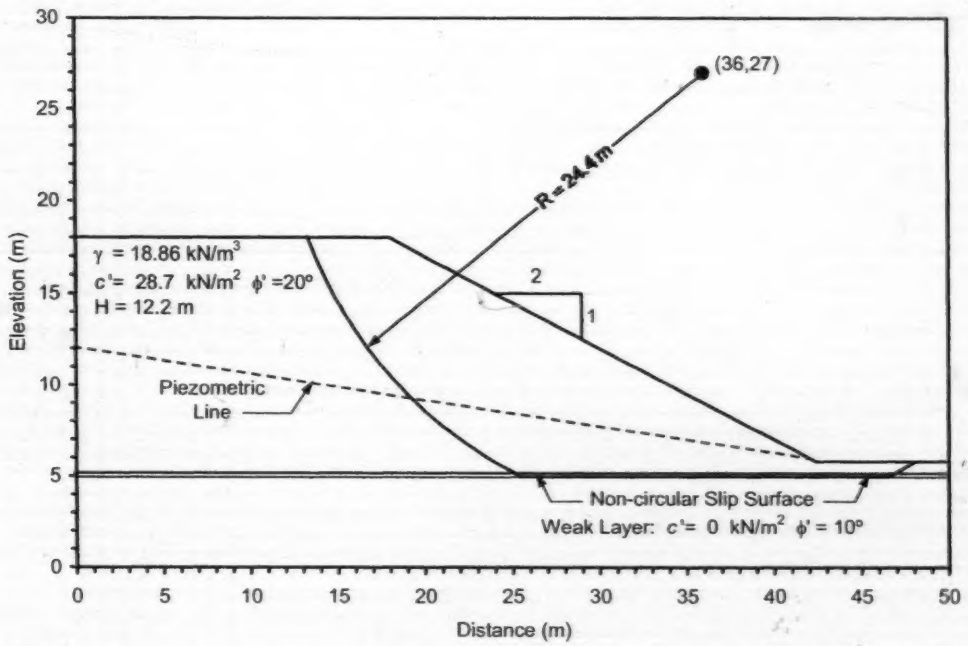

Figure 4.9: A two-dimensional cross-section illustrating the geometry and soil properties for verification example No. 2. H is the height of the slope and *R* is the radius of the ellipsoid.

The factor of safety is computed for the composite slip surface shown in Figure 4.9, considering two conditions. The first case does not include the piezometric line

and considers an ellipsoidal slip surface that encompasses 13,000m^3 of soil. The second case includes the water table and considers a slip surface that encompasses 16,000m^3 of soil.

4.4.2.1 Finite Element Stress Analysis for Verification Example No. 2

The finite element analysis used to compute the internal stress state for the slope is presented in Figure 4.10. Roller boundary conditions are applied to all sides of the problem, the bottom of the problem is pinned, and the top surface of the problem is free to move. The internal stress distribution is computed based on an isotropic linear elastic model using the 'switch on' gravity technique. A sensitivity study is also performed to observe the effects of Poisson's ratio on the factor of safety calculation. The linear elastic stresses are generated considering Poisson's ratio values equal 0, 0.1, 0.2, 0.3, 0.4, and 0.49. The values of Young's modulus are arbitrarily selected to be 15,000 kPa in the medium soil and 5,000 kPa in the weak layer.

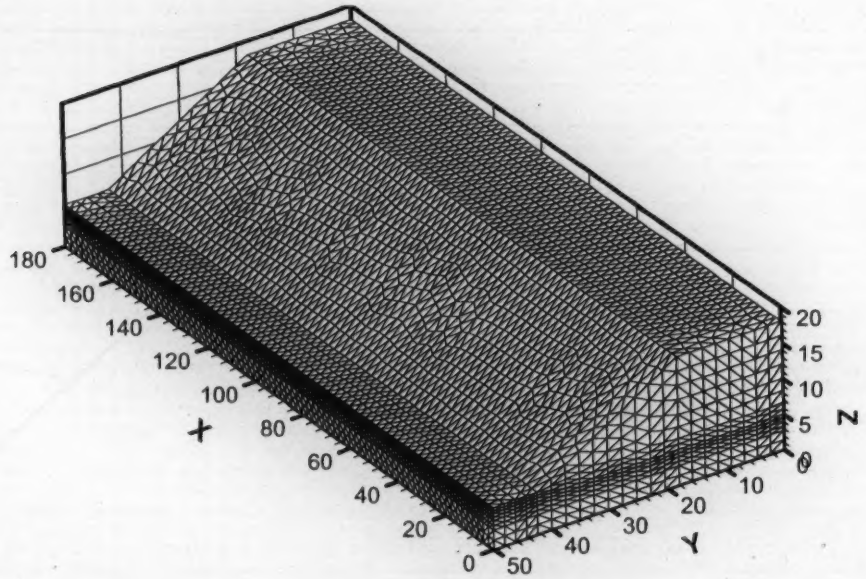

Figure 4.10: Finite element mesh used to calculate the internal stress state for verification example No. 2.

4.4.2.2 Slope Stability Results for Verification Example No. 2

Figure 4.11 illustrates the slip surface for Case 1 where the volume of soil encompassed by the slip surface is approximately 13,000 cubic meters. A sensitivity study was completed for Case 1 to determine the appropriate finite element mesh density, intermediate grid density, and the number of planes that should be used to discretize the slip surface. The resulting parameters were also used to compute the factor of safety for the second case considering a slide volume of 16,000m^3.

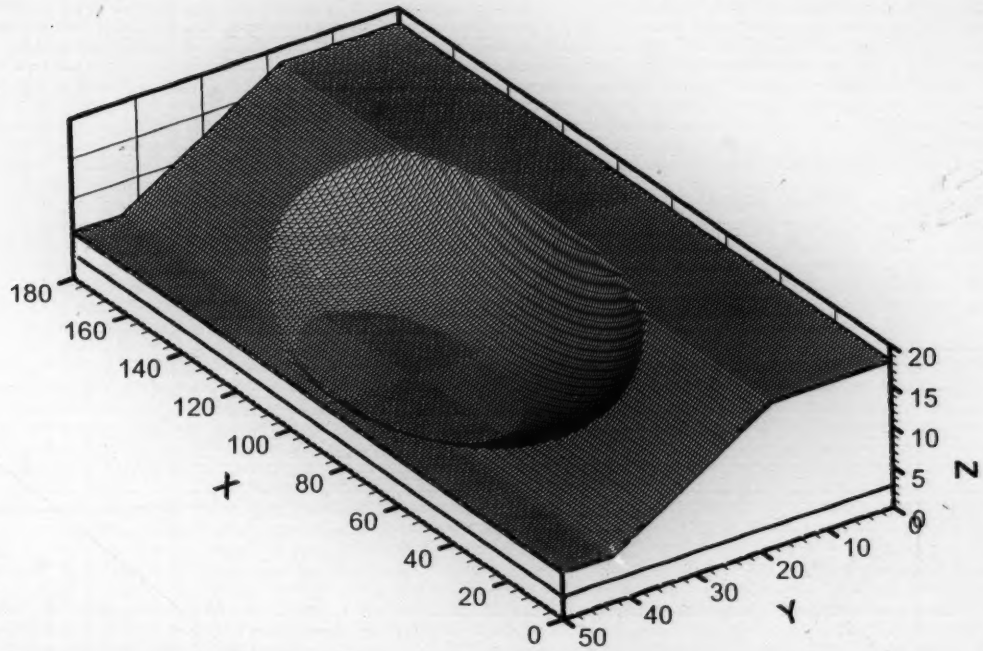

Figure 4.11: Slip surface generated for Case 1 considering a slide volume of 13,000m^3.

Initially, the internal stress state was calculated using a finite element mesh with NGRID equal to 10 (i.e., grid spacing = 180m/10 = 18m). The computed stresses were exported to an intermediate grid with 45 increments in the x-direction (4m spacing), 25 increments in the y-direction (2m spacing), and 36 increments in the z-direction (0.25m spacing). The initial grid spacing for the intermediate grid was selected with the understanding that: 1) a small spacing would be required in the z-direction due to the weak layer, 2) the largest spacing would be allowed in the x-direction because the soil properties and geometry are continuous, and 3) the spacing in the *y*-direction should be somewhere in between.

A series of slope stability models were generated to determine the relationship between the computed factor of safety and the number of planes used to discretize the slip surface (Figure 4.11). The relationship for NGRID equal to 10 is shown in

Figure 4.12. The factor of safety decreases from 1.763 to 1.713 as the number of planes increases from 1,200 to 19,200.

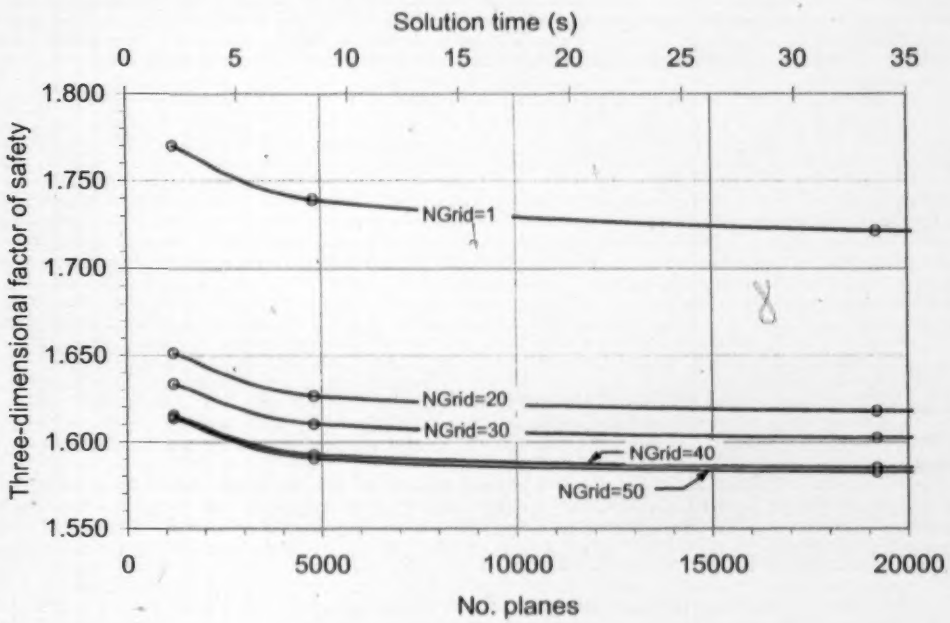

Figure 4.12: Results of a sensitivity study used to determine the appropriate density for the finite element mesh for Case 1.

The remaining curves in Figure 4.12 illustrate the effect of increasing the density of the finite element mesh by increasing NGRD from 10 to 50 in four equal increments. Each curve is shifted downward until convergence is obtained when NGRID is equal 50. A number of additional trials were completed in a separate analysis to determine the appropriate grid density for the intermediate grid linking the finite element stresses with the factor of safety calculation. The factors of safety for both cases were calculated with NGRID equal to 50, an intermediate grid with 45, 25, and 90 increments in the x, y, and z-directions, and approximately 20,000 planes to discretize the critical slip surface.

The factor of safety for Case 1 is equal to 1.607 while the factor of safety for Case 2 is equal to 1.514. The factors of safety computed for Case 1 and Case 2 are

compared to the results from other studies in Table 4.2. The results from the stress-based slope stability method appear to be within the limits of uncertainty associated with slope stability calculations.

Table 4.2: A comparison between the factors of safety computed for verification example No. 2.

Author	method	Case 1: without water table 13,000 m^3	Case 2: with water table 16,000 m^3
Xing (1988)	Ordinary	1.553	1.441
Hungr (1989)	Bihsop's simplified	1.620	1.54
Lam (1993)	General limit equilibrium method	1.603	1.508
Huang and Tsai (2000)	Upper bound limit analysis	1.665	-
Chen (2004)	Upper bound limit analysis	1.656	-
Current Study	Stress based method	1.607	1.514

The results confirm that the proposed method can be effective for larger-scale problems involving thousands of cubic meters of material. The analysis also illustrates the ability of the proposed method to evaluate cases involving non-circular failure surfaces with consideration of force and moment equilibrium.

4.4.2.3 Influence of Poisson's Ratio on the Three-Dimensional Factor of Safety

A sensitivity analysis was completed to determine the influence of Poisson's ratio (v) on the computed factor of safety for the slope conditions considered in Case 1 (i.e., Slide volume of 13,000 m^3 and no piezometric surface). A series of models were completed considering six values of Poisson's ratio including 0.0, 0.1, 0.2, 0.3, 0.4, and 0.49.

Figure 4.13 illustrates the relationship between Poisson's ratio (v) and the computed three-dimensional factor of safety for Case 1. The range of Poisson's ratio values are listed on the *x*-axis and the corresponding three-dimensional factors of

safety are shown on the y-axis. The percent difference from the factor of safety determined from the sensitivity analysis (i.e., 1.607) is reported on the right y-axis. The figure also provides information regarding the number of inadmissible planes along the slip surface depending on the Poisson's ratio selected in the finite element stress analysis.

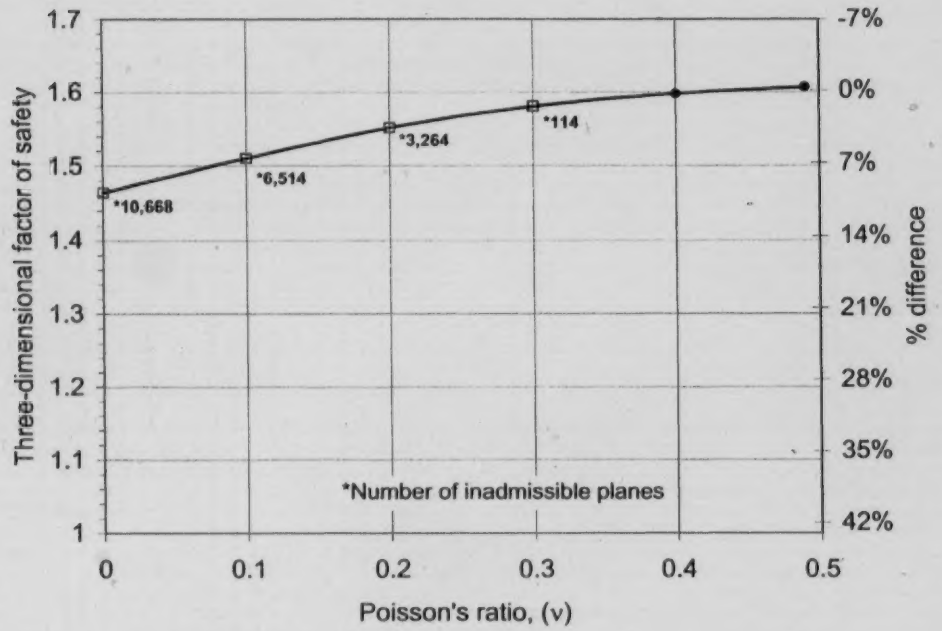

Figure 4.13: Influence of Poisson's ratio on the three-dimensional factor of safety for Case 1.

The factor of safety increases from 1.464 when Poisson's ratio is equal to 0 to 1.607 when Poisson's ratio is equal to 0.49. The factor of safety varies by approximately 10% over the range of Poisson ratio values considered in the sensitivity study. The number of inadmissible planes has the same effect on the factor of safety calculation in that the factor of safety is closest to the accepted value when no planes violate the admissibility criteria; however, the overall effect of Poisson's ratio seems to be less dramatic.

4.4.3 Verification Example No. 3: Leshchinsky et al. (1985)

Leshchinsky et al. (1985) presented an analytical method where the equations of equilibrium are arranged as an isoperimetric problem and variational calculus is applied to determine the critical log-spiral failure surface. The method was used to evaluate the stability of the embankment described by the cross-section shown in Figure 4.14. The characteristics of the slope were selected such that the two-dimensional factor of safety is equal 1.0. A three-dimensional slope stability analysis was carried out to determine the entry point along the crest of the slope for the slip surface with the lowest factor of safety. The critical slip surface was forced to pass through the toe of the slope and the width-to-length ratio was selected to result in a slip surface similar to the one shown in Figure 4.15. The entry point near the crest of the slope was determined through a trial and error procedure.

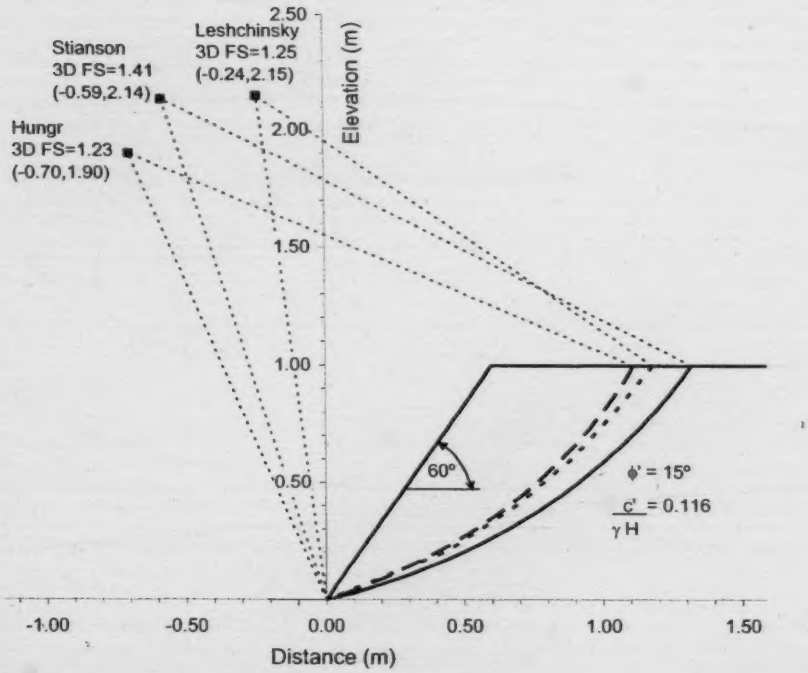

Figure 4.14: Comparison of the factor of safety for the three-dimensional slip surfaces found using the variational approach developed by Leshchinsky et al. (1985), the method of columns approach developed by Hungr et al. (1989), and the procedure developed for the current study.

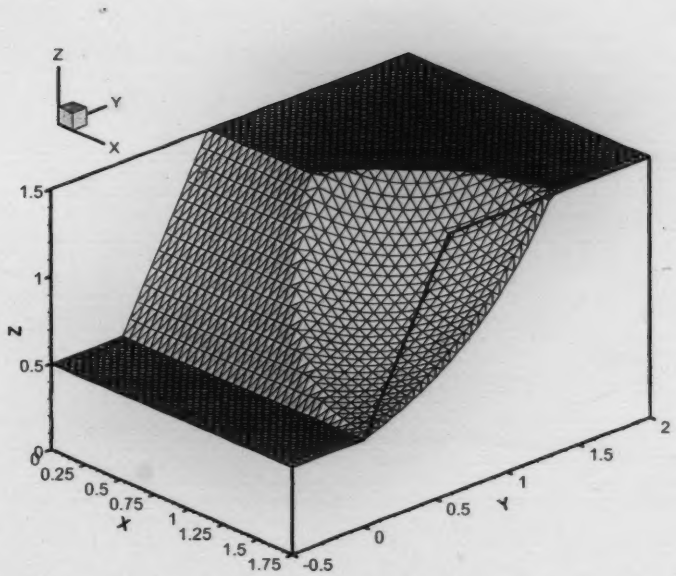

Figure 4.15: Three-dimensional slip surface found using the procedure developed for the current study.

A similar analysis was completed using the proposed slope stability method to determine the factor of safety and the centre for the critical ellipsoidal failure surface with a comparable width-to-length ratio. The width-to-length ratio was controlled by considering ellipsoidal slip surfaces with an aspect ratio equal to 0.66, as suggested by Hungr et al. (1989). The results from all three studies are compared in Figure 4.14.

The most significant difference between the results is that the factor of safety computed based on finite element stresses is approximately 11% larger than the factors of safety computed using the other methods. The difference is not surprising considering the potential differences in the stresses used to compute the factor of safety. The formulation presented by Leshchinsky et al. (1985) was found to be independent of the stresses acting on the sip surface. The extension of Bishop's simplified method to three-dimensions (Hungr et al. 1989) involves vertical and

moment equilibrium and follows a procedure similar to the original two-dimensional formulation. The stress distribution along potential failure surfaces associated with Bishop's method of analysis are known to have different characteristics when compared to the stress distribution associated with finite element slope stability analyses, especially near the toe of the slope (Krahn 2003). The stresses near the toe of the slope are generally higher from a finite element analysis and can lead to an increase in the normal stresses acting on the slip surface. Higher normal stresses can contribute to the stability of the slope resulting in larger factors of safety.

4.4.4 Verification Example No. 4: Dennhardt and Forster 1985

Dennhardt and Forster (1985) presented an analytical method to calculate the factor of safety for a three-dimensional ellipsoidal slip surfaces. The method was used to identify the ellipsoidal slip surface with the lowest factor of safety for the three-dimensional slope shown in Figure 4.16. A three-dimensional failure was generated by loading the slope over a 5 x 2 meter area, with one meter of material. The material was assigned a unit weight equal 55 kN/m3 to simulate a surcharge equal to 55 kPa. The load was placed along the axis of symmetry, 1m behind the crest of the slope. The geometrical characteristics and the factor of safety for the critical ellipsoidal slip surface found by Dennhardt and Forster (1985) are presented in Figure 4.16.

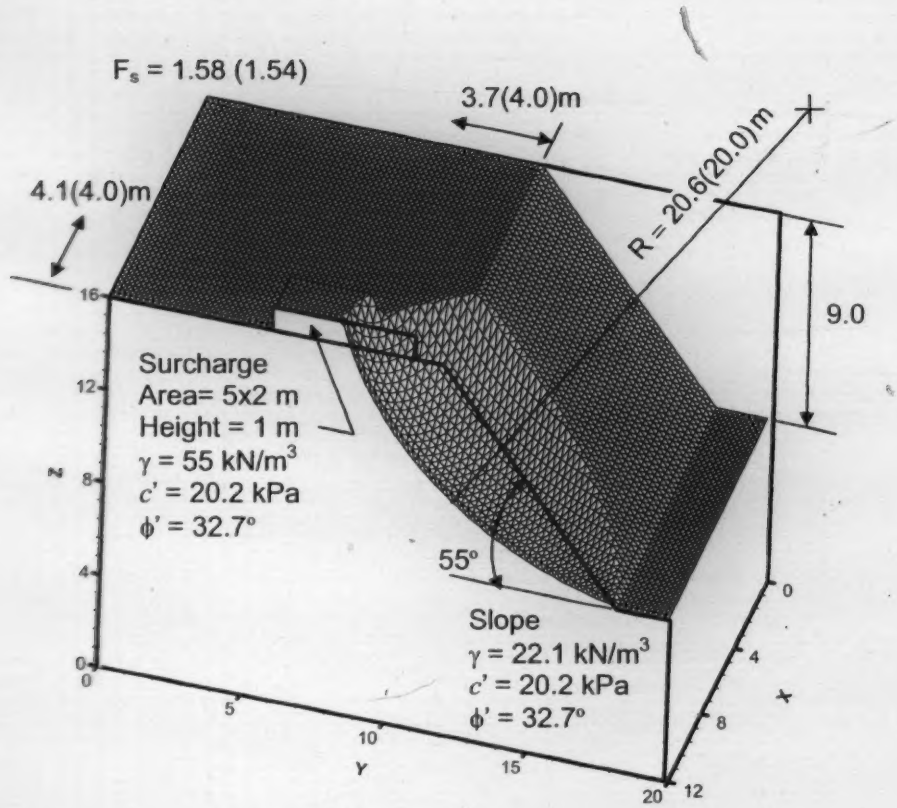

Figure 4.16: Slope stability results for a three-dimensional slope with a surcharge load of 55 kPa. Numbers without parentheses are from Hungr et al. (1989). Numbers with parentheses are from Dennhardt and Forster (1985).

Hungr et al. (1989) used the results published by Dennhardt and Forster (1985) to evaluate the three-dimensional method of columns formulation based on Bishop's simplified method. The slip surface found by Hungr et al. (1989) displayed similar characteristics to the slip surface found by Dennhardt and Forster (1985). The results reported by both authors are compared in Figure 4.16.

The overall factor of safety and some of the geometrical characteristics of the critical ellipsoidal slip surface found using the proposed technique are different from those reported by Dennhardt and Forster (1985) and Hungr et al. (1989). The most significant difference is that the slip surface with the lowest factor of safety is

cylindrical, corresponding to plane strain failure. Another less significant difference is that the slip surface does not pass directly through the toe of the slope. The slip surface exits a small distance above the toe of the slope avoiding areas with increased stress that contribute to the overall stability of the slope. The entry point on the top of the slope was determined to be 3.5m from the crest of the slope, similar to the distances reported by Dennhardt and Forster (4.0m) and Hungr et al. (3.7m). A sensitivity analysis was completed to determine the factors contributing to the differences observed in the exit distance of the slip surface in the *x*-direction. First, two- and three-dimensional plane strain analyses were carried out, for both loaded and unloaded conditions, to identify the conditions that should be satisfied to result in a typical three-dimensional failure surface (i.e., a failure surface that does not extend infinitely in the *x*-direction). Next, a series of three-dimensional analyses were completed to determine the relationship between the three-dimensional factor of safety (i.e., surcharge load) and the exit distance in the x-direction.

The three-dimensional factor of safety for the loaded plane strain scenario (i.e., cylindrical slip surface) is dependent on the length of the slope in the *x*-direction. If the length of the slope is equal to the width of the surcharge (2m), the three-dimensional factor of safety for the loaded plane strain case should be equal to the loaded two-dimensional case. The factor of safety for the loaded two-dimensional case is equal to 1.32, based on stresses from a finite element analysis (Dennhardt and Forster (1985) reported 1.29 using the Morgenstern and Price Method). If the length of the slope is increased infinitely in the *x*-direction, the effect of the surcharge load will eventually become insignificant. The three-dimensional factor of safety for the cylindrical slip surface increases and approaches the two-dimensional unloaded case. The two-dimensional factor of safety for the case with no load applied is equal to 1.54, based on stresses from a finite element analysis (1.44 using the two-dimensional Morgenstern and Price or Bishop Simplified method). For a typical three-dimensional failure surface to be the most critical, it seems reasonable to expect that the factor of safety should be less than the unloaded plane strain case. It is interesting to observe that the three-dimensional factors of safety reported by Dennhardt and

Forster (1.54) and Hungr et al. (1.58) are higher than the unloaded plane strain case (1.44).

The results from a series of loaded three-dimensional models are presented to investigate the relationship between the exit distance of the slip surface and the factor of safety. In one case, the factor of safety is controlled by increasing or decreasing the surcharge applied to the crest while Poisson's ratio is equal 0.48. In the other case, Poisson's ratio is equal 0.30. The exit distance of the slip surface is controlled by the aspect ratio of the ellipsoid. The exit distance increases as the aspect ratio is increased. An exit distance equal to 4m corresponds to an aspect ratio of approximately 0.5 while an exit distance equal to 10m corresponds to an aspect ratio of approximately 1.2. An aspect ratio of 1,000 represents an infinite slip surface (i.e., plane strain conditions).

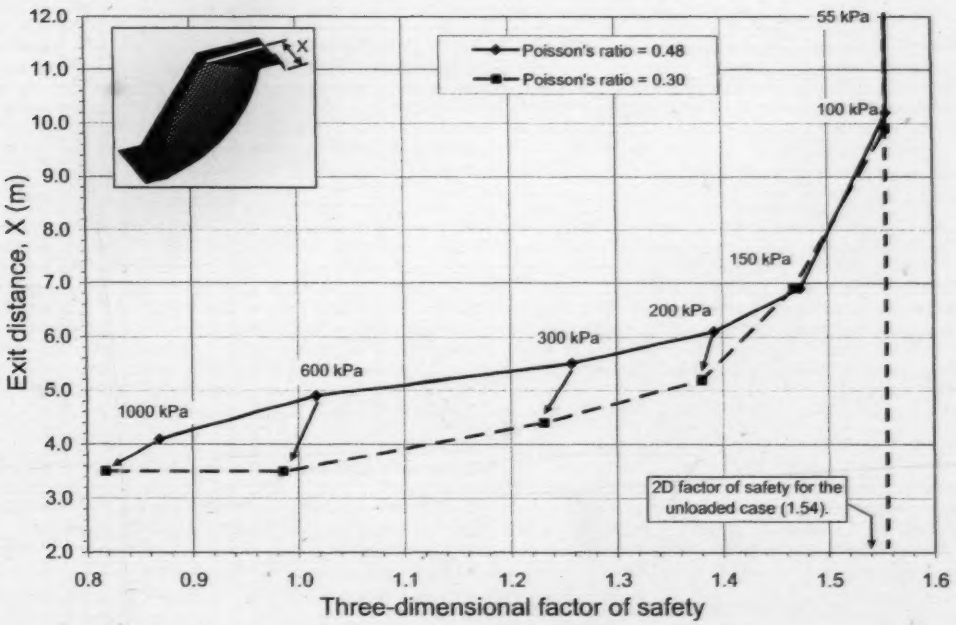

Figure 4.17: Relationship between the exit distance of the three-dimensional failure surface and the three-dimensional factor of safety.

The exit distance increases exponentially as the three-dimensional factor of safety approaches the unloaded two-dimensional plane strain case. A distinct three-dimensional failure surface, contained within the 24m length of slope (see Figure 4.16), does not begin to emerge until the three-dimensional factor of safety decreases to approximately 1.47. A factor of safety equal to 1.47 is approximately 5% lower than the factor of safety for the unloaded plane strain case and corresponds to a surcharge equal to 150 kPa. The results seem to support the thinking that the three-dimensional factor of safety should be lower than the factor of safety for the unloaded plane strain condition to develop a typical three-dimensional failure (i.e., including end effects). The exit distance steadily decreases as the three-dimensional factor of safety is reduced due to the application of additional load. The exit distance approaches the values reported by Dennhardt and Forster (1985) and Hungr et al.

(1989) once the surcharge load is increased beyond 600 kPa or the three-dimensional factor of safety decreases below 1.0.

One additional model was completed for each surcharge load with Poisson's ratio equal to 0.3. Poisson's ratio affects the exit distance of the slip surface as well as the factor of safety. The curve describing the relationship between the exit distance and the three-dimensional factor of safety for the case where Poisson's ratio was equal to 0.3 is shown in Figure 4.17. The curve is shifted down and to the left when compared to the relationship determined using Poisson's ratio equal to 0.48. It appears that the exit distance decrease as Poisson's ratio is decreased.

4.5 Discussion

The results from each comparison demonstrate that the proposed slope stability method provides a reliable estimate of the three-dimensional factor of safety. The accuracy of the factor of safety calculation is affected by the density of the finite element mesh used to compute the internal stresses, the intermediate grid used to link the finite element analysis and the slope stability calculations, the discretization of the slip surface, and the admissibility of individual planes along the slip surface. Detailed sensitivity studies are presented in the first and second examples to show that the density of each mesh can be increased to a level where the variation in the factor of safety is no longer significant. The procedure is shown to provide reasonable estimates of the factor of safety for large scale failures often encountered in practice.

Sensitivity studies are also presented to demonstrate the influence of Poisson's ratio on the three-dimensional factor of safety. The Poisson's ratio selected in the 'switch on' gravity analysis partially controls the relationship between the horizontal and vertical stresses (i.e., $K_o = \sigma_x/\sigma_y = \nu/(1 - \nu)$). Selecting different values for Poisson's ratio can influence the direction of forces acting on individual planes along the slip surface. In some cases, certain planes can be considered kinematically inadmissible because the shear force acts contrary to the assumed direction of failure.

It appears that the overall variability in the factor of safety increases as the number of inadmissible planes increases. The factor of safety is shown to be the most reliable when Poisson's ratio is selected so that a minimum number of planes violate the kinematic admissibility criteria. The results confirm the conclusion made by Stianson (2008) that finite element slope stability results can be misleading if slip surfaces of a certain shape are automatically assumed to be admissible.

The third and fourth example problems are examples of other cases where the characteristics of the finite element stress distribution can result in differences in the slope stability calculations. The factor of safety computed in the third example is approximately 11% higher than the factor of safety computed using the method of columns. The increase in the factor of safety is considered to be due to the presence of stress concentrations near sharp breaks in the geometry at the toe of the slope. The fourth example considers a case where a surcharge is applied on the crest of the slope to initiate a three-dimensional failure. A significantly higher surcharge is required in the finite element analysis to produce a slip surface with similar characteristics as the slip surface found using the method of columns.

4.6 Conclusion

A procedure is developed where stresses from a separate finite element analysis are incorporated into a limit equilibrium framework to evaluate the stability of three-dimensional slopes. The resulting three-dimensional finite element factor of safety equation is determinate and satisfies all conditions of equilibrium. In addition, the factor of safety can be computed directly and does not require the use of complex iterative procedures. The proposed method is used to re-analyze a series of published example problems. The results from each comparison demonstrate that the stress-based finite element method provides a reliable estimate of the three-dimensional factor of safety. The stability of each slope considered in the current research is evaluated using symmetrical ellipsoidal failure surfaces. The ability to satisfy all conditions of equilibrium means that the procedure can be used to evaluate the factor

of safety for three-dimensional slip surfaces of any arbitrary shape provided that the slip surface is kinematically admissible. This research has set the stage to go the next step and incorporate non-linear searching techniques to alleviate assumptions regarding the shape of the three-dimensional slip surface.

4.7 Bibliography

Baligh, M.M., and Azzouz, A.S. 1975. End effects of stability of cohesive slopes. Journal of the Geotechnical Engineering Division, ASCE, 101(GT 11): 1105-1117.

Bishop, A.W. 1955. The use of the slip circle in the stability analysis of slopes. Geotechnique, 5: 7-17.

Chen, J. 2004. Slope stability analysis using rigid elements. Dissertation, Hong Kong Polytechnic University, Hong Kong.

Chen, R.H., and Chameau, J.L. 1982. Three-dimensional limit equilibrium analysis of slopes. Geotechnique, 32(1): 31-40.

Chen, Z.Y., Wang, J., Wang, Y.J., Yin, J.H., and Haberfield, C. 2001. A three-dimensional slope stability analysis method using the upper bound theorem - Part II: numerical approaches, applications and extensions. International Journal of Rock Mechanics and Mining Sciences, 38(3): 379-397.

Dennhardt, M., and Forster, W. 1985. Problems of three-dimensional slope stability. *In* Proceedings, 11th International Conference on Soil Mechanics and Foundation Engineering. San Francisco, Vol.2, pp. 427-431.

Fan, K., Fredlund, D.G., and Wilson, G.W. 1986. An interslice force function for limit equilibrium slope stability analysis. Canadian Geotechnical Journal, 23(3): 287-296.

Fellenius, W. 1936. Calculations of the stability of earth dams. *In* Transaction of the 2nd Congress on Large Dams. Washington DC, Vol.4, p. 445

Fredlund, D.G., and Krahn, J. 1977. Comparison of slope stability methods of analysis. Canadian Geotechnical Journal, 14(3): 429-439.

Fredlund, D.G., and Rahardjo, H. 1993. Soil Mechanics for Unsaturated Soils. John Wiley & Sons, Inc., New York, N. Y.

Fredlund, D.G., Krahn, J., and Pufahl, D.E. 1981. The relationship between limit equilibrium slope stability methods. *In* Proceedings of the International Conference on Soil Mechanics and Foundations Engineering. Stockholm, Sweden, Vol.3, pp. 409-416.

Fredlund, D.G., Scoular, R.E.G., and Zakerzadeh, N. 1997. Using finite element stress analysis to compute the factor of safety. *In* 52nd Canadian Geotechnical Conference. Regina, Saskatchewan, Canada, pp. 73-80.

Gens, A., Hutchinson, J.N., and Cavounidis, S. 1988. Three-dimensional analysis of slides in cohesive soils. Geotechnique, 38(1): 1-23.

Hungr, O. 1987. An extension of Bishop's simplified method of slope stability analysis to three dimensions. Geotechnique, 37(1): 113-117.

Hungr, O. 2001. CLARA-W: Slope Stability Analysis in two or three Dimensions for microcomputers. O. Hungr Geotechnical Research, Vancouver, B.C.

Hungr, O., Salgado, F.M., and Byrne, P.M. 1989. Evaluation of a three-dimensional method of slope stability analysis. Canadian Geotechnical Journal, 26(4): 679-686.

Janbu, N., Bjerrum, L., and Kjaernsli, B. 1956. Soil mechanics applied to some engineering problems. Norwegian Geotechnical Institute, Publication No. 16 (in Norwegian).

Krahn, J. 2003. The 2001 R.M. Hardy Lecture: The limits of limit equilibrium analyses. Canadian Geotechnical Journal, 40(3): 643-660.

Kulhawy, F.H. 1969. Finite element analysis of the behavior of embankments. Dissertation, University of California, Berkeley, California, USA.

Lam, L., and Fredlund, D.G. 1993. General limit equilibrium model for three-dimensional slope stability analysis. Canadian Geotechnical Journal, 30(6): 905-919.

Leshchinsky, D., Baker, R., and Silver, M.L. 1985. Three-dimensional analysis of slope stability. International Journal for Numerical and Analytical Methods in Geomechanics, 9(3): 199-223.

Loehr, J.E. 1998. Development of a hybrid limit equilibrium-finite element procedure for three-dimensional slope stability analysis. Dissertation, The University of Texas at Austin, Texas, USA.

Morgenstern, N.R., and Price, V.E. 1965. The analysis of slope stability of general slip surfaces. Geotechnique, 15(1): 79-63.

Pham, H.T.V. 2002. Slope Stability Analysis Using Dynamic Programming Method Combined With a Finite Element Stress Analysis. Thesis, University of Saskatchewan, Saskatoon, Canada.

Scoular, R.E.G. 1997. Limit equilibrium slope stability analysis using a stress analysis. Thesis, University of Saskatchewan, Saskatoon, Canada.

Silvestri, V. 2006a. A three-dimensional slope stability problem in clay. Canadian Geotechnical Journal, 43(2): 224-228.

Silvestri, V. 2006b. Erratum: A three-dimensional slope stability problem in clay. Canadian Geotechnical Journal, 43(10): 1.

Spencer, E. 1967. A method for analysis of the stability of embankments assuming parallel interslice forces. Geotechnique, 17(1): 11-26.

Stianson, J.R. 2008. A three-dimensional slope stability method based on finite element stress analysis and dynamic programming. Dissertation, University of Alberta, Canada.

Xing, Z. 1988. Three-dimensional stability analysis of concave slopes in plan view. Journal of Geotechnical Engineering, ASCE, 114(6): 658-671.

Chapter 5

Three-Dimensional Slope Stability Based on Dynamic Programming and Finite Element Stresses Analysis

5.1 Introduction

Admissibility criteria play a critical role in the application of searching procedures to locate the critical slip surface in two- and three-dimensional limit equilibrium slope stability analyses. Admissibility criteria can be used to train the searching procedure to distinguish between reasonable and unreasonable slip surfaces. The goal is to select admissibility criteria that are sufficiently flexible to provide an exhaustive search (i.e., the most likely failure surface is included in the search) yet restrictive enough to result in a search that is efficient (i.e., meaningless slip surfaces are excluded from the search). Neglecting to use appropriate admissibility criteria can compromise the efficiency of the search by including unreasonable slip surfaces that have little resemblance to real cases.

The ability to invoke admissibility criteria is closely related to the method used to compute the factor of safety. Traditional two-dimensional method of slices techniques invoke no kinematical considerations regarding soil behavior and hence require assumptions regarding the overall shape of potential failure surfaces (Morgenstern and Price 1965). Assumptions regarding the shape of the slip surface are generally justified on the grounds that the computational procedure is made simpler. However, Ching and Fredlund (1983) provide examples where an analyst

might seemingly select a reasonable shape (i.e., circular or composite) that in the end might result in the violation of basic soil behavior principles including cases where the factor of safety is less than zero or tensile forces exist within the sliding mass. Ching and Fredlund (1983) developed an admissibility criterion based on active and passive earth pressure theory that can be used to identify and modify the shape of problematic failure surfaces. The earth pressure constraint acts as a secondary admissibility criterion used to modify the primary shape of the slip surface selected by the analyst. Similar admissibility criteria are applied in the three-dimensional method of columns techniques for the calculation of factor of safety. The primary shape of the slip surface is typically assumed to be an ellipsoid and is subject to secondary modifications.

More sophisticated admissibility criteria have been developed as a result of the application of two-dimensional stress-based slope stability methods (Pham and Fredlund 2003). The admissibility criterion developed by Pham and Fredlund (2003) can be used to govern the shape of the overall slip surface without the use of arbitrary assumptions. The criterion includes both circular and non-circular failure surfaces and is made possible as a result of calculating the internal stress distribution prior to performing the slope stability calculations. It is reasonable that the admissibility criteria developed for two-dimensional finite element slope stability calculations be extended to three-dimensional slope stability problems.

The objective of this research is to demonstrate a proeedure that can be used to simultaneously determine the shape, location, and factor of safety for the critical slip surface in three-dimensional slope stability problems. The procedure is designed to use stresses from an independent finite element analysis to compute the factor of safety. The dynamic programming methodology is used to search for the critical slip surface. The shape of the critical slip surface is not pre-defined, however, that does not mean that the dynamic programming searching procedure indiscriminately considers every possible slip surface. The searching procedure is trained to distinguish between reasonable and unreasonable slip surfaces through the use of a series of admissibility criteria. The admissibility criteria used to govern the three-

dimensional slope stability calculations are developed based on extensions of admissibility criteria that have been successfully applied in two-dimensional slope stability methods.

5.2 Background

Admissibility criteria are used to judge whether or not a potential slip surface is worthy of consideration in the slope stability analysis. It is possible to distinguish between two classes of admissibility; namely, geometric and kinematic admissibility criteria. Geometric admissibility criteria (GAC) are based strictly on the geometric properties of the slip surface. Kinematic admissibility criteria (KAC) can be formulated based on principles of soil behavior, equilibrium considerations, and the kinematics required to produce physically realistic slip surfaces. Kinematic admissibility criteria are typically considered to be more flexible than geometric admissibility criteria. The application of certain admissibility criteria is closely related to the method used to compute the factor of safety and the procedure used to search for the critical slip surface. A number of geometric and kinematic admissibility criteria identified in the literature are summarized in Table 5.1 and Table 5.2.

Table 5.1: Geometric admissibility criteria applied in two-dimensional slope stability formulations.

Geometric Admissibility Criteria	
Circle (traditional limit equilibrium methods) (Nguyen 1985), (De Natale 1991)	$(x-x_c)^2+(y-y_c)^2=R^2$
Concave (Baker 1980)	$\partial^2 y/\partial^2 x \geq 0$

The circular GAC is one of the simplest and most restrictive admissibility criteria. The advantage of using the circular GAC is that the shape and location of potential slip surfaces can be described using three parameters. 'Grid and radius' searching techniques have been developed to systematically evaluate various combinations of the parameters to identify the slip circle with the lowest factor of safety. Steps have also been taken to consider composite slip surfaces by including the ability to specify pre-defined lines of intersection. The lines of intersection are used to simulate the location of weak layers within the slope. The critical composite slip surface and the critical circular slip surface are typically identified in separate searches.

The application of the dynamic programming searching technique in two-dimensional slope stability promoted the development of a more general GAC. The GAC developed by Baker (1980), $\partial^2 y / \partial x^2 \geq 0$, considered the use of concave slip surfaces. The searching procedure proposed by Baker (1980) is considerably more flexible than the grid and radius approach and can be used to consider circular and composite slip surfaces in the same search. The concave GAC should be used in combination with factor of safety equations satisfying all conditions of equilibrium.

Classic earth pressure theory has been used to develop KAC to limit the angle of inclination of individual line segments along a slip surface. The inclination of the slip surface in the active zone should not exceed the limit of $45+\phi/2$ and the inclination of the slip surface in the passive zone should not exceed $45-\phi/2$. Boutrup and Lovell (1980) used the earth pressure constraints to control the shape of randomly generated slip surfaces while Ching and Fredlund (1983) used earth pressure constraints to modify the slip surface at the end of a method of slices analysis. Ching and Fredlund (1983) found that specifying a circular or composite slip surface could result in the violation of basic soil behavioral principles. In moderate cases, the factor of safety might be under-estimated but in more severe cases the factor of safety could be negative. The results indicated that GAC might result in slip surfaces that violate certain principles of soil mechanics if used in isolation of other considerations.

Table 5.2: Kinematic admissibility criteria applied in two-dimensional slope stability formulations.

Kinematic Admissibility Criteria	
Theoretical Principle	Governing Equation
Earth Pressure Theory (Boutrup and Lovell 1980) (Ching and Fredlund 1983)	Active Case: $\theta \leq 45 + \phi/2$ Passive Case: $\theta \leq 45 - \phi/2$
Force Equilibrium (Baker 1980), (Greco 1996)	$p_{\alpha_i} = \cos(\alpha_i - \theta)\left[1 + \frac{\tan\phi_i}{F}\tan(\alpha_i - \theta)\right] > 0.3 - 0.4$
Failure criterion of the soil (Morgenstern and Price 1965)	The line of thrust, computed based on moment equilibrium, must not pass below the slip surface.
Kinematics of the sliding mass (Pham and Fredlund 2003)	$\tau_n = \tau_{xy}\left(\sin^2\theta - \cos^2\theta\right) - \left(\frac{\sigma_x - \sigma_y}{2}\right)\sin 2\theta$

Baker (1980) proposed an additional admissibility criterion to be used in combination with Spencer's method of slices technique. The criterion was based on the rationale that force equilibrium should be satisfied for individual slices if the slip surface is to be considered reasonable. The criterion is not related to the geometric properties of the slip surface and is therefore classified as a KAC. The expression used to evaluate individual slices along the slip surface is listed in Table 5.2. The expression is used as part of the procedure to compute the inter-slice forces. The restriction that P_α be in the range of 0.3 to 0.4 is necessary to ensure that force equilibrium is satisfied (i.e., the force polygon for an individual slice closes). Similar expressions can be developed for other method of slices techniques to evaluate the satisfaction of force equilibrium for individual slices. Greco (1996) presented a summary of the expressions used in combination with various method of slices techniques including Bishop's Simplified method, Janbu's method, and Spencer's method. Greco (1996) confirmed that slip surfaces violating the criterion (i.e., P_α

>0.3 to 0.4) tend to assume shapes that are kinematically inadmissible and can be excluded from the analysis.

Morgenstern and Price (1965) introduced an admissibility criteria based on the rationale that the failure criterion for the soil must not be violated. The failure criterion is considered to be violated if a state of tension is implied within the soil mass above the slip surface. Morgenstern and Price (1965) indicated that it is possible to determine whether or not a state of tension is implied by computing the location of the line of thrust. The line of thrust is computed using moment equilibrium and describes the line of action of the resultant inter-slice forces acting on individual slices. Tension is considered to exist within the sliding mass if the line of the thrust passes below the slip surface. Slip surfaces that result in a violation of the failure criterion of the soil are excluded from the analysis.

Pham and Fredlund (2003) developed a KAC based on the consideration that the actuating force should act in the same direction as mass movement. The admissibility of individual line segments along a potential slip surface is evaluated by computing the direction of the actuating shear stress based on a Mohr's Circle analysis of the finite element stresses. The criterion is more flexible than the concave criterion because it can be used to model cases where weak layers within the slope might result in a slip surfaces that are not strictly concave.

The application of admissibility criteria in three-dimensional slope stability is less advanced. In most cases, GAC are used to restrict the shape of potential slip surfaces to pre-defined mathematical shapes such as ellipsoids. Composite slip surfaces are often considered in a separate analysis involving a procedure where the ellipsoid is intersected with a plane corresponding to the location of a weak layer. Yamagami and Jiang (1997) developed a three-dimensional slope stability method based on the combination of dynamic programming and Spencer's method of slices technique. The concave admissibility criterion originally proposed by Baker (1980) was adopted to relax the restrictions typically placed on the shape of three-dimensional slip surfaces. However, difficulties were encountered as a result of the extremely large number of potential slip surfaces that needed to be considered in even the simplest

three-dimensional slope stability analysis. Yamagami and Jiang (1997) used random number generation to limit the number of slip surfaces to be considered in the dynamic programming search to reduce the computational time required to complete an analysis. The current three-dimensional slope stability method is formulated considering the possibility of improving the efficiency of three-dimensional searching procedures by combining existing GAC with KAC. It is possible to investigate the application of more advanced KAC as a result of the development of three-dimensional slope stability methods where the factor of safety is computed based on finite element stresses and the search for the critical slip surface is completed using dynamic programming (Stianson 2008).

5.3 Application of the Dynamic Programming Optimization Technique to Three-Dimensional Slope Stability

The dynamic programming method is a numerical algorithm used to optimize sequential multi-stage decision problems (Bellman 1957). Multi-stage decision problems are solved using a system of *stages* and *states*. The *stages* associated with the dynamic programming search are in no way related to other staged systems typically referred to in slope stability literature (i.e., staged construction sequence, etc.). Likewise, the *states* associated with the dynamic programming search are in no way related to soil behavior (i.e., stress state, limit state, critical state soil mechanics etc.). Dividing the slope stability calculation into a *stage-state* system facilitates the calculation of the factor of safety for trial slip surfaces while at the same time searching for the slip surface with the lowest factor of safety. The details regarding the development of the *stage-state* system, the factor of safety equation, and the optimization procedure used to search for the critical slip surface are presented in the following sections.

5.3.1 Development of a *Stage-State* System

Yamagami and Jiang (1997) developed a scheme for dividing the three-dimensional slope stability calculations into a *stage-state* system. *Stages* were defined as a series of two-dimensional cross-sections aligned perpendicular to the assumed direction of failure (i.e., *stage cross-sections*). A *state* was defined as one curve on one *stage cross-section* (i.e., *state curve*). The shaded region shown in Figure 5.1 results from the connection of *state curve* (jj) from *stage* [i] to *state curve* (kk) in *stage* [i+1] and represents a narrow section of a three-dimensional slip surface. A complete three-dimensional slip surface can be generated by connecting one *state* curve from each *stage cross-section*.

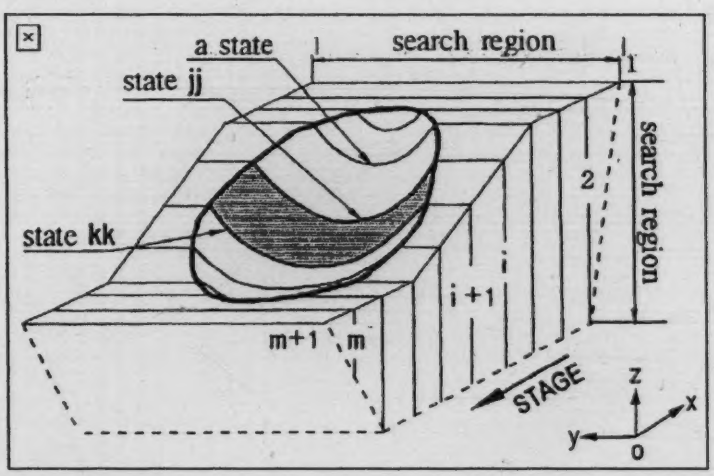

Figure 5.1: Stage-state system proposed by Yamagami and Jiang (1997).

A separate numerical procedure involving random number generation was developed to generate a specified number of concave *state curves* on each *stage cross-section*. Once a sample of *state curves* was generated on each *stage cross-section*, the dynamic programming algorithm was used to determine the combination

of *state curve* connections that resulted in the three-dimensional slip surface with the lowest factor of safety.

The proposed formulation uses a similar procedure to divide the three-dimensional slope stability calculations into a *stage-state* system. The main difference between the procedure developed by Yamagami and Jiang (1997) and the proposed procedure is the numerical technique used to generate *state curves* on each *stage cross-section*. More detail regarding the generation of *state curves* is provided in the following section.

5.3.2 Admissibility Criteria Governing the Shape of the Slip Surface Perpendicular to Movement

The generation of *state curves* is an intermediate step in the overall slope stability evaluation. First, a discretization scheme is used to generate a two-dimensional grid (*cross-section grid*) of points on each *stage cross-section*.

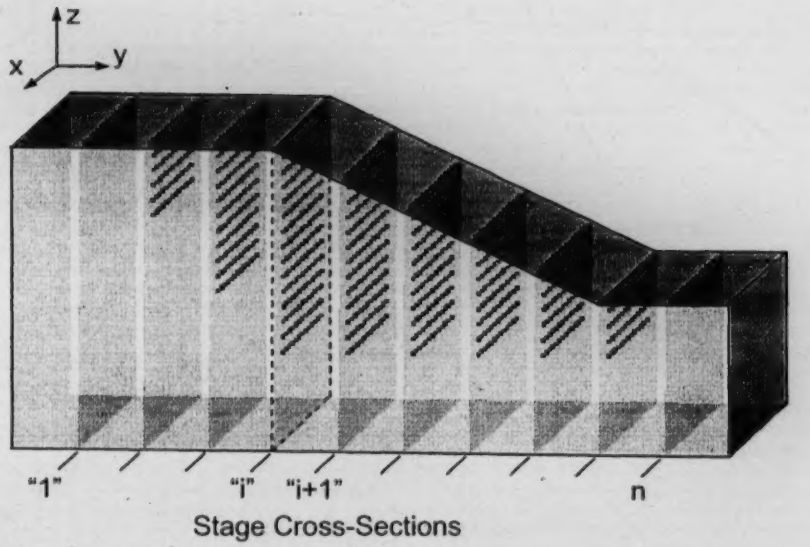

Figure 5.2: A series of regular two-dimensional *cross-section grids* generated for a number of *stage cross-sections* for a three-dimensional slope.

The regular *cross-section grid* shown in Figure 5.3 represents *stage cross-section* "*i*" outlined in Figure 5.2 and was generated by specifying a common spacing between points in the *x* and *z*-directions. A numerical procedure is used to systematically iterate from the first to the last column, connecting one grid point from each column. A broken line segment (*state curve*), extending from one side of the *cross-section grid* to the other, is formed after one complete iteration. It is evident from Figure 5.3 that *state curves* describe the shape of the slip surface in the direction perpendicular to failure. In practice, a number of iterations are performed to generate the total number of *state curves* passing certain admissibility criteria (i.e., a random number generator is not used to generate a pre-defined number of state curves on each stage cross-section). Once the *state curves* have been generated on each *stage cross-section*, the dynamic programming method is used to search for the combination of *state curves* that result in the slip surface with the lowest factor of safety.

Yamagami and Jiang (1997) suggested that the slope stability evaluation could be considered sufficiently rigorous if a few hundred *state curves* were randomly

generated for each *stage cross-section*. A detailed study was undertaken to investigate the numerical difficulties that might be encountered if a more rigorous treatment of *state curve* generation was considered.

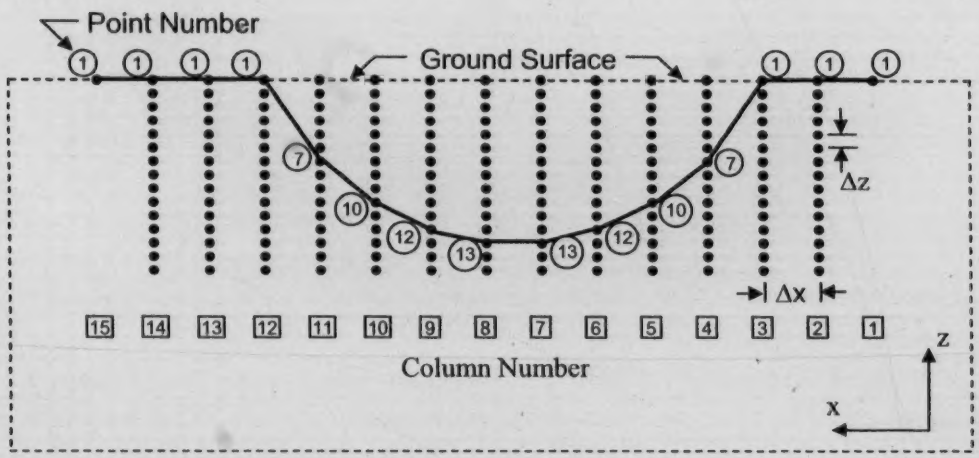

Figure 5.3: Illustration to describe the generation of state curves.

The *cross-section grid* shown in Figure 5.3 contains a total of 15 columns, each with 15 points except for the first and last columns. The points below the ground surface were excluded from the first and last columns to indicate that all *state curves* exit the slope. If *state curves* of any shape were allowed, including those that result in oscillatory slip surfaces, there would be a total of 1.95E15 (i.e., 15^{13}) *state curves* that could be generated for the grid shown in Figure 5.3. The time required to evaluate the *state curve* connections between two cross-sections is sensitive to the number of *state curves* included on each cross-section. At this point, it is prudent to discuss the number of *state curves* that the dynamic programming optimization technique can evaluate within a reasonable amount of time, given the available computing resources in a typical desktop computer.

The computer code developed for the current research has been used to solve a number of example problems. Each example has provided additional experience regarding the time required for the dynamic programming algorithm to search

through a given number of curve connections. Figure 5.4 represents a typical relationship between computer time and the total number of curve connections to be considered by the dynamic programming algorithm. The relationship shown in Figure 5.4 can be used to approximate the solution time given a certain number of curve connections or recommend the number of curve connections that will result in a reasonable solution time. The simulations were run on a 3.00GHz Pentium 4 processor with 1.0GB of random access memory (RAM).

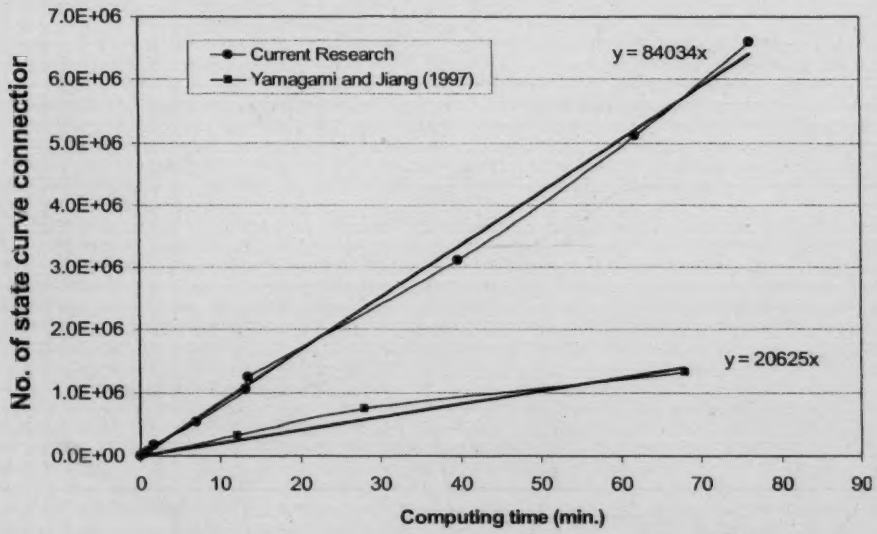

Figure 5.4: Relationship between computing time and the number of *state curve* connections.

Consider the case where the dynamic programming algorithm would be used to determine the critical curve connections between two stage cross-sections similar to the one shown in Figure 5.3. The total number of curve connections between the two cross-sections can be computed by multiplying the total number of curves in cross-section *i* by the number of curves in cross-section *i+1*. The total number of curve connections would be equal to, 1.95E15 * 1.95E15 = 3.8E30 curve connections. The solution time can be estimated using the straight line equation used to approximate

the relationship shown in Figure 5.4. The approximate solution time would be equal to 3.8E30 / 84034 = 4.52e25 minutes or 8.6E19 years! The following calculation demonstrates the need for the application of admissibility criteria to identify only those *state curves* that result in physically realistic slip surfaces. The question regarding the number of *state curves* left over after the application of appropriate admissibility criteria remains to be answered.

5.3.2.1 Concave Admissibility Criteria

Yamagami and Jiang (1997) recognized that *state curves* resulting in oscillatory slip surfaces can be excluded from the analysis on the basis that a large number of actual sliding surfaces are smooth curves. It was suggested that only *state curves* passing the admissibility criterion $\partial^2 z / \partial^2 y \geq 0$, should be included in the analysis. The admissibility criterion includes *state curves* similar to the curves shown in Figure 5.5 including concave curves (curve *a*), flat bottom curves with concave sides (curve *b*) or flat bottom curves with planar (curve *c*) sides. The admissibility criteria can be classified as GAC as it is based on the geometric properties of the slip surface.

There are at least two special cases (i.e., Eq. [5.2] and Eq. [5.3] given below) included within the overall concave admissibility criteria that will result in meaningful slip surfaces but are slightly more restrictive, resulting in fewer state curves.

[5.1] $\partial^2 z / \partial^2 y \geq 0$

[5.2] If $\partial z / \partial y = 0$ then $\partial^2 z / \partial^2 y \geq 0$ else $\partial^2 z / \partial^2 y > 0$

[5.3] $\partial^2 z / \partial^2 y > 0$

Equation [5.2] includes curves similar to curves *a* and *b* but excludes curves like *c*. Equation [5.3] only includes curves where the slope of consecutive line segments is always decreasing (i.e., curves similar to curve *a*). The variations of the concave constraint can be used to limit the number of *state curves* included in the analysis depending on the soil conditions being considered. For example, it might not be necessary to include flat bottom planar curves in simple homogeneous slopes consisting of cohesive material with no well-defined weak layers. It is well known from two-dimensional analysis that slip surfaces in homogeneous cohesive slopes are generally smooth curves.

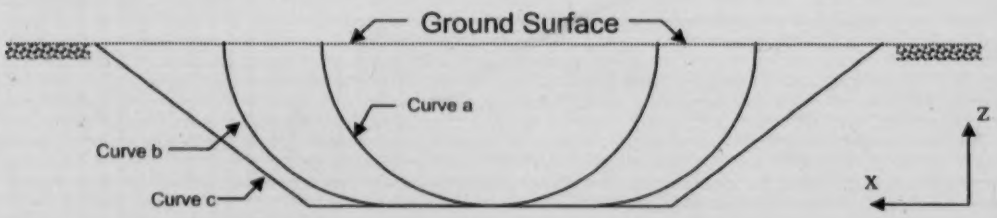

Figure 5.5: An illustration of the differences between state curves allowed by the three proposed variations of the concave constraint.

Applying the concave admissibility criteria reduces the number of state curves for the *cross-section grid* shown in Figure 5.3 from 1.95E15 curves to just over 350,000 curves. According to Figure 5.4, the computer time required to optimize the critical curve connections between two stages with 350,000 *state curves* would still be in the order of three years.

Yamagami and Jiang (1997) suggested that the total number of *state curves* could be reduced to a reasonable level by randomly selecting 100-200 *state curves* for simple symmetrical problems or 400-500 *state curves* for non-symmetrical slopes. Randomly selecting 500 curves from a sample of approximately 350,000 concave curves would mean that hundreds of thousands of potentially admissible *state curves* would indiscriminately be removed from the analysis. Ching and Fredlund (1984) also demonstrated that the application of GAC in isolation might result in slip

surfaces that violate basic principles of soil behavior. It is possible that the development of more advanced admissibility criteria might offer the ability to reduce the number of *state curves* to a reasonable level while still providing a rigorous treatment of *state curve* generation.

5.3.2.2 Earth Pressure Admissibility Criteria

Classic earth pressure theory can be used to control the inclination of line segments used to generate *state curves*. Controlling the inclination of individual line segments based on earth pressure theory will ensure the shape of the slip surface is reasonable and provide a meaningful admissibility criterion that can be used to reduce the number of *state curve* combinations. All of the *state curves* that contain line segments elevated at angles less than or equal to $45+\phi'/2$ in an active zone, or $45-\phi'/2$ in a passive zone, should be included in the search for the most critical slip surface. In practice, it is not necessary to predetermine active and passive zones if only the active constraint is applied. The sample of curves satisfying the active constraint will include all of those curves that satisfy the passive constraint. (i.e., $45+\phi'/2$ automatically includes curves passing $45-\phi'/2$). It is understood that applying only the active constraint will result in a certain number of extra curves in zones where passive failure is expected. The application of the earth pressure constraint is not the final check for slip surface admissibility and is only meant to provide a meaningful constraint that can be used to reduce the number of *state curve* combinations. The final check for admissibility is carried out using a kinematic admissibility criterion applied during the dynamic programming search.

5.3.2.3 Grid Aspect Ratio Constraint

The number of *state curves* included in the analysis after applying the earth pressure admissibility criterion depends on the friction angle of the soil and the aspect ratio of the cross-section grid. The aspect ratio of the cross-section grid is the relationship

between the horizontal grid spacing to the vertical grid spacing. The aspect ratio for the cross-section grid shown in Figure 5.3 is 1:4 (i.e., the vertical grid spacing of 0.5m results in four times as many grid points as the horizontal grid spacing of 2m). Figure 6 illustrates how the aspect ratio of the cross-section grid and the earth pressure admissibility criteria can be used to control the number of state curves to be included in the analysis.

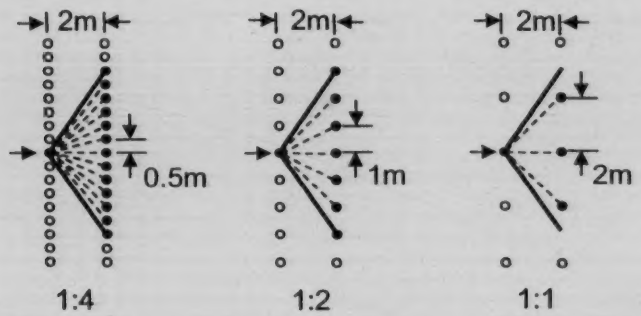

Figure 5.6: Illustration showing how the number of *state curve* combinations can be increased or decreased depending on the aspect ratio selected for the cross-section grid.

The aspect ratio for the grid on the left is 1:4. The middle grid and the grid on the right have aspect ratios equal to 1:2 and 1:1, respectively. If the soil has a friction angle equal to the 30 degrees, only those state curves with line segments elevated at angles less than 60 degrees ($45+\phi'/2=60$) are included in the analysis. The solid black lines have been drawn at 60 degrees to illustrate the number of line segments that are considered for a single point on the cross-section grid. The 1:4 grid contains approximately twice as many line combinations as the 1:2 grid (i.e., at least twice as many *state curve* combinations). The number of admissible combinations decreases as the friction angle of the soil decreases or the aspect ratio of the cross-section grid is decreased. Difficulties can arise if the angle permitted by the earth pressure constraint approaches the minimum angle between points on the cross-section grid.

For example, in the extreme case where the friction angle of the soil is equal to zero, the maximum line segment elevation permitted by the earth pressure admissibility criteria is equal to 45 degrees. If the cross-section grid aspect ratio is less than 1:1, the minimum angle between grid points is greater than 45 degrees resulting in a case where there are zero admissible *state curves*.

The aspect ratio of the dynamic programming search grid can be selected lower during preliminary analysis to reduce the number of *state curves* and expedite the dynamic programming search. The aspect ratio should not be reduced lower than 1:2 and should be sufficiently large to provide enough resolution to account for thin weak layers that might dominate the stability analysis. The aspect ratio can be increased once the search grid is focused around the likely location of the critical slip surface identified from preliminary searching.

5.3.2.4 Application of Admissibility Criteria during *State Curve* Generation

The numerical procedure used to generate *state curves* can be formulated to permit the application of various combinations of the admissibility criteria described above. Selecting *state curves* based on the proposed admissibility criteria is considered to be rigorous because *state curves* are not arbitrarily excluded from the analysis. All of the *state curves* passing the applied admissibility criteria are considered. A sensitivity study was undertaken to investigate whether or not the admissibility criteria can be used to reduce the number of *state curve* combinations to a number that can be managed with available computing resources.

Various combinations of the admissibility criteria were applied during the generation of *state curves* for the cross-section grid shown Figure 5.3 (Table 5.3). In each case, the number of admissible *state curves* is reported along with an estimate of the solution time in hours. The solution time represents the time required by the dynamic programming algorithm to determine the optimum *state curve* connection

between two stage cross-sections each containing a certain number of state curves. The results of the sensitivity study are presented in Table 5.3.

Table 5.3: Results of a sensitivity study regarding the rigorous treatment of *state curve* generation.

			Concave constraint					
			No. 1		No. 2		No. 3	
Grid aspect ratio	ϕ'	Earth pressure constraint (°)	State curves	Solution time (hrs.)	State curves	Solution time (hrs.)	State curves	Solution time (hrs.)
1:4	0 to 12	51	32 821	214	1 361	0.4	467	0.04
1:4	0 to 20	55	83 844	1 394	3 423	2.3	1 258	0.3
1:4	0 to 30	60	157 181	4 900	8 154	13.2	3 161	2.0
1:2	0 to 30	60	3 463	2.4	567	0.1	183	0.01

The largest number of *state curves* was reported for the combination where the cross-section grid aspect ratio was 1:4, the friction angle of the soil was 30 degrees, and the most flexible concave criteria was used (i.e., Eq. [5.1]). This combination resulted in approximately 157,000 admissible *state curves*. According to Figure 5.4, approximately 4,900 hours of computer time would be required to optimize all of the combinations. The results show that the number of *state curves* can be reduced if the friction angle of the soil is lower, if the density of cross-section grid is reduced by considering an aspect ratio of 1:2, or if one of the more restrictive variations of the concave criteria is invoked. In reality, the angle of internal friction corresponds to the strength of the soil and cannot be modified to control the number of *state curve* connections. The solution time can be reduced to 13 hours or less by selecting the concave criteria corresponding to Eq. [5.2] and to 2 hours or less by selecting the concave criteria corresponding to Eq. [5.3]. The solution time was reduced to 2 hours or less when an aspect ratio of 1:2 was selected, for all three variations of the concave criteria.

The solution time can also be significantly reduced by incorporating information from field investigations. In many cases, it is possible to estimate the volume of soil

that is moving or even isolate the general location of the slip surface at discrete points using slope inclinometer data.

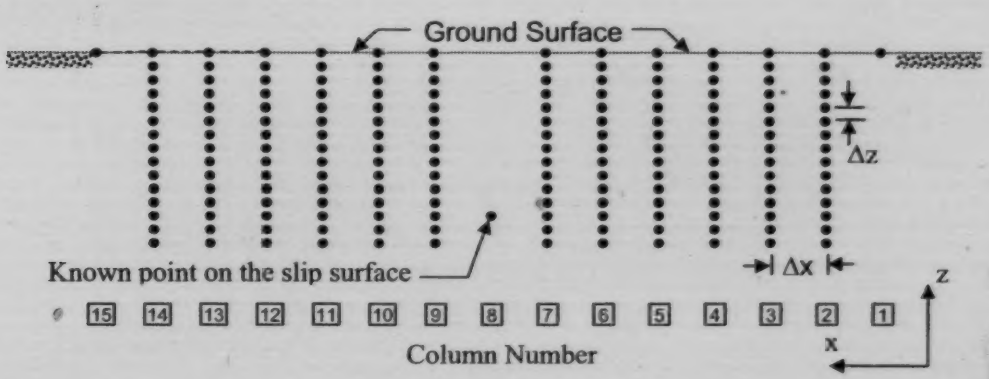

Figure 5.7: Illustration showing how information from field investigations can be used to reduce the total number of admissible *state curves* and reduce the solution time.

Let us consider the combination from Table 5.3 where the grid aspect ratio is 1:4, the friction angle of the soil is 30 degrees, and the concave criterion corresponds to Eq. [5.1]. The total number of admissible *state curves* for this case is 8,154. If one point on the slip surface can be identified, the remaining points in the column could be removed from the cross-section grid, as shown in Figure 5.7. In this case, isolating one point on the failure surface reduces the total number of admissible *state curves* from 8,154 to 647, reducing the solution time from nearly 13 hours to approximately 5 minutes.

Admissibility criteria are necessary to increase the efficiency of the search by excluding *state curves* that do not result in reasonable slip surfaces. In practice, it is possible to carry out more restrictive preliminary analysis to determine the approximate location of the slip surface. Once the approximate location of the slip surface has been identified, it is possible to focus the grid on each cross-section around the anticipated area and relax the admissibility criteria. The admissibility

criteria described in this paper can be used to investigate the stability of a large number of conditions typically encountered in practice.

5.3.3 Admissibility Criteria Governing the Shape of the Slip Surface in the Direction of Movement

Kinematic admissibility criteria used in three-dimensional slope stability formulations is less developed than those used in two-dimensional formulations. The idea of using the dynamic programming algorithm to search for concave failure surfaces was extended to three-dimensions by Yamagami and Jiang (1997). However, it appears that the concave restriction was only applied in the direction perpendicular to failure. Yamagami and Jiang (1997) did not report on the use of a criterion to ensure the shape of the slip surface in the direction of failure was kinematically admissible. The criterion proposed by Pham and Fredlund (2003) has been extended to three-dimensions for use in the current research. The criterion serves as the final check for admissibility of the overall three-dimensional slip surface.

5.3.4 Definition of the Factor of Safety

The factor of safety equation for an arbitrary three-dimensional slip surface can be defined as

$$[5.4] \qquad F_S = \frac{\int \tau_f \, dA}{\int \tau \, dA}$$

where τ_f is the shear strength of the soil, τ is the mobilized shear stress, and dA is an incremental area on the slip surface. It is assumed that the critical slip surface can be approximated by series of triangular surfaces (Figure 5.8). The triangular surfaces

form the connection between the critical *state curves* from successive stage cross-sections. The factor of safety can be written in the form:

$$[5.5] \quad F_S = \sum_{ijk=1}^{mn2} \tau_{f_{ijk}} A_{ijk} \Big/ \sum_{ijk=1}^{mn2} \tau_{ijk} A_{ijk} = \sum_{ij=1}^{mn} R_{ij} \Big/ \sum_{ij=1}^{mn} S_{ij}$$

where m is the number of dividing lines in the x-direction, n is the number of dividing lines in the y-direction, $\tau_{f_{ijk}}$ is the shear strength, τ_{ijk} is the mobilized shear stress, and A_{ijk} is the area of one triangular plane. The resisting force R_{ij} and the shear force S_{ij} can be calculated by multiplying the shear strength and the mobilized shear stress, obtained from the finite element analysis, by the area of each plane. R_{ij} and S_{ij} are the addition of the resisting forces and shear forces acting on the combination of two triangular planes (i.e., $k = 1$ and 2 as shown in Figure 5.8). The slip surface shown in Figure 5.8 is discretized with a total of $m*n*2$ triangular planes. The two triangles between the dividing lines i and $i+1$ in the x-direction and j and $j+1$ in the y-direction can be identified according to the incremental areas A_{ij1} and A_{ij2}, as shown in Figure 5.8.

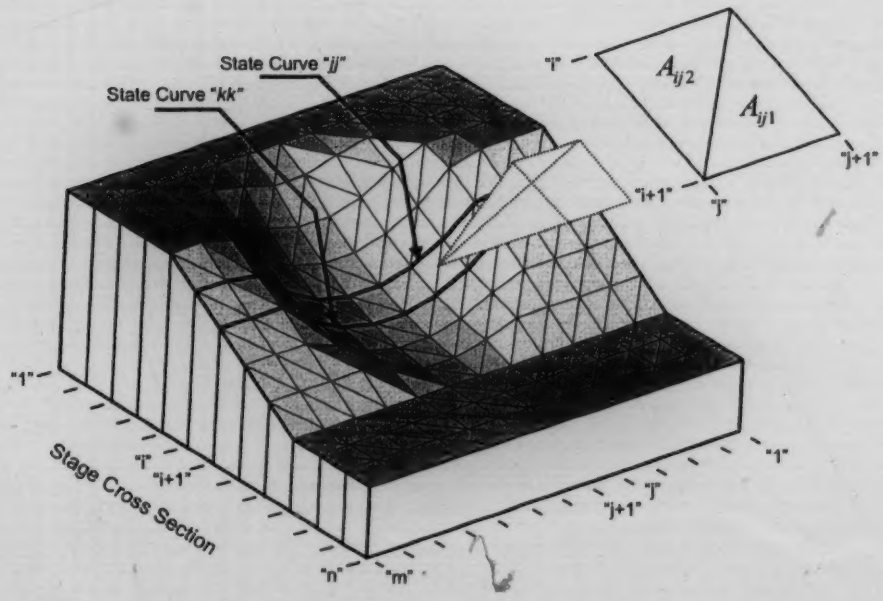

Figure 5.8: A three-dimensional slip surface discretized into a series of triangular planes.

The procedure used to compute the resisting force, R_{ijk}, and the shear force, S_{ijk}, for triangle A_{ijk}, has been described by Stianson (2008). The normal stress and mobilized shear stress acting on the incremental area, A_{ijk}, are obtained from a separate finite element stress analysis. The shear force, S_{ijk}, is calculated by multiplying the mobilized shear stress by the area of the triangle, A_{ijk}. The shear strength provided by each incremental area, A_{ijk}, can be calculated using the extended Mohr-Coulomb equation for saturated-unsaturated soil (Fredlund and Rahardjo 1993):

$$[5.6] \qquad \tau_{f_{ijk}} = c' + (\sigma_n - u_a)\tan\phi' + (u_a - u_w)\tan\phi^b$$

where c', ϕ', and ϕ^b are the shear strength parameters of a saturated-unsaturated soil, $(\sigma_n - u_a)$ is the net normal stress, and $(u_a - u_w)$ is the matric suction. The resisting

force, R_{ijk}, is computed by multiplying the shear strength of the soil, $\tau_{f_{ijk}}$, by the area of the triangle A_{ijk}.

5.3.5 Dynamic Programming Optimization Procedure

The three-dimensional slope stability calculations have been divided into a *stage-state* system and the factor of safety equation has been defined. It is now possible to introduce an auxiliary functional that is evaluated for each *state curve* connection and can be used to determine the slip surface with the lowest factor of safety. It was shown by Baker (1980) that the minimum factor of safety for two-dimensional slope stability problems can be found by rearranging the factor of safety equation into an auxiliary functional. Eq. [5.7] is the extension of the auxiliary functional proposed by Baker (1980) to three-dimensional slope stability analysis and is the result of rearranging Eq. [5.4].

$$[5.7] \quad G_i = \sum_{ij=1}^{mn} \left[R_{ij} - FS_{ij} \right]$$

Figure 5.8 illustrates a portion of a three-dimensional sip surface resulting from the connection of *state curve* (*kk*) from stage [*i*+1] to *state curve* (*jj*) from *stage* [*i*]. The *state curves* are connected by a series of triangular planes. The value of the auxiliary functional for the connection shown in Figure 5.8 is determined by summing the result of the right hand side of Eq. [5.7] evaluated for each plane combination (i.e., one plane combination consists of areas A_{ij1} and A_{ij2}. R_{ij} and S_{ij} are the addition of the resisting forces and actuating forces acting on the areas A_{ij1} and A_{ij2}.).

The optimal function shown in Eq. [5.8] is introduced to record and compare the return function values, G_i, calculated for each trajectory as the search for the slip surface with the minimum factor of safety proceeds.

[5.8] $$H_{i+1}(kk) = \min_{jj=1-s_i} \left\{ H_i(jj) + G_i(jj,kk) \right\}_{kk=1-s_{i+1}}^{i=1-I}$$

$$H_1(jj) = 0; \qquad jj = 1 - s_1$$

$G_i(jj,kk)$ is the value of the return function that is calculated from the trajectory between *state curve* (*kk*) in *stage* [*i*+1] to *state curve* (*jj*) in *stage* [*i*]. $H_i(jj)$ is the value of the optimal function recorded at the *state curve* (*jj*) in *stage* [*i*]. The value of the optimal function, $H_1(jj)$, for all of the *state curves* in the initial *stage* (i.e., *state curves* 1 through *s*) is set to zero according to the boundary condition listed in Eq. [5.8]. The *state curve* (*jj*) that results in the minimum value of the brace {} (i.e., the trajectory with the lowest factor of safety), is recorded and the calculation proceeds to the *state curve* (*kk*+1). When the calculation reaches the final *stage* [*n*] the *state curve* (*kk*) resulting in the minimum optimal function value is determined. Starting at the minimum *state curve* in the final *stage*, it is possible to trace back the minimum trajectory to each previous *stage* using the recorded (*jj*) values at each [*i*] and (*kk*). The combination of each minimum trajectory is the trace of the slip surface with the lowest factor of safety.

5.4 Comparisons with Published Three-Dimensional Solutions

New slope stability methods are often evaluated by re-analyzing a selection of cases from the literature. There are a limited number of published cases where the search for the critical three-dimensional slip surface is performed using dynamic programming (Yamagami and Jiang 1997; Jiang et al. 2003; Jiang and Yamagami 2004). In each case, the overall factor of safety is computed using a method of columns technique based on the extension of one of the methods of slices including Janbu's Simplified method (Yamagami and Jiang 1997; Jiang et al. 2003) or Spencer's method (Jiang and Yamagami 2004). The authors are not aware of any

cases where the factor of safety is computed based on finite element stresses and the search for the critical three-dimensional slip surface is performed using dynamic programming.

A series of examples were selected from the literature to evaluate the application of the dynamic programming searching procedure in combination with the proposed admissibility criteria. Valuable information can be obtained through the comparisons even though the factors of safety are not computed using the same procedure. In some cases, the results are also compared with the critical ellipsoidal slip surface computed based on the procedure developed by Stianson (2008).

5.4.1 Loaded Homogeneous Slope

The first example involves a simple homogeneous slope elevated at a 2:1 angle and subject to a distributed load in addition to gravity forces (Figure 5.9). The load is distributed over a square eight meter by eight meter area. Only one-half of the load is shown in Figure 5.9 due to the symmetry of the slope. The internal stress distribution of the slope was computed using an isotropic linear elastic finite element analysis using the 'switch on' gravity technique with Young's modulus equal to 20,000 kPa and Poisson's ratio equal to 0.48. The effective cohesion, effective angle of internal friction, and unit weight of the material were taken to be 10 kPa, 10°, and 18 kN/m^3, respectively.

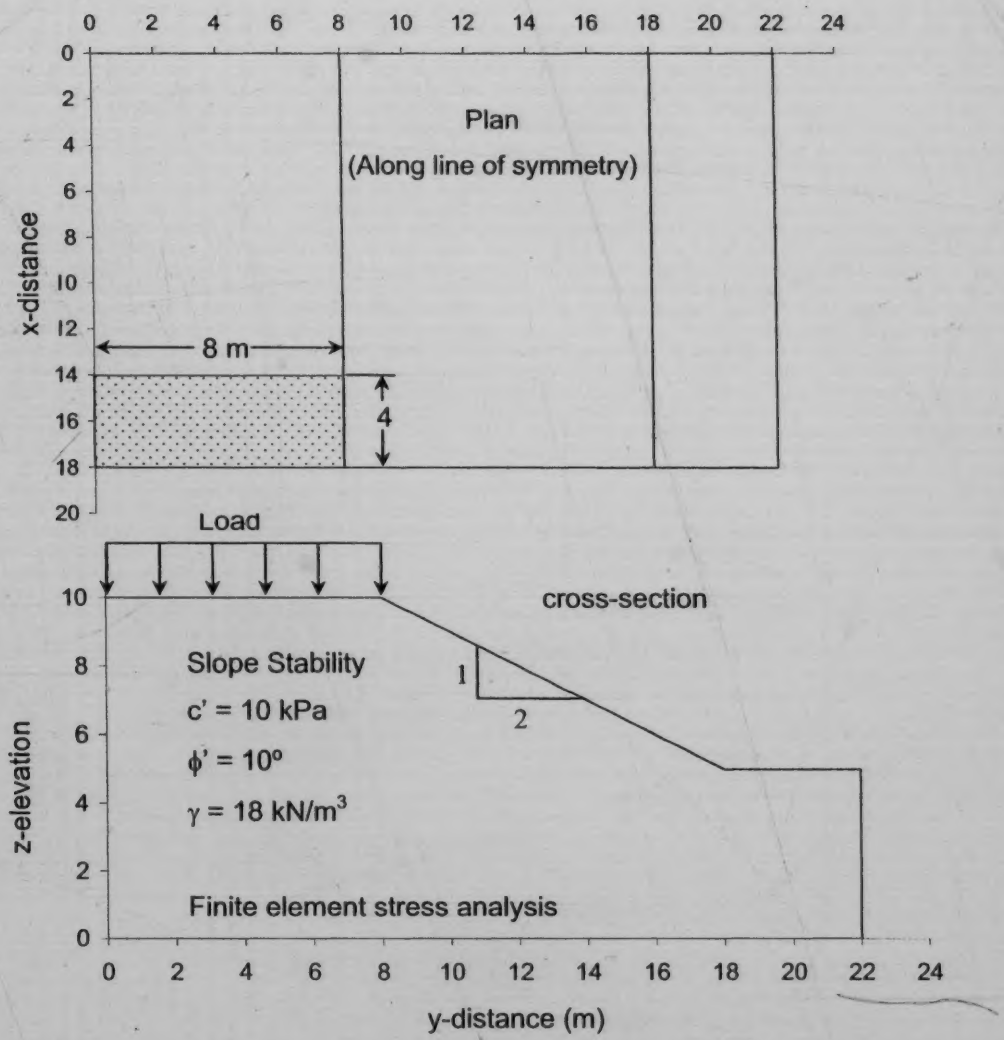

Figure 5.9: Plan view and cross-section view of the simple homogeneous slope considered in Example No. 1.

The example was originally evaluated by Yamagami et al. (1991) using a three-dimensional slope stability method involving the random generation of surfaces. The problem has been re-analyzed by Yamagami and Jiang (1997) to investigate if the efficiency of the slope stability method might be improved if the search technique

based on the random generation of surfaces was replaced with dynamic programming. The solution time was reduced from 4 hours to 12 minutes and the dynamic programming search identified a slip surface with a lower factor of safety. The factor of safety for the case where the slope was subject to a load of 50 kPa was estimated to be 1.141 using random generation of surfaces and 1.026 using dynamic programming.

5.4.1.1 Application of the Dynamic Programming Searching Procedure in Combination with Admissibility Criteria

The slope stability analysis consists of a preliminary search followed by a series of refined searches (Table 5.4). Initially, the dynamic programming search grid was defined by selecting an appropriate spacing in the *y*-direction (i.e., spacing between stage cross-sections in the direction of failure), in the *x*-direction (i.e., the spacing between columns of grid points perpendicular to failure) and the *z*-direction (i.e., vertical spacing between grid points). The spacing between grid points was selected keeping in mind the dimensions of the overall area to be searched and the desired aspect ratio (i.e., no less than 1:2.). Subsequent refinements to the search grid were completed based on the results from the preliminary search.

The concave admissibility criteria was selected according to the soil conditions, keeping in mind that a more restrictive criterion results in fewer *state curve* combinations and in turn shorter run times. The critical slip surface was expected to be circular because the slope consists of homogeneous material. The concave criterion corresponding to Eq. [5.2] includes circular and composite curves and was considered to be a reasonable starting point for preliminary analysis. If the shape of the slip surface from the preliminary analysis turned out to be circular, Eq. [5.3] could be applied in the refined searches (i.e., it would likely not be necessary to consider composite *state curves*). In this case, Eq. [5.1] was used in the refined search to

provide an indication regarding the run times that might be expected when the most general concave admissibility criterion is applied.

Table 5.4: The parameters used to define the dynamic programming search and a summary of the solution details for the comparison involving the loaded homogeneous slope.

Parameter	Preliminary search	Refined search
Search grid spacing (m)		
*y-direction	2	1
x-direction	2	1
z-direction	1	0.5
Aspect ratio (x:z)	1:2	1:2
Concave admissibility criteria	Eq. [2]	Eq. [1]
Number of state curves	700	19 000
State curve connections	43 000	30 000 000
Solution time	5 minutes	5.5 hours

* Assumed direction of failure.

The grid spacing and admissibility criteria selected in the preliminary analysis resulted in a total of 700 *state curves* distributed over 10 stage cross-sections. There were a total of 43,000 potential *state curve* connections. The number of *state curve* connections represents the total number of unique slip surfaces evaluated during the search. The density of the search grid was increased for the refined search while the aspect ratio of the grid remained the same. The number of *state curves* included in the refined analysis increased dramatically as a result of increasing the grid density and relaxing the concave constraint. There were approximately 19,000 *state curves* included in the analysis distributed over 16 stage cross-sections resulting in over 30 million *state curve* connections (i.e., 30 million slip surface combinations). The solution time increased from approximately 5 minutes for the preliminary analysis to 5.5 hours for the refined analysis.

5.4.1.2 Slope Stability Results

Initially, the stability of the slope was evaluated considering a case where a load equal to 50 kPa was applied on the crest of the slope (Figure 5.10). The critical slip surface is symmetrical and approximately circular along a cross-section corresponding to the line of symmetry. The shape of the slip surface seems to correspond with the types of failures typically expected in homogeneous material. The factor of safety for the slope is 1.121 indicating that the slope is near the point of failure.

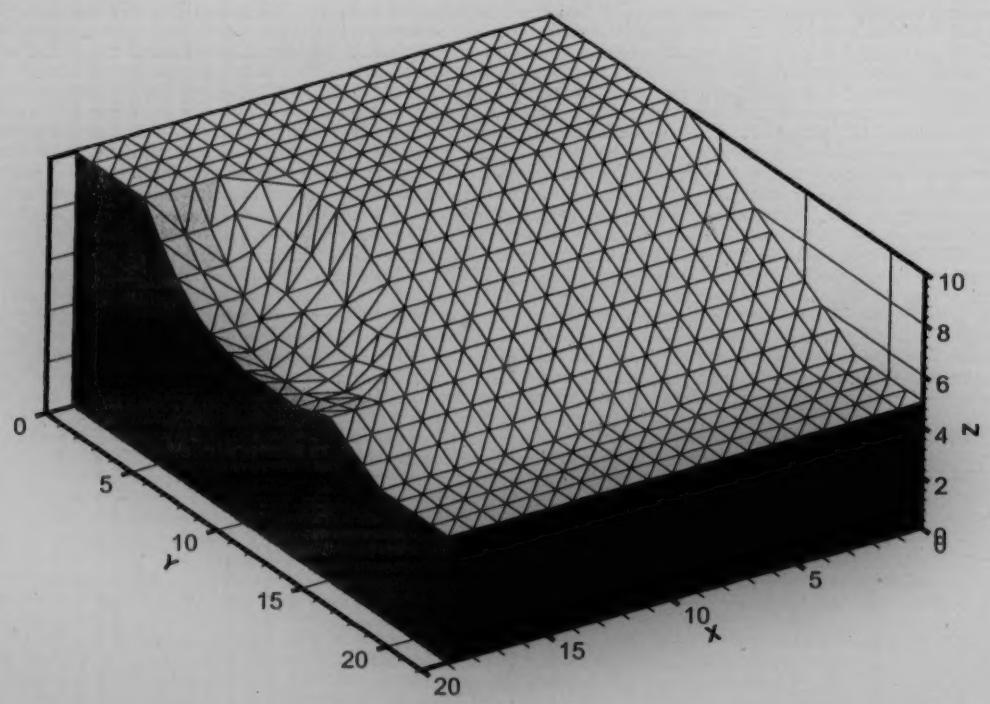

Figure 5.10: Critical slip surface found using the proposed slope stability method.

The results reported by Yamagami and Jiang (1997) are similar to the results reported in Figure 5.10 in that the slip surface is symmetrical and approximately circular along the line of symmetry. The slip surface found using the proposed procedure exits the slope a significant distance above the toe. The slip surface

reported by Yamagami and Jiang (1997) is deeper, exits at the toe of the slope and the factor of safety was estimated to be 1.026. The variation in the results is likely due to the different procedures used to compute the overall factor of safety.

Additional stability calculations were completed to observe the change in the character of the slip surface as a result of decreasing the load applied on the crest of the slope. The load was decreased from 50 kPa to zero in five regular increments. The slip surface moved deeper into the slope as the magnitude of the applied load was reduced. Reducing the load to 30 kPa resulted in a slip surface with similar geometrical characteristics as the slip surface reported by Yamagami and Jiang (1997), for the 50 kPa load case (Figure 5.11). Reducing the load to zero resulted in a slip surface with cylindrical characteristics indicative of plane strain failure.

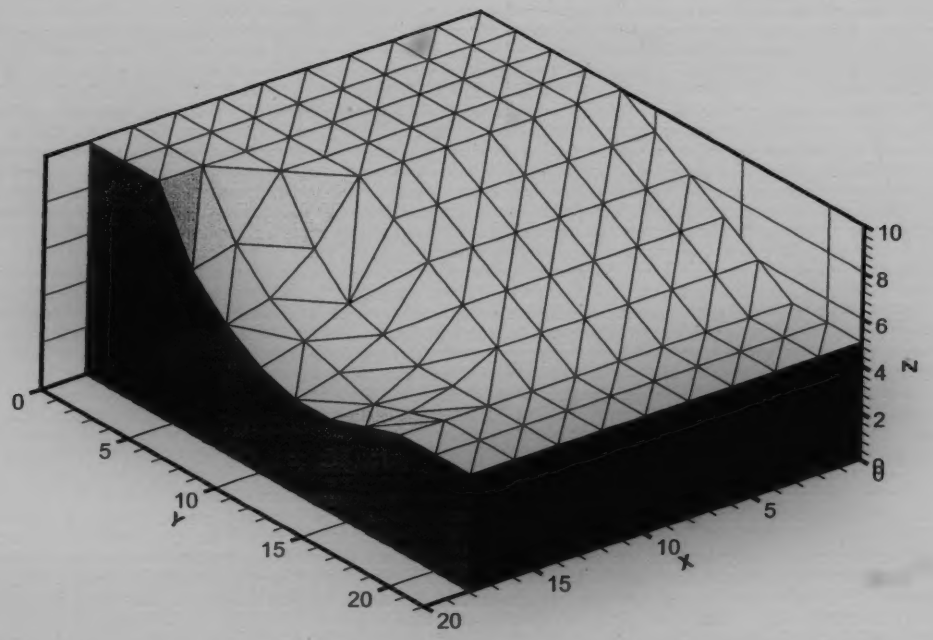

Figure 5.11: Critical slip surface for the case where the load applied on the crest of the slope is equal to 30 kPa ($F_s = 1.30$).

5.4.1.3 Comparison with Critical Ellipsoidal Failure Surface

The soil (homogeneous) and loading (symmetrical) conditions considered in the first example resulted in a symmetrical slip surface that can be reasonably approximated using an ellipsoidal shape. The critical slip surface identified by the dynamic programming searching technique can be compared to the critical slip surface identified using the grid and radius searching procedure designed to search for the critical ellipsoidal slip surface (Stianson 2008).

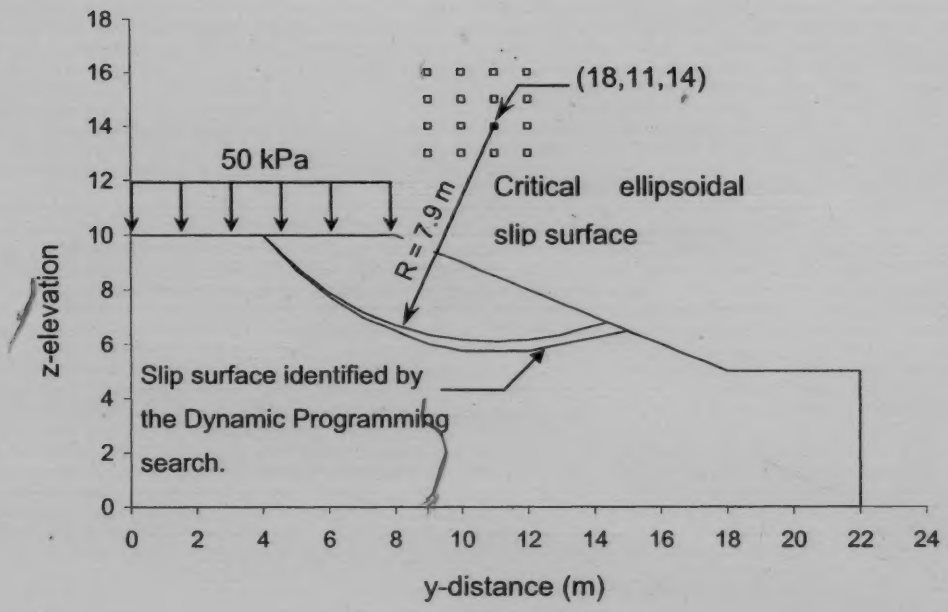

Figure 5.12: Comparison between the critical slip surface found using the dynamic programming search technique with the critical ellipsoidal slip surface found using a simple grid and radius search technique.

Figure 12 shows a comparison between the trace of the critical ellipsoidal slip surface with the trace of the slip surface found using dynamic programming, along the line of symmetry of the slope (i.e., x = 18m). The centre of the critical ellipsoid is located at the coordinate (18, 11, 14) and the radius is equal to 7.90 meters. The ellipsoidal slip surface is in close agreement with the slip surface determined from the dynamic programming search. The trace of the ellipsoidal slip surface shown in Figure 5.12 is in better agreement with the dynamic programming slope stability results than the results reported by Yamagami and Jiang (1997). The agreement is likely due to the fact that the factor of safety calculation adopted in the current method is similar to the method developed by Stianson (2008). Yamagami and Jiang (1997) computed the factor of safety using a method of columns technique based on the extension of Janbu's simplified method of slices.

The shape of the dynamic programming slip surface in the direction of failure is governed by kinematic admissibility criteria rather than assumptions regarding the specific geometric shape. The kinematic admissibility criteria used to control the shape of the slip surface in the direction of failure is more general than assuming that the slip surface conforms to an ellipsoid. However, the shape of the critical slip surface identified by the dynamic programming optimization technique is nearly circular. The results provide evidence that the dynamic programming searching technique can be used to successfully evaluate the stability of slope and identify the shape of the critical slip surface.

5.4.2 Loaded Homogeneous Slope with Modified Soil Properties

The slope conditions considered in the first comparison can be modified to demonstrate the flexibility of the admissibility criteria used to govern the dynamic programming search. A weak layer is included in the slope as shown in Figure 5.13. The shape of the weak layer was selected to promote a condition where the failure surface might not be strictly concave. The weak layer can be considered to be an idealized representation of the two-dimensional slope conditions evaluated by Zienkiewicz et al. (1975), where a fill material was placed over an existing geological feature. The weak layer is strictly cohesive with $c' = 4$ kPa and unit weight equal to 18 kN/m3. The load applied on the crest of the slope is equal to 30 kPa. The results for the loaded weak layer case can be compared to the results reported in Figure 5.11, corresponding to a case with the same loading conditions but homogeneous soil properties.

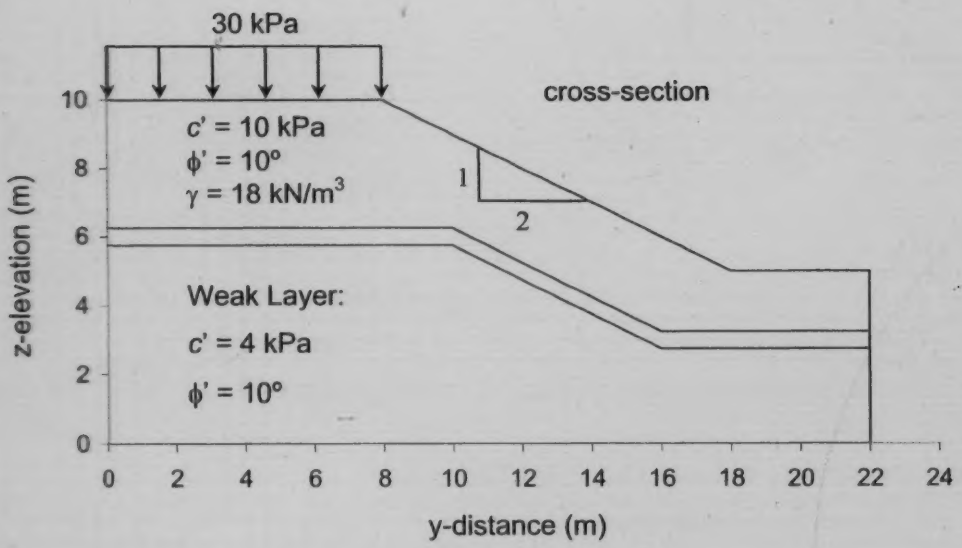

Figure 5.13: Cross-section view of the modified slope conditions considered in Example No. 2.

5.4.2.1 Slope Stability Results

The slope stability results for the weak layer case are presented in Figure 5.14. The results demonstrate the ability of the proposed searching procedure to evaluate the stability of slopes where the critical slip surface might not be strictly concave due to certain geological or man-made conditions. The presence of the weak layer has changed the character of the slip surface and reduced the factor of safety from 1.3 to 1.0 when compared to the homogeneous case (i.e., Figure 5.11).

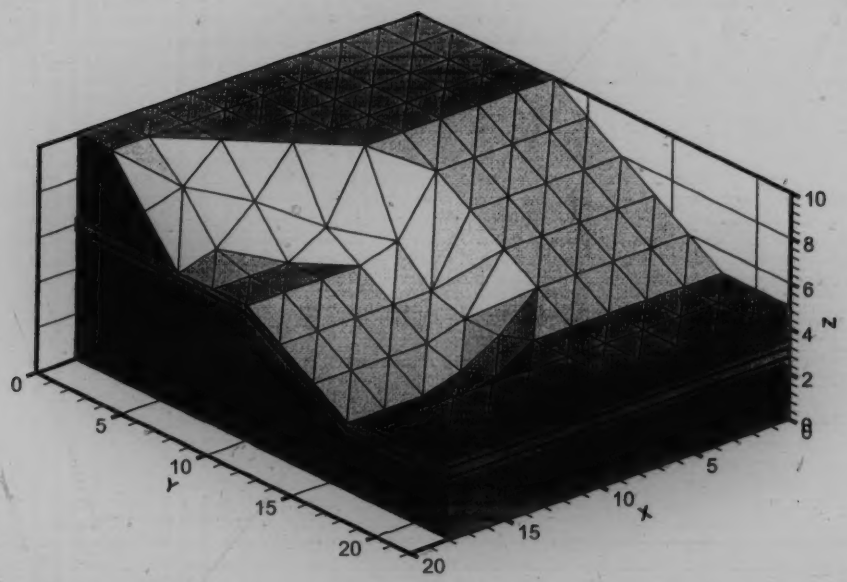

Figure 5.14: Slope stability results for the second example where an irregular weak layer is included in the slope.

The stability of the slope was also evaluated using the grid and radius searching procedure developed by Stianson (2008). The analysis was completed to demonstrate that assumptions regarding the overall shape of the slip surface can affect the computed factor of safety. The factor of safety for the slope was determined to be 1.15. The factor of safety is over-estimated by approximately 13% due to the assumption that the slip surface was ellipsoidal.

5.4.3 Convex Slope Including Pore-Water Pressures and a Weak Layer

The slope was originally considered by Yamagami and Jiang (1997) as part of the testing program carried out to evaluate a similar slope stability method involving dynamic programming. The slope consists of a conical heap of soil as shown in Figure 5.15. The slope is similar to other three-dimensional geometries found in

practice including the outside corner of an embankment or excavation. The stability of the slope was evaluated for three separate cases including homogeneous soil with no pore-water pressure, homogeneous soil with pore-water pressure, and multi-layered soil conditions with pore-water pressure. The distribution of pore-water pressure was defined using a phreatic surface that was taken to be the surface of a cone with a vertical to horizontal inclination of 1:4 (Yamagami and Jiang 1997). The multi-layered slope conditions, including the phreatic surface, are shown in Figure 5.15.

Material	Thickness (m)	γ (kN/m^3)	c' (kPa)	ϕ'
Layer 1	7	19.2	29.3	10
Layer 2	5.5	18	17.5	10
Layer 3	0.5	19.2	0	10
Layer 4	10	19.2	0	30

Radius to the crest of the slope is equal to 12m.
Radius to the toe of the slope is equal to 35m.

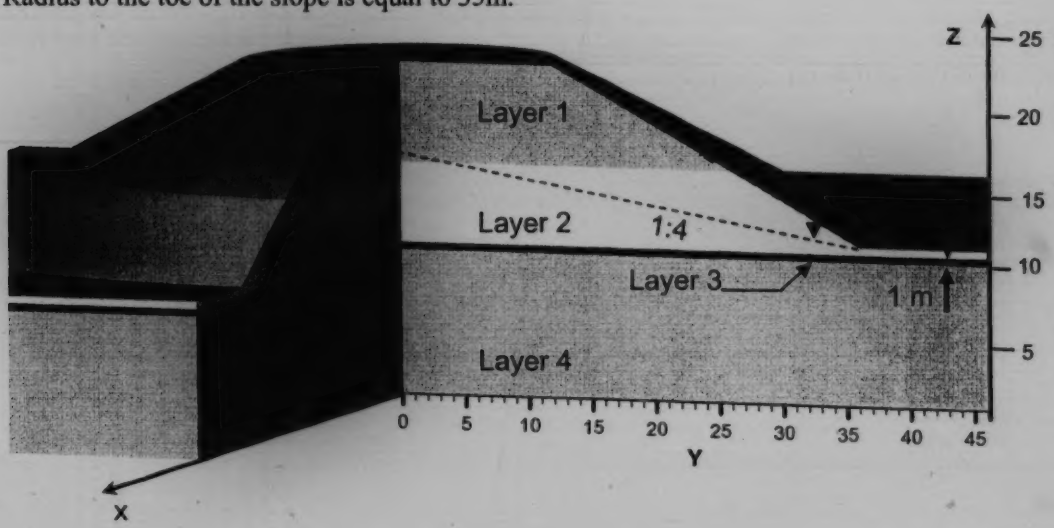

Figure 5.15: Slope geometry and soil conditions considered in the multi-layer conical heap example problem.

Initially, the soil conditions were considered to be homogeneous. Two additional cases were considered where the slope conditions were modified to decrease the

overall stability of the slope and increase the complexity of the search for the critical failure surface. The complexity of the search for the critical slip surface was considered to increase as the number of *state curves* increased. The number of *state curves* can increase as a result of expanding the search area or by relaxing the admissibility criteria to accommodate more complex soil conditions.

The critical slip surfaces were expected to be symmetrical in all cases because the geometry and soil conditions are such that a line of symmetry exists regardless of the assumed direction of failure. However, it was possible that the shape and location of the critical slip surface might be different between certain cases. The critical slip surface in the second case could have been deeper (with a lower factor of safety) when compared to the first case, as a result of the reduced effective stress below the phreatic surface. The critical slip surface in the third case might have been composite (i.e., follow along the weak layer) while in the first two cases the critical slip surface was expected to be a smooth surface because the soil properties are homogeneous. The search for the critical slip surface becomes more complex as the slope conditions are modified from the homogeneous case to the multi-layered case including pore-water pressure. The objective was to demonstrate that the proposed searching procedure can be used to identify the critical slip surface for various soil conditions.

5.4.3.1 Slope Stability Results

The slope stability results for the first case (i.e., no pore-water pressure) and the second case (i.e., with pore-water pressure) are shown in Figure 5.16*a*) and Figure 5.16*b*), respectively. The critical slip surface for the second case passes deeper into the slope as a result of the reduced effective stress below the phreatic surface. The factor of safety for the third case was calculated to be 0.535. The soil conditions considered in the third case result in a slip surface with a completely different shape than the soil conditions considered in the first two cases. The results demonstrate that the dynamic programming searching procedure can be used to search for the slip surface in a variety of soil conditions.

a) Soil Properties:

$\phi' = 20°$; $c' = 29.3$ kPa; $\gamma = 19.2$ kN/m^3; $E = 20\,000$ kPa; $\nu = 0.48$; F_s=1.75

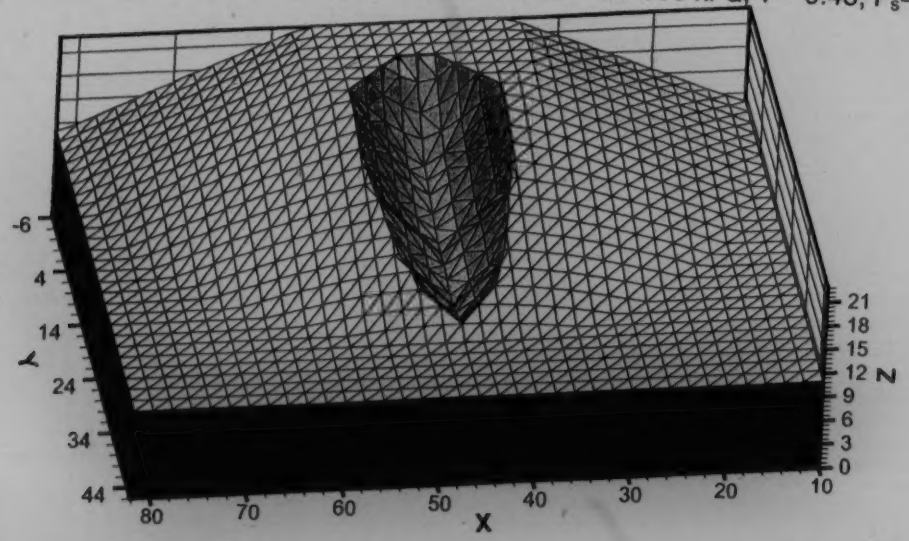

b) Soil Properties:

$\phi' = 20°$; $c' = 29.3$ kPa ; $\gamma = 19.2$ kN/m^3 ; $E = 20\,000$ kPa ; $\nu = 0.48$; F_s=1.62

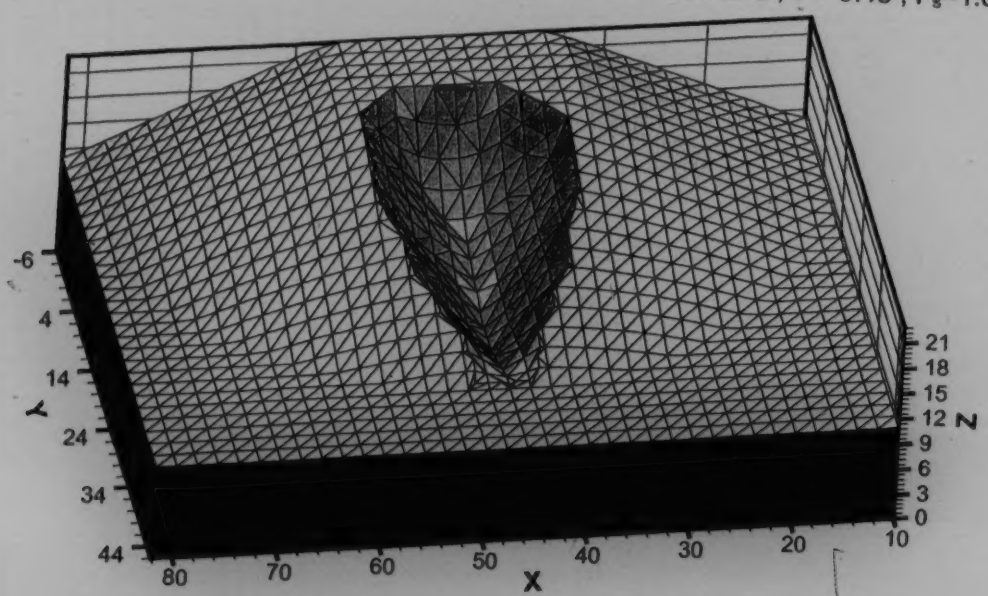

c) Soil Properties: Multi-Layered Slope; $F_s = 0.535$

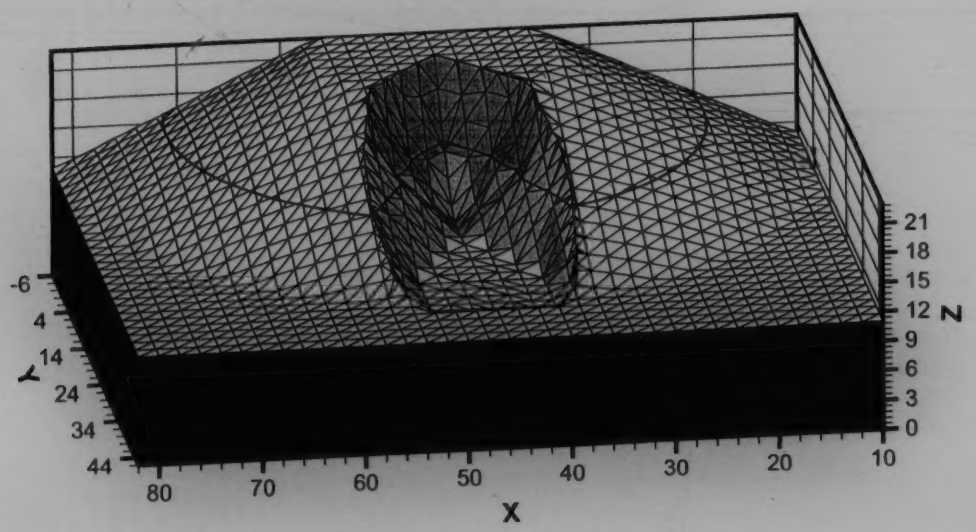

Figure 5.16: Slope stability results for Example No. 3.

The factors of safety computed by Yamagami and Jiang (1997) and the values computed using the current slope stability procedure are presented in Table 5.5. The factors of safety computed using the current slope stability method are consistently lower than the factors of safety reported by Yamagami and Jiang (1997). The two most significant factors contributing to the differences between the factors of safety include the method used to compute the factor of safety and the procedure used to generate state curves to search for the critical slip surface.

Table 5.5: Comparison between factors of safety computed by Yamagami and Jiang (1997) and the current slope stability method for Example No. 3.

Case	Yamagami and Jiang (1997)	Current study	Difference %
Homogeneous	2.06	1.75	15%
Homogeneous (Including phreatic surface)	1.83	1.619	12%
Four layers (Including phreatic surface)	1.08	0.535	50%

Yamagami and Jiang (1997) computed the factor of safety using a three-dimensional method of columns procedure originally developed by Ugai (1988) and Ugai and Hosobori (1988). The procedure is based on an extension of the two-dimensional Janbu Simplified method to an equivalent method of columns procedure. The factor of safety is computed considering horizontal and vertical force equilibrium. Moment equilibrium was not satisfied and the effects of inter-column shear forces were not taken into consideration. The factor of safety computed based on finite element stresses satisfies horizontal force, vertical force, and moment equilibrium and considers all of the forces acting within the sliding mass. Both procedures use dynamic programming to search for the critical slip surface. The main difference between the two searching procedures is the method used to generate *state curves*. Yamagami and Jiang (1997) consider a random sample of 100-500 concave *state curves* while the current procedure considers all of the *state curves* passing a series of admissibility criteria.

In the first case, the soil is homogeneous and the phreatic surface is not included in the slope. Yamagami and Jiang (1997) computed the factor of safety to be 2.06. The factor of safety was computed to be 1.75 (i.e., 15% lower) using the proposed slope stability method. It appears that the critical slip surface is more shallow and narrow when compared to the results reported by Yamagami and Jiang (1997). The reduction in the factor of safety is primarily attributed to the differences between the procedures used compute the factor of safety (i.e., method of columns versus finite element stresses). It is possible that the reduction in the factor of safety is due in part to using a more rigorous searching procedure. However, it is anticipated that either searching procedure will provide a similar level of performance when the shape of the slip surface is relatively simple and can be approximated using restrictive admissibility criteria. The searching procedure will likely play a more significant role when more flexible admissibility criteria are necessary to locate the slip surface with the lowest factor of safety.

In the second case, the soil remains homogeneous but the phreatic surface is included in the slope. The search region is expanded to consider that the slip surface

will likely move deeper in the slope as a result of the phreatic surface. The admissibility criteria remains the same as the first case but the number of *state curves* considered in the analysis increases as a result of the expanded searching area. Both slope stability procedures confirm that the stability of the slope is reduced and that the critical slip surface moves deeper into the slope. The factor of safety computed using the current slope stability method is 12% lower than the factor of safety reported by Yamagamig and Jiang (1997). The results seem to follow a similar pattern as the first case.

In the third case, the slope is divided into four soil layers including a thin weak layer. The admissibility criteria used to generate *state curves* was relaxed to consider slip surfaces that might follow along the thin weak layer. Relaxing the admissibility criteria increases the number of *state curves* that should be considered in the analysis. The difference between the factors of safety for this case is significantly greater than the previous two cases and is in the order of 50%. It appears that the influence of using a more rigorous searching procedure becomes more significant in cases where more flexible admissibility criteria are required to identify the slip surface with the lowest factor of safety.

5.5 Discussion

The method used to search for the critical slip surface should fit the complexity of the slope conditions being evaluated. In the first example, the slope consists of homogeneous material. The search for the critical slip surface is completed using two separate procedures including: 1) a 'grid and radius' search assuming that the slip surface is ellipsoidal (i.e., circular in the direction of failure) and 2) the dynamic programming technique using the proposed geometric and kinematic admissibility criteria to govern the shape of the slip surface. The factor of safety is calculated based on stresses from an independent stress-deformation analysis in both cases. The critical slip surfaces identified by both searching procedures are compared in Figure 5.12. The results demonstrate that there are practical uses for 'grid and radius'

searching procedures where the critical slip surface is assumed to be ellipsoidal. The ability to perform a reasonable slope stability analysis using a 'grid and radius' searching procedure significantly reduces the overall computing time. However, the value of the dynamic programming searching procedure is demonstrated as the soil conditions within the slope become more complex (i.e., second example in Figure 5.14) and the last case of the third example (Figure 5.16c)).

The factor of safety calculation requires the slip surface to be discretized into a series of triangular planes. The size of the triangles can influence the accuracy of the factor of safety calculation as well as the resolution in the shape of the final slip surface. Currently, the size of the triangles is controlled by the number of points included in the dynamic programming search grid. The density of the dynamic programming search grid must be increased to reduce the size of the triangles and improve the accuracy of the factor of safety calculation. However, the time required to complete the dynamic programming search can increase as the density of the search grid increases. In many cases, the shape of the slip surface can be reasonably approximated using a lower density when compared to the density required to improve the factor of safety calculation. It is possible to provide a second level of discretization, independent of the search grid density, to improve the overall factor of safety calculation. The triangles formed by connecting the points on the search grid can be discretized into a series of smaller triangles as part of a separate procedure independent of the dynamic programming search. The secondary discretization can improve the factor of safety calculation without significantly increasing the time required to search for the critical slip surface.

5.6 Conclusions

The proposed slope stability procedure can be used to simultaneously determine the shape, location and the factor of safety for the critical slip surface in three-dimensional slope stability problems. The procedure is designed to use stresses from a separate finite element analysis to compute the factor of safety and dynamic

programming to search for the critical slip surface. The finite element factor of safety equation is determinate and linear making it possible to direct more computer resources towards the search for the critical slip surface.

There are significant numerical difficulties that must be overcome to develop rigorous three-dimensional searching procedures where the shape of the slip surface is not pre-defined. The numerical difficulties are associated with the overwhelming number of slip surface combinations that would be included in the analysis without the use of meaningful criteria to exclude unreasonable slip surfaces. A procedure was introduced whereby 'geometric' and 'kinematic' admissibility criteria were used to train the searching procedure to distinguish between reasonable and unreasonable slip surfaces. The admissibility criteria can be used in place of a random number generator and provide a rigorous treatment of state curve generation. The flexibility of the admissibility criteria can be adjusted to provide a balance between the solution time and the complexity of the soil conditions.

5.7 Bibliography

Baker, R. 1980. Determination of the critical slip surface in slope stability computations. International Journal for Numerical and Analytical Methods in Geomechanics, 4(4): 333-359.

Bellman, R. 1957. Dynamic Programming. Princeton University Press, Princeton, N.J.

Boutrup, E., and Lovell, C.W. 1980. Search Technique in slope stability analysis. Engineering Geology, 16(1): 51-61.

Ching, R.K.H., and Fredlund, D.G. 1983. Some difficulties associated with the limit equilibrium method of slices. Canadian Geotechnical Journal, 20(4): 661-672.

Ching, R.K.H., and Fredlund, D.G. 1984. Quantitative comparison of limit equilibrium methods of slices. In Proceedings of the 4th International Symposium on Landslides. Toronto, Canada, pp. 373-379

De Natale, J.S. 1991. Rapid identification of critical slip surface: structure. Journal of Geotechnical Engineering, ASCE, 117(10): 1568-1589.

Fredlund, D.G., and Rahardjo, H. 1993. Soil Mechanics for Unsaturated Soils. John Wiley & Sons, Inc., New York, N. Y.

Greco, V.R. 1996. Efficient Monte-Carlo technique for locating critical slip surface. Journal of Geotechnical Engineering, ASCE, 122(7): 517-525.

Jiang, J.-C., and Yamagami, T. 2004. Three-dimensional slope stability analysis using an extended spencer method. Soils and Foundations, 44(4): 127-135.

Jiang, J.C., Baker, R., and Yamagami, T. 2003. The effect of strength envelope nonlinearity on slope stability computations. Canadian Geotechnical Journal, 40(2): 308-325.

Morgenstern, N.R., and Price, V.E. 1965. The analysis of slope stability of general slip surfaces. Geotechnique, 15(1): 79-63.

Nguyen, V.U. 1985. Determination of critical slope failure surfaces. Journal of Geotechnical Engineering, ASCE, 111(2): 238-250.

Pham, H.T.V., and Fredlund, D.G. 2003. The application of dynamic programming to slope stability analysis. Canadian Geotechnical Journal, 40(4): 830-847.

Stianson, J.R. 2008. A Three-dimensional slope stability method based on finite element stress analysis and dynamic programming. Dissertation, University of Alberta, Edmonton, Alberta, Canada.

Ugai, K. 1988. Three-dimensional slope stability analysis by slice method. In Proceedings of the 6th International Conference on Numerical Methods in Geomechanics. Innsbruck, Austria, Vol.2, pp. 1369-1374.

Ugai, K., and Hosobori, K. 1988. Extension of simplified Bishop method, simplified Janbu method, and Spencer method to three-dimensions. Proceedings Japanese Society of Civil Engineers, No. 394(III-9): 21-26 (In Japanese).

Yamagami, T., and Jiang, J.C. 1997. A search for the critical slip surface in three dimensional slope stability analysis. Soils and Foundations, 37(3): 1-16.

Yamagami, T., Kojima, K., and Taki, M. 1991. A search for the three-dimensional critical slip surface with random generation of surfaces. In Proceedings of

36th symposium on slope stability analyses and stabilizing construction methods., pp. 27-34 (In Japanese).

Zienkiewicz, O.C., Humpheson, C., and Lewis, R.W. 1975. Associated and non associated visco-plasticity and plasticity in soil mechanics. Geotechnique, 25(4): 671-689.

Chapter 6

Summary and Conclusions

The development of a procedure that can be used to simultaneously determine the shape, location and factor of safety for the critical slip surface in three-dimensional slope stability calculations was presented. The procedure was developed following a natural progression from two- to three-dimensional analysis. Two-dimensional studies were undertaken to provide a better understanding of the interaction between the stress-deformation analysis and the slope stability calculations including the influence of the stress-strain characteristics of the soil, the influence of Poisson's ratio and the application of admissibility criteria. The two-dimensional studies provided the background necessary to extend the stress-based method factor of safety calculations to three-dimensions and develop the three-dimensional dynamic programming searching procedure.

Dynamic programming is applied as a numerical technique to search for the critical slip surface. The algorithm does not require the existence and uniqueness of derivatives making it suitable for application to a layered profile where such derivatives are not properly formed (Baker 1980). The sequential nature of the procedure also permits the application of admissibility criteria as the search for the critical slip surface progresses. The application of the numerical procedure can be memory intensive. The memory and time requirements can increase markedly with the size and density of the search grid. The size of the search grid is selected according to the anticipated dimensions of the unstable soil mass. The density of the search grid is selected with enough resolution to consider the influence of key soil layers (i.e., thin weak zones.), provide a reasonable representation of the shape of the slip surface and can influence the accuracy of the factor of safety in some cases.

Memory and time requirements can be easily managed in two-dimensional problems but can become excessive in three-dimensional problems where the dimensions of the unstable mass are large and the shape of the slip surface is complex. The influence of the search grid density on the accuracy of the factor of safety can be minimized by including a second level of discretization on the mesh used to approximate the slip surface. Each triangle on the mesh can be discretized into a number of smaller triangles. The second level of discretization can be included to improve the accuracy of the factor of safety calculation and is not meant to alter the shape of the slip surface.

The application of the dynamic programming algorithm requires that the factor of safety equation be re-written in the form of an additive Auxiliary Functional. Application of dynamic programming yields the absolute minimum of the Auxiliary Functional that corresponds to a minimum of the factor of safety functional for the slope but not necessarily the lowest one (Baker 1980). The search grid is typically constructed with a number of points outside the boundaries of the slope which helps to minimize this difficulty. The points above the crest of the slope are required to determine the entry point of the slip surface and can be viewed as different starting points along the factor of safety functional for the slope. The ability to initiate the search at a number of locations along the factor of safety functional can eliminate local minima from the search and reduce the likelihood of becoming trapped. This characteristic is different from other searching procedures that are initiated by specifying one initial slip surface.

6.1 Two-Dimensional Studies

A comparative study was completed to investigate concerns that a linear elastic analysis might not provide a reliable estimate of the factor of safety in slopes where there is potential for extensive yielding. The study was limited to normally consolidated soil conditions where the internal stress distribution can be estimated using the 'switch on' gravity technique. A number of different slope configurations

were evaluated to determine the differences between slope stability analyses based on linear elastic or elasto-plastic soil behavior. The results demonstrated that there can be significant differences in the local factor of safety distribution as a result of local yielding but the shape, location and overall factor of safety are similar. The similarities in the slope stability results were observed in cases where there was extensive yielding (i.e., F_s =1.0) even though the shear stress increased beyond the strength of the soil in the linear elastic analysis.

Calculating the factor of safety based on the results of a stress-deformation analysis introduces new variables that are not typically associated with slope stability calculations; namely, Young's modulus and Poisson's ratio. A review of the literature indicated that researchers generally agree that Young's modulus does not have a significant influence on the slope stability results but there appeared to be different reports regarding the influence of Poisson's ratio. The results from a number of studies indicated that the slope stability analysis is not sensitive to the selection of Poisson's ratio while other studies reported that the factor of safety could vary by as much as 20%. Another study involving three-dimensional slope stability evaluations reported that Poisson's ratio can contribute to fluctuations in three-dimensional factors of safety in the order of 100% (Loehr 1998). A second two-dimensional study was completed to examine the interaction between the stress-deformation analysis and the slope stability calculations with special attention directed towards the influence of Poisson's ratio.

Poisson's ratio partially controls the relationship between the horizontal and vertical stress and can influence the orientation of the failure surfaces predicted by Mohr's theory. Therefore, the amount of stress rotation required to promote the development of a continuous slip surface depends on Poisson's ratio to some degree. A linear elastic analysis was shown to provide a poor prediction of the stress rotations required to bring the internal stress distribution into alignment in some cases. The limitations associated with the linear elastic analysis resulted in elevated factors of safety in cases where the search was based on geometric admissibility. Searching procedures based on kinematic admissibility criteria were shown to be more sensitive

resulting in irregular shaped slip surfaces and elevated factors of safety. The influence of stress rotation was shown to be significant in normally consolidated cases where the slip surface is shallow and excavations made in over-consolidated soil conditions. A more reasonable representation of the internal stress distribution was achieved through the use of an elasto-plastic analysis.

Searching procedures based exclusively on geometric admissibility criteria can result in slip surfaces that are not compatible with the internal stress distribution. The influence on the overall stability analysis was shown to depend on how much of the slip surface was inadmissible and how the presence of negative mobilized shear stresses were treated. The dynamic programming searching procedure was designed to exclude slip surfaces that were not completely admissible through the application of kinematic admissibility criteria. The strict application of kinematic admissibility criteria was considered to be appropriate based on observations made from shear zones in natural clays and laboratory tests (Morgenstern and Tchalenko 1967; Skempton and Petley 1967).

6.2 Three-Dimensional Studies

The details surrounding the extension of the stress-based slope stability method to three dimensions were presented. The results from an independent stress-deformation analysis were imported into the three-dimensional limit equilibrium slope stability analysis in the form of a regular grid. Slip surfaces were initially assumed to be ellipsoidal and were approximated using a triangular discretization scheme. The normal force and shear force acting at the centroid of individual triangular planes was computed based on the imported stress field using an interpolation scheme. The accuracy of the three-dimensional factor of safety calculation was shown to depend on: 1) the density of the finite element mesh, 2) the density of the intermediate stress grid linking the stress-deformation analysis and the factor of safety calculation, 3) the discretization of the slip surface and 4) the compatibility between the internal stress distribution and the shape of the slip surface. The results from a number of sensitivity

analyses demonstrated that the mesh refinement could be increased to an appropriate level without increasing the cost of the analysis to a degree that would discourage the application of the method in practice.

Additional sensitivity studies were completed to investigate the influence of Poisson's ratio. The results confirmed that the factor of safety can be sensitive to the value selected for Poisson's ratio in cases where the shape of the specified slip surface is not completely compatible with the stresses from the stress analysis. The level of compatibility was evaluated by reporting the number of inadmissible triangular planes on the slip surface. The fluctuations in the factor of safety increased as the number of inadmissible planes on the slip surface increased. The computed factor of safety was in agreement with published values when Poisson's ratio was selected so that there were no inadmissible planes on the slip surface. A series of verification examples were presented to confirm that the proposed method provides the required accuracy and flexibility to assess the stability of slopes typically encountered in practice. The successful application of the stress-based method in three-dimensions involves similar steps and provides similar advantages as the corresponding two-dimensional method. The factor of safety equation is linear, satisfies all conditions of force equilibrium and provides the ability to develop more advanced three-dimensional searching procedures based on kinematic admissibility criteria.

The final stage of the research involved the development of a slope stability method based on the combination of the stress-based method to compute the factor of safety and dynamic programming to search for the critical slip surface. There were numerical difficulties associated with the overwhelming number of slip surface combinations that were included in the analysis without meaningful criteria to exclude unreasonable slip surfaces. A combination of geometric and kinematic admissibility criteria were used to train the dynamic programming searching procedure to distinguish between reasonable and unreasonable slip surfaces. The flexibility of the admissibility criteria was adjusted to provide a balance between the slip surfaces included in the analysis and the solution time.

6.3 Recommendations for Future Research

All of the slope stability calculations were completed with no consideration of the strain values computed from the stress-deformation analysis. Additional research could be completed to determine if knowledge of the strain values could be used to improve the limit equilibrium slope stability calculations. Strength parameters (i.e., c' and ϕ') are typically assigned based on the assumption that the values are constant throughout individual soil units. It is possible that strength of the soil could be included in the slope stability analysis as a function of the amount of strain computed from the stress-deformation analysis in an attempt to capture the strain softening characteristics of the soil. Knowledge of the strain could also provide the basis for the development of new admissibility criteria. The admissibility criteria could be used to further reduce the number of slip surfaces considered in two- and three-dimensional searching algorithms.

It is clear that the searching procedure based on the dynamic programming algorithm represents a significant advancement over traditional trial and error techniques where the shape of the slip surface is assumed. The application of the dynamic programming algorithm has remained the subject of research for some 20 years and has only recently been incorporated into a commercially available software product for the evaluation of two-dimensional slope stability problems (SoilVision Systems Ltd. 2006b). Other commercial software products based on the method of slices or stress-based methods could also benefit from the ability to provide a more thorough search for the critical slip surface. stress-based slope stability methods can take advantage of geometric and kinematic admissibility criteria to completely integrate the search for the critical slip surface with the stress distribution used to compute the factor of safety. Results from this dissertation have indicated that it is prudent to confirm that the shape of the slip surface is compatible with the internal stress distribution when the shape of the slip surface is specified.

Finally, this dissertation confirms that the stress-based method can be extended and successfully applied to compute the factor of safety for three-dimensional slip

surfaces. The development of three-dimensional modeling products with CAD interfaces as well as advanced visualization products could provide the tools required to apply the stress-based method in engineering practice. The stress-based procedure can be economically combined with traditional searching procedures to provide the ability to evaluate three-dimensional effects in many cases. The three-dimensional dynamic programming searching procedure is clearly more costly than traditional trial and error searching procedures but represents a viable option that can be applied in complex situations where the increased cost is warranted. The practice of geotechnical engineering will benefit from the development of cost-effective three-dimensional slope stability methods given the pressure to design steeper slopes in response to the ever increasing value of natural resources, water storage requirements and property value. This dissertation has demonstrated that the numerical difficulties associated with three-dimensional slope stability analyses can be effectively managed providing the ability to carry out further analyses of case history examples.

6.4 Bibliography

Baker, R. 1980. Determination of the critical slip surface in slope stability computations. International Journal For Numerical and Analytical Methods in Geomechanics, 4(4): 333-359.

Loehr, J.E. 1998. Development of a hybrid limit equilibrium-finite element procedure for three-dimensional slope stability analysis. Dissertation, The University of Texas at Austin, Texas, USA.

Morgenstern, N.R., and Tchalenko, J.S. 1967. Microstructural observations on shear zones from slips in natural clays. *In* Proceedings Geotechnical Conference. Oslo, Norway, Vol.1, pp. 147-152.

Skempton, A.W., and Petley, D. 1967. The strength along structural discontinuities in stiff clays. *In* Proceedings Geotechnical Conference, Oslo, Norway, pp. 55-69.

SoilVision Systems Ltd. 2006b. SVDynamic Version 1.23, Saskatoon, SK.

Appendix A

Comparing Slope Stability Analysis Based on Linear Elastic or Elasto-Plastic Stresses Using Dynamic Programming Techniques[1]

A.1 Introduction

Conventional limit equilibrium slope stability methods require assumptions regarding stresses within the slope and the shapes of potential slip surfaces to render the problem determinate. These assumptions have been overcome with the use of the dynamic programming method (Brito et al. 2004) in combination with stresses from a finite element analysis. However, slope stability calculations based on stresses from finite element analysis have not become popular for slope stability studies due to intense computational requirements and difficulties in assessing the stress versus strain characteristics of the soil (Scoular 1997). If the Dynamic Programming Method (DPM) of analysis is to be adopted in practice, these issues must be addressed and continuing verification of the method must be provided.

The focus of this study is to address the above concerns by providing additional verification of the DPM and guidance as to the appropriate constitutive model to use in stability calculations. Verification of the DPM is provided through the comparison

[1] This chapter has been presented as a paper at the 2004 Canadian Geotechnical Conference (Stianson et al. 2004).

of a vertical cut analysis with Taylor's stability charts. Guidance on appropriate constitutive models is provided through a comparison of stability results based on either linear elastic (LE) or elasto-plastic (EP) stresses. The comparison includes a series of stable and failing slopes. It is of interest to determine if stresses from a plastic analysis are required to correctly determine the shape, location, and factor of safety of critical slip surfaces for slopes at or near failure.

A.2 Background

Much research has been focused on developing techniques to overcome assumptions used in limit equilibrium methods. Variational calculus was one of the first of such techniques. The calculus of variations provides a mathematical procedure to find the shape of an extremal, a curve that maximizes or minimizes the value of an integral along that line (De Josselin De Jong 1980). The benefit of such a method is that the factor of safety is determined without any prior assumptions regarding the shape or location of the critical slip surface. While the calculus of variations was popular with several researchers, it was shown to contain a degeneration (De Josselin De Jong 1981). The degeneration was related to the non-existence of unique derivatives within the formulation.

The DPM, in combination with Spencer's (1967) assumptions, was first applied to slope stability problems by Baker (1980). It was used to overcome assumptions regarding the shape of potential slip surfaces and degenerations reported with variational calculus. Baker notes that while the DPM is similar in concept to the calculus of variations it does not require the existence and uniqueness of derivatives to determine the critical slip surface. Instead, the minimization is completed numerically through the direct comparison of values. While numerical methods may have been laborious in the past, they are much less of a problem with the high speed computers readily available today.

The formulation of the DPM in combination with stresses from a finite element analysis was first developed by Yamagami and Ueta (1988b). The purpose of the

study was to employ limit equilibrium methods to yield an overall factor of safety while accounting for the constitutive relationship and initial stress state of the soil using stresses from a finite element analysis. The benefit of determining the shape of the slip surface without assumptions was also realized. Further verification has been provided by testing the technique over a wide range of slope conditions using a large parametric study (Pham 2002). The technique has also been applied to the analysis of transient embankment stability by Gitirana and Fredlund (2003).

A.3 Verification

A.3.1 Vertical Cut analysis

The ϕ-Circle Method was proposed by Gilboy and Casagrande with the hope that a completely graphical solution method may be developed to solve for the stability of a homogeneous slope. Applied to any circular slip surface, the result is a vector whose length represents the quantity $2c/\gamma$, where c is the cohesion and γ is the unit weight required for equilibrium (Taylor 1937). Dividing the length of the vector by the height of the slope (H), resulted in an abstract number that could describe the equilibrium conditions for a slope of any height for a given slope and friction angle, $2c/\gamma H$. Taylor (1937) modified the form of this abstract number resulting in the following dimensionless expression called the "Stability Number" with F_s representing the factor of safety.

$$\frac{c}{F_s \gamma H} \qquad [6.1]$$

The traditional factor of safety equation becomes independent of the normal stress when ϕ' is equal to zero. If the linear elastic constitutive model is used, the calculation of the factor of safety using the DPM should be independent of Young's modulus and Poisson's ratio. These realizations allow for the comparison of the

DPM with the stability charts developed by Taylor (1937) which are also independent of stress. The reliability of the DPM will be tested by comparing the factor of safety obtained for a strictly cohesive vertical cut with Taylor's stability chart.

A slope with cohesion equal to 30 kPa, internal angle of friction equal to zero, and a unit weight of $18kN/m^3$ was used to compare the DPM with Taylor's stability chart. Assuming a factor of safety of one, Taylor's stability number predicts the critical height for a vertical cut with the noted properties to be 6.4m. A stress analysis is completed for a vertical cut with this height using the linear elastic constitutive model. Two values of Poisson's ratio (0.48 and 0.33) and Young's modulus (20,000 kPa and 100,000 kPa) are chosen to test if the DPM is independent of stress for the $\phi'=0$ analysis.

A.4 Comparison of Slope Stability Results Based on Linear Elastic or Elasto-Plastic Stress Analysis

The purpose of this comparison is to address issues related to basing a slope stability analysis on stresses generated from a numerical analysis. More specifically, investigating the use of linear elastic stresses in slopes where the factor of safety is low enough to allow overstressing to occur. In such slopes, a constitutive model that accounts for yielding may be required to correctly calculate the factor of safety and determine the shape and location of the critical slip surface. However, use of plastic constitutive models is more involved causing computing times to increase. Therefore, it is necessary to determine if a plastic analysis is in fact required.

A.4.1 Scope

A variety of increasingly complex problems are chosen to ensure that the comparison will encompass a small range of typical conditions. The range of problems includes homogeneous slopes and multi-layered slopes with various Poisson's ratios, pore

pressure conditions and slope angles. Space does not permit the presentation of every model so representative results are chosen that best illustrate the observed behavior for each condition.

The FLAC stress analysis software package is chosen to complete the comparison. FLAC is chosen based on three requirements. The software must include an elasto-plastic constitutive model, a linear elastic constitutive model, and must have the ability to incorporate the computed stress data into the DP slope stability analysis. It should also be noted that the finite difference solution technique employed by FLAC results in similar stress fields when compared with finite element results for the range of slopes in this study.

A.4.1.1 Homogenous Slopes

Ideally, the comparison between the LE and EP models will be carried out over a range of safety factors. Beginning with safety factors for which the majority of the slope behaves in an elastic manner progressing to safety factors where the slope experiences yielding. Soil properties are chosen such that three factors of safety will result including ~1.3, ~1.0, and < 1.0. Factors of safety of 1.3 and 1.0 result in slopes that are mostly elastic with some yielding and slopes that are at failure, respectively. The majority of engineering design is completed using factors of safety greater than 1.2 while successful back analysis requires a factor of safety of 1.0. Factors of safety less than 1.0 are impossible in reality but are included for discussion purposes.

Table A.1: Homogeneous slope soil properties

Unit Weight γ (kN/m^3)	Poisson's Ratio ν	Effective Cohesion c' (kPa)	Effective Friction Angle ϕ' (degrees)
18	0.48	20	10
		17	7
		15	5
18	0.40	20	10
		17	7
		15	5
18	0.33	20	10
		17	7
		15	5
18	0.20	20	10
		17	7
		15	5

The range of soil properties used in the homogeneous slopes is shown in Table A.1. The effective cohesion (c') and effective friction angle (ϕ') are chosen such that a factor of safety of ~1.3 results, given a unit weight of 18 kN/m^3 and a 2:1 slope angle. The slope is brought to failure by decreasing the cohesion and friction of the material by equal increments resulting in factors of safety of ~1.0 and <1.0 respectively. A set of analysis was also completed bringing the slope to failure by increasing the unit weight of the material. Using cohesion equal to 20 kPa and friction angle equal to 10° the desired range of safety factors was achieved by using unit weights of 18 kN/m^3, 30 kN/m^3, and 50 kN/m^3. Bringing the slope to failure by increasing the unit weight produced similar results therefore only the strength reduction results are presented.

Four values of Poisson's ratio are chosen including 0.48, 0.40, 0.33, and 0.2. Varying Poisson's ratio in a LE analysis is equivalent to setting different in-situ stress conditions. The range of K_o values achieved using the above values for Poisson's ratio include 0.25, 0.5, 0.7, and ~1.0. These values are calculated according to the

following relationship, $K_o = \nu / 1-\nu$. This relationship is only a guide, as stress conditions generated in a slope vary with depth. It should also be noted that Young's modulus was held constant at 20,000 kPa for all homogeneous analysis. The convergence criteria (δ) for the dynamic programming search remained 0.001 for all analyses.

A.4.1.2 Wet and Submerged Slopes

Water is included for the case of Poisson's ratio equal to 0.48, cohesion equal to 20 kPa, friction angle equal to 10° and slope angle of 2:1. Two pore-water conditions are generated including a wet slope condition where the water table is drawn down to the toe of the slope and a submerged slope condition where the water is two meters deep at the toe of the slope.

A.4.1.3 Slope Angle

Three slope angles are chosen including 3:1, 2:1 and 1:1. These slope angles are applied to the case where Poisson's ratio is 0.48 and the unit weight is 18 kN/m^3. Given these conditions the factor of safety ranges from ~1.6 to 1.0.

A.4.1.4 Multi-Layered Slopes

Multi-layered slopes are included to compare conditions where a contrast in Young's modulus exists and a weak soil layer is included. Two conditions are considered including a 2-layer slope and a 3-layer slope under dry and wet conditions.

A.5 Results

A.5.1 Vertical Cut

The factor of safety calculated by the DPM is virtually the same as that predicted by Taylor's stability chart. Focusing on the first two slip surfaces listed in Figure A.1, the factor of safety calculated using a constant Poisson's ratio is exactly the same whether the Young's modulus is 20,000 kPa or 100,000 kPa. The slip surfaces for the first two cases also plot one on top of the other. Therefore, the factor of safety and the critical slip surface calculated using the DPM method is independent of Young's modulus.

Comparing the results using a Poisson's ratio of 0.48 to 0.33 yields a slight difference in the factor of safety and the location of the critical slip surface. As noted by (Gitirana and Fredlund 2003), the overall effect of the value of ν results in higher σ_x/σ_y ratios inside the embankment for larger values of ν. The larger values of σ_x/σ_y inside the embankment drive the slip surface to shallower regions where the lower σ_x/σ_y ratios occur. While the effect is almost negligible in this case, the slip surface for ν equal to 0.33 is slightly deeper than for the 0.48 case. In this comparison it appears that various in-situ stress states result in only minor differences.

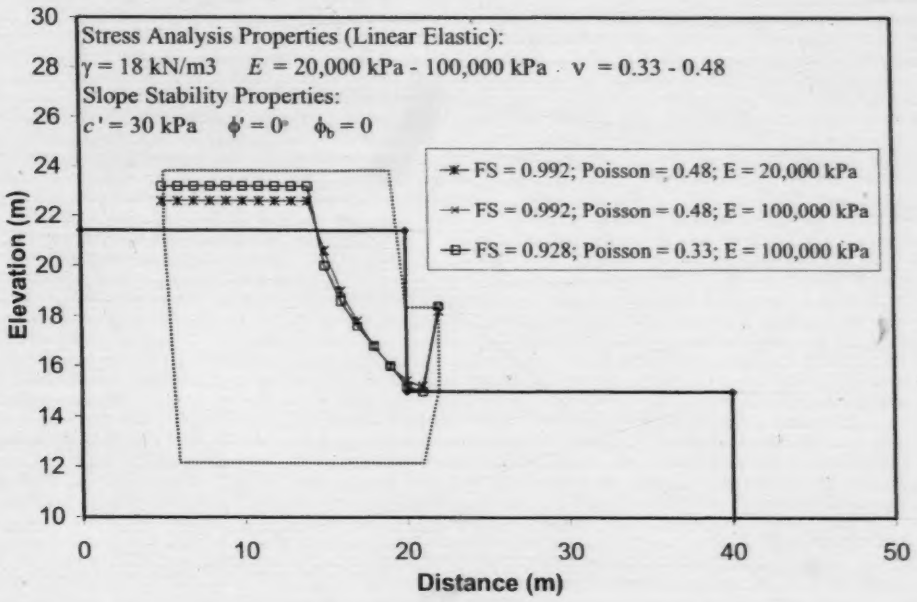

Figure A.1: Vertical cut comparison

A.5.2 Homogeneous Slope

The results for the case of Poisson's ratio equal to 0.48 are used to illustrate the observed behavior for all dry homogeneous slopes. There are three figures, one for each factor of safety including ~1.3, ~1.0, and <1.0. It should be noted that the legend for each slip surface records whether the analysis was elastic or elasto-plastic and the calculated factor of safety. The factor of safety calculated by the Morgenstern and Price (MP) method using a half sine function is also included for comparison. One summary plot at the end of the section shows the relationship between the initial K_o conditions and the factor of safety.

Figure A.2, A.3 and A.4 illustrate the difference between slope stability analysis based LE or EP stress analysis. The shape and location of the critical slip surfaces are very similar for conditions where the factor of safety is equal to or greater than one. The calculated factors of safety for these conditions are also very similar. The

following reasoning explains why the differences between these two analyses are very small.

The distribution of stress computed by any stress analysis is governed mainly by the geometry of the problem, the boundary conditions and the soil properties. Therefore, it is reasonable to expect that critical areas of high stress will develop in similar locations within a slope using either the LE or EP constitutive model. This can be verified by using extremely high strength in an EP stress analysis and observing that the stress distribution is the same as the equivalent LE stress analysis.

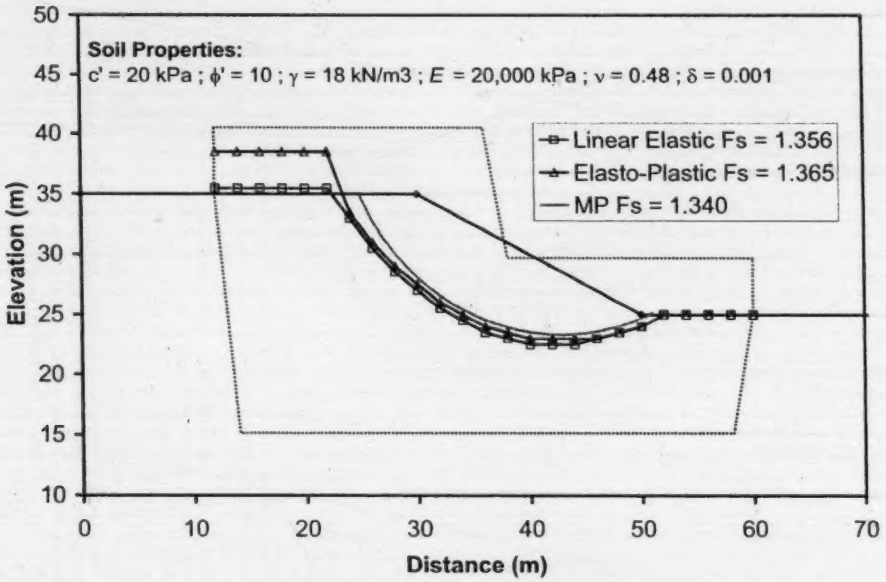

Figure A.2: Dry Homogeneous Slope, F_s~1.3.

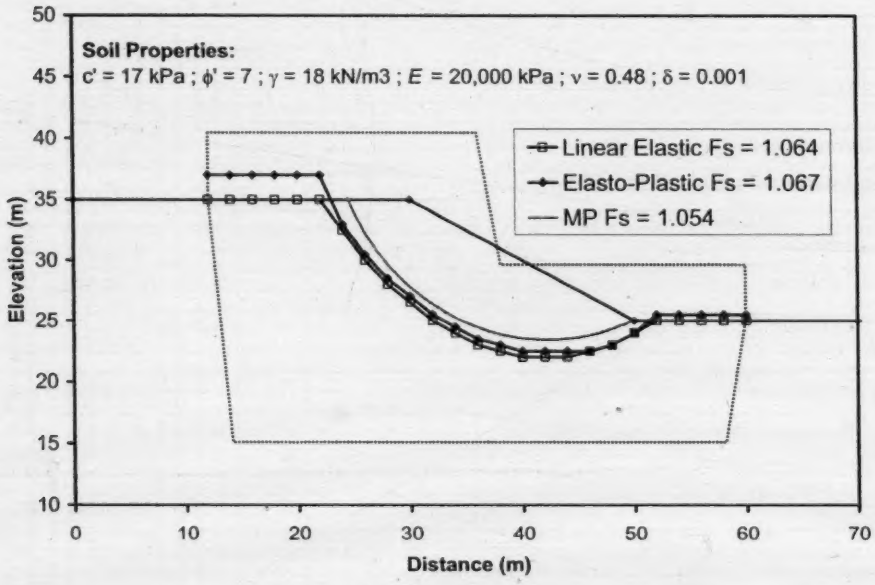

Figure A.3: Dry Homogeneous Slope, F_s~1.0

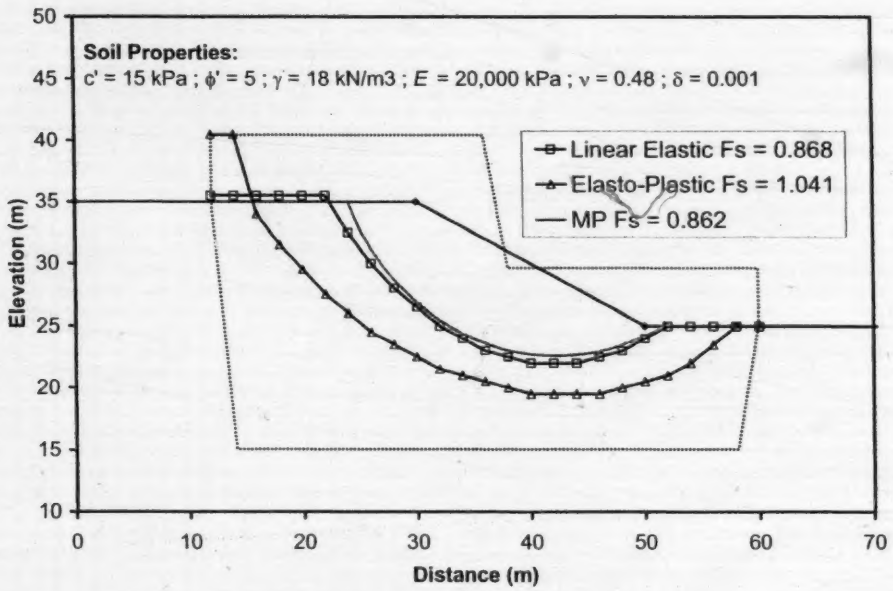

Figure A.4: Dry Homogeneous Slope, F_s<1.0

However, in most cases the EP stresses are only allowed to increase to a certain level before excess stresses are redistributed to surrounding soil. As shown in Figure A.2 and A.3, this does not cause large differences in the location of the critical slip surface when the factor of safety is equal to or greater than 1.0. Excess stresses are redistributed to adjacent areas of high stiffness and lower mobilized strength. The DP stability analysis searches for the path of lowest mobilized strength. Therefore, it is not surprising that the DP search determines the critical slip surface to be in similar locations using either constitutive model. This has also been verified by comparing displacement vectors determined from EP stress analysis with the critical slip surface determined from DP stability analysis. If additional load is added to the slope or the strength of the slope is decreased, large displacements occur. Additional stresses are redistributed to surrounding soil increasing the amount of failed soil. This causes

large differences in the location of the critical slip surface determined from LE or EP stresses as shown in Figure A.4.

The discussion above is also useful for explaining differences observed in the distribution of the factor of safety but overall agreement in the average factor safety. If strength properties used in an EP model are such that a factor of safety of 1.0 will result, the factor of safety computed for individual line segments along the critical slip surface will be approximately the same. If DP stability analysis is completed using the equivalent LE stresses, the distribution of the factor of safety is highly variable and in some cases exists below 1.0. This difference is also due to the redistribution of stresses that occurs in an EP analysis. Although there are differences in the distribution of the factor of safety along the critical slip surface, agreement in the overall factor of safety results from three conditions: 1) the same geometry, boundary conditions and elastic constants are used to generate the stress state, 2) the same strength properties are used to perform the stability analysis and 3) the calculated factor of safety for the slope is equal to or greater than 1.0.

The same trend is observed when the initial stress state is changed. There remain only small differences in stability analysis based on either LE of EP stress analysis. However, it should be noted that changing the initial stress state causes subtle variations in the shape of the critical slip surface from both analysis. The slip surface becomes less circular with decreasing Poisson's ratio (i.e. decreasing K_o). The effects are more pronounced near the crest of the slope. Figure A.5 illustrates the relationship between factor of safety and initial stress state computed using LE stresses. The plot shows that there is virtually no change in the factor of safety as K_o is varied from 0.3 to ~1. The remaining examples have been included to examine if similar results will be observed for more complex slopes.

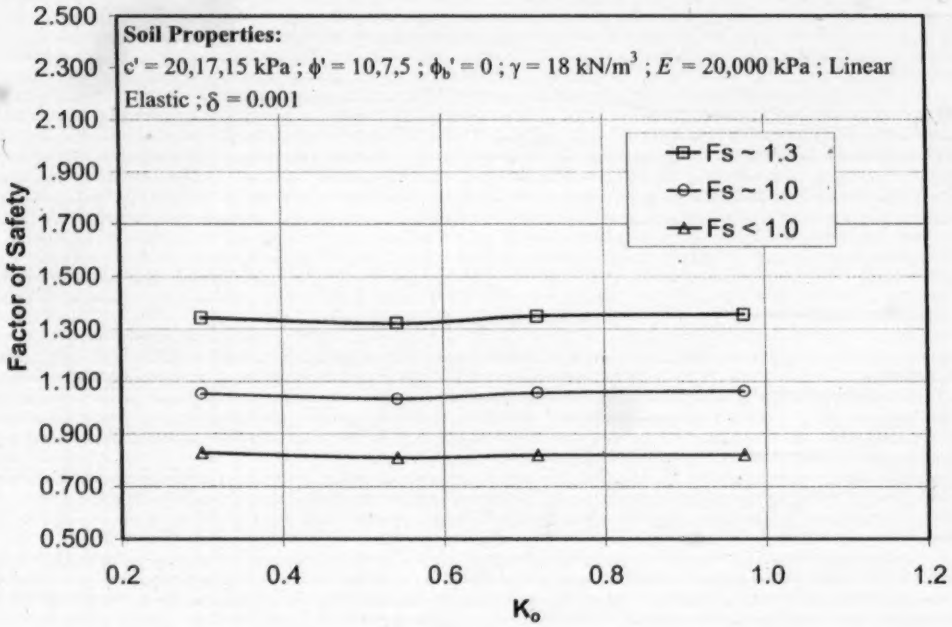

Figure A.5: Effect of initial stress state on the factor of safety.

A.5.3 Wet and Submerged Slope

Figure A.6 shows the comparison of LE wet (Elastic-W), EP wet (Plastic-W), LE submerged (Elastic-S), and EP submerged (Plastic-S) results.

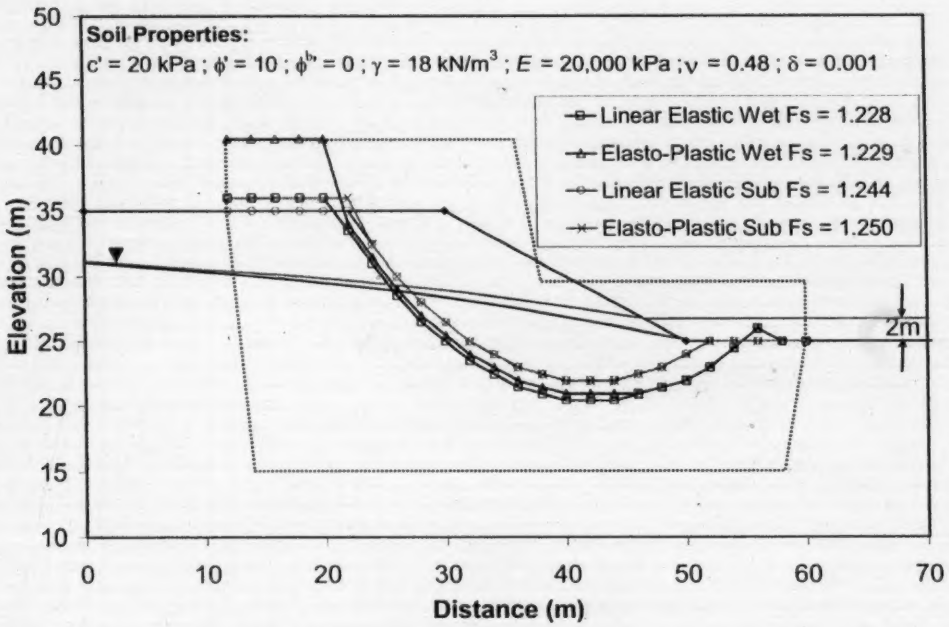

Figure A.6: Wet and Submerged Slope

As anticipated the critical slip surface rises and the factor of safety increases slightly as the slope is submerged with water. This occurs due to the added pressure of the standing water at the toe of the slope. It can be seen that the shape and location of the critical slip surfaces are again quite similar for both the wet and submerged conditions. From Figure A.6, the dark lines correspond to the wet condition and the light lines correspond to the submerged condition.

A.5.4 Slope Angle

As expected, the factor of safety decreases as the slope angle becomes steeper. The results also show the same similarities between the shape and location of the critical slip surface when using either LE or EP stresses.

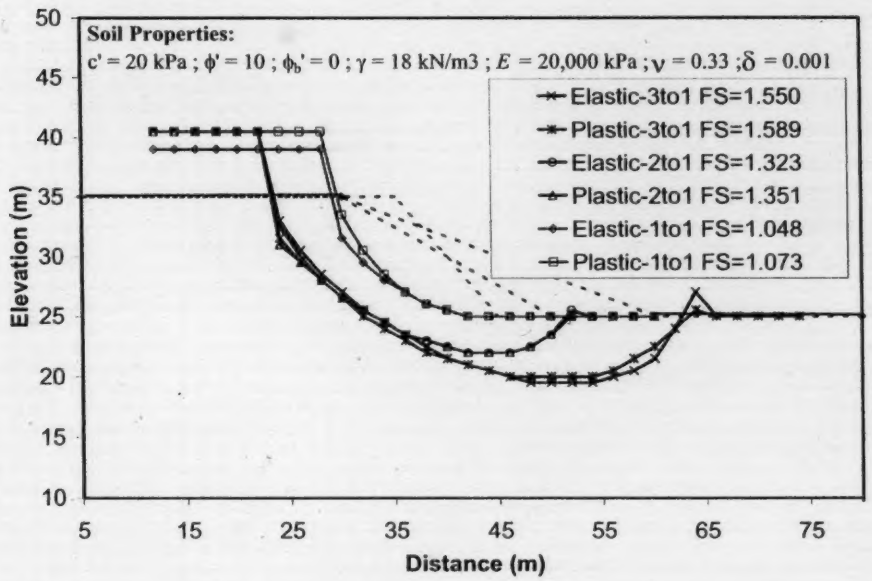

Figure A.7: Slope Angle.

A.5.5 Multi-Layer Slopes

A.5.5.1 Two Layer Slope

Figure A.8 illustrates the results for the 2-Layer slope at a factor of safety of ~1.0 and dry conditions. Only small differences exist between the location of the critical slip surface and the calculated factor of safety. The two methods differed by similar amounts when water was included.

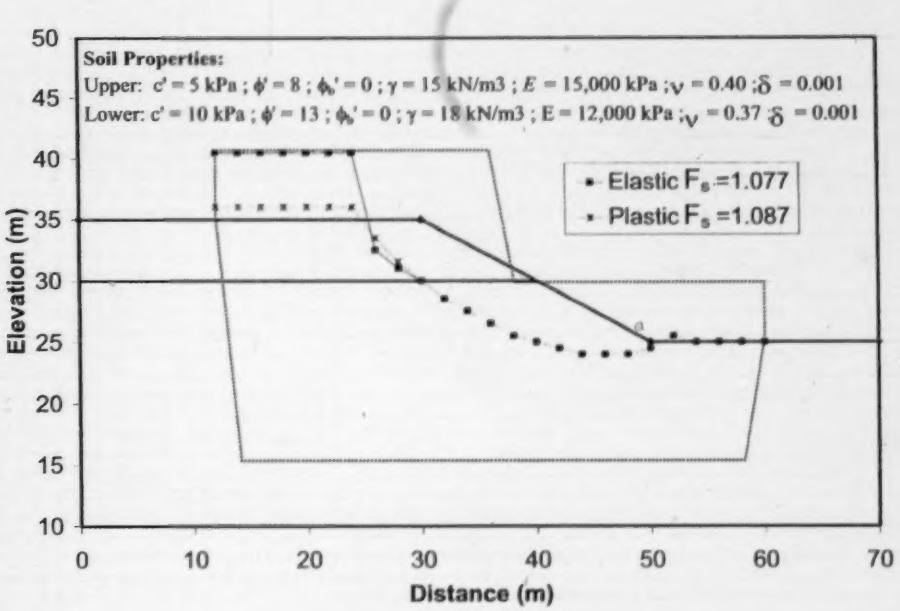

Figure A.8: Two Layer Slope

A.5.5.2 Three Layer Slope

The three layer slope models a condition of a much larger stiffness contrast, as well as the inclusion of a weak layer. The results from the dry condition are shown in Figure A.9. While these results show almost no deviation, it should be noted that a limitation was encountered in this analysis. The thickness of the weak layer was originally 1m thick. The results from this condition showed larger deviations near the toe of the slope and through the weak layer. This deviation was due to the search grid density relative to the dimensions of features within the slope. When the thickness of the weak layer is increased to 2m, the results calculated are as shown in Figure A.9. More testing is required to determine the optimum grid density relative to the size of important features within the slope.

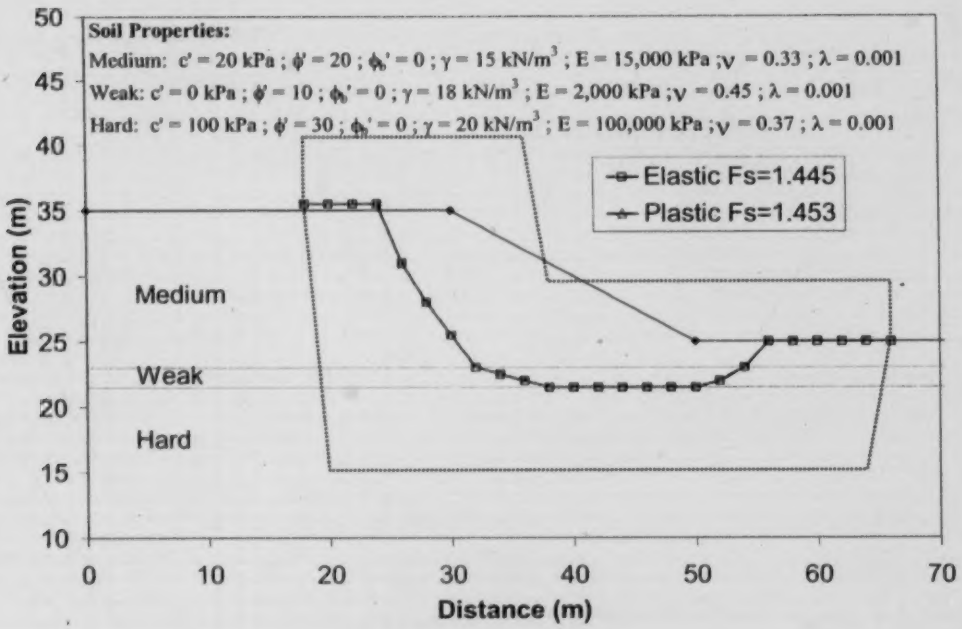
Soil Properties:
Medium: c' = 20 kPa ; φ' = 20 ; φb' = 0 ; γ = 15 kN/m3 ; E = 15,000 kPa ;ν = 0.33 ; λ = 0.001
Weak: c' = 0 kPa ; φ' = 10 ; φb' = 0 ; γ = 18 kN/m3 ; E = 2,000 kPa ;ν = 0.45 ; λ = 0.001
Hard: c' = 100 kPa ; φ' = 30 ; φb' = 0 ; γ = 20 kN/m3 ; E = 100,000 kPa ;ν = 0.37 ; λ = 0.001
Elastic Fs=1.445
Plastic Fs=1.453
Medium
Weak
Hard
Elevation (m)
Distance (m)
50
45
40
35
30
25
20
15
10
0
10
20
30
40
50
60
70

Figure A.9: Three layer slope.

A.6 Conclusions

The reliability of the DPM is confirmed in the vertical cut analysis. The DPM predicted the same factor of safety as Taylor's stability charts for a vertical strictly cohesive cut. It was also demonstrated that the factor of safety and slip surface were relatively unaltered by Young's modulus and only minor changes resulted from changing Poisson's ratio.

The differences between stability analyses based on LE or EP stresses are also presented. The largest differences are shown to occur in the fabricated condition where the factor of safety is less than one. Only small differences were found when the slope was modeled under more realistic conditions where the factor of safety is equal to or greater than 1.0. It would seem then that LE stress analysis is sufficient to calculate the overall stability of a slope. Due to the various conditions considered, it is reasonable to conclude that elastic stress analysis is adequate for a large range of

slope conditions frequently encountered in practice. This is of benefit as elastic stress analysis is less involved requiring much less computer time. However, more research is required to determine if this conclusion will hold true for every possible slope condition encountered in practice.

A.7 Bibliography

Baker, R. 1980. Determination of the critical slip surface in slope stability computations. International Journal For Numerical and Analytical Methods in Geomechanics, 4(4): 333-359.

De Josselin De Jong, G. 1980. Application of the calculus of variation to the vertical cut off in cohesive frictionless soil. Geotechnique, 30(1): 1-16.

De Josselin De Jong, G. 1981. A variational fallacy. Geotechnique, 31(2): 289-290.

Gitirana, J.G.F.N., and Fredlund, D.G. 2003. Analysis of transient embankment stability using the dynamic programming method.

Pham, H.T.V. 2002. Slope Stability Analysis Using Dynamic Programming Method Combined With a Finite Element Stress Analysis. Thesis., University of Saskatchewan, Saskatoon.

Scoular, R.E.G. 1997. Limit equilibrium slope stability analysis using a stress analysis. Thesis, University of Saskatchewan, Saskatoon.

Spencer, E. 1967. A method for analysis of the stability of embankments assuming parallel interslice forces. Geotechnique, 17(1): 11-26.

Taylor, D.W. 1937. Stability of earth slopes. Journal of Boston Society of Civil Engineers, 24(3): 337-386.

Yamagami, T., and Ueta, Y. 1988b. Search for critical slip lines in finite element stress field by dynamic programming. *In* Proceedings of the 6th International Conference on Numerical Methods in Geomechanics. Innsbruck, pp. 1347-1352.

Appendix B

Methodology to Perform a Three-Dimensional Dynamic Programming Slope Stability Analysis

B.1 Finite Element Analysis

A significant amount of the information required to complete the slope stability analysis is generated or managed during the completion of the stress deformation analysis. The results of the finite element analysis are exported to a regular three-dimension grid in preparation for performing the slope stability evaluation (Figure B.1). The strategy for preparing the information required in the slope stability analysis is outlined below.

Table B.1 lists the parameters input into the stress-deformation analysis. It is beneficial to assign values for the supporting parameters even though the information is not required to compute the internal stress distribution. The Dynamic Programming optimization procedure does not have to be designed to identify the boundaries of the soil layers since each point in the exported three-dimensional grid inherits the correct strength and stress values from the stress-deformation analysis. Many stress-deformation software packages provide the ability to define additional variables to facilitate the management of the supporting parameters that will be used to compute the factor of safety in later stages of the slope stability analysis. It is important to note that the coordinate system selected in the stress-deformation analysis is maintained throughout the rest of the slope stability analysis. The current

formulation is designed such that the y-direction corresponds to the assumed direction of failure.

Table B.1: Parameters input into the stress-deformation analysis.

Stress Deformation Analysis	Required to compute internal stresses distribution	[1]Required for slope stability analysis
Linear Elastic	E, v	c', ϕ', ϕ^b, u_w
Elasto-Plastic	E, v, c', ϕ'	ϕ^b, u_w

[1]The slope stability parameters are not used to compute the internal stress distribution. The stress deformation software manages the assignment of the supporting parameters to the various soil units in preparation for the stability analysis.

The internal stress state computed from the finite element analysis is used to determine the forces acting along the three-dimensional slip surface. The interpolation procedure required to determine the stresses acting at discrete points along the slip surface is dependent on the mesh configuration used in the three-dimensional stress-deformation analysis (i.e., tetrahedron, hexahedron etc.). A separate interpolation procedure is required for individual mesh configurations. For simplicity, the stresses and soil parameters from the finite element analysis are exported to a rectangular grid configuration, referred to as the intermediate grid (Figure B.1 b). The information stored in the intermediate grid is used to compute the factor of safety for the triangular planes that are connected to form potential slip surfaces during the slope stability analysis. In many cases, the stress and strength parameters are required at points that do not align exactly with the points on the intermediate grid. The values of the parameters are linearly interpolated from surrounding grid points on the intermediate grid. The density of the intermediate grid is selected to minimize the influence of the linear interpolation procedure and provide an accurate factor of safety calculation.

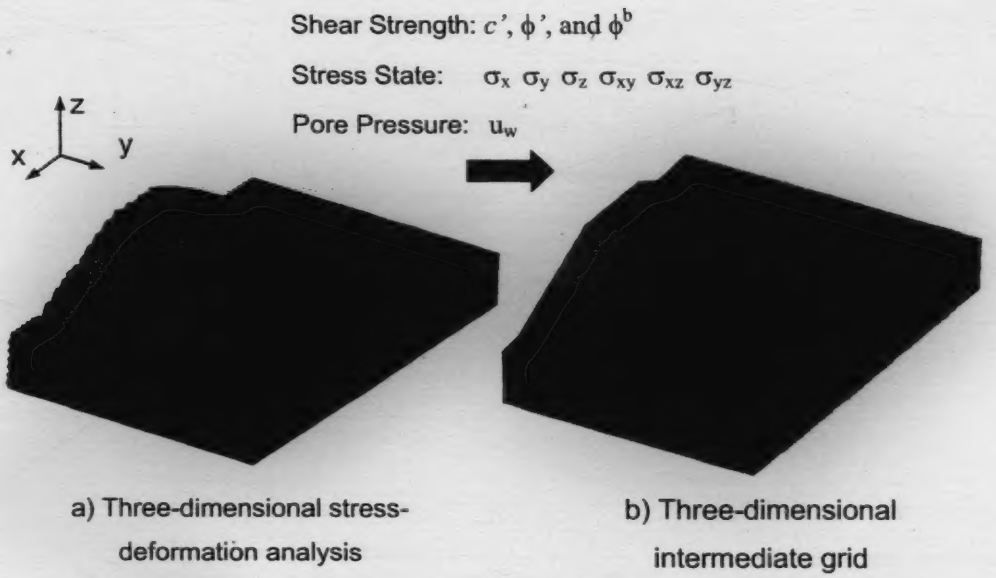

Figure B.1: Illustration of the three-dimensional grid linking the stress-deformation analysis with the slope stability calculations.

B.2 Development of the *Stage-State* System

The dynamic programming method is a numerical algorithm used to optimize sequential multi-stage decision problems. Multi-stage decision problems are solved using a system of *stages* and *states*. Dividing the slope stability calculation into a *stage-state* system facilitates the calculation of the factor of safety for trial slip surfaces while at the same time searching for the slip surface with the lowest factor of safety. The details regarding the development of the *stage-state* system is presented in the following sections.

B.2.1 Three-Dimensional Dynamic Programming Search Grid

A previous section described how the stress-deformation analysis is used to prepare an intermediate grid that stores the soil parameters required to compute the factor of safety for a potential slip surface. The current section introduces one more three-dimensional grid referred to as the dynamic programming search grid. The points on the search grid are used construct triangular planes that are connected together to form the slip surfaces evaluated during the slope stability analysis. The search grid is designed so that the connection of triangular planes is completed according to a *stage-state* system.

The two-dimensional dynamic programming slope stability formulation proposed by Pham (2000) used the concept of an intermediate grid to store the soil properties and generate potential slip surfaces. In other words, the points on the intermediate grid are used to generate potential slip surfaces instead of developing a separate search grid. It might seem reasonable to eliminate the requirement of a separate search grid to reduce the effort required to prepare a two- or three-dimensional search. However, it is recommended that the intermediate grid and the search grid remain separate.

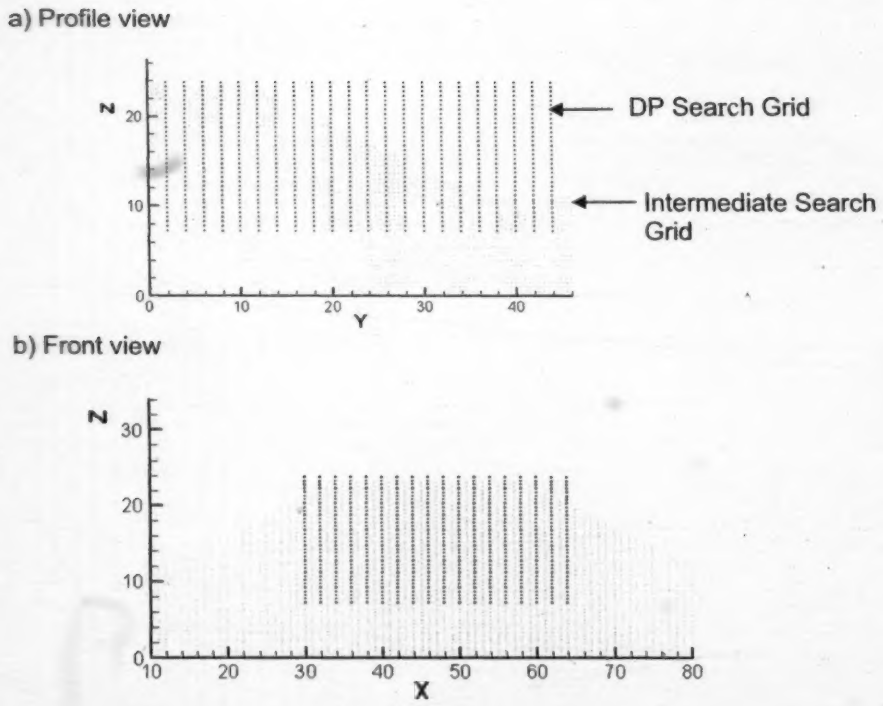

Figure B.2: Profile view (a) and front view (b) illustrating the separation between the intermediate grid and the search grid.

The density of the intermediate grid is selected to provide the ability to compute an accurate factor of safety. The density of the search grid is selected to build slip surfaces that can reasonably represent the shape of the critical slip surface. In many cases the density of the intermediate grid must be increased to a higher level than would be required to represent the shape of the critical slip surface. As a result, the dynamic programming searching procedure would be required to evaluate extra slip surface combinations if the intermediate grid was used in place of a separate search grid, increasing the overall solution time. The increase in the solution time resulting from using one grid might not be considered significant in certain two-dimensional problems. However, the solution time can increase drastically in three-dimensional analyses and the best search grid design might not be achieved. Therefore, it is best to separate between the grid used to store the information from the stress-deformation

analysis and the grid used to construct potential slip surfaces during the dynamic programming search (In both two- and three-dimensional formulations.).

The input required to generate the three-dimensional search grid is summarized in Table B.2. The resulting search grid is regular in that the *x*, *y* and *z* spacing between points is constant (Further research in this area should consider the possibility of increasing the density of the dynamic programming search grid around thin weak layers or other problem areas in the slope. Doing so would provide another reason to separate between the intermediate grid and the dynamic programming search grid.). The grid is initially rectangular and intersects the slope in the area of interest as shown in

Figure B.3 a). The grid should be viewed as a series of two-dimensional cross-sections called *stages*. *Stages* are aligned perpendicular to the assumed direction of failure (i.e., the *y*-direction in the current formulation). *Stages* divide the slope stability analysis into a number of smaller optimization problems.

Table B.2: Parameters required to build the dynamic programming Search Grid.

Parameter	Description
xc, yc, zc	Starting coordinates
x, y, z	Spacing between points in each direction
i, j, k	Number columns/rows to generate

The spacing between points in the *z*-direction is typically selected based on the presence of thin weak layers or other requirements regarding the shape of the slip surface. The spacing between points in the *x*- and *y*- directions is typically three to four times larger than the *z* spacing. The selection of the spacing is related to the presence of soil features and the admissibility criteria applied during the generation of *state curves*. The relationship between the spacing and the admissibility criteria is described in the following section.

The final step in preparing the search grid is to delete unnecessary points above the ground surface. The points are deleted using a three-dimensional surface like the one shown in

Figure B.3 (i.e., all points above the surface are deleted.). The surface is designed to leave a certain number of grid points above the ground surface near the outside of the search grid. These grid points are needed to evaluate the entry and exits points of the critical slip surface. The surface deletes a certain number of grid points below the ground surface, approximately in the middle of the search grid. These points are deleted so that potential slip surfaces are forced to pass through the slope. The final search grid is shown in Figure B.3b).

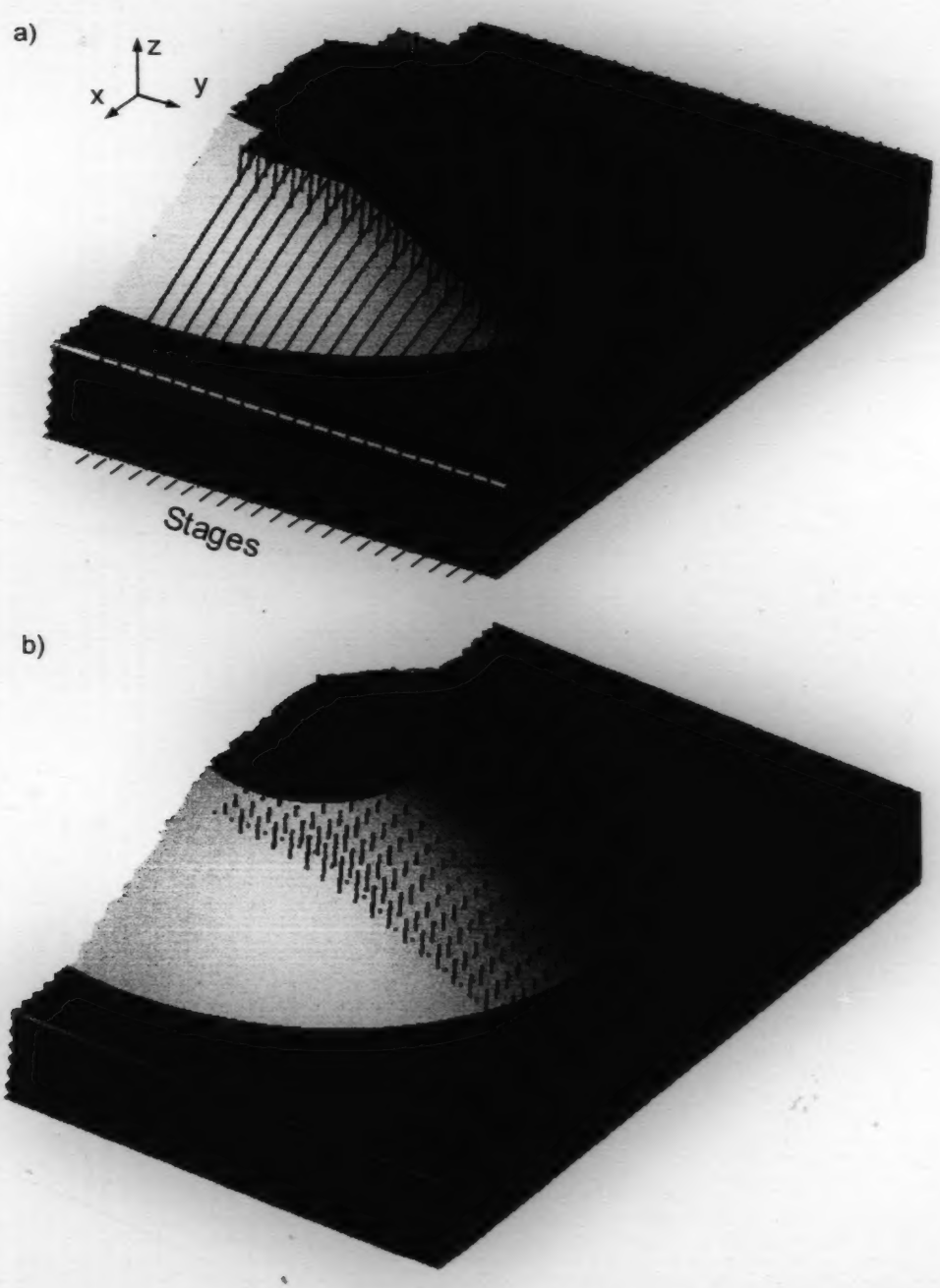

Figure B.3: Illustration describing the design of the dynamic programming search grid.

Figure B.4 illustrates two profiles taken through the centre of the problem parallel to the assumed direction of failure (i.e., the *y*-direction). The profiles illustrate that there are certain number of points above the crest and the toe of the slope. These points provide the ability to locate the entry and exit of the critical slip surface. The profiles also illustrate that points along the face of the slope are deleted so that the slip surfaces are forced to enter the slope.

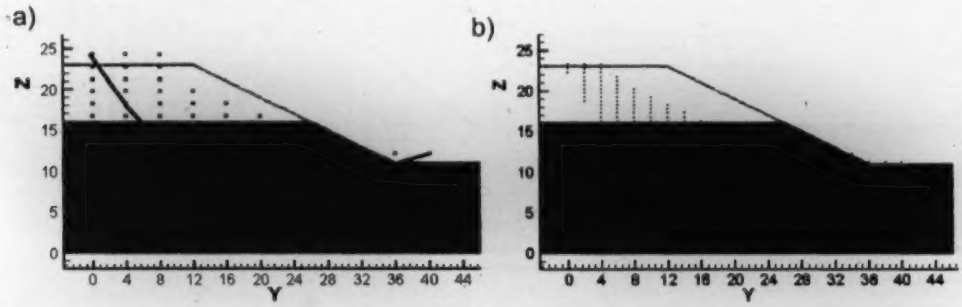

Figure B.4: Search grid configurations to facilitate different searching strategies.

The profiles demonstrate a potential searching strategy that can be used to maximize the efficiency of the dynamic programming optimization procedure. An initial search can be completed using a coarse grid similar to the one shown in Figure B.4 a). The coarse grid is spread over a large area of the slope to identify the most likely location of the critical slip surface. It is understood that the shape of the slip surface will likely be approximate at this stage. The next step is to focus the search grid around the critical slip surface identified in the preliminary search. The internal modifications to the search grid are applied using a surface similar to the procedure for deleting points above the ground surface.

B.2.2 State Curve Generation

The final step in preparing the skeleton of the dynamic programming search is to further divide the analysis into a series of *states*. Figure B.5 represents a typical

profile view of one *stage*. *States* are defined as curves generated by connecting a series of points from one *stage*. It is evident from Figure B.5 that *state curves* describe the shape of the slip surface in the direction perpendicular to failure. The numerical procedure to generate *state curves* is divided into steps depending on the number of admissibility criteria that are used to control the shape of the curves. The current formulation is divided into two steps that correspond to the application of the earth pressure admissibility criteria described in section 5.3.2.2 and the concave admissibility criteria described in section 5.3.2.1.

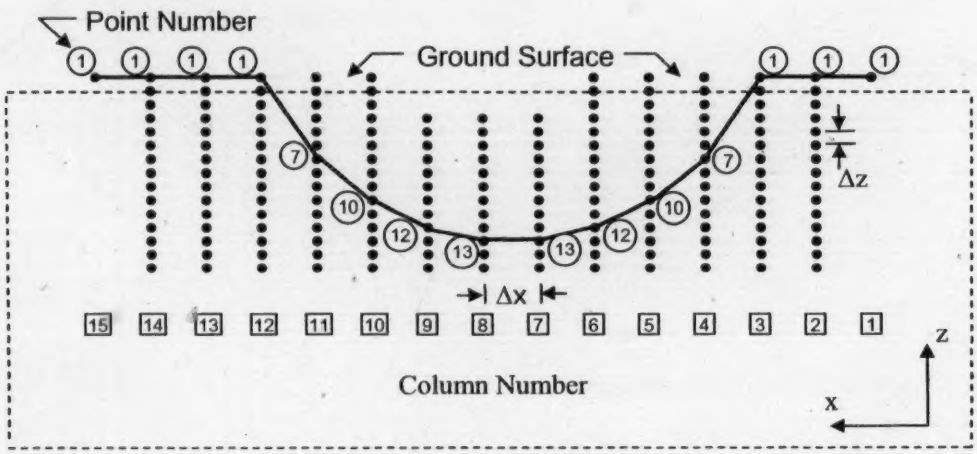

Figure B.5: Profile view of one stage from

Figure B.3 a) illustrating the numbering scheme used in the numerical procedure to generate *state curves*.

The earth pressure admissibility criterion is applied first and follows the numbering scheme illustrated in Figure B.5. The procedure begins at point, [k = 1], in column, [i = 2]. The angle of inclination (θ) for the line segment connecting point, k, to each point [j=*1*] to [j=n] in column [i – 1] is computed and compared to the angle of inclination permitted by the earth pressure admissibility criteria (i.e., $45+\phi'/2$). The connections that result in line segments with angles of inclination, $|\theta| \leq 45+\phi'/2$, are stored. The procedure is repeated until the connections for each

point in the grid have been evaluated. Figure B.6 a) and b) illustrates the results of the procedure for point k in column i. Figure B.6 a) illustrates all of the connections evaluated for a point k. The solid lines in Figure B.6 b) represent line segments that pass the earth pressure admissibility criteria. Applying the earth pressure admissibility criteria first, reduces the number of connections evaluated during the application of the concave admissibility criteria.

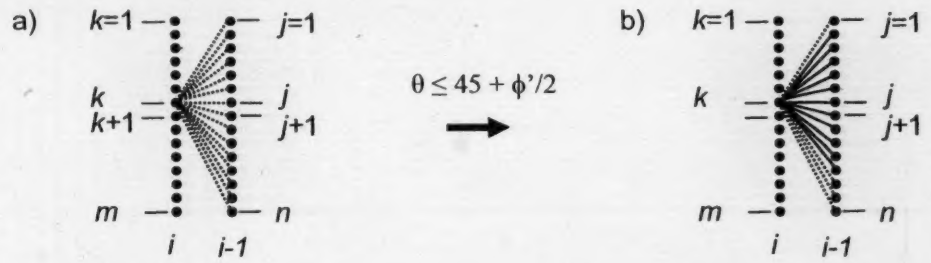

Figure B.6: Schematic illustrating the application of the earth pressure admissibility criteria.

The application of the concave admissibility criteria follows a similar procedure. The procedure begins in column, [$i = 2$]. The slope (i.e., $\partial z / \partial x$) of each of each line segment connection between points [$k = 1$] to [m] and points [$j = 1$] to [n] that pass the earth pressure admissibility criteria are calculated and stored at the corresponding point [k]. The procedure moves on to the next column (i..e, $i = i+1$). The procedure computes the slope of each admissible connection between points [k] in columns [i] and points [j] in column [$i - 1$], similar to the first step. It is important to point out that each point [j] in column [$i - 1$] contains information regarding the slope of the line segments from column [i-2] leading to that point, as shown in Figure B.7 a). Now the procedure computes the difference between the slope of connections between columns [i-2] and [i-1] and columns [i-1] and [i] (i.e., $\partial^2 z / \partial^2 x$ is computed). The connections that pass the required concave admissibility criteria (i..e, Equations [5.1], [5.2] or [5.3]) are recorded. Figure B.7 b) illustrates the admissible connections after the application of the concave admissibility criteria corresponding to Equation [5.1]. The line segments between column [$i - 2$] and [$i - 1$] were

recorded during the application of the earth pressure admissibility criteria. The solid lines represent the connections that passed the concave admissibility criteria. The procedure continues through the remainder of the grid until all of the admissible state curves have been recorded.

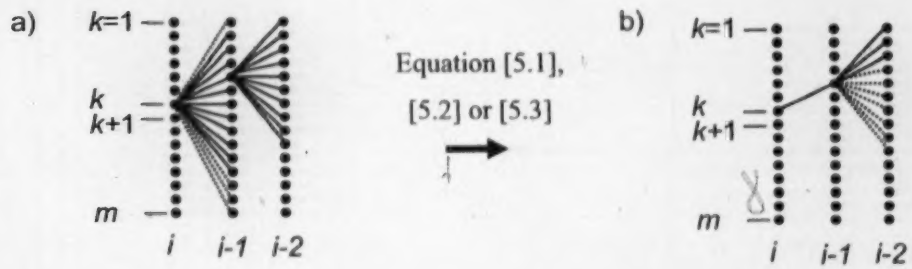

Figure B.7: Schematic illustrating the application of the concave admissibility criteria.

Figure B.8 illustrates a completed sample of state curves on one *stage*. Each admissible *state curve* is stored in an array in preparation for the completion of the dynamic programming search. Figure B.9 illustrates a completed *stage-state* system that is ready to be searched (The top layer has been made "see through" in an attempt to illustrate the internal portion of the *stage state* system.).

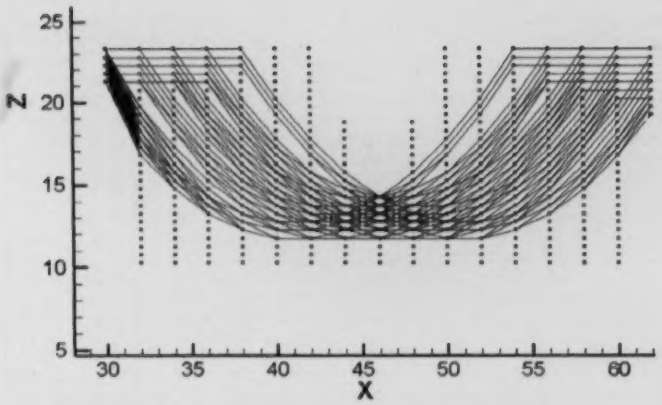

Figure B.8: Illustration of a completed sample of *state curves*.

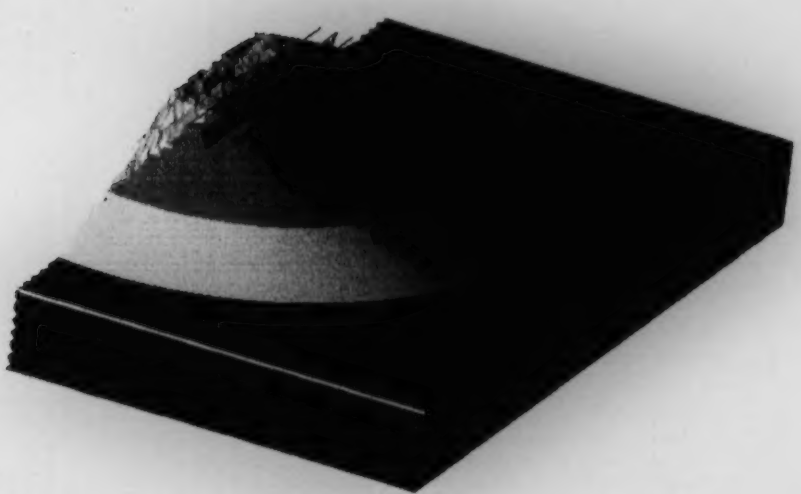

Figure B.9: Illustration of a completed *stage-state* system.

B.3 Dynamic Programming Search

The dynamic programming search is completed according to the stage-state system described above. The following sections describe the procedure to compute the factor

of safety followed by a description of the dynamic programming optimization procedure.

B.3.1 Calculating the Factor of Safety

The points on the dynamic programming search grid are used construct triangular planes that are connected together to form the slip surfaces evaluated during the slope stability analysis. The factor of safety for individual triangular planes is evaluated and used to compute the overall factor of safety for the slip surface. The following discussion describes the procedure to compute the factor of safety for one triangular plane.

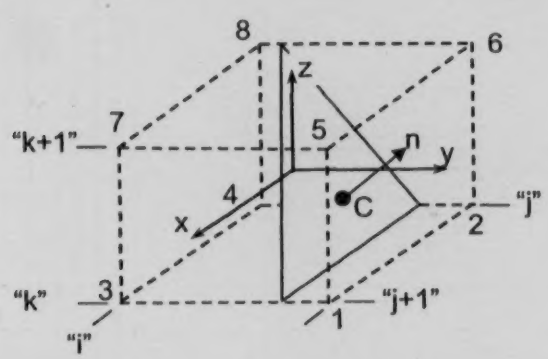

Figure B.10: Illustration of one triangular plane intersecting an element from the intermediate grid.

A search is performed through the intermediate grid to determine the eight grid points surrounding the centroid of the triangle (Figure B.9). The soil parameters and stress state from the surrounding eight grid points are used to determine the soil parameters and stress state at the centroid of the triangle using standard tri-linear interpolation. First, a local coordinate system is defined with an origin located at the centre of the element. Next, the local coordinates (x_c, y_c, z_c) for the centroid, C, of the triangular plane can be computed using the expressions shown in Eq. [4.3].

[6.2] $$x_c = 2 * \frac{(x - x_i)}{(x_{i+1} - x_i)} - 1 \; ; \; y_c = 2 * \frac{(y - y_j)}{(y_{j+1} - y_j)} - 1 \; ; \; z_c = 2 * \frac{(z - z_k)}{(z_{k+1} - z_k)} - 1$$

The values x, y, z are the coordinates for the centroid of the triangular plane based on the global coordinate system. Likewise, the coordinates x_i, y_i, and z_i are based on the global coordinate system. The local coordinates computed using the expressions given in Eq. [4.3] will always result in values between negative one and one. The local coordinates of the centroid can be used to compute an interpolation factor, N, for each of the eight nodes using the set of expressions given in Eq. [4.4].

[6.3]
$$N_1 = (1 / 8) * (1 + x_c) * (1 + y_c) * (1 - z_c)$$
$$N_2 = (1 / 8) * (1 - x_c) * (1 + y_c) * (1 - z_c)$$
$$N_3 = (1 / 8) * (1 + x_c) * (1 - y_c) * (1 - z_c)$$
$$N_4 = (1 / 8) * (1 - x_c) * (1 - y_c) * (1 - z_c)$$
$$N_5 = (1 / 8) * (1 + x_c) * (1 + y_c) * (1 + z_c)$$
$$N_6 = (1 / 8) * (1 - x_c) * (1 + y_c) * (1 + z_c)$$
$$N_7 = (1 / 8) * (1 + x_c) * (1 - y_c) * (1 + z_c)$$
$$N_8 = (1 / 8) * (1 - x_c) * (1 - y_c) * (1 + z_c)$$

The soil parameters (i.e., c', ϕ', ϕ^b, u_w) and stress state (i.e., σ_x, σ_y, σ_z, σ_{xy}, σ_{xz}, σ_{yz}) at the centroid of the triangular plane can be computed as the sum of the parameter multiplied by the corresponding interpolation factor for each of the eight nodes (e.g., $\sigma_x = \sum_{i=1}^{8} \sigma_{x_i} N_i$ etc.). The unit normal vector, n, can be determined using the three coordinates from the triangular plane.

Knowing the stress state at the centroid of the triangle and the unit vector normal to the plane, it is possible to calculate the components of the traction $T^{(n)}$ shown in Figure B.11, using Eq. [4.5].

[6.4] $T_i^{(n)} = \sigma_{ij} n_j$

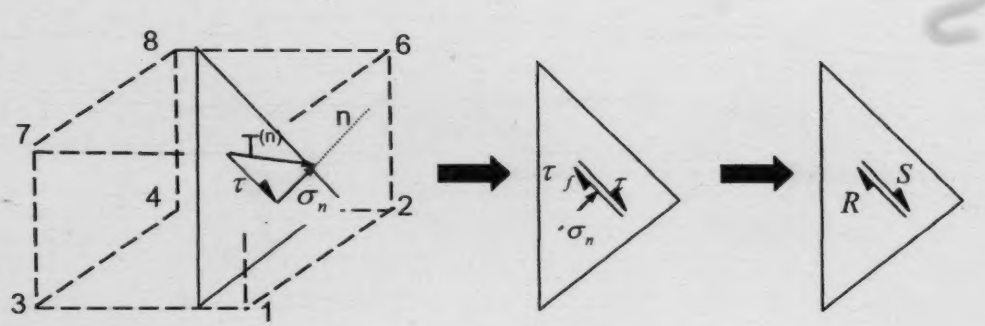

Figure B.11: Calculating the resisting force, R, and shear force, S, based on the normal stress, σ_n, and mobilized shear stress, τ, acting at the centroid of a triangular plane.

The normal stress, σ_n, can be calculated by evaluating the dot product of the traction $T^{(n)}$ and the unit normal vector, n, using Eq. [4.6].

[6.5] $\sigma_n = T^n \bullet n$

Finally, Pythagoras' theorem can be used to determine the magnitude of the mobilized shear stress, τ, acting at the centroid of the triangle using Eq. [4.7].

[6.6] $\tau = \sqrt{\left|T^{(n)}\right|^2 - \left|\sigma_n\right|^2}$

The shear force, S, is calculated by multiplying the mobilized shear stress, from Eq. [4.7], by the area of the triangle.

The shear strength provided over the area of the triangle can be calculated using the extended Mohr-Coulomb equation for saturated-unsaturated soil (Fredlund and Rahardjo 1993):

$$[6.7] \qquad \tau_f = c' + (\sigma_n - u_a)\tan\phi' + (u_a - u_w)\tan\phi^b$$

where c', ϕ', and ϕ^b are the shear strength parameters of a saturated-unsaturated soil, $(\sigma_n - u_a)$ is the net normal stress, and $(u_a - u_w)$ is the matric suction. The resisting force, R, is computed by multiplying the shear strength of the soil, τ_f , by the area of the triangle A.

The same procedure can be used to compute the resisting force and shear force for each triangular plane on the slip surface. The summation of the resisting forces divided by the summation of the shear forces can be used to compute the overall factor of safety for the slip surface, according to Eq. [4.2].

B.3.2 Optimization Procedure

The three-dimensional slope stability calculations have been divided into a *stage-state* system and the factor of safety equation has been defined. It is now possible to introduce an auxiliary functional (G) that is evaluated for each *state curve* connection and can be used to determine the slip surface with the lowest factor of safety. Eq. [5.7] represents the auxiliary functional and is the result of rearranging Eq. [5.4].

$$[6.8] \qquad G_i = \sum_{ij=1}^{mn} \left[R_{ij} - FS_{ij} \right]$$

Figure B.12 illustrates a portion of a three-dimensional sip surface resulting from the connection of *state curve* (*kk*) from stage [*i*+1] to *state curve* (*jj*) from *stage* [*i*]. The *state curves* are connected by a series of triangular planes. The value of the

auxiliary functional for the connection shown in Figure B.12 is determined by summing the result of the right hand side of Eq. [5.7] evaluated for each plane combination.

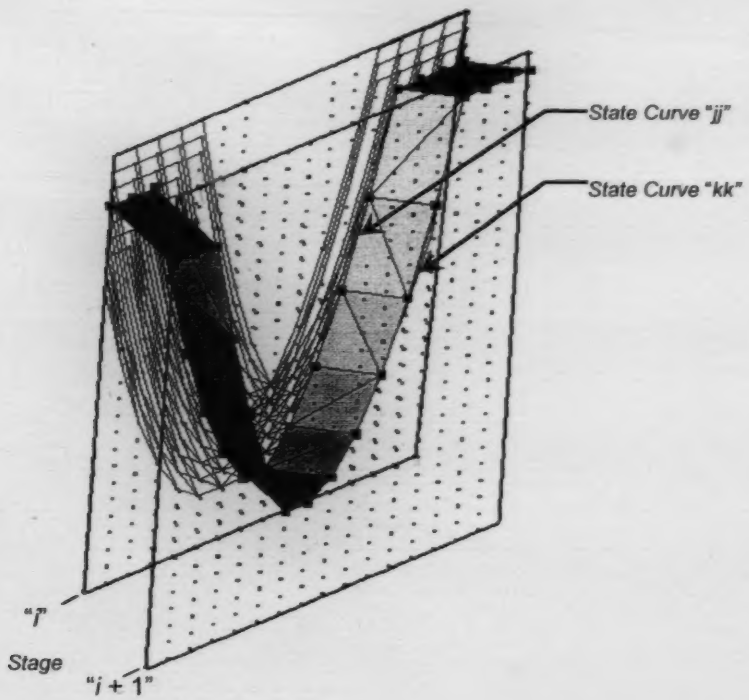

Figure B.12: One state curve connection between stage [i] and [$i-1$].

The optimal function shown in Eq. [5.8] is introduced to record and compare the return function values, G_i, calculated for each trajectory as the search for the slip surface with the minimum factor of safety proceeds.

[6.9] $$H_{i+1}(kk) = \min_{jj=1-s_i} \left\{ H_i(jj) + G_i(jj,kk) \right\}_{kk=1-s_{i+1}}^{i=1-I}$$

$$H_1(jj) = 0; \qquad jj = 1 - s_1$$

The value of the optimal function, $H_1(jj)$, for all of the *state curves* in the first *stage* (i.e., *state curves* 1 through s) is set to zero, the factor of safety is initialized with a reasonable guess and the convergence criteria (δ) is set according to the desired accuracy in the factor of safety. The numerical procedure evaluates the state curve connections between every stage beginning with stage [i] to stage [n-1]. The return function $G_i(jj,kk)$ is calculated for each trajectory between *state curve* (kk) in *stage* [i+1] to *state curves* [(jj) = 1-s_i] in *stage* [i]. In other words, R and S is calculated for each triangular plane on the state curve connection and used together with the current value of F to compute the return function value. $H_i(jj)$, the value of the optimal function recorded at the *state curve* (jj) in *stage* [i], is added to the return function value. The *state curve* (jj) that results in the minimum value of the brace {} (i.e., the trajectory with the lowest factor of safety), is recorded and the calculation proceeds to the *state curve* (kk+1) until all of the connections between stage [i] and [i+1] have been evaluated. When the calculation reaches the final *stage* [n] the *state curve* (kk) resulting in the minimum optimal function value is determined. Starting at the minimum *state curve* in the final *stage*, it is possible to trace back the minimum trajectory to each previous *stage* using the recorded (jj) values at each [i] and (kk). The combination of each minimum trajectory is the trace of the slip surface with the lowest factor of safety. The factor of safety (F_s) for the slip surface is computed and compared to F (i.e., the factor of safety from the previous iteration). If, $|F\text{-}F_s| \leq \lambda$, then convergence is achieved and the optimization procedure is complete. If not, F is set to the value F_s and the optimization procedure is repeated. Convergence is typically achieved in less than five iterations.

B.4 Evaluating the Results

It is possible to artificially restrict the shape of the slip surface depending on the design of dynamic programming search grid or the intermediate grid. The final slip surface should be inspected to make sure that it does not touch the boundaries of either grid. It is possible to design the computer program to identify the locations

where the slip surface is restricted by the search grid, automatically expand the search grid in the problem area and perform another iteration.